

Fachbereich Biologie/Chemie
Institut für Chemie neuer Materialien

Dissertation

Zur Erlangung des Grades eines Doktors der Naturwissenschaften
(Dr. rer. nat.)

**Viologen-nucleobase derivatives: building
blocks for functional materials**

von

Marius Ciobanu

aus Rumänien

Osnabrück 2015

This work is dedicated to my beloved parents

„The most fundamental and lasting objective of chemistry is not production of new compounds, but production of properties.”

George S. Hammond (1921 – 2005)

This doctoral work was carried out at the Institute of Chemistry of New Materials, Faculty of Biology/Chemistry (FB/05) in the group Organic Materials Chemistry I (Prof. Dr. Beginn), University of Osnabrück, under the supervision of Prof. Dr. Simona Asaftei. The doctoral studies were performed in the period from April 2010 to March 2015.

Hauptberichterstatter: Prof. Dr. Uwe Beginn, University of Osnabrück

Zweitberichterstatter : Prof. Dr. Simona Asaftei, University of Applied Science
Osnabrück

Weitere Mitglieder : Prof. Dr. Markus Haase, University of Osnabrück
Dr. Dietrich Steinmeier, University of Osnabrück

Acknowledgments

This dissertation was the most extensive and complex project I ever accomplished and the people around me were playing a determining role on achieving this goal. Therefore, I would like in the following to express my appreciation to those who guide, help and support me over the PhD time.

I would like first to express my deepest gratitude to my supervisor Prof. Dr. Simona Asaftei, for her continuous support, understanding, guidance and encouragement throughout my doctoral studies at the University of Osnabrück. I appreciate her generosity in sharing knowledge, ideas and precious time which was critical for my development as a research scientist.

I would like to express my appreciation to my co-advisor Prof. Dr. Uwe Beginn for give me the opportunity to make my PhD in his research group, for interesting discussions and careful advices and for the big freedom to use all available laboratory resources.

I would like to thank to Prof. Dr. Helmut Rosemeyer and Prof. Dr. Lorenz Walder for the very helpful individual discussions or at the literature seminars.

I would like to thank to Prof. Dr. Markus Haase and Dr. Dietrich Steinmeier for accepting of being members of my evaluation commission.

Further, I would like to thank to Ana-Maria Lepadatu for being a great colleague and friend and for her support and the time spent together in the lab that I will always remember with pleasure.

I would like to thank all alumni PhD students and actual colleagues from OMC I group: Dr. Enfeng Song, Dr. Ralf Beckmann, Dr. Edith Malecki, Dr. Sandra Schwitke, Dr. Marina Zorn, Miriam Brandt, Adrian Dragulelei, Eduard Belke, Xihomara Lizzet Casallas Cruz, Christine Knies, Eduard Belke and Emma Werz, for the very nice knowledge exchange that we had over the time in the Monday's work seminar. I would also like to thank to all Erasmus students that I co-advised through their own projects and that help me in the daily work in the laboratory.

Special thanks to Dr. Alina Veronica Constantin, Dr. Dereje Hailu Taffa and Seyyed Mohsen Beladi-Mousavi for the nice scientific discussions close-related to my research topic.

I appreciate the effort of Marianne Gather-Steckhan for introduce me into the NMR technique measurements and help me with patience to improve my German language. Many thanks to Petra Bösel who provides me help with chemical and accessories and for the many practical advices. I would like to thank also to the all co-workers from the Institute of Chemistry of New Materials for their support: Anja Schuster for IR and elemental analysis, Kerstin Rücker for TGA, Iris Helms and Elisabeth Michalek for ordering chemicals and various helping in laboratory.

I would like to thank to my friend Dr. Cristina Gruian and Mrs. Ruth Bonazza from Schreibwerkstatt, University of Osnabrück, for their advices regarding scientific English writhing that were so helpful in the writhing of my own dissertation.

I would like to thank to the secretary of our research group, Gertrud Strunk for her great professionalism in help me with the administrative work. Many thanks also to Ms. Monika Dubiel.

I would like to express my appreciation to Dr. Dietrich Steinmeier for the friendly advices and for the bicycle that was so useful to make the 5 km distance between Institute and home. Of course, I would like to thank to all my friends in Osnabrück for the very nice moment spent together and for their friendship.

Last, but not least, I would like to thanks to my parents that invest in me and my education for which I will be always grateful. Special thanks to my dear Audrey for encouragement and being near to me all over this time.

Table of contents

Acknowledgments	1
Table of contents	3
CHAPTER 1	
Introduction.....	6
1.1 Background.....	6
1.2 Concept and objectives	7
1.3 State of the art	9
1.3.1 Viologens – properties, applications and methods of characterization	9
1.3.2 Nucleobases as supramolecular motifs	10
1.3.3 Templated self-assembly of functional molecules.....	12
1.3.4 Viologen-based ionic liquid crystals.....	14
1.3.5 Hydrogen bonded layer-by-layer self-assembly	19
1.3.6 Mesoporous TiO ₂ film as solid support for electrochemical devices	20
1.3.7 Electrochromic devices - principle and construction.....	21
CHAPTER 2	
Viologen-Nucleobase Derivatives: Synthesis and Characterization	23
2.1 Synthesis of viologen-nucleobase derivatives	24
2.1.1 Nucleobases alkylation	26
2.1.2 Coupling of the alkylated nucleobases to 4,4'-bipyridinium unit	26
2.2 Study of physico-chemical properties.....	31
2.2.1 Optical and spectroelectrochemical properties	31
2.2.2 Electrochemical properties	36
2.2.3 Chemical reduction	39

CHAPTER 3**Interaction of Viologen-Thymine Derivatives with ssDNA and Analogue ssPNA.. 41**

- 3.1 Hydrogen-bonded self-assemblies of viologen-thymine derivatives with ssDNA 42
- 3.2 Electrostatic interaction of viologen-thymine derivatives with ssDNA 45
- 3.3 Viologen-thymine derivatives as gene carriers..... 49
- 3.4 Hydrogen-bonded self-assemblies of viologen-thymine derivatives with ssPNA 50

CHAPTER 4**Mesogenic Viologen-Nucleobase Derivatives with Self-Association Behavior in Low Polar Solvents 55**

- 4.1 Synthesis 57
- 4.2 Hydrogen bonded self-association in low-polar solvents 58
- 4.3 Electrochemical properties in low-polar solvents..... 63
- 4.4 Thermotropic characterization 66
- 4.5 Ionic conductivity and cyclic voltammetry in LC state 70
- 4.6 Thermal-induced electrochromism in LC state 73

CHAPTER 5**Hydrogen Bonded Layer-by-Layer Deposition of Viologen-Nucleobase Derivatives on Mesoporous TiO₂ Film for Optoelectronic Devices 77**

- 5.1 Synthesis of a phosphonate-viologen derivative 4/Br⁻ 79
- 5.2 ssDNA-modified TiO₂ film 81
- 5.2.1 Preparation and electrochemical characterization 81
- 5.2.2 Evaluation of ssDNA surface coverage (Γ_{ssDNA}) 84
- 5.2.3 Stability of ssDNA monolayer..... 85
- 5.3 Deposition of a viologen-thymine derivative by hydrogen bonding on ssDNA-modified TiO₂ surface – proof of the concept 87

5.4 LbL deposition of viologen-nucleobase derivatives on TiO ₂ electrode modified with ssDNA as anchoring layer	89
5.5 LbL deposition of viologen-nucleobase derivatives on TiO ₂ surface modified with derivative 4 as anchoring layer	93
5.6 Fabrication of an electrochromic device.....	95
CHAPTER 6	
Experimental part.....	98
6.1 Materials	98
6.1.1 Commercial available chemicals	98
6.1.2 Synthesized chemicals.....	99
6.2 Synthesis	102
6.2.1 Synthesis of precursors	102
6.2.2 Synthesis of viologen-nucleobase derivatives 1/An ⁻ -3/An ⁻	105
6.2.3 Synthesis of ionic complexes 1 ²⁺ (DOBS) ₂ , 2 ²⁺ (DOBS) ₂ and 3 ²⁺ (DOBS) ₂	108
6.2.4 Synthesis of phosphonate-viologen derivatives.....	114
6.3 Methods	115
6.3.1 General techniques of characterization.....	115
6.3.2 Preparative procedures.....	118
6.4 Numerical experimental data	120
Summary and outlook	127
Zusammenfassung und Ausblick.....	129
Abbreviations	132
References.....	134
Curriculum Vitae.....	150

CHAPTER 1

Introduction

1.1 Background

Chemical compounds with multiple functionalities are promising building blocks for construction of functional materials with enhanced properties. This is because the combination of two or more distinct functions may have a synergetic effect on the overall properties and features of the corresponding material.

Particular attention has been directed towards the synthesis of compounds with two functionalities consisting of a core responsible for physico-chemical properties (i.e. electrochemical, optical, etc.) and nucleotide bases as capping groups capable of molecular recognition [1-10]. A major motivation of designing such compounds lies in the ability of nucleobases to direct the self-assembly process of functional molecules which may result in a modulation of physico-chemical properties of the corresponding materials. For example, White et al. [1] have reported on the synthesis of metal–polypyridyl complexes with pendant adenine or thymine groups. The obtained material exhibited enhanced luminescent properties as a result of supramolecular arrangement induced by nucleobases. In addition, Maiya et al. [2] have made use of the same self-assembly approach of a porphyrin and an anthracene derivative respectively, capped by complementary nucleobases, to modulate the optical properties of the respective bichromatic system. Other authors have claimed that such compounds offer great potential as building blocks for the construction of highly ordered and monodispersed nano-aggregates incorporating redox or optical functionalities [5-9]. In respect with this, the optoelectronic properties can be very efficiently tuned by controlling self-assembly approach of functional molecules in the presence of complementary templates.

Moreover, the application potential of dual functional derivatives is not restricted to the examples mentioned above. Compounds simultaneously combining supramolecular interaction abilities (i.e. hydrogen bonding, electrostatic) with optical or electrochemical function make them suitable for self-assembled monolayers (SAM's) studies, functional liquid crystals, optoelectronic materials or electrochemical devices construction.

Therefore, the design of small building blocks molecules with dual functionality continues to be an exciting topic for chemistry, biology, physics or supramolecular material sciences.

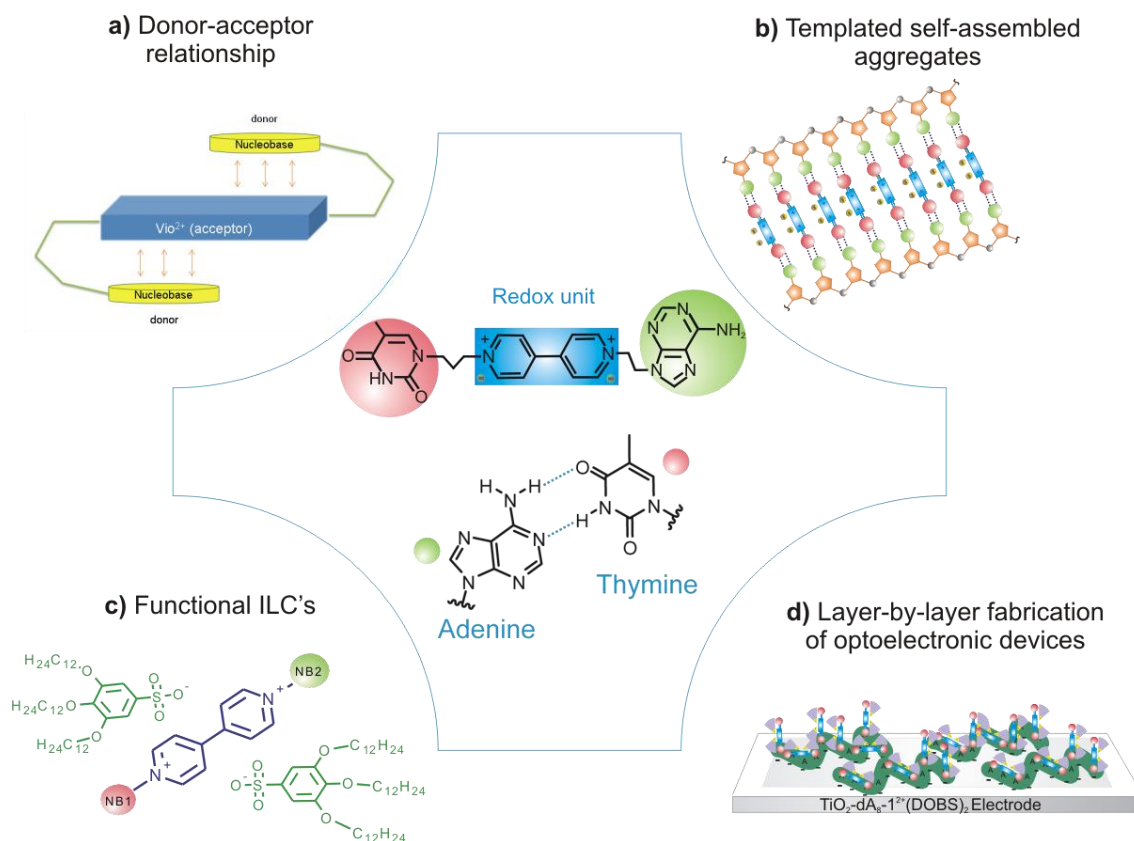
Despite the significant amount of examples in literature of compounds with dual function, there are still many possibilities for exploring new combinations of well-known functionalities which may lead to new interesting functional materials.

1.2 Concept and objectives

The main idea behind this thesis resides in rational designing of small bi-functional molecules consisting in a 4,4'-bipyridinium unit as a redox core and nucleobases (i.e. thymine and adenine) as capping groups. The combination of these two functionalities and unique structural topology of such compounds are expected to induce a series of new features:

- (i) Tuneable optical and electrochemical properties due to an intra/intermolecular charge transfer (CT) relationship between 4,4'-bipyridinium core as charge acceptor and nucleobase units as charge donors (Scheme 1.1a);
- (ii) Self-organization abilities induced by the hydrogen bonding interaction between nucleobases, by itself (Scheme 1.1d) or in the presence of complementary templates such as ssDNA or ssPNA analogues (Scheme 1.1b);
- (iii) Ionic exchange capability can be exploited to incorporate viologen-nucleobase derivatives into a liquid crystalline matrix by ionic exchange with amphiphilic anions (Scheme 1.1c) or to interact electrostatically with DNA and form polyplexes with biological importance.

The above mentioned features are expected, by one side, to have influence on the physico-chemical properties of the resulted new materials and, on the other side, to open new perspectives/possibilities for application of such molecular building blocks in the field of supramolecular optoelectronic materials, functional liquid crystals, for construction of electrochemical devices or as potential non-viral delivery vectors. The building block design and some possible applications of “viologen-nucleobase” derivatives are shown in Scheme 1.1.



Scheme 1.1 Viologen-nucleobase building blocks and their potential applications

On the basis of the molecular design concept presented above and the promising futures and applications of viologen-nucleobase derivatives, it was planned to achieve within this thesis the following objectives:

- (1) To synthesize a series 4,4'-bipyridinium compounds capped by thymine and/or adenine nucleobases and investigate the impact of unusual combination of the two functionalities on the chemical, electrochemical and optical properties;
- (2) To create well-defined supramolecular structures by using templated self-assembly approach of viologen-nucleobase derivatives in the presence of ssDNA or ssPNA and thymine-adenine base pairing as driving force interaction;
- (3) To investigate the capacity of viologen-nucleobase derivatives to condense electrostatically oligonucleotides or plasmid DNA as potential non-viral delivery vectors;
- (4) To combine viologen-nucleobase derivatives by ion pairing with amphiphilic 3,4,5-tris(dodecyloxy)benzene sulfonate (**DOBS**⁻) anions, and to investigate their phase behaviour;

- (5) To develop a new approach for construction of optoelectronic device components by using hydrogen bonded layer-by-layer self-assembly process of viologen-nucleobase derivatives on TiO₂ surface.

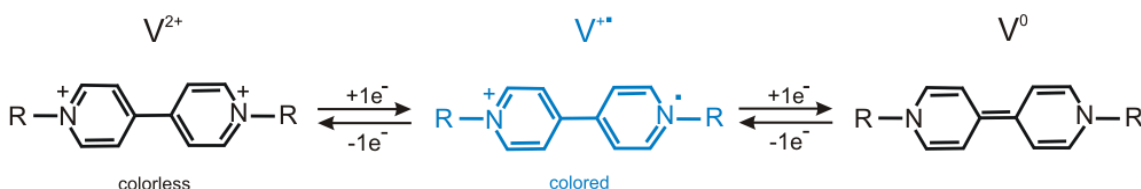
1.3 State of the art

The viologen-nucleobase derivatives were discussed in this thesis in a series of applications which required knowledge related to supramolecular chemistry, liquid crystalline materials or electrochemical devices principle and construction. Therefore, in the subsequent text, the main concepts, methodologies and the most recent achievements in the respective fields will be presented.

1.3.1 Viologens – properties, applications and methods of characterization

The N,N'-disubstituted 4,4'-bipyridinium derivatives ("viologens") are dicationic salts obtained mainly by diquaternization of 4,4'-bipyridyl. There are two general synthetic pathways to prepare the viologens: the first one starts from the synthesis of 1-substituted pyridines which are subsequently coupled [11], and the second one (also applied in this thesis) consisting in the nucleophilic substitution reaction of 4,4'-bipyridine with excess of an alkyl halide substrate. The preparation of bipyridilium salts implying this later method was performed first by Anderson [12] in 1855. This reaction, better-known as Menshutkin reaction [13], follows a S_N2 mechanism.

Viologen derivatives are particularly interesting for their redox and electrochromic properties. The dicationic form (V²⁺), which is almost stable state, is known as a good electron acceptor and can undergo two subsequently one electron reduction steps to form first, a colored radical cation (V^{•+}), and second at a more negative potential, a neutral quinoidal species (V⁰) (Scheme 1.2) [14].



Scheme 1.2 The redox states of viologen

The reduction potential and the color of the radical cationic species (blue/violet/green) strongly depend on the substituents at the nitrogen atoms of the 4,4'-bipyridinium core

[11]. The redox properties of viologens were exploited in several applications such as electrochromic devices [15, 16], photovoltaic cells [17], sensors [18, 19], ionic liquid crystalline devices [20-22], light-harvesting [23], catalysis [24-27] or potential oxidant agent for cancer radiation therapy [5].

One of the most used techniques to characterize the redox behavior of viologens is cyclic voltammetry (CV). Very briefly, CV is an electrochemical method which implies the variation of the potential with a constant rate, in one direction and backward, between a working electrode and a counter electrode while the current response is monitored. The electrical potential is applied relative to the potential of a third electrode, so-called reference electrode. The shape of the resulted current-potential curve (cyclic voltammogram) provides insights into both, the kinetic and thermodynamic of electrochemical systems. Excellent review articles and textbooks dedicated to the fundamental aspects and applications of cyclic voltammetry can be found in literature [28-30]. The most important quantities derived from CV data are the pick potentials E_{pc} and E_{pa} with the corresponding currents I_{pc} and I_{pa} respectively. For reversible and quasi-reversible processes the ratio $I_{pc}/I_{pa}=1$. The separation of the peak potential ($\Delta E=E_{pa}-E_{pc}$) gives also information about the reversibility of the electron transfer (ET). For a one-electron transfer reversible process which occurs with a very fast rate of electron transfer the separation peak should not exceed 59 mV.

The electrochromic properties of viologens are investigated by spectroelectrochemical methods (SEC) [30]. The electrochromism is the property of a material to change its color as a certain potential is applied. The method consist in coupling of an electrochemical cell setup with a spectrophotometer and monitoring *in situ* the electrochemically generated species by mean of UV-Vis spectroscopy (SEC-UV-Vis). In the case of the viologens, SEC-UV-Vis technique is used to study the change in color as a result of electrochemical reduction from dicationic species to colored radical-cationic species.

1.3.2 Nucleobases as supramolecular motifs

The nucleobases (adenine, guanine, cytosine, thymine and uracil) are well-known heterocyclic compounds existing in nature in the structure of DNA or RNA biopolymers. The nucleobases are classified in two main groups: purines (adenine and guanine) and pyrimidines (thymine, uracil and cytosine). Their ability to recognize and

bind specifically by hydrogen bonding (T-A, G-C) represents the key mechanism in the duplication and transmission of the genetic information in biological systems. For the point of view of materials science the nucleobases have a great potential as supramolecular motifs due to their high ability to form in-plane multiple intermolecular hydrogen bonds, stacking interaction perpendicular to the plane or metal-nucleobase coordination interaction [31]. These features were used in a variety of supramolecular systems with applications in specific recognition of biological receptors [32-34], as cross-linkage for polymer systems [35-37] or as connecting unit for supramolecular polymers [38]. The use of nucleobases as supramolecular motif is excellently reviewed by Rowan (2004) [31] and Araki (2005) [39]. Figure 1.1 shows the donor and acceptor hydrogen bonding sites of the four nucleobases.

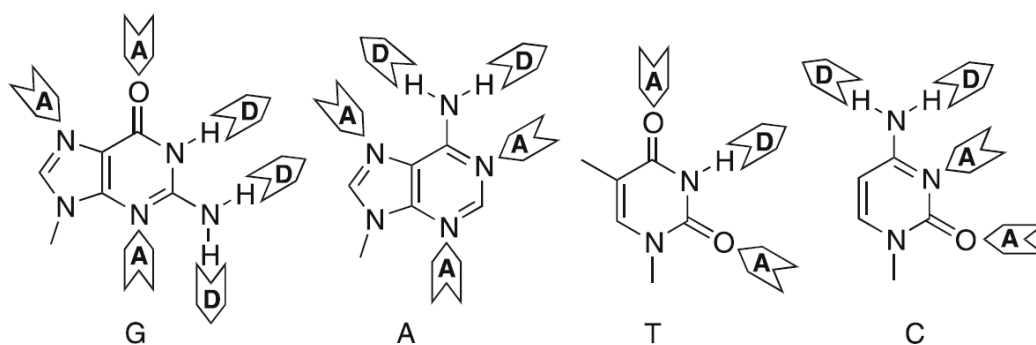


Figure 1.1 Hydrogen-bonding donor (D) and acceptor (A) sites of guanine (G), adenine (A), thymine (T) and cytosine (C) [39]

A special care in the covalent incorporation of nucleobase moieties into a certain chemical matrix is given to the preservation of their molecular recognition function. Therefore, it is desirable to connect covalently nucleobases on a certain position which does not affect hydrogen bonding sites.

The preparation of purinic and pyrimidinic nucleobases has been well-documented from long time ago [40]. However, the synthesis of their alkylated derivatives continues to be a challenge for organic chemists since the direct alkylation of nucleobases suffers of two major drawbacks: 1) poor solubility in organic solvent, and 2) no regioselectivity, hence nucleobases can be alkylated simultaneously on several positions [41, 42]. Most popular approach towards alkylation of nucleobases is direct nucleophilic displacement of halide substrates [43-45]. The specific alkylation of the nucleobase using this approach require in many cases the protection of functional groups prior the alkylation reaction [44, 46].

1.3.3 Templated self-assembly of functional molecules

Supramolecular self-assembly process, pioneered by Lehn [47, 48] in the early 90`s, has emerged as a powerful strategy to create well-defined functional nanostructures and to enhance the physico-chemical properties of the materials. Self-assembly process involves the binding of building blocks molecules by non-covalent interactions such as hydrogen bonding, π - π stacking, electrostatic or Van-der-Waals. A variety of supramolecular entities like supramolecular gelators [49-51], vesicles [52, 53], liquid crystals [54, 55] and nanofibers [6-8, 56-58] were constructed using this approach. Particularly, templated self-assembly approach driven by molecular recognition has been attracted considerable attention as an efficient pathway to construct highly ordered supramolecular nanostructures [59]. In the terms of supramolecular chemistry, a template is a molecular entity which serves as a pattern to construct supramolecular structures with well-defined architecture. Accordingly, single stranded DNA molecule with pre-defined size and shape is a reasonable template to construct supramolecular functional materials. Even the natural double helix DNA represents itself the best example of a sophisticated and highly ordered self-assembled system. Starting with year 2000, several groups have used molecular recognition function of nucleobases and ssDNA (single stranded DNA) as template to direct the self-assembly process of small functional molecules. Janssen and co-workers [6-8, 60] have incorporated chromophore molecules into monodispersed supramolecular aggregates by using synthetic homo oligonucleotides as templates (Figure 1.2).

In a similar way, Iwaura [9, 57, 58] has created nano- and microfibers by using nucleobase-appended bolaamphiphiles as guest components and complementary ssDNA as template.

Recently, Wong [5] reported on the formation of self-assembled nanofibers from a thymine-appended oligo(p-phenylenevinylene) derivative and oligoadenine 20-mer. The resulted supramolecular structures, stabilized by adenine-thymine hydrogen bonding and π - π staking interactions, exhibited enhanced fluorescence properties. To summarize, all the above mentioned authors emphasised that DNA templated self-assembly approach of functional molecules is an efficient and easy way to modulate optical and electronic properties of the materials.

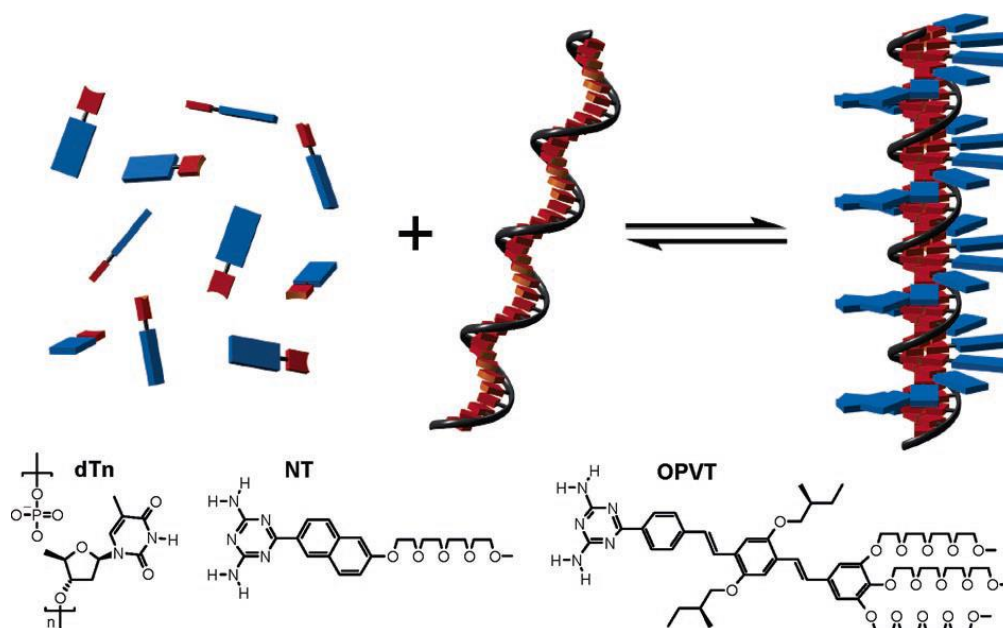


Figure 1.2 A schematic representation of ssDNA templated self-assembly of chromophores: ssDNA (black strand); chromophores (blue bar); hydrogen bonding unit (red bar) and molecular structures of dTn, NT and OPVT (reproduced from ref. [8])

DNA templated approach continues to be a dynamic topic of research and efforts are focussed on (1) designing new functional molecules that can be used as building blocks for self-assembly and (2) replacing ssDNA (which restrict the scope to aqueous environment) with other templates. Some advancement for the latter case was already achieved by using polypeptide nucleic acids (PNA) or nucleobase-functionalized syntactical polymers as templates [10, 61, 62]. The DNA self-assembled suprastructures may find application in the field of molecular electronics, sensing or optoelectronic devices.

The self-assembly process of functional molecules can be demonstrated by a variety of techniques including: gel permeation chromatography (GPC), viscometry, light scattering methods, mass spectrometry (MS), atomic force microscopy (AFM), etc. An extensive review about methodologies and techniques used in the characterization of supramolecular systems was published by Liu et al. [63].

In the following paragraphs, a brief introduction of the diffusion ordered spectroscopy (DOSY) will be given since this method was employed in the current thesis to demonstrate the self-assembly process of viologen-nucleobase derivatives by hydrogen bonding (cf. Chapter 4).

DOSY is a powerful NMR technique which gives information about the diffusion coefficient of molecules which is connected to their size and shape, as well as properties of the surrounding environment (i.e. viscosity and temperature) of each chemical species in solution. The technique consists in measurements of diffusion of the chemical species by observing the attenuation of the NMR signals during a pulsed field gradient experiment. The degree of signal attenuation is a function of \mathbf{G} (the magnetic gradient pulse amplitude) and occurs at a rate which is proportional to the coefficient of diffusion (\mathbf{D}). Assuming that a line in spectrum at a fixed chemical shift \mathbf{f} belongs to a single component \mathbf{N} with diffusion constant \mathbf{D}_N , the signal attenuation $\mathbf{S}(\mathbf{f},\mathbf{z})$ can be written:

$$\mathbf{S}(\mathbf{f},\mathbf{z}) = \mathbf{S}_N(\mathbf{f}) \exp(-\mathbf{D}_N\mathbf{Z}) \quad (1.1)$$

where $\mathbf{S}_N(\mathbf{f})$ is the spectral intensity of component \mathbf{N} in zero gradient (“normal” spectrum of \mathbf{N}), \mathbf{D}_N is its diffusion coefficient and \mathbf{Z} encodes the different gradient amplitudes used in the experiment [64].

1.3.4 Viologen-based ionic liquid crystals

Liquid crystalline state (LC) is considered “the fourth state of matter” [65]. The properties of the LC materials are intermediate between that of a liquid and a crystalline solid. A material existing in liquid crystalline state flows like a liquid but the positional order in the molecular arrangement is still preserved on a certain extent. The LC’s properties (mechanical, magnetic susceptibility, electric permittivity, refractive index, etc.) are anisotropic which means that their quantities vary with the direction in which the properties are measured. Thus, the LC’s has found a variety of applications in display construction [66], as molecular sensors and detectors [67, 68], or as optical connectors and switches [69].

Liquid crystalline materials can be classified in two main categories: lyotropic and thermotropic liquid crystals. A liquid crystal is lyotropic if phases having long-ranged orientational order are caused by the addition of a solvent. In contrast, thermotropic liquid crystals are materials in which the mesomorphic state and the respective degree of order of the corresponding components are determined by the temperature.

Typically, a LC molecule consists of a rigid unit and one or more flexible parts. The rigid unit aligns the LC molecules in one direction, whereas the flexible part is

responsible for the fluidity. The optimum balance of these two components is critical to form liquid-crystalline materials. The liquid crystalline molecule is referred to as mesogen. Accordingly with the type of mesogenic units, liquid crystals are divided in two main classes: 1) calamitic liquid crystals, in which the mesogen has a rod-like shape and 2) columnar liquid crystals, whereas the mesogen is a flat-shaped core that makes the molecules to stack in one direction. Depending on the type of the mesogenic unit and temperature, liquid crystals exhibit a variety of LC phases. Some of them are depicted in Figure 1.3.

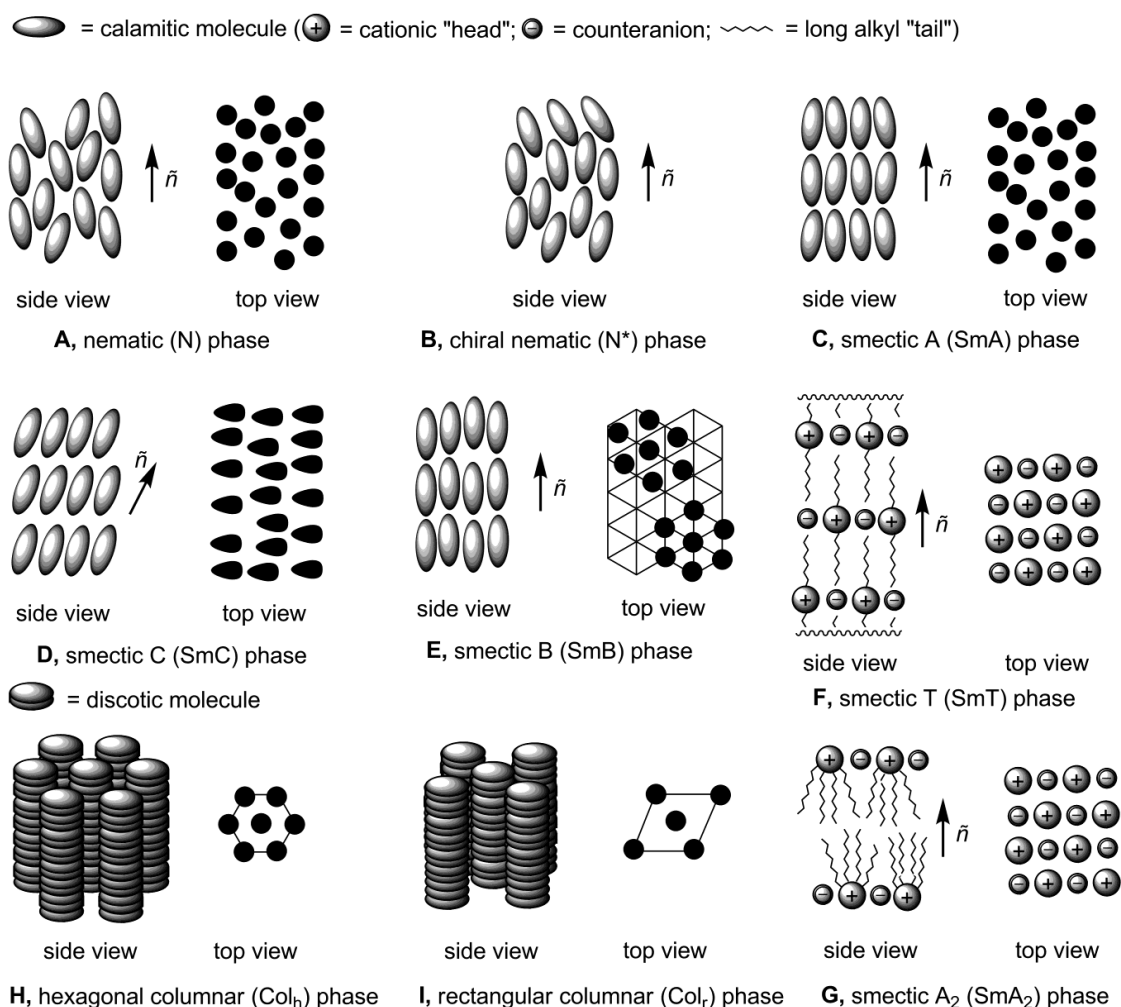


Figure 1.3 Different types of liquid crystalline phases [70]

To identify the occurrence and the type of liquid crystalline phases, a series of methods and standard techniques are used [71]. In the following, the basic concepts and principle of two important techniques employed in this thesis will be presented:

Differential scanning calorimetry (DSC)

DSC analysis is a widely used technique for study of chemical and physical processes that occur with exchange of heat. Basically, differential scanning calorimetry is a thermoanalytical method that measures the heat difference per unit of time between a sample and a reference, as a function of temperature. Because the selected reference should not exhibit any thermal transition in the measurement range, the specific heat variation of the sample is directly correlated with the heat difference between the sample and the reference. During the phase transition, the system makes automatically a thermal compensation that is monitored against the temperature. The resulted heat fluxes will cause an endothermic or exothermic peak in the corresponding thermogram. Two main parameters can be obtained from the DSC analysis: the onset temperature, which represents the temperature at which the phase transition starts, and the area between the peak and baseline which is associated to the transition enthalpy (ΔH) [72].

DSC is a frequently used technique in characterization of liquid crystalline materials and permits the identification of the multi-phase transitions: crystal-to-mesophase, mesophase-to-mesophase or mesophase-to-liquid. In generally, the enthalpy of crystal-to-mesophase transition is larger comparatively with the enthalpy of mesophase-to-liquid transition [73]. However, the DSC method is not able to identify the exact type of transition and combination with other methods is absolutely required for a complete characterization of liquid crystalline materials.

Thermo-optical polarizing microscopy (TOPM)

Thermo-optical polarizing microscopy [74] is another important technique in the standard characterization of liquid crystals. In contrast with the DSC, this method has the advantage of providing intuitive information regarding the type of mesophase. The method consists in observing a specimen placed between two glass plates under polarized light illumination, while its temperature is varied to identify the phase occurrence. The origin of optical patterns observed by polarized light microscope is the refractive index anisotropy (i.e. birefringence) of liquid crystals. When the polarized light enters a birefringent specimen the incident light is separated into two components of different velocity: the slow ray (called the extraordinary ray) and the fast ray (called the ordinary ray). Both the rays are polarized under mutual perpendicular orientation of their polarization planes. Because the two components pass the birefringent media with

different velocities, the corresponding light waves get out of phase. When the ordinary and extraordinary rays are recombined beyond the “analyser” polarizer, the state of polarization has changed because of the difference in phase. Furthermore, a specific wavelength becomes extinguished by interference of the two phase-shifted beams. Upon illumination of the sample with white light this gives rise to a colored light. The color will depend on the materials birefringence, its thickness, and the angle between the optical axis of the LC phase and the analyser [75]. Hence, upon cooling below the transition temperature from isotropic state to mesophase, the LC materials starts to become colored in the polarized light (the materials becomes anisotropic). In contrast to DSC, by TOPM it can be directly observed if the anisotropic material is a solid or a liquid and consequently it is easy to identify the occurrence of mesophase.

The growing of the mesophase results in many structural “defects”, i.e. local variations of the mesogen orientation, which give rise to a multi-colored specific pattern, called texture [73]. The analysis of the texture may provide useful information about the mesophase type but an unequivocal mesophase type assignment is not possible in most cases, because different mesophase types can exhibit identical optical textures.

In conclusion, TOPM is not a unique method to fully characterize liquid crystalline materials but combined information from the complementary methods such as DSC, thermo-optical polarizing microscopy or X-Ray Diffraction (XRD) may reveal the mesophase type and structure.

Viologen-based ionic liquid crystals – recent achievements

A particular class of LC materials are ionic liquid crystals (ILC's). As the name says, the mesogenic unit is composed by cations and anions. Therefore, ionic liquid crystals are materials that combine the properties of classic ionic liquids with that of liquid crystalline materials. The typical feature of ILC's is their anisotropic ionic conductivity which makes them ideally suitable for the field of molecular electronics. The ILC's materials were reviewed by Binnemans (2005) [76] and more recently by Axenov (2011) [70]. Those authors established a classification of ionic liquid crystals as function of mesogenic ionic unit. According to their taxonomy, there is a variety of subclasses including: ionic mesogens with organic cations, metal carboxylates, phosphates and phosphonates, ionic dendrimers, etc.

The viologen-based ILC's materials are particularly interesting because they combine redox/electrochromic properties of 4,4'-bipyridinium unit with anisotropic properties of liquid crystals [77]. The first viologen-based ionic liquid crystal consisting of a 4,4'-bipyridinium unit symmetrically substituted at the nitrogen atoms with 3,6,9-trioxatridecyl chains has been synthesized in 1986 by Tabushi et al. [78]. The group of Saielli showed that the substituted viologen salts with sufficiently long alkyl chains ($> C_7H_{14}$) exhibit in generally smectic mesophase in a wide range of temperature (0 – 140 °C) since such molecules are rod-like mesogens [79-81]. However, the viologen-based redox active ILC's forming columnar phases were later reported by Kato [21] which designed the discotic mesogens shown in Figure 1.4.

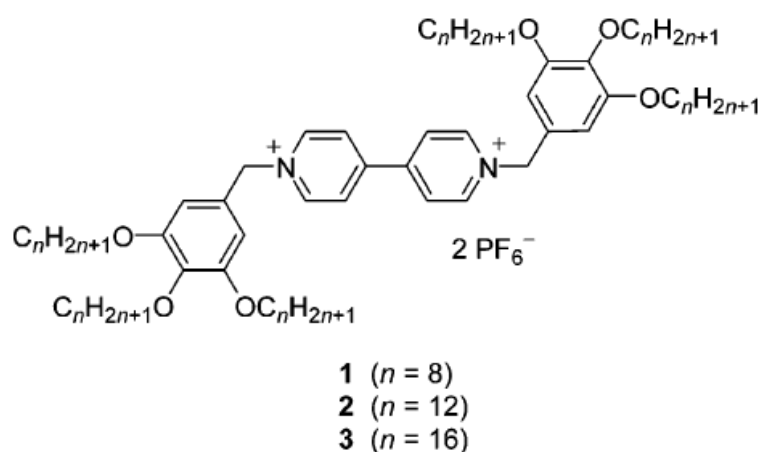


Figure 1.4 The first columnar liquid-crystalline viologens reported by Kato et al. [21]

N,N' -Aryl viologens possessing para-alkylbenzene sulfonate as counter anion were also synthesized and they show a smectic A liquid crystalline phase. In the mesophase this ILC exhibits a reversible redox photochromism in the presence of UV light [82-84]. This property makes such ionic liquid crystals very interesting for the development of optical writable devices.

In this context the incorporation of redox viologens into a LC matrix, by ion pairing with amphiphilic anions is a promising approach that can be used to develop new functional materials combining the redox/electrochromic properties of viologen with the anisotropic characteristics of liquid crystalline materials. Moreover, efforts could be directed towards designing of viologen-based mesogens containing functional groups (i.e. with hydrogen bonding abilities) as a strategy to enhance the physico-chemical properties of the corresponding ILC's.

1.3.5 Hydrogen bonded layer-by-layer self-assembly

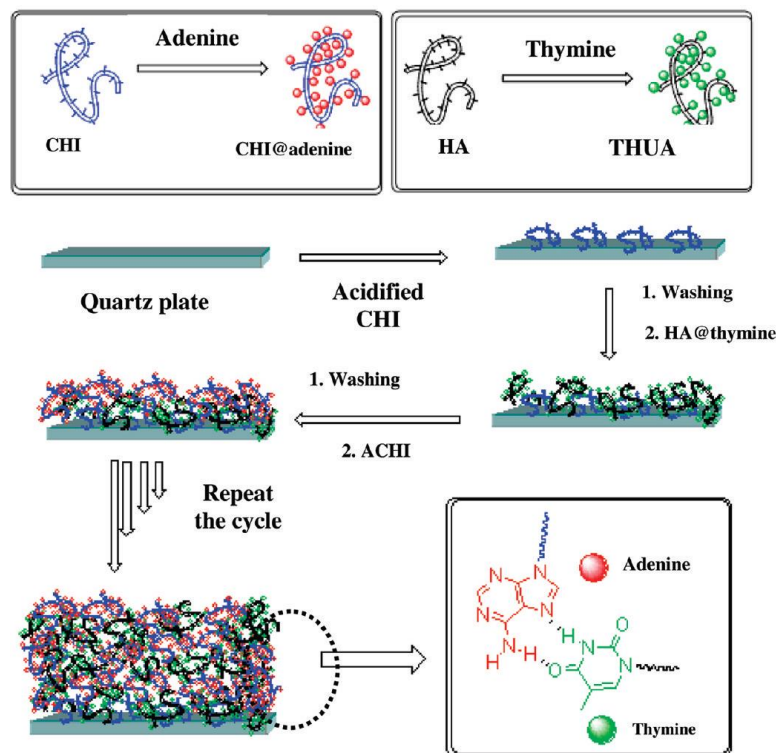
The design of smart surfaces by using small building units and exploring suitable intramolecular interactions such as electrostatic [85, 86], hydrogen bonding [87-91], π - π stacking [92, 93], hydrophobic or van der Waals forces [94] represents a promising approach for potential applications in the fields of biosensors [95], catalysis [96], optical data storage [97], molecular electronics [98] or surface property switching [99].

The surface functionalization using layer-by-layer (LbL) technique [100] has become a versatile and simple option for making nanostructured films under mild conditions, which is an important issue for preserving, for example, the activity of biomolecules. Simplified, layer-by-layer technique consists in depositing alternating layers of a certain material with wash steps in between. The deposition may be achieved by dip-coating, spray-coating, spin-coating, etc. The LbL technique has a series of advantages like: (1) it is simple, (2) it can be inexpensive, (3) a wide variety of materials can be deposited, i.e., polyions, metals, ceramics, nanoparticles, biological molecules and, (4) the thickness of deposited layer can be easily controlled. This last advantage arises from the linear growth of the film thickness with the number of deposition steps. Characterization of LbL films is typically done by optical methods such as ellipsometry or UV-Vis spectroscopy but not restricted to.

The LbL technique was developed in the early 90's by Decher which applied this method to deposit polyelectrolytes with opposite charge on solid support [85, 101]. Particularly, layer-by-layer assembly based on hydrogen bonding interactions was demonstrated in 1997, simultaneously by the groups of Rubner [89] and Wang [88]. Since then, a lot of studies were reported on thin-film fabrication based on hydrogen bonded LbL deposition by using a variety of building blocks [102-106]. Hydrogen bonded layer-by-layer assembly approach is a relatively young area of research which is receiving growing attention. The possibilities of controlling the hydrogen bonded films stability by simply changing parameters such as ion strength, pH or temperature make such films attractive for controlled release applications [107].

The hydrogen bonded layer-by-layer deposition based on molecular recognition of DNA nucleobases was successfully applied by Manna et al. [87] to self-assembly adenine-modified chitosan and thymine-modified hyaluronic acid on quartz solid

support (cf. Scheme 1.3). Park et al. [108] used thymine-adenine molecular recognition to immobilize zeolite microcrystals on glass substrate.



Scheme 1.3 Fabrication of H-bonded multilayer thin film using the Watson-Crick base pairing Principle. CHI = chitosan, HA = hyaluronic acid [87]

The layer-by-layer deposition using the hydrogen bonding between natural nucleobases is an intriguing approach that could be applied to generate very easy functional surfaces with great potential in the biosensoric field.

1.3.6 Mesoporous TiO₂ film as solid support for electrochemical devices

Titanium dioxide (TiO₂) has emerged as an important metal oxide in the development of nanostructured substrates with good technological and physico-chemical characteristics such as: good refractive index ($n=2.4$), semiconductive properties, biological compatibility and easy processability. Therefore, TiO₂ has been widely used as a suitable support for a variety of applications in the field of biosensors [109, 110], electrochromic windows [111-115], dye-sensitized solar cells (DSSC) [116, 117], photocatalysis [118], etc. The TiO₂ films are prepared by several methods including spray coating [119, 120], screen printing [121, 122] or liquid phase crystal deposition (LPCD) [123]. The thickness and structure of TiO₂ nanostructured film are dependent on the method of fabrication. Particularly, TiO₂ film (cf. Figure 1.5), prepared by *doctor*

blade method [112] has a mesoporous internal structure composed of nano-sized crystalline particles (diameter range 10-100 nm) sintered together in an interconnected network. The mesopores diameter is in the range 10-15 nm [124, 125]. Such TiO₂ film has found application as support for construction of electrochromic devices for two reasons: firstly, it has a considerably high surface availability for functionalization [126] and secondly has good affinity for a variety of anchoring functional groups like salicylate, carboxylate, phosphonate, sulfonate, pyridine and its derivatives, ketones and aldehydes, silanes, etc. [127, 128].

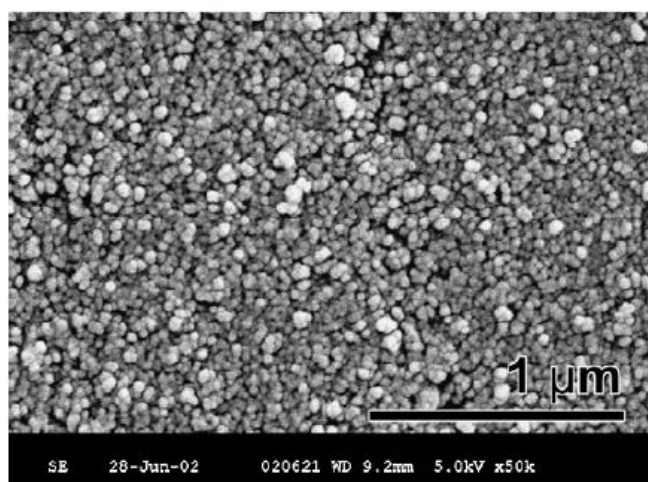


Figure 1.5 Scanning electron micrograph of nanostructured TiO₂ used for Nanochromics™ displays [129]

1.3.7 Electrochromic devices - principle and construction

Electrochromic devices (ECD) are one kind of electrochemical cells [126]. The basic structure of electrochromic devices embodies five superimposed layers in a laminated configuration on one substrate or positioned between two substrates. Figure 1.6 shows schematically the prototype of an EC device with its components [130]: i) two optical transparent electrodes (OTE) comprising in a glass slide coated with a conductive film such as indium tin oxide (ITO) or fluorine tin oxide (FTO); ii) an electrochromic layer (EC) which is usually an inorganic oxide (WO₃ widely used) but can be also an organic film; iii) an ion storage layer (or a secondary EC film) deposited on the opposite counter electrode; iv) an electrolyte solution (or gel) sandwiched between the two optical transparent layers. When a voltage is applied between the electrodes, the electrochromic film is reduced concomitantly with changing of its color. During the redox process, the electrolyte solution/gel ensures the charge transport between the two electrodes.

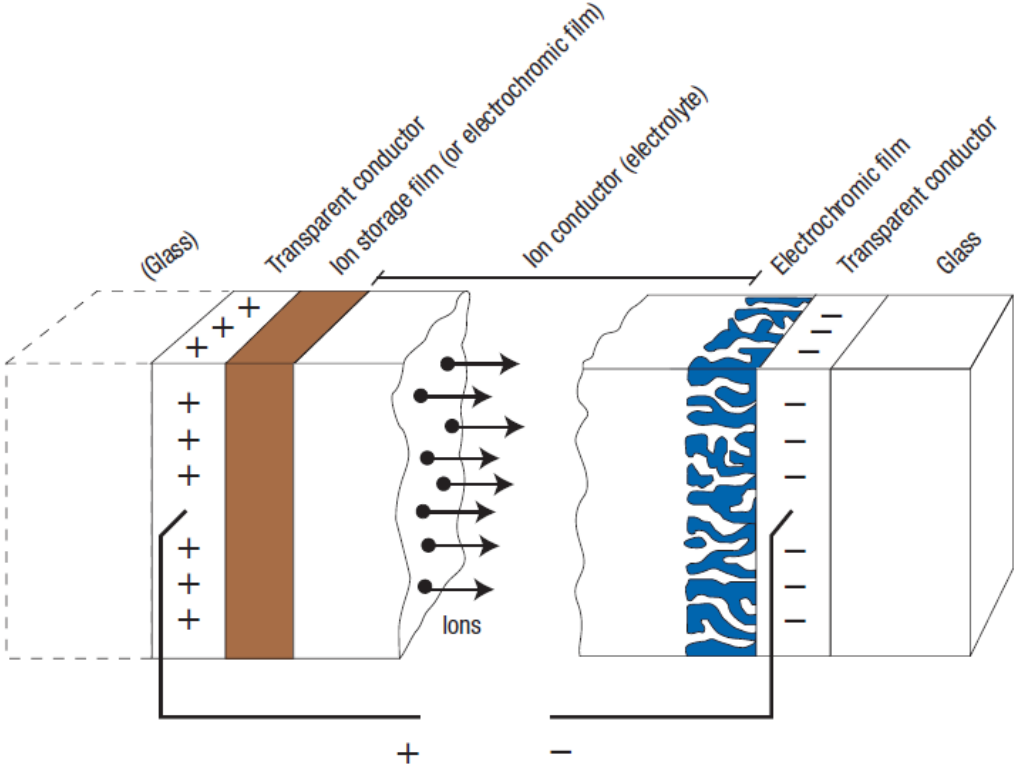


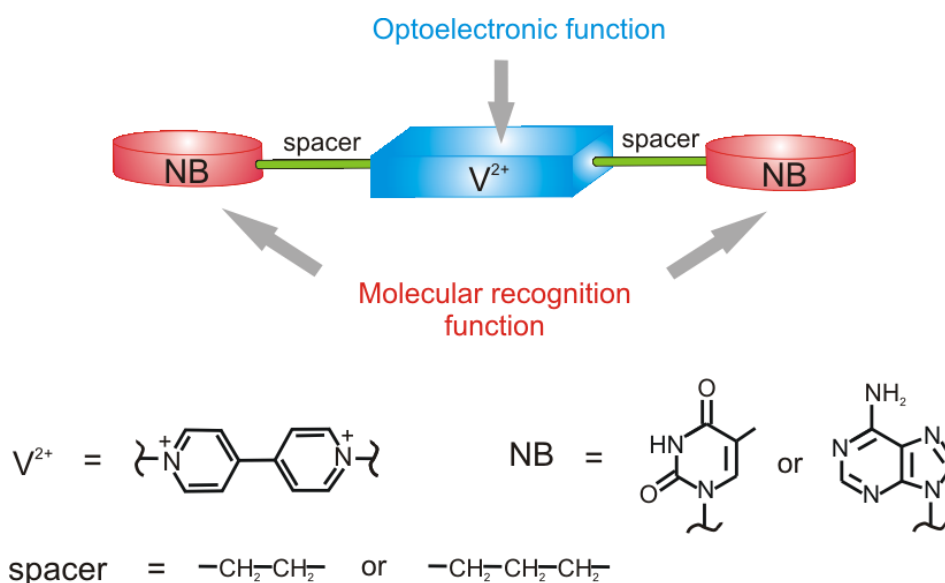
Figure 1.6 Electrochromic device design showing the movement of ions under an externally applied electric field [130]

CHAPTER 2

Viologen-Nucleobase Derivatives: Synthesis and Characterization

The design of small bifunctional molecules consisting of a redox core and capping groups with molecular recognition function is of great interest for creating new supramolecular materials with enhanced physico-chemical properties [3]. In respect with this, the current study aims to describe the synthesis and properties of a new class of self-assembling, electroactive molecules, consisting of a viologen core and nucleobase terminal groups. Such a combination is interesting since the 4,4'-bipyridinium, known as good acceptor used in electrochemical processes [11] may interact with electron rich systems like nucleobases [131] with consequences on the electronic properties.

The molecular design consists in a “triad” molecule *nucleobase-viologen-nucleobase* in which the functional tails are connected by flexible polymethylene spacers $-(\text{CH}_2)_n-$ (Scheme 2.1). There are two main features that may arise from the unique structural topology of such derivatives: (1) an intra/intermolecular donor-acceptor relationship between viologen core and nucleobases and, (2) a self-assembly ability due to the nucleobases properties to interact by hydrogen bonding.



Scheme 2.1 The molecular design of viologens capped by nucleobases

In this Chapter it will be discussed the synthetical pathway of a series of three new viologen-nucleobase derivatives based on a redox active 4,4'-bipyridinium core capped by thymine (**1/An⁻**), adenine (**2/An⁻**) or thymine/adenine (**3/An⁻**), respectively, and their corresponding precursors **P1/An⁻** and **P2/An⁻** (Scheme 2.2). A major attention has been paid to connect the nucleobases via a short alkyl spacer using the N(1) position of thymine or N(9) position of adenine as connection points. In this way, the molecular recognition function by hydrogen bonding of the nucleobases is preserved as in the case of natural DNA. Such a molecular design permits to exploit simultaneously both functionalities (redox and molecular recognition). The series of compounds **1/An⁻-3/An⁻** in which the nucleobase capping groups are varied systematically, allows to investigate how the attached nucleobase (i.e. purine or pyrimidine) will influence the overall properties, as well as their differences are. Despite the effort to obtain a fully systematic system, the use of the same connection spacer between nucleobase and viologen was not possible due to the limitations in the synthesis of alkylated nucleobase precursors containing the same alkyl group as will be discussed in the Section 2.1.1.

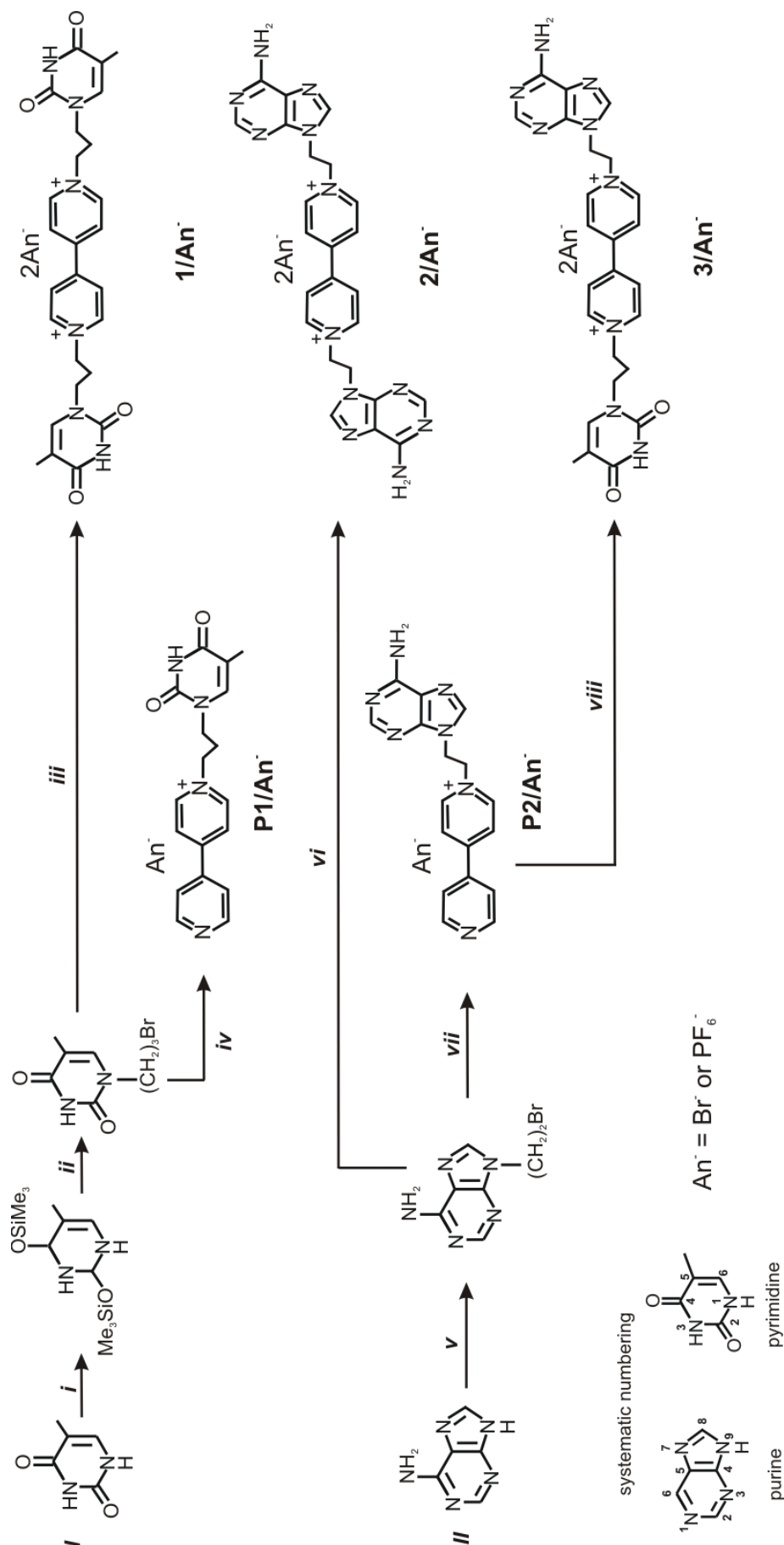
Electrochemical, spectroelectrochemical and optical properties of the new materials were investigated. The influence of the nucleobases capping groups on the redox and optical properties of the 4,4'-bipyridinium core was especially addressed.

The synthesized molecules containing a viologen core with redox properties, and biologically active capping groups nucleobase units are new and offer an unusual combination with several functionalities such fast electron transfer reactions, charge-transfer or low potential reduction for biological systems.

2.1 Synthesis of viologen-nucleobase derivatives

The strategy of the synthesis implies two main stages:

- i) Regioselective alkylation of nucleobases (i.e. thymine or adenine) with alkyl dihalides;
- ii) Coupling of the alkylated nucleobases at the nitrogen atoms of the 4,4'-bipyridine core.



Scheme 2.2 Synthetic pathway to prepare compounds **1-3/An⁻** and monosubstituted precursors **P1/An⁻** and **P2/An⁻**: (i) HMDS and Me₃SiCl (cat.), 2lh, reflux, 95%, (ii) 3 equiv. of 1,3-dibromopropane, DMF, 24h, 80°C, 34%, (iii) 4,4'-bipyridine, DMF, 4 days, 80°C, 76% (**1/Br⁻**); (iv) 4,4'-bipyridine, nitrobenzene, 48 h, 110°C, 83% (**P1/Br⁻**); (v) 1,2-dibromoethane, K₂CO₃ in DMF, 48 h, r.t., 61%, (vi) precursor **P2/Br⁻**, H₂O, 17 days, 80°C, 85% (**2/Br⁻**); (vii) 4,4'-bipyridine, nitrobenzene, 48 h, 110°C, 92%; (viii) **P2** as PF₆⁻ salt with two-fold excess of 1-(3-bromopropyl)thymine, DMF, 70 h, 80°C, 45% (**3/PF₆⁻**)

2.1.1 Nucleobases alkylation

Two alkylated nucleobase derivatives, 1-(3-bromopropyl)thymine [132, 133] and 9-(2-bromoethyl)adenine [134], were synthesized according to the protocols adopted from previously published literature.

Difficulties arose during alkylation of thymine because of a lack in regioselectivity. Thymine can be simultaneously alkylated at the N(1), N(3), O(2) and O(4) positions. Moreover, Nawrot et al. [42] reported the formation of a variety of internal cyclization products or covalently-bridged thymine dimers for the reaction of thymine with dialkyl halides. The regioselectivity problem was solved by protection of carbonyl functional groups according to the procedure reported by Vorbrüggen [133]. The thymine was preliminary converted to bis-(O-silylated) analogue derivative in reaction with HMDS (Scheme 2.2, step i) and subsequently alkylated with 1,3-dibromopropane to obtain 1-(3-bromopropyl)thymine in 34% overall yield (Scheme 2.2, step ii). The synthesis of analogue derivative 1-(2-bromoethyl)thymine using the above mentioned procedure gives the desired product in very low yield (< 10%). For this reason the preparation of ethylene-spacer containing thymine compounds was no longer followed.

The alkylation of adenine at the N(9) position was performed directly with 1,2-dibromoethane in DMF to afford 9-(2-bromoethyl)adenine as the main product in 62% yield without any protection of the purine ring (Scheme 2.2, step v). The alkylation with 1,3-dibromopropane in the similar conditions gives predominantly an cyclic ionic derivative as reported by Schall [132], hence the preparation of propyl-spacer adenine compounds was abandoned.

2.1.2 Coupling of the alkylated nucleobases to 4,4'-bipyridinium unit

The monosubstituted precursors **P1/An⁻**, **P2/An⁻** and viologen-nucleobase derivatives **1-3/An⁻** were synthesized by means of the Menshutkin reaction of 9-(2-bromoethyl)adenine or 1-(3-bromopropyl)thymine with 4,4'-bipyridine.

The **P1/Br⁻** and **P2/Br⁻** derivatives were obtained in 68% and 92% yield respectively, by reacting 1-(3-bromopropyl)thymine and 9-(2-bromoethyl)adenine with two-fold excess of 4,4'-bipyridine in nitrobenzene (Scheme 2.2, step iv and vii). The ¹H-NMR spectra of both the compounds are depicted in Figure 2.1, showing the assignments of signals, and structural elements.

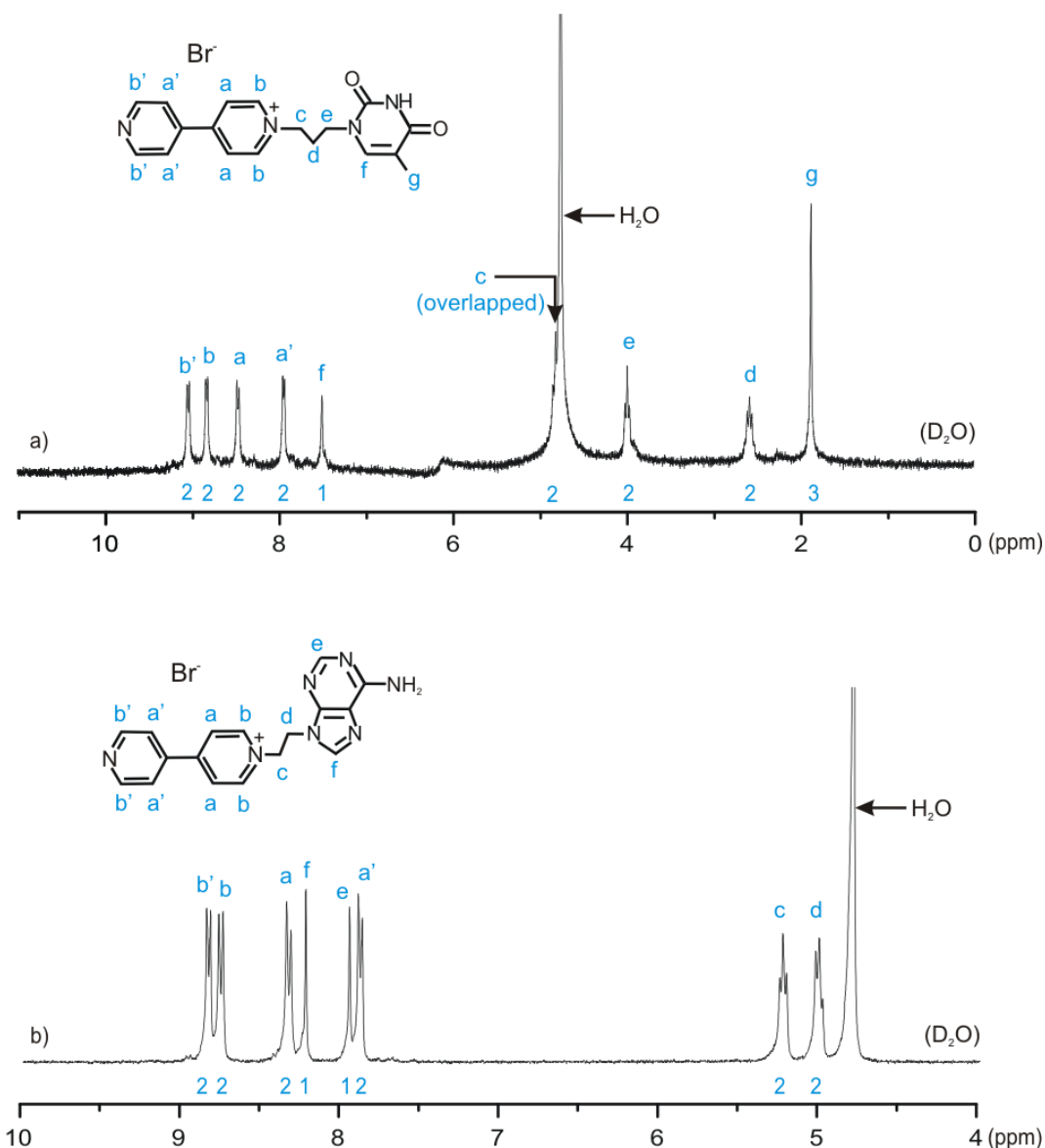


Figure 2.1 $^1\text{H-NMR}$ spectra of P1/Br^- (a) and P2/Br^- (b)

The kinetic of synthesis reaction of P1/Br^- and P2/Br^- was investigated. In Figure 2.2 is depicted the plot of conversion rate (wt%) of the alkylation substrates 1-(3-bromopropyl)thymine and 9-(2-bromoethyl)adenine over the reaction time. It can be observed that the monoalkylation of 4,4'-bipyridine occurred faster and in higher yield in the presence of 1-(3-bromopropyl)thymine compared with 9-(2-bromoethyl)adenine under the same reaction conditions.

P1/An^- and P2/An^- were further used as precursors in the synthesis of disubstituted viologen-nucleobase derivatives 2/An^- and 3/An^- , according with the Scheme 2.2, or as dendrons in the divergent synthesis of viologen-based dendrimers capping nucleobase units at the periphery [4].

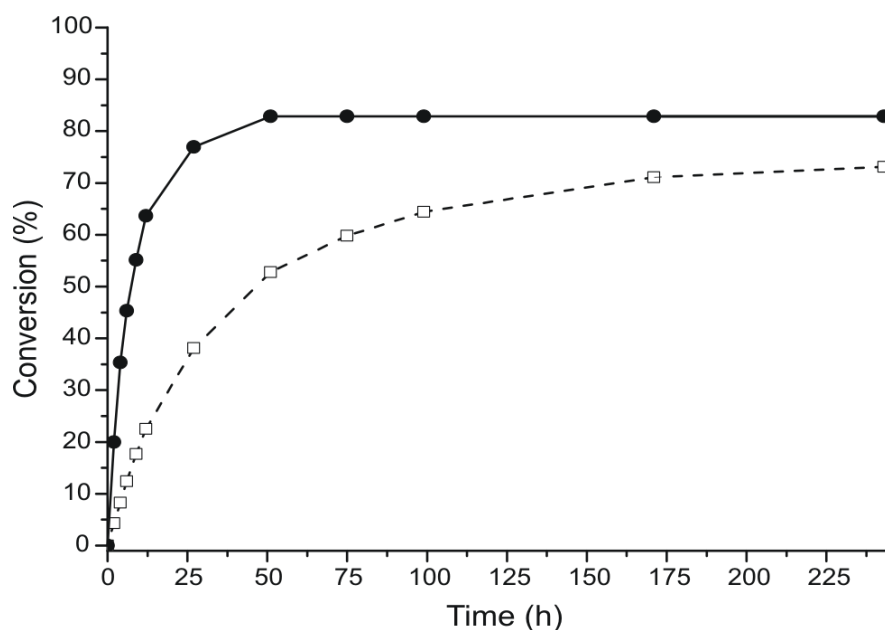
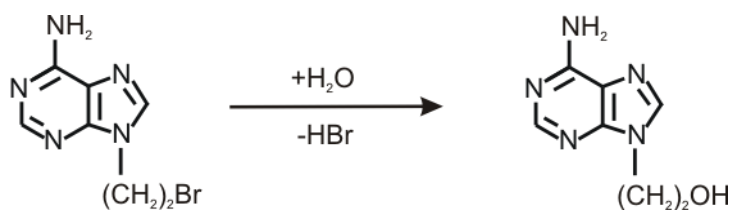


Figure 2.2 Reaction kinetic for **P1/Br⁻** (continues line) and **P2/Br⁻** (dashed line) in nitrobenzene at 110°C

The symmetrical N,N'-disubstituted viologen-thymine derivative **1/Br⁻** was prepared in 76% yield in a one pot dialkylation of 4,4'-bipyridine with 4.6-fold excess of 1-(3-bromopropyl)thymine in DMF (Scheme 2.2, reaction step iii).

The one pot synthesis of compound **2/Br⁻**, which involves dialkylation of 4,4'-bipyridine with 9-(2-bromoethyl)adenine, failed in solvents such as DMF or acetonitrile. The low solubility of the adenine substrate corroborated with the formation of insoluble monobromide salt during monoalkylation of 4,4'-bipyridine caused a partial precipitation of the monosubstituted salt before the second quaternization was completed. The best yield of 85% and complete conversion into disubstituted product **2/Br⁻** was achieved in water, using the precursor **P2/Br⁻** as nucleophilic substrate, at 80°C, and 17 days of reaction time (Scheme 2.2, step vi). In this case, the rate of the reaction was slow since the nucleophile was sterically shielded due to the hydrogen bonding with the protic solvent. Supplementary addition of 9-(2-bromoethyl)adenine was necessary during the reaction because the alkylation substrate was partially transformed in 9-(2-hydroxyethyl)adenine in the course of a side reaction with the solvent (Scheme 2.3). *In situ* ¹H-NMR of the reaction mixture showed the evolution of two new triplets (4.02 ppm and 4.41 ppm) and two new singlets (8.30 ppm and 8.33 ppm) typically to the formation of 9-(2-hydroxyethyl)adenine [135]. The occurrence of the hydrolysis was also confirmed by the gradually decreasing of the pH over the reaction time as a result of hydrobromic acid formation.



Scheme 2.3 Conversion of 9-(2-bromoethyl)adenine into 9-(2-hydroxyethyl)adenine in the presence of water

Generally, the synthesis of asymmetric 1,1'-disubstituted 4,4'-bipyridinium derivatives requires two steps [11]. In a first step, the solvent used in Menshutkin reaction should be sufficiently low-polar to allow the precipitation of the monosubstituted product before the formation of the symmetrical 1,1'-disubstituted 4,4'-bipyridinium derivative. In the second reaction step, a solvent of higher polarity is required to facilitate the dissolution of the monosubstituted 4,4'-bipyridinium derivative and allows for the alkylation reaction in the presence of the second alkylation substrate. Thus, compound **3/PF₆⁻** was prepared following the above mentioned synthesis strategy. Starting from 4,4'-bipyridine, the monoalkylation reaction was performed first with 9-(2-bromoethyl)adenine in nitrobenzene to yield compound **P2/Br⁻** (Scheme 2.2, step vii). Subsequently, **P2/Br⁻** was converted quantitatively by metathesis reaction in the analogue derivative **P2/PF₆⁻**. In the second step, the compound **P2** as PF₆⁻ salt was treated with 3 fold excess of 1-(3-bromopropyl)thymine in DMF to yield the corresponding asymmetrically 1,1'-disubstituted 4,4'-bipyridinium compound **3/PF₆⁻** in **45%** yield after purification (Scheme 2.2, step viii).

The full characterization of viologen-nucleobase derivatives **1/An⁻**-**3/An⁻** and monoalkylated precursors (**P1/An⁻** and **P2/An⁻**) were confirmed by ¹H-, ¹³C-NMR and elemental analysis (cf. Chapter 6). The **1/Br⁻**-**3/Br⁻** salts are slightly hygroscopic compared with analogues derivatives **1/PF₆⁻**-**3/PF₆⁻**. Figure 2.3 depicts the ¹H-NMR spectra of the compounds **1/Br⁻** (Figure 2.3a), **2/Br⁻** (Figure 2.3b) and **3/PF₆⁻** (Figure 2.3c) together with the respective structure formulas. The spectra confirm the molecular structures of the substances, since each signal could be assigned to the corresponding structure elements. The same holds true with the ¹³C-NMR spectra (not shown here), cf. Chapter 6. Their purity estimated from the ¹H-NMR spectra was around 95%, however elemental analysis provided the purity of viologen-nucleobase derivatives **1/PF₆⁻**-**3/PF₆⁻** to exceed 98%.

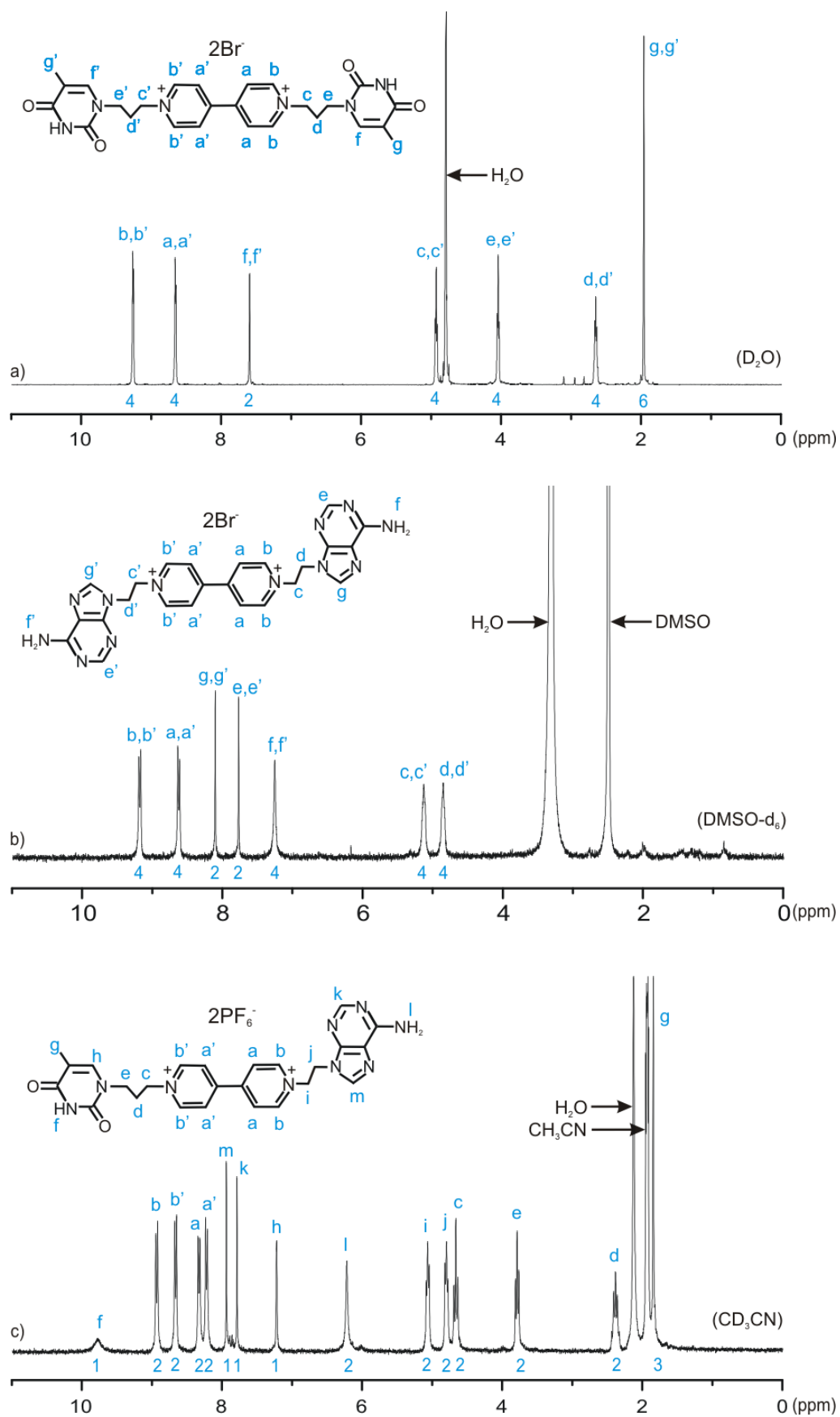


Figure 2.3 $^1\text{H-NMR}$ spectra of $1/\text{Br}^-$ (a), $2/\text{Br}^-$ (b) and $3/\text{PF}_6^-$ (c)

2.2 Study of physico-chemical properties

2.2.1 Optical and spectroelectrochemical properties

The optical properties of dicationic derivatives **1/An²⁺-3/An²⁺** were investigated by means of UV-Vis spectroscopy, as bromide salts in aqueous solution or as PF₆⁻ salts in DMF. The UV-Vis measurements in DMF were performed with, or without addition of tetrabutylammonium hexafluorophosphate (TBAPF₆), to investigate the influence of ionic strength on the optical characteristics. All UV-Vis measurements were performed at 21°C.

Figure 2.4 shows the normalized UV spectra, $A_{\text{norm}[0,1]} = (A - A_{\text{min}}) / (A_{\text{max}} - A_{\text{min}})$, of compounds **1/Br⁻-3/Br⁻** in aqueous solution. In their dicationic state the compounds **1/Br⁻-3/Br⁻** absorb light in UV range due to the overlapping electronic transitions of the chromophoric units, i.e. thymine, adenine, and 4,4'-bipyridinium. The wavelength of the maximum absorption shifts slightly to the red region for compounds capped by thymine ($\lambda_{\text{max}}(\mathbf{1/Br}^-) = 268 \text{ nm}$; $\lambda_{\text{max}}(\mathbf{2/Br}^-) = 260 \text{ nm}$; $\lambda_{\text{max}}(\mathbf{3/Br}^-) = 263 \text{ nm}$).

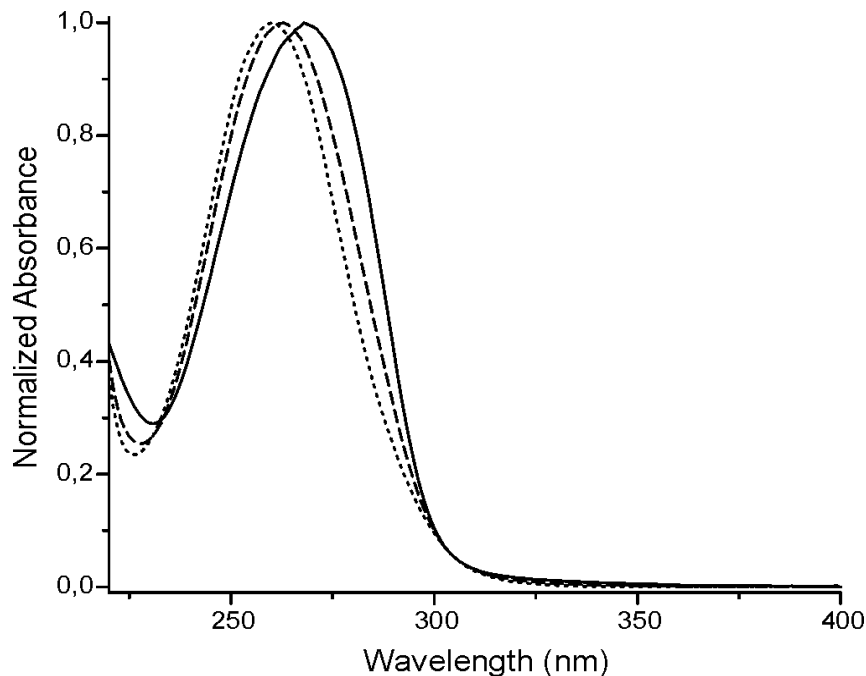


Figure 2.4 UV spectra of compounds **1/Br⁻** (continues line), **2/Br⁻** (dotted line), and **3/Br⁻** (dashed line) ($5 \cdot 10^{-5} \text{ mol} \cdot \text{l}^{-1}$) in aqueous solution

In contrast to UV-Vis measurement of $1/\text{Br}^-$ - $3/\text{Br}^-$ in aqueous solution, the analogues compounds $1/\text{PF}_6^-$ - $3/\text{PF}_6^-$ in DMF exhibited a second absorption band in the visual range of the spectra with $\lambda_{\text{max}2}$ at about 400 nm (cf. Figure 2.5).

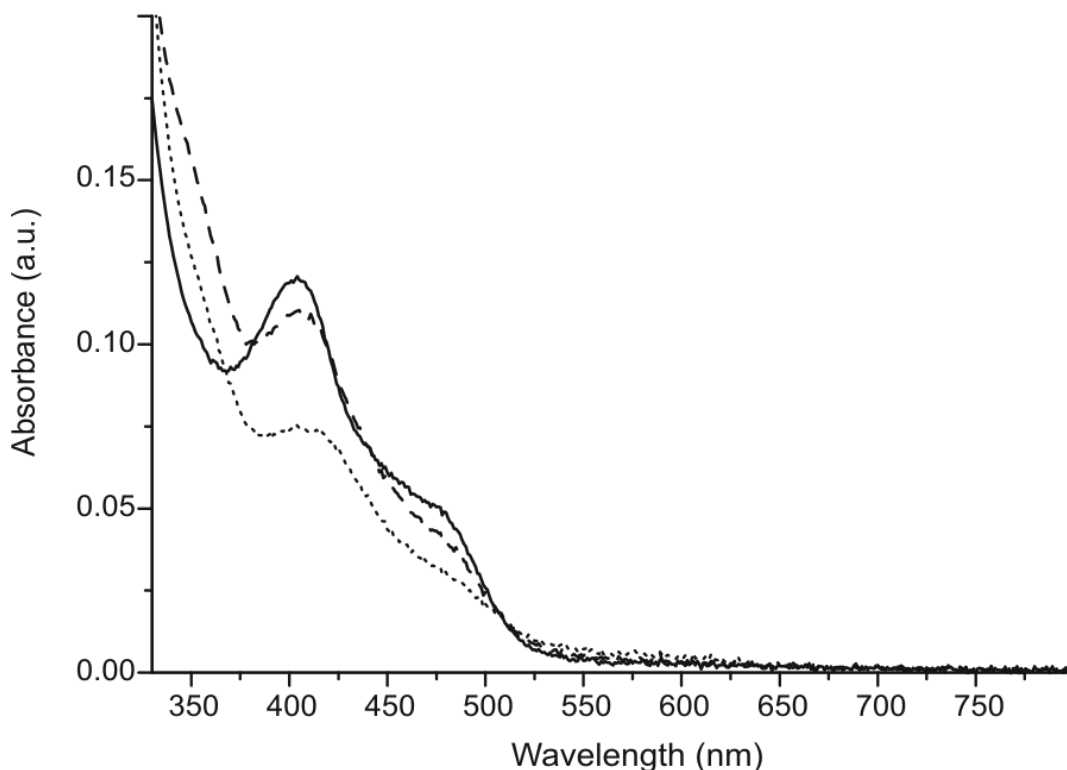


Figure 2.5 CT absorption band of compounds $1/\text{PF}_6^-$ (continues line) $2/\text{PF}_6^-$ (dashed line) and $3/\text{PF}_6^-$ (dotted line); concentration 0.1 mM in DMF

Since the analogue 1,1'-dibenzyl-4,4'-bipyridinium derivative (BV^{2+}) shows only one UV band at 260 nm [11], the second absorption band of compounds $1/\text{PF}_6^-$ - $3/\text{PF}_6^-$ observed in DMF must be caused by the presence of the nucleobase units. Since pure thymine and adenine do not absorb light around 400-500 nm [136] it must be concluded the presence of a charge transfer interaction (CT) of the thymine and adenine moieties with 4,4'-bipyridinium unit. The 4,4'-bipyridinium compounds in dicationic state (V^{2+}) are known as electron deficient derivatives [11], capable to interact as charge acceptor (A) in a CT system with electron rich molecules such crown ethers [137], indoles [138] or naphtholes derivatives [139, 140]. Moreover, the nucleobases are known as aromatic electron rich systems capable to interact as charge donors (D) with electron deficient derivatives [131]. The CT band is characterized by a broad shape and a low extinction coefficient which is typical for the CT interaction of 4,4'-bipyridinium derivatives [141]. The possible ion pair charge-transfer (IPCT) between viologen core and the counter anion can be excluded since the PF_6^- (used as counter anion in this study) is

known as a non-coordinative anion [142]. Noteworthy, the extinction coefficient of CT band (ϵ_{CT}) increases in the order $2 < 3 < 1$ (cf. Table 2.1). This trend suggests a higher extent of CT complexation in the case of viologen derivatives capped by thymine.

With the goal to elucidate the type of charge transfer interaction (intra- or intermolecular) an UV-Vis study was performed in which the extinction coefficient at 404 nm of the CT band (ϵ_{CT}) was monitored in the concentration range from $2.5 \cdot 10^{-6}$ to $5 \cdot 10^{-4}$ mol/l). The experiment was performed in DMF at 21°C. The molar extinction coefficient of the CT band decreases with the increase of concentration as can be observed in Figure 2.6a when no additional salt was added. This trend shows that the CT interaction between 4,4'-bipyridinium unit and the nucleobases is suppressed by the increase of intrinsic ionic strength. This behavior is in accordance with the studies of Monk which investigated the influence of ionic strength on the CT interactions of viologens with a variety of neutral or anionic donors [141].

In a second series of experiments the ionic strength was kept constant ($I=0.1$ mol/l) by adding inert salt TBAPF₆ and the extinction coefficient of the CT band was monitored

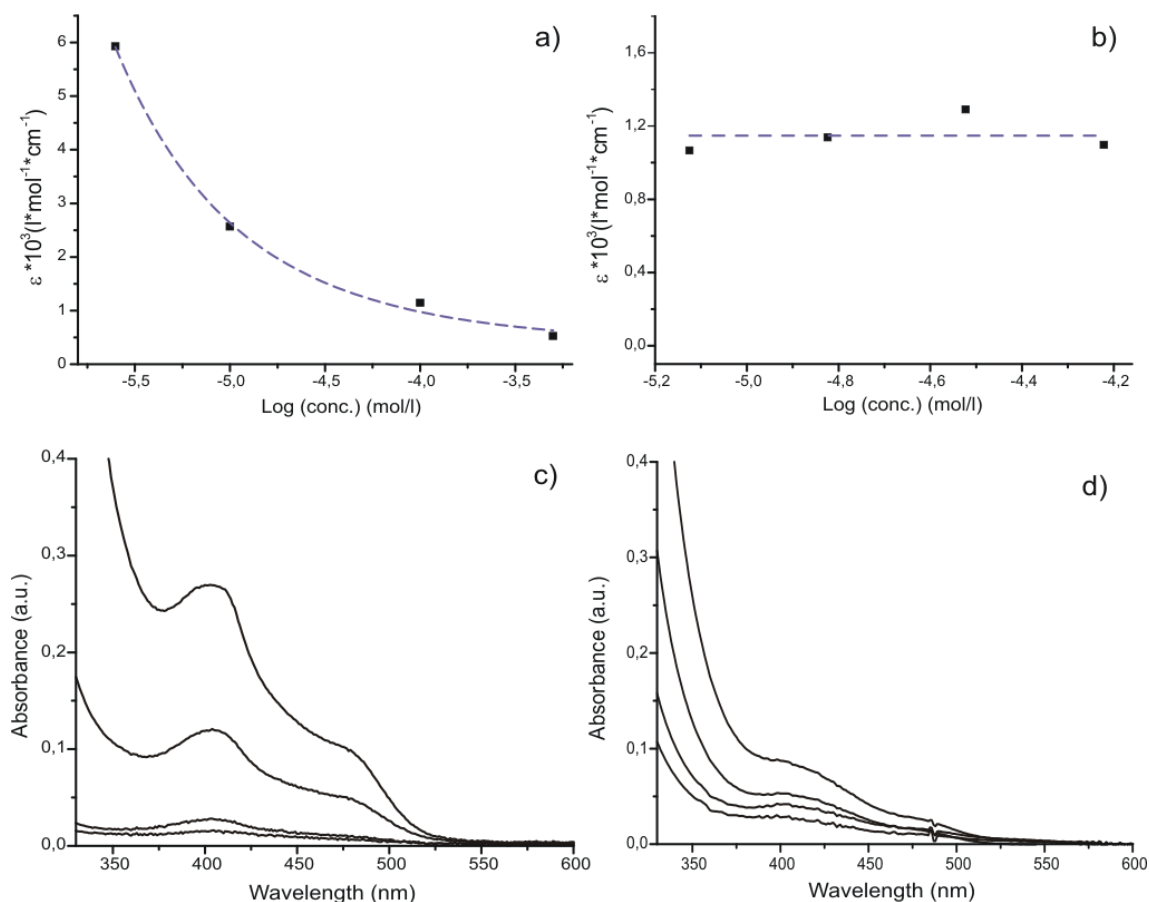


Figure 2.6 Concentration dependency of molar extinction coefficient at 404 nm of compound **1/PF₆⁻**: a) in the absence or, b) in the presence of 0.1 M TBAPF₆ and the corresponding CT bands (c and d)

in the concentration range from $7.5 \cdot 10^{-6}$ to $6 \cdot 10^{-5}$ mol/l. In this case no variation of ϵ_{CT} over the concentration was observed (Figure 2.6b). This result demonstrates that the charge transfer interaction between nucleobase and viologen unit occurred intramolecular. In order to undergo intramolecular CT, the nucleobase moieties have to fold in a parallel face-to-face conformation with the viologen unit. In this particular case, the difference in CT association constant observed between the compounds capped by thymine and those capped by adenine can be explained by the better flexibility of the propylene spacer compared to ethylene which permits to the donor moiety to fold and stack with the acceptor core in a co-facial manner. However, the intensity of the CT absorption spectrum is also dependent on the donor nature (i.e. purine or pyrimidine) and their auxochromic groups with mesomeric effects +M or -M. For this reason, the exact discrimination between the effect of the spacer length and the nature of nucleobase is difficult in this system.

Among the examples discussed in literature [143-145] this is the first intramolecular CT system between viologen and nucleobases. Figure 2.7 represents a computed molecular model of intramolecular CT interaction in viologen-nucleobase derivatives.

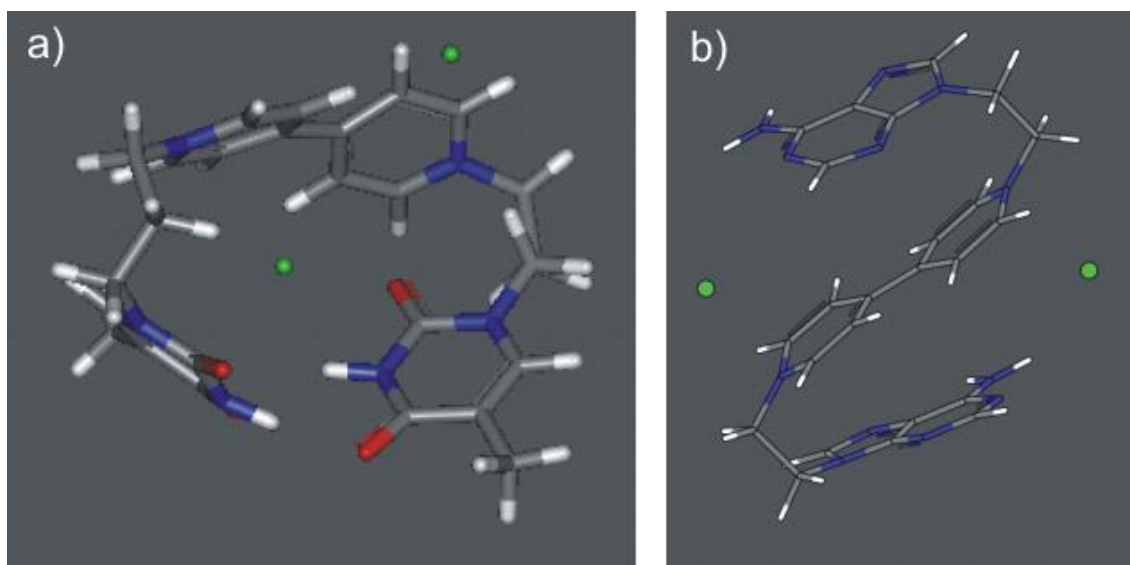


Figure 2.7 Computed models of intramolecular CT interaction between viologen and nucleobases in compound **1/Cl⁻** (a) and **2/Cl⁻** (b), respectively

The optical characterization of viologen-nucleobase derivatives **1/PF₆⁻**-**3/PF₆⁻** in their reduced state was performed at 21 °C using a three-electrode electrochemical cell, Ag/AgCl as reference electrode, and NaClO₄/DMF as supporting electrolyte.

Figure 2.8a shows a series of UV-Vis spectra obtained from $1/\text{PF}_6^-$ on stepwise increasing of the applied potential from 0 to -600 mV. While the absorption at 260 nm decreases, both absorption bands at $\lambda_{\text{max}3}=401$ nm and $\lambda_{\text{max}4}=607$ nm become stronger.

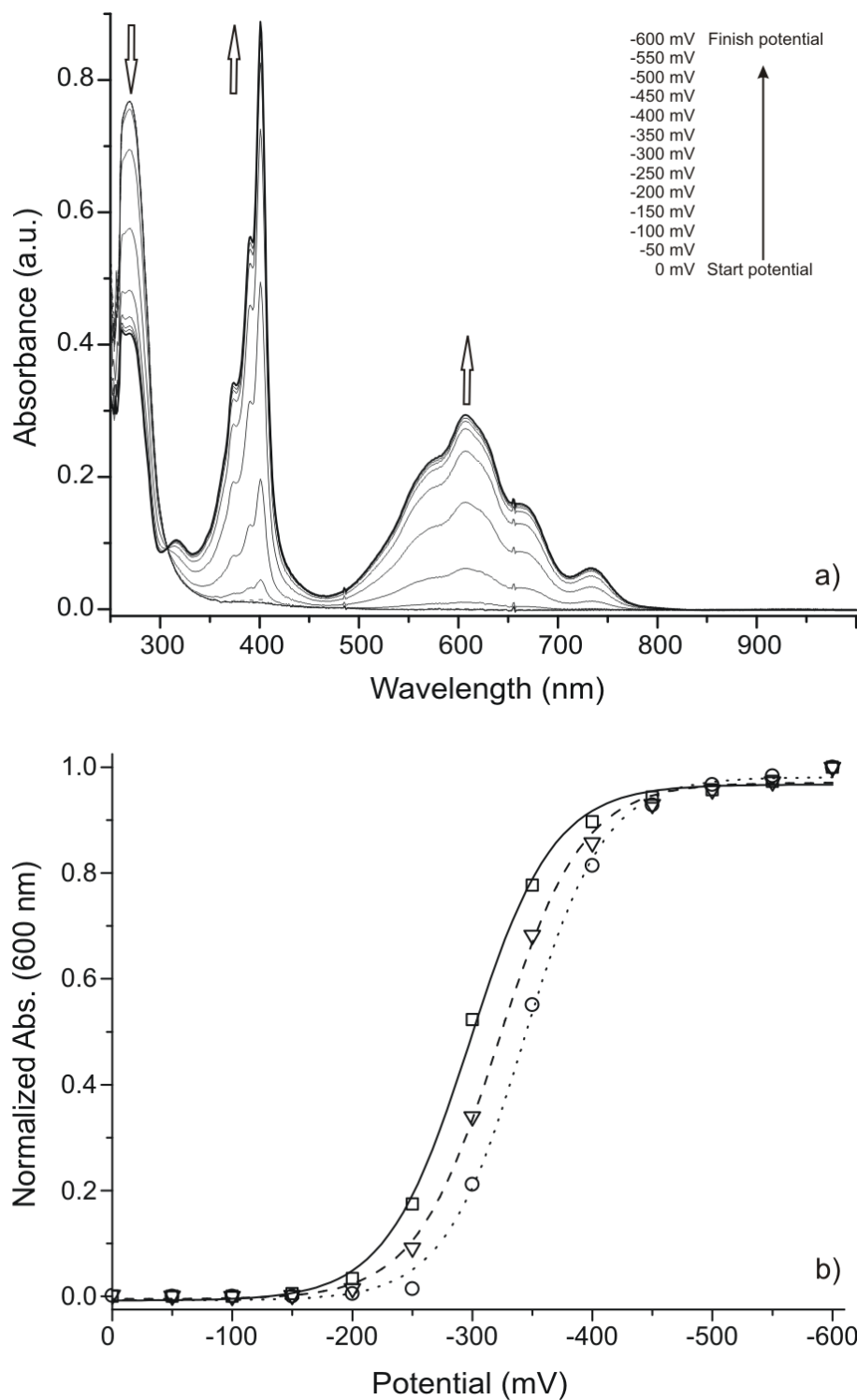


Figure 2.8 (a) UV-VIS spectra of compound $1/\text{PF}_6^-$ (0.1 mmol/l) in 0.1 M $\text{NaClO}_4/\text{DMF}$ electrolyte during electrochemical titration. The arrows indicate the evolution of the spectra from 0 to -600 mV. (b) Plot of normalized absorbance at 600 nm for compounds $1/\text{PF}_6^-$ - $3/\text{PF}_6^-$ versus potential

In the reduced state ($V^{+\bullet}$), compounds $1/PF_6^-$ - $3/PF_6^-$ show the typical absorption band of 1,1'-dialkylated 4,4'-bipyridinium unconjugated derivatives with maximum wavelengths at 401 nm, and 605 nm ($\lambda_{\max 3}$ and $\lambda_{\max 4}$ in Table 2.1) respectively corresponding to blue colour. By monitoring the absorption at 600 nm as a function of the applied potential, the corresponding sigmoidal curves from Figure 2.8b were obtained. The potential value for which half of the V^{2+} species are reduced to the blue radical-cation species ($V^{+\bullet}$) (inflection point of the sigmoidal curves) corresponds to the half-wave potential of the first reduction step ($E_{1/2}$).

The optical characteristics derived from the corresponding UV-Vis spectra of $1/PF_6^-$ - $3/An^-$ in dicationic state (V^{2+}) and radical-cationic state ($V^{+\bullet}$) respectively, are summarized in Table 2.1

Table 2.1 UV-Vis absorption wavelengths and molar extinction coefficients of $1/An^-$ - $3/An^-$ ^[a]

Compound	Oxidized state (V^{2+})		Reduced state ($V^{+\bullet}$)	
	$\lambda_{\max 1}(\epsilon)^{[b]}$	$\lambda_{\max 2}(\epsilon)^{[c]}$	$\lambda_{\max 3}(\epsilon)^{[d]}$	$\lambda_{\max 4}(\epsilon)^{[d]}$
1/An⁻	268 (46.1)	404 (1.21)	401 (44.40)	607(14.69)
2/An⁻	260 (45.5)	412 (0.74)	401 (37.67)	605 (13.43)
3/An⁻	263(44.4)	405 (1.1)	401 (38.50)	606 (13.08)

^[a]Wavelength of maximum absorption (λ_{\max}) expressed in nm and extinction coefficient (ϵ) in parenthesis expressed as $10^3 \cdot l \cdot mol^{-1} \cdot cm^{-1}$; ^[b]Determined for $1/Br^-$ - $3/Br^-$ (0.05 mM) in H_2O ; ^[c]Determined for $1/PF_6^-$ - $3/PF_6^-$ (0.1 mM) in DMF; ^[d]Determined for $1/PF_6^-$ - $3/PF_6^-$ (0.1 mM) electrolyte solution $NaClO_4/DMF$ (0.1 M).

2.2.2 Electrochemical properties

Compounds $1/PF_6^-$ - $3/PF_6^-$ (conc. = 0.5 mM) were characterized by cyclic voltammetry in 0.1 M $NaClO_4/DMF$ electrolyte at the surface of a glassy carbon electrode and using $Ag/AgCl$ as reference electrode. All electrochemical measurements were performed at 21°C. The corresponding cyclic voltammograms of compounds $1/PF_6^-$ - $3/PF_6^-$ (cf. Figure 2.9a) represent the typical reduction of the 4,4'-bipyridinium units from the dication state (V^{2+}) to radical cation ($V^{+\bullet}$) and further to the neutral species (V^0) [14]. The reduction mechanism implies two subsequent one-electron transfer steps. The ratio of the cathodic and anodic current peaks (I_{pc}/I_{pa}) was calculated after baseline correction of the corresponding cyclic voltammograms and satisfies the condition for reversibility

($I_{pc}/I_{pa}=1$). The first reduction step of compounds $1/PF_6^-$ - $3/PF_6^-$ is a diffusion-controlled process in the range of scan rate from 0.1 to $1 \text{ V}\cdot\text{s}^{-1}$ as it can be observed from the linear plot of current (I_{pc1}) versus the square root of the scan rate (Figure 2.9b).

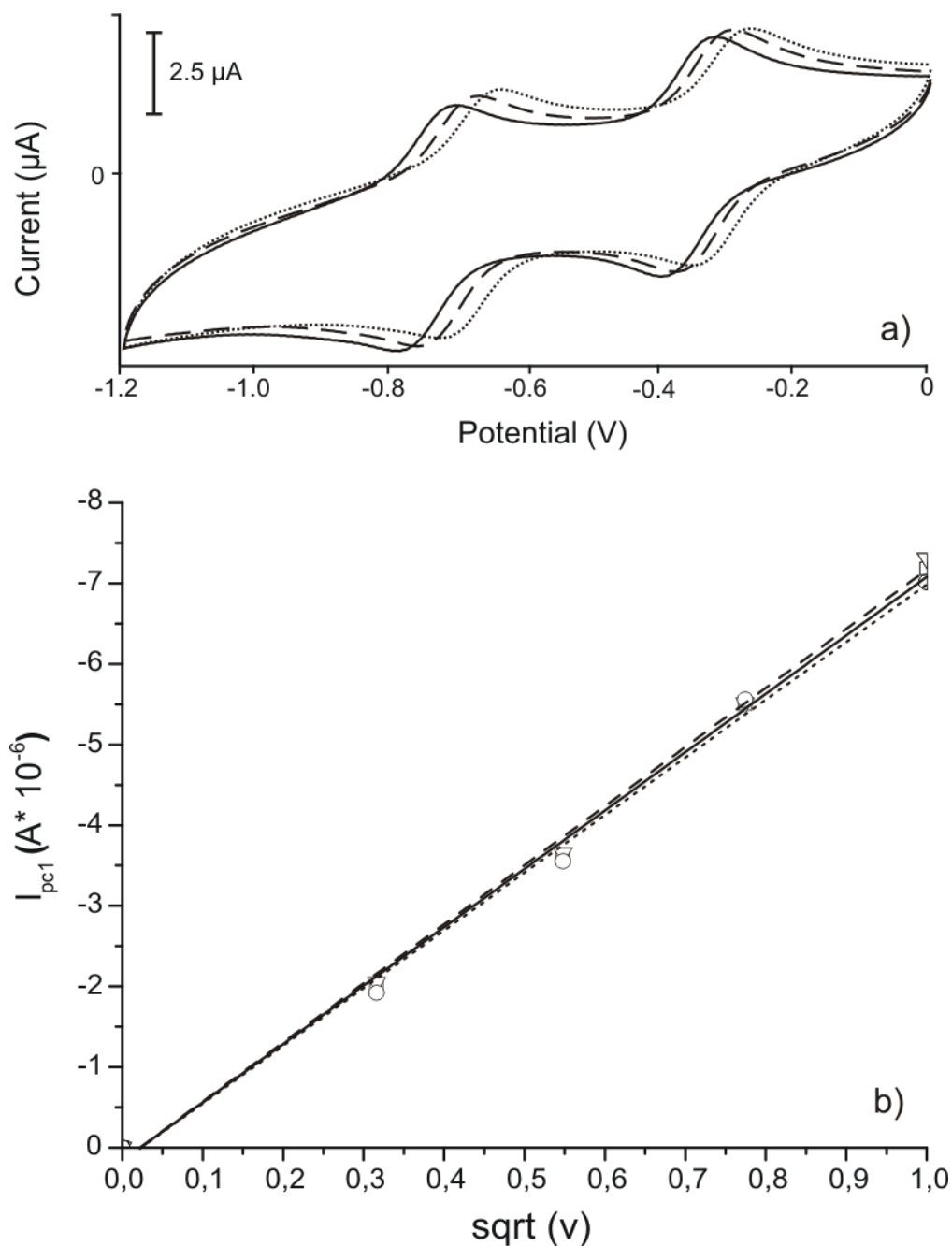


Figure 2.9 a) Cyclic voltammograms of compound $1/PF_6^-$ (continues line), $2/PF_6^-$ (dotted line) and $3/PF_6^-$ (dashed line) at $0.1 \text{ V}\cdot\text{s}^{-1}$ scan rate versus Ag/AgCl (3M KCl) in $0.1 \text{ M NaClO}_4/\text{DMF}$; b) Linear regression of peak current (I_{pc1}) versus the square root of the scan rate

The diffusion coefficients of the dicationic species in DMF (cf. Table 2.2) were calculated from the voltammetric data using a derivative form of Randles–Sevcik equation (2.1):

$$D = [B / (2.69 \cdot 10^5 \cdot z^{3/2} \cdot A \cdot c)]^2 \quad (2.1)$$

where D is the diffusion coefficient, B is the slope of the linear regression of the peak current (I_{pc1}) versus the square root of the scan rate, A is the area of the surface of the electrode (0.031 cm^2), z is the number of electron transferred ($z=1$) and c is the concentration of the analyte in electrolyte solution ($5 \cdot 10^{-7} \text{ mol} \cdot \text{cm}^{-3}$). The diffusion coefficients have similar values for all three compounds which suggest no self-association of the dicationic viologen-nucleobase species in a polar solvent such as DMF.

The electrochemical parameters of the compounds $1/\text{PF}_6^-$, $2/\text{PF}_6^-$ and $3/\text{PF}_6^-$ are presented in Table 2.2. The formal potential values E^0_1 and E^0_2 , corresponding to each electron transfer step, are more negative (approx. 60 mV) in the case of compound $1/\text{PF}_6^-$ compared with compound $2/\text{PF}_6^-$, while the formal potential values E^0_1 and E^0_2 of compound $3/\text{PF}_6^-$ are situated between the values recorded for the compounds $1/\text{PF}_6^-$ and $2/\text{PF}_6^-$.

Table 2.2 Electrochemical parameters for the compounds $1/\text{PF}_6^-$ - $3/\text{PF}_6^-$ from cyclic voltammetry^[a]

Compound	D	ν	$E_{pc1}^{[b]}$	E_{pa1}	$E^0_1^{[c]}$	$\Delta E_1^{[d]}$	E_{pc2}	E_{pa2}	E^0_2	ΔE_2
$1/\text{PF}_6^-$	$3.3 \cdot 10^{-6}$	0.1	-391	-330	-360	61	-781	-718	-750	63
		0.3	-393	-325	-359	68	-784	-715	-750	69
		0.6	-393	-320	-357	73	-789	-720	-755	69
		1	-393	-317	-355	76	-791	-715	-753	76
$2/\text{PF}_6^-$	$3.4 \cdot 10^{-6}$	0.1	-342	-273	-308	69	-715	-649	-682	66
		0.3	-342	-269	-306	73	-723	-649	-686	74
		0.6	-344	-269	-307	75	-725	-649	-687	76
		1	-342	-266	-304	76	-732	-659	-696	73
$3/\text{PF}_6^-$	$3.1 \cdot 10^{-6}$	0.1	-366	-298	-332	68	-752	-681	-717	71
		0.3	-366	-298	-332	68	-757	-684	-721	73
		0.6	-369	-295	-332	74	-764	-686	-725	78
		1	-366	-288	-344	78	-771	-684	-727	87

^[a]All potential parameters are expressed in mV versus Ag/AgCl, the diffusion coefficients (D) in $\text{cm}^2 \cdot \text{s}^{-1}$ and the scan rate (ν) in $\text{V} \cdot \text{s}^{-1}$; ^[b] E_{pc1} , E_{pa1} , E_{pc2} and E_{pa2} represent the corresponding half-wave potentials; ^[c] E^0_1 and E^0_2 represent the calculated formal potentials; ^[d] ΔE_1 and ΔE_2 represent the separation potential.

Compounds **1/PF₆⁻-3/PF₆⁻** were reduced at much more positive potential compared to well-known analogue 1,1'-dimethyl-4,4'-bipyridinium ($E^0_1 = -380$ mV versus Ag/AgCl) measured in the similar experimental conditions [146]. The low reduction potentials observed in the case of derivatives **1/PF₆⁻-3/PF₆⁻** could be attributed to the electronic effects of the substituents 9-(2-ethylene)adenine and/or 1-(3-propylene)thymine attached covalently to the nitrogen atoms. However, the observed potential shift cannot be explained by the intermolecular association, because Figure 2.9b demonstrates equal diffusion coefficients, i.e. equal hydrodynamic radii with compounds **1/PF₆⁻-3/PF₆⁻** in DMF.

2.2.3 Chemical reduction

The chemical reduction of viologens in the presence of strong reduction agents such as sodium dithionite ($E = -0.66$ V) [25] are of special interest since the reduced species can be used as redox indicators in photosynthetic studies [147, 148], as electron transfer catalysts (ETC) in the reduction of aldehydes and ketones [24] or for hydrogen generation [149].

The chemical reduction was performed by adding 0.05 ml aqueous solution of Na₂S₂O₄ (10 mM) in 2 mL Tris-H₂SO₄ buffer (pH 8.5) solution of compounds **1/Br⁻-3/Br⁻** (conc. = 0.5 mM) under nitrogen atmosphere. The reduction reaction was monitored *in situ* by UV-Vis spectroscopy. The initial spectra of compounds **1/Br⁻**, **2/Br⁻** and **3/Br⁻** in the oxidized state contain an absorption band in UV range attributed to the nucleobases adenine, thymine and dicationic 4,4'-bipyridinium moieties as previously discussed in Section 2.2.1. Upon addition of Na₂S₂O₄, the color of the solution of all three compounds changes to blue with two absorption maxima at about 401 nm and 605 nm (Figure 2.10), typical for the formation of the radical cation state (V^{•+}) [11]. The absorption at 315 nm ($\epsilon = 8043$ L·mol⁻¹·cm⁻¹) is attributed to the dithionite anion present in the solution [150]. The inset in Figure 2.10 represents the absorption band of pure Na₂S₂O₄ in Tris-H₂SO₄ buffer at pH = 8.5. Upon air contact, the reduced solutions of 4,4'-bipyridinium derivatives **1/Br⁻-3/Br⁻** lost their blue color and become colorless. The absorption band in the visible range attributed to the radical cation species gradually decreased and concomitantly, the absorption at 260 nm increased implying that the V^{•+} species were oxidized back to V²⁺ species in the presence of atmospheric oxygen after complete consuming of reducing agent SO₂^{•-}. The compounds **1/Br⁻-3/Br⁻**

could play the role of catalyst for an electron transfer reaction for the reduction of carbonyl compound or nitroarenes by $\text{Na}_2\text{S}_2\text{O}_4$ [24, 151].

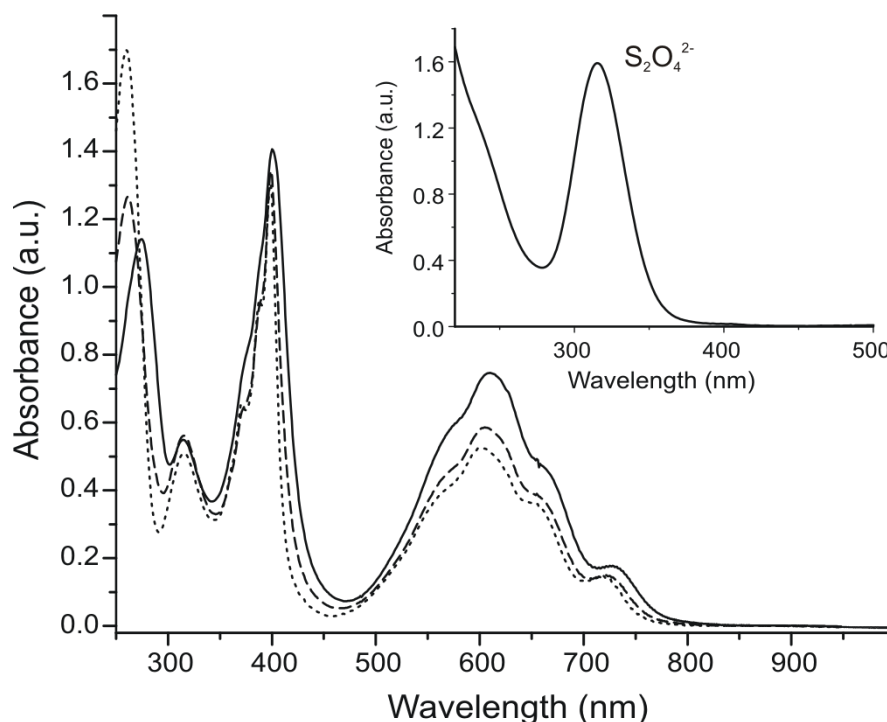


Figure 2.10 UV-Vis spectra of the reduced species of $1/\text{Br}^-$ - $3/\text{Br}^-$ (0.5 mM) in the presence of 0.05 ml $\text{Na}_2\text{S}_2\text{O}_4$ (10 mM) in Tris- H_2SO_4 buffer solution (pH 8.5). Inset: UV spectra of dithionite anion

In conclusion, a new series of bifunctional derivatives ($1/\text{An}^-$ - $3/\text{An}^-$) based on combination of redox active “viologen” with nucleobases was prepared by coupling the nucleobase units to the 4,4'-bipyridine core via nucleophilic substitution reactions. Depending on the attached “capper” nucleobase, i.e. if 4,4'-bipyridinium core is capped by thymine, adenine, or thymine/adenine, significantly different characteristics were observed in optical and electrochemical behavior. An intramolecular charge-transfer interaction between the viologen as acceptor and nucleobases as donor was demonstrated by UV-Vis spectroscopy. On the other hand, the aromatic purinic or pyrimidinic substituents played an important role in the modulation of necessary energy for the electron transfer (ET) to the viologen units. The radical cation state ($\text{V}^{\cdot+}$) of derivatives $1/\text{PF}_6^-$ - $3/\text{PF}_6^-$ had the typical color of the unconjugated viologens such as 1,1'-dibenzyl-4,4'-bipyridinium derivative ($\text{DBV}^{\cdot+}$). The anaerobic reduction in the presence of reducing agents like sodium dithionite leads to transformation of compounds $1/\text{Br}^-$ - $3/\text{Br}^-$ into the reduced radical cation state, which could be used as catalyst in organic synthesis or as low potential reductants for biological systems.

CHAPTER 3

Interaction of Viologen-Thymine Derivatives with ssDNA and Analogue ssPNA

The ability to control the molecular arrangement and packing order of the molecules represents a useful approach for tuning and optimizing the materials properties, apart from the chemical functionalization. For instance, bio-inspired self-assembly process driven by molecular recognition has been recognized as a powerful approach to create well-defined hierarchical supramolecular assemblies [152]. A good template to organize small functional molecules and to construct nanostructures with controlled size and shape is single stranded DNA. Several research groups have used ssDNA as template to assemble functional π -conjugated molecules and to form well-defined aggregates or nanostructures with enhanced electronic properties [5-10, 57, 60, 153]. The viologen-thymine derivatives are also promising building blocks for construction of self-assembled supramolecular structures in a “biomimetic way” with complementary oligonucleotides (ssDNA) or analogues peptide nucleic acids (ssPNA) due to their molecular recognition functionality. As a result of self-assembly process, the new nanostructured materials are expected to exhibit enhanced optical and optoelectronic properties with application in the field of supramolecular electronics [154, 155].

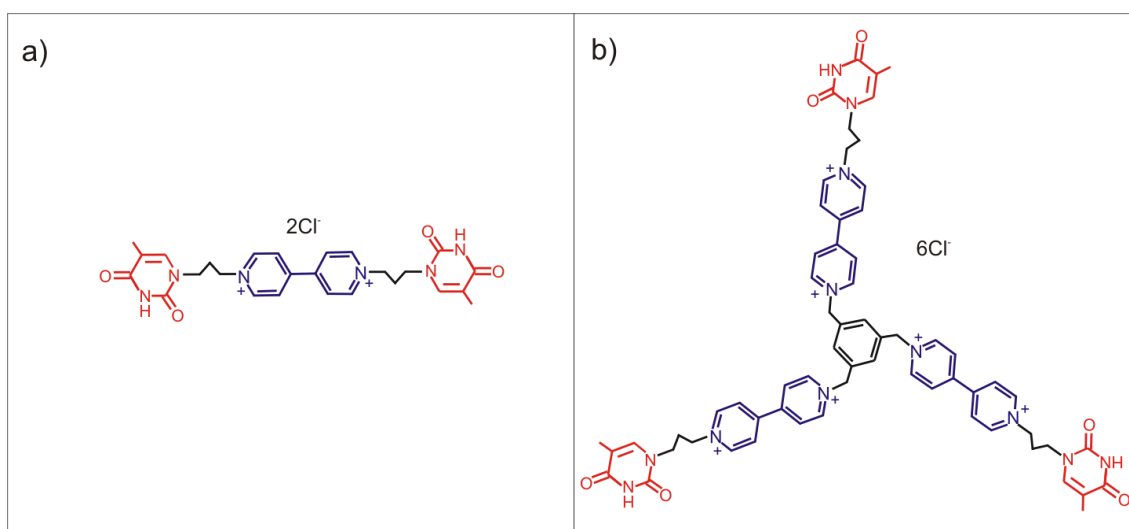
Furthermore, viologen-nucleobase derivatives with polycationic scaffold can interact electrostatically with the negatively charged phosphate backbone of oligonucleotides, leading to DNA condensation [156]. This aspect makes such polycationic derivatives interesting for the field of gene therapy as potential non-viral delivery vectors [157].

Considering these possible applications, this chapter discusses the interaction of viologen-thymine derivatives with complementary adenylic oligomers (dA_n) or analogues adenylic peptide nucleic acid (PNA) in aqueous solution. The temperature-absorbance dependence experiments (T_m), were performed to study the formation of self-assembled aggregates by hydrogen bonding. UV-Vis and circular dichroism spectroscopy were used as methods to characterize and quantify the amount of electrostatically condensed oligonucleotide. Additionally, the ability of polycationic viologen-nucleobase derivatives to condense luciferase plasmid DNA as potential gene

delivery carriers has been discussed. Standard methods such as electrophoresis and ethidium bromide assay were carried out to characterize the condensation process.

3.1 Hydrogen-bonded self-assemblies of viologen-thymine derivatives with ssDNA

Two viologen-thymine derivatives were chosen for the current study: rod-like molecule **1/Cl⁻**, capped by two thymine units and “Y-shaped” molecule **G0/Cl⁻**, capped by three thymine units (Scheme 3.1). They differ in shape, number of thymine units and positive charges per molecule. The compound **1/Cl⁻** was synthesized as reported in Chapter 2, and subsequently converted by metathesis reaction with tetrabutylammonium chloride in the analogue chloride salt. **G0/Cl⁻** derivative was synthesized by Ms. Ana-Maria Lepadatu following a previously reported procedure [3]. Both compounds as chloride salts were characterized by means of ¹H-NMR spectroscopy (cf. Experimental part in Chapter 6). Their purity exceeds 95% accordingly with the NMR data.



Scheme 3.1 Structure of viologen-thymine derivatives: a) **1/Cl⁻** and b) **G0/Cl⁻**

The mixtures (**1/Cl⁻**):(**dA₄₀**) and (**G0/Cl⁻**):(**dA₄₀**), were prepared at 21°C in a phosphate buffer (pH=7) by mixing corresponding stock solutions of viologen-thymine derivatives **1/Cl⁻** and **G0/Cl⁻** respectively, with oligonucleotide **dA₄₀** in equimolar thymine/adenine ratio ($[T] = [A] = 20 \mu\text{M}$).

It is noteworthy to mention first that a fraction of oligonucleotide **dA₄₀** precipitated spontaneously after mixing with respective viologen-thymine derivative, as a result of competitive electrostatic interaction between polycationic scaffold of viologen and

negatively charged riboso-phosphate backbone of dA₄₀. It was found that **1/Cl⁻** precipitates 24% while compound **G0/Cl⁻** precipitated almost 70% of the entire oligonucleotide. Detailed experimental description for determination of the amount of precipitated oligonucleotide will be presented in Section 3.2. However, the analysis of supernatant solutions of (**1/Cl⁻**):(**dA₄₀**) and (**G0/Cl⁻**):(**dA₄₀**) respectively, showed that oligonucleotide dA₄₀ coexists in solution with viologen-thymine compounds below a critical concentration and is expected to form hydrogen-bonded aggregates.

The self-assembly process by hydrogen bonding was demonstrated with an optical method, a so called “denaturation experiment”. Melting point DNA (T_m) or denaturation experiments consist in monitoring the UV absorption of nucleobases at a fixed wavelength (usually 260 nm) while the sample is heated up with a constant heating rate. The temperature-induced hydrogen bond breaking between nucleobases decreases the degree of π - π stacking interaction between adjacent nucleobases in the DNA strand and, as consequence, a cooperative hyperchromic effect is observed over the temperature range. Usually, the typical profile of a DNA denaturation experiment is a sigmoidal curve over temperature in which the inflection point (also called “melting point”) represents the temperature at which half of the hydrogen bonds in double stranded DNA are broken. T_m experiments are widely used to investigate the stability of the double stranded DNA.

T_m curve profiles of the mixture (**1/Cl⁻**):(**dA₄₀**) and (**G0/Cl⁻**):(**dA₄₀**), show a sigmoidal trend of absorption upon heating with the inflection point at about 37°C (Figure 3.1a and b). This non-linear hyperchromic effect over the temperature was not observed when the denaturation experiment was performed on the individually components **1/Cl⁻** (10 μ M), **G0/Cl⁻** (6.66 μ M) and oligonucleotide dA₄₀ (0.5 μ M), respectively (Figure 3.1c, d and e). The sharp hyperchromic changing at 260 nm over the temperature is typical for the cooperative hydrogen bond breaking of complementary nucleobases thymine and adenine as in the case of dsA-T [5]. These results suggest that the viologen-thymine derivative **1/Cl⁻** and **G0/Cl⁻** respectively, is hydrogen bonded to oligonucleotide dA₄₀. The mixture (**1/Cl⁻**):(**dA₄₀**) exhibited a sharper hyperchromic effect over the temperature, compared to the mixture (**1/Cl⁻**):(**dA₄₀**) suggesting a stronger cooperativity of the hydrogen bonding formation in the assembled aggregates. This is firstly explained by the different shape and structure of derivative **G0/Cl⁻** compared with the compound **1/Cl⁻**, which influences the supramolecular arrangement

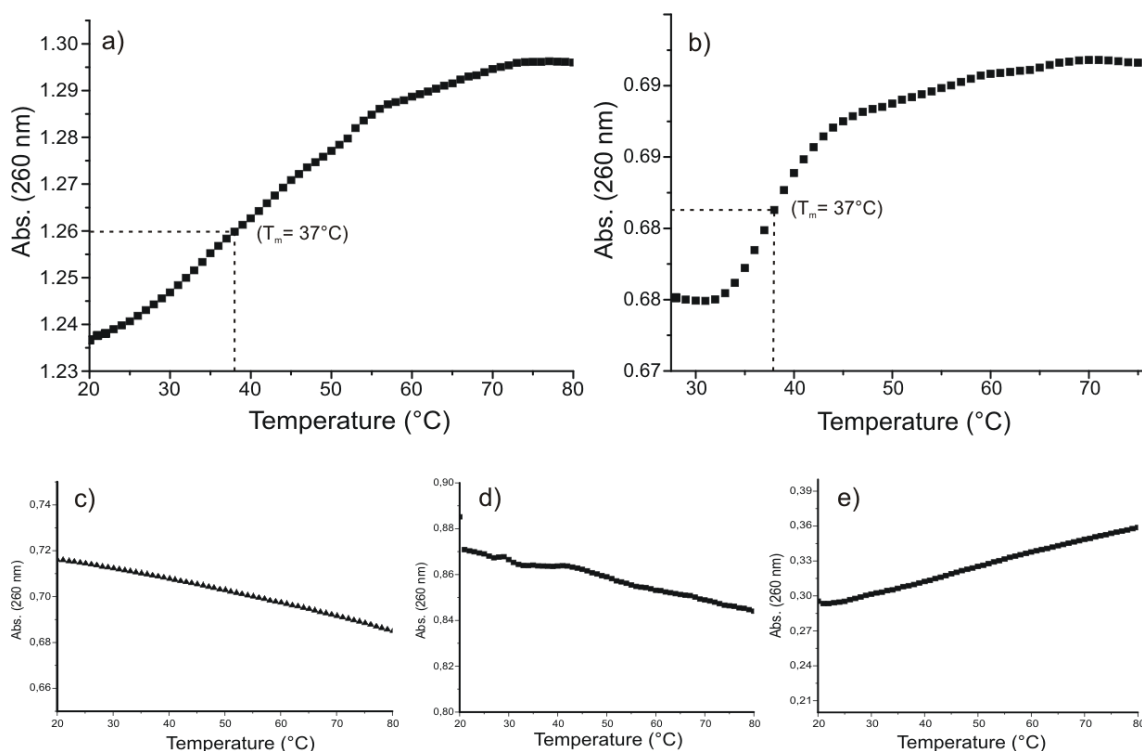
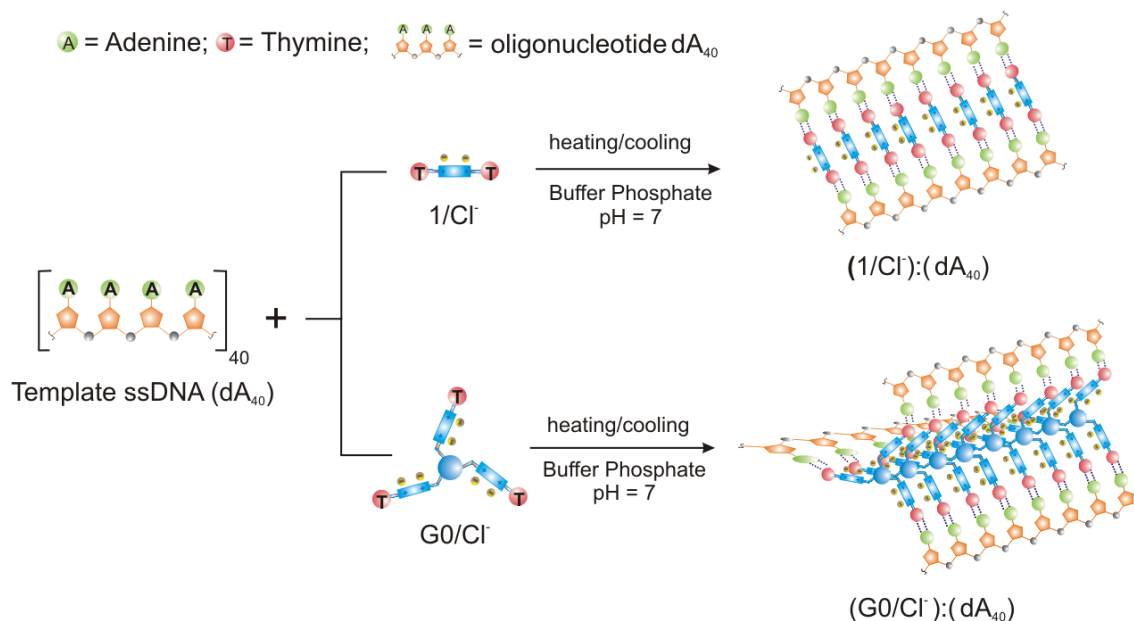


Figure 3.1 Denaturation experiments of the mixtures $(\mathbf{1/CI}):(\mathbf{dA}_{40})$ (a), $(\mathbf{G0/CI}):(\mathbf{dA}_{40})$ (b), and individually components $\mathbf{1/CI}$ ($10 \mu\text{M}$) (c), $\mathbf{G0/CI}$ ($6.66 \mu\text{M}$) (d) and \mathbf{dA}_{40} ($0.5 \mu\text{M}$) (e) in phosphate buffer solution ($\text{pH} = 7$)

and thermodynamic stability of the corresponding supramolecular aggregates. Secondly, the derivative $\mathbf{G0/CI}$ is capable to bind stronger with the oligonucleotide \mathbf{dA}_{40} since it contains three thymine units compared with the compound $\mathbf{1/CI}$ that contains only two thymine units. The self-assembly process by hydrogen bonding is enhanced by the increase of the number of thymine units per viologen-thymine derivative, but becomes unfavourable with the increase of number of positive charges per molecule due to electrostatic precipitation of the oligonucleotide.

An hypothetical self-assembled supramolecular model of the compounds $\mathbf{1/CI}$, respectively $\mathbf{G0/CI}$ by hydrogen bonding with \mathbf{dA}_{40} is represented in the Scheme 3.2. In this model, the oligonucleotide \mathbf{dA}_{40} with fibrillar structure plays the role of a template that directs the formation of the self-assembled nanostructure. The supramolecular aggregates are stabilized mainly by hydrogen bonding between the complementary nucleobases adenine and thymine units. Other forces, such as π - π staking or hydrophobic interactions between adjacent nucleobases may also contribute energetically to the stabilization of the supramolecular assemblies, in a similar way as seen in the double stranded DNA (dsDNA). The two theoretical models are inspired by the plenty of examples in the literature referring to the ability of single stranded DNA to

direct the formation of hydrogen-bonded supramolecular structures with fibrillar architectures [5-9, 57, 60]. Further investigations in the solid state, i.e. crystallographic characterization or transmission electron microscopy (TEM) are needed to confirm the proposed theoretical models.



Scheme 3.2 Hypothetic hydrogen-bonded self-assembly models of compounds **1/Cl⁻** and **G0/Cl⁻** respectively, with dA₄₀ oligonucleotide as template

3.2 Electrostatic interaction of viologen-thymine derivatives with ssDNA

The electrostatic neutralization of DNA by polycationic compounds reduces considerably the repulsion between DNA molecules and they tend to agglomerate until finally precipitate from solution. This phenomenon is known as DNA condensation [156, 158, 159]. The potential of polycationic derivatives to condense DNA is of great interest because such compounds can be potentially used as non-viral vectors in gene therapy. For this reason, the interaction between viologen-thymine derivatives and ssDNA was investigated using optical methods. Figure 3.2 shows the corresponding UV spectra of the mixture **(G0/Cl⁻):(dA₄₀)** and of the individually components **(G0/Cl⁻** and respectively dA₄₀). The strong and irreversible diminishing of UV absorption band around 260 nm of the mixture **(G0/Cl⁻):(dA₄₀)**, compared with the spectra of individually components **G0/Cl⁻** and dA₄₀ oligomer respectively, was assigned to the partially precipitation of the oligonucleotide dA₄₀ due to the electrostatic neutralization.

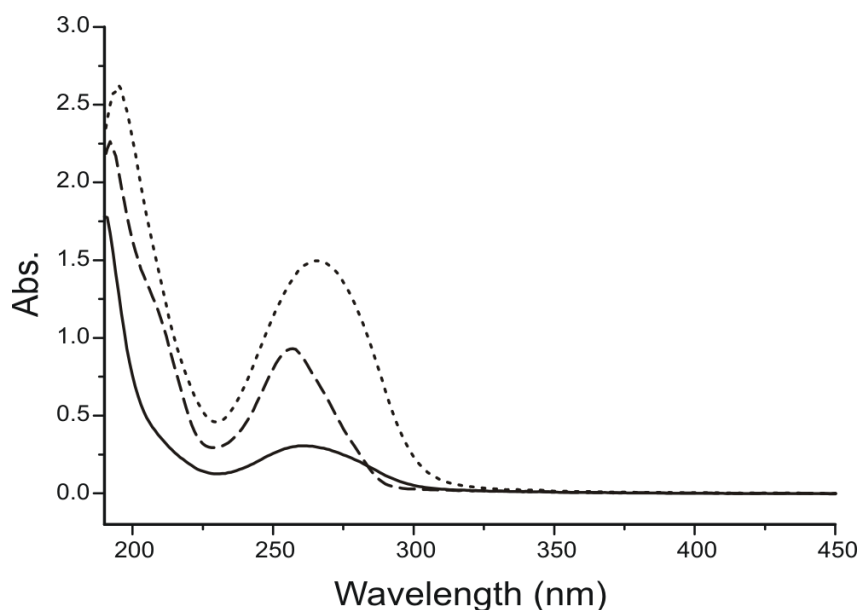


Figure 3.2 UV-Vis spectra of **G0** [6.66 μM] (dotted line), **dA₄₀** [0.5 μM] (dashed line) and mixture (**G0/Cl**):(**dA₄₀**), [6.66 μM]:[0.5 μM] in phosphate buffer (pH=7)

The precipitation of **dA₄₀** in the presence of derivative **G0/Cl** was confirmed by circular dichroism spectroscopy. Figure 3.3 shows the CD spectra of oligonucleotide **dA₄₀** and of the supernatant mixture (**G0/Cl**):(**dA₄₀**) respectively. The CD signature of **dA₄₀** is characterized by three major peaks: at 214 nm (positive), 245 nm (negative) and 273 nm (positive) which are corresponding to a random-coiled conformation of ssDNA [160]. When the oligonucleotide **dA₄₀** was mixed with the compound **G0/Cl**, a dramatic diminishing of the CD signal of the **dA₄₀** was observed and was caused by the

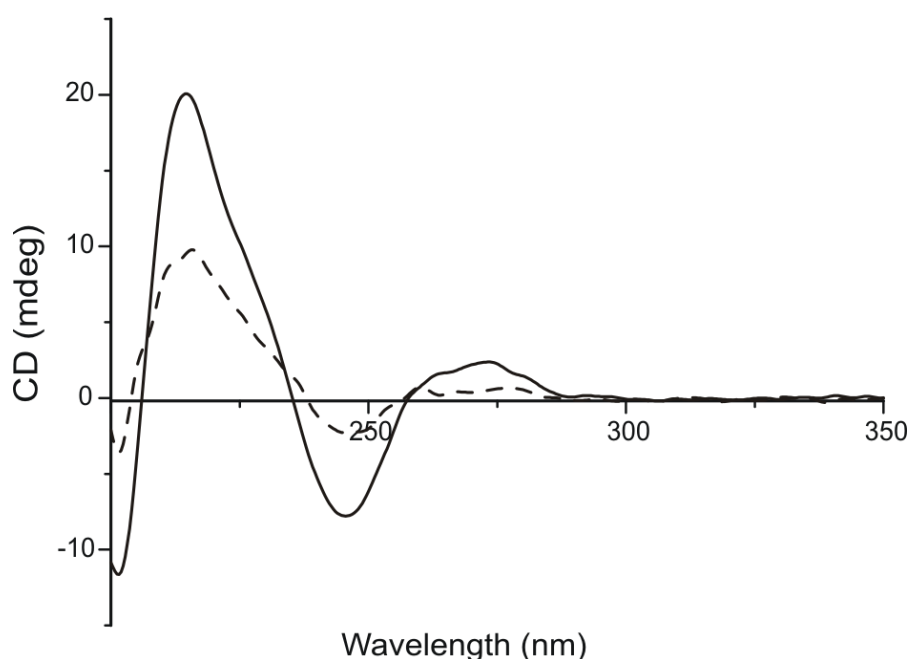
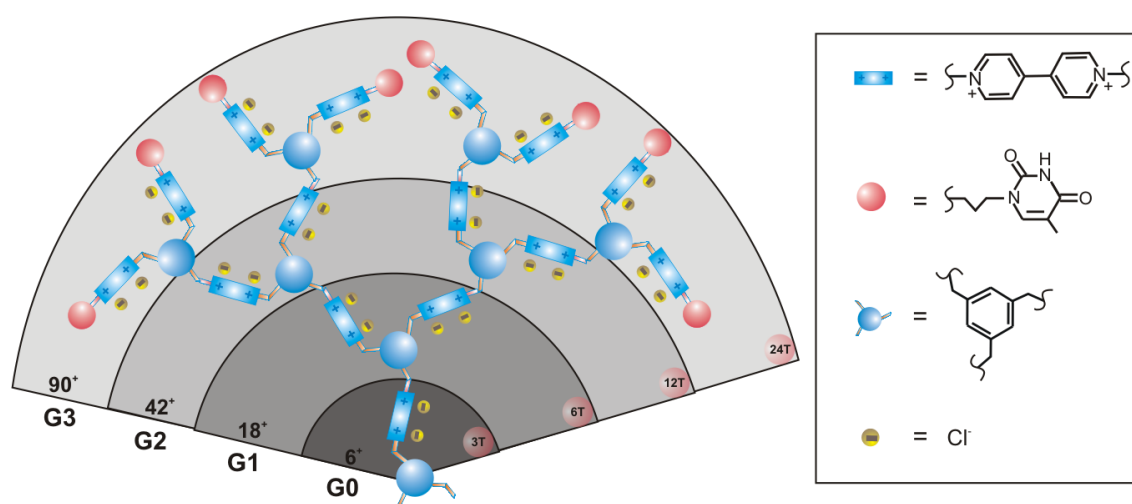


Figure 3.3 CD spectra of **dA₄₀** [0.5 μM] (continuous line) and mixture (**G0/Cl**):(**dA₄₀**) [6.66 μM] : [0.5 μM] (dashed line) in phosphate buffer (pH=7)

oligonucleotide precipitation from the bulk solution due to the electrostatic interaction with the polycationic **G0/Cl⁻** derivative.

In a further series of experiments the influence of positive charge number per molecule of viologen-thymine derivative and the oligonucleotide length on the precipitated amount of oligonucleotide was systematically investigated. For this propose, the viologen-thymine derivative **1/Cl⁻**, carrying two positive charges, and four viologen-based spheroidal dendrimers with polycationic scaffold, carrying 6 (**G0/Cl⁻**), 18 (**G1/Cl⁻**), 42 (**G2/Cl⁻**) and 90 (**G3/Cl⁻**) positive charges, respectively 3 (**G0/Cl⁻**), 6 (**G1/Cl⁻**), 12 (**G2/Cl⁻**) and 24 (**G3/Cl⁻**) thymine terminal groups on the periphery (Scheme 3.3) were used in interaction studies with adenylic oligonucleotides dA_n of different lengths (n= 20, 40, 80, 140). The synthesis of dendrimers **G0-3/Cl⁻** was performed by Ms. Ana-Maria Lepadatu accordingly with a previously published procedure and do not make the subject of this thesis [3, 4]. Their molecular structure and purity (>95%) as chloride salts was checked by ¹H-NMR spectroscopy (cf. Chapter 6).



Scheme 3.3 Schematic representation of dendritic compounds **G0-3/Cl⁻** capped by thymine groups at periphery

The corresponding solution mixtures in phosphate buffer (pH=7) of viologen-thymine derivatives with oligonucleotides (dA_n) were obtained by mixing Stock solutions of the components in equimolar ratio T/A, as previously described (cf. Section 3.1) at 21°C. After mixing, spontaneously precipitation occurred. The supernatant solution phase was isolated and further analysed by means of circular dichroisms spectroscopy. The advantage of using circular dichroism over UV-Vis spectroscopy lies in the possibility to determine the oligonucleotide amount individually, since the oligonucleotide is the

only optically active in CD due to the chirality of desoxyribose moieties. The percentage amount of precipitated dA_n (%mol dA_n) was calculated by the formula:

$$\% \text{mol } dA_n = [1 - (\Delta A_1 / \Delta A_2)] \cdot 100 \quad (3.1)$$

where, ΔA_1 is the CD absorbance of the mixture at 245 nm, and ΔA_2 is the CD absorbance of the individually oligonucleotide¹ at 245 nm.

The calculation was done considering that the CD signal decreased proportionally with the amount of precipitated oligonucleotide according with the Lambert-Beer law for circularly-polarized light:

$$\Delta A(\lambda) = \Delta \epsilon \cdot c \cdot l \quad (3.2)$$

where, $\Delta A(\lambda)$ is the difference between absorption of the left and right circularly-polarized light; $\Delta \epsilon$ is the difference between extinction coefficients for the left and right circularly-polarized light; c is the concentration of the optical active species in solution and l is the pathlength.

Figure 3.4a illustrates the influence of the number of positive charges per molecule of viologen-thymine derivatives on the percentage amount of precipitated dA_{40} . Except the compound **1/Cl⁻** and **G0/Cl⁻**, which produced a partial precipitation, the dendritic compounds (**G1-3/Cl⁻**) precipitated practically the entire amount of oligonucleotide dA_{40} . Furthermore, the amount of condensed oligonucleotide in the presence of

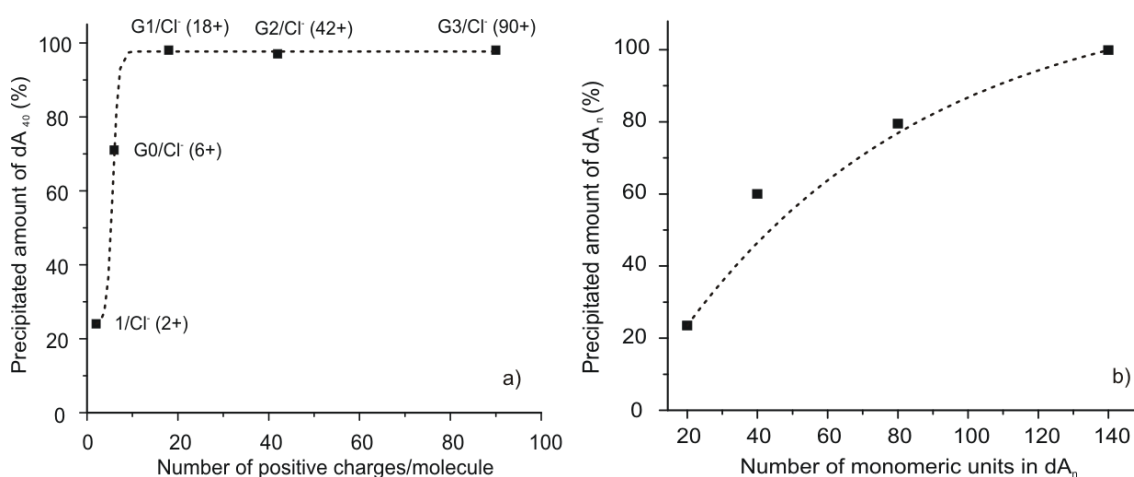


Figure 3.4 Amount of precipitated dA_{40} as a function of number of positive charges per molecule of viologen-thymine derivative (a) and as oligonucleotide length in the presence of **G0/Cl⁻** (b)

¹ The concentration of individually solution of dA_n was the same as used in the mixture dA_n ; viologen-thymine derivative

compound **G0/Cl⁻** increased with the length of the oligonucleotide dA_n (Figure 3.4b).

3.3 Viologen-thymine derivatives as gene carriers

In an additional study the polycationic viologen-thymine derivatives were tested *in vitro* for their function to condense a plasmid DNA (i.e. luciferase). The study was performed by the members of the research group of Prof. David Oupický (Center for Drug Delivery and Nanomedicine, Department of Pharmaceutical Sciences, University of Nebraska Medical Center, United States). Experimental details can be found in the lit. [161].

Condensation of luciferase in the presence of viologen-nucleobase derivatives **1/Cl⁻**-**3/Cl⁻** (cf. Scheme 2.2 in Chapter 2 for structural details) or polycationic viologen-based dendrimers **G0-3/Cl⁻** (cf. Scheme 3.2) respectively, was first investigated by ethidium bromide (EBr) exclusion assay. This method consists in monitoring the fluorescence of the uncomplexed DNA that is accessible for intercalation with EBr at a given nitrogen/phosphate (N/P) ratio. The compounds **1/Cl⁻**-**3/Cl⁻** with the lowest number of positive charges per molecule (2+) failed to condense plasmid DNA as indicated by the nonsigmoidal shape of the condensation curves (Figure 3.5a). In the presence of viologen-thymine dendrimers **G0-3/Cl⁻**, the plasmid DNA was fully condensed showing a typical sigmoidal shape (Figure 3.5b). These findings are in agreement with literature results obtained with non nucleobase-capped viologen dendrimers [162].

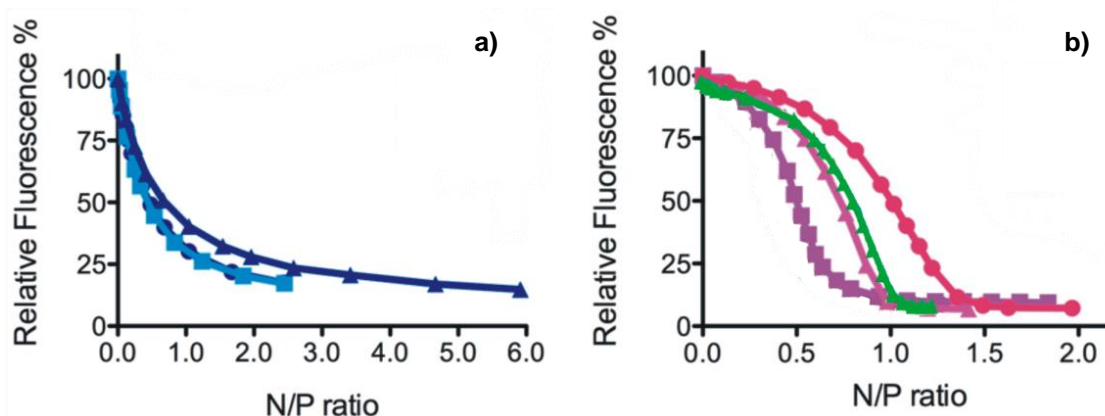


Figure 3.5 DNA condensation ability of viologen-thymine derivatives evaluated by EBr exclusion assay in 10 mM HEPES buffer: a) **1/Cl⁻**, **2/Cl⁻**, **3/Cl⁻** and b) dendrimers **G0/Cl⁻**, **G1/Cl⁻**, **G2/Cl⁻**, **G3/Cl⁻** [161]

The DNA condensation in the presence of viologen-nucleobase derivatives was confirmed by agarose gel electrophoresis (Figure 3.6). The complete condensation of DNA with dendrimers **G0-3/CI** and formation of stable polyplexes was demonstrated by the absence of plasmid band on the gel. By contrast, the compounds **1/CI-3/CI** were not able to condense DNA since the characteristic band of unprecipitated luciferase was present in the gel.

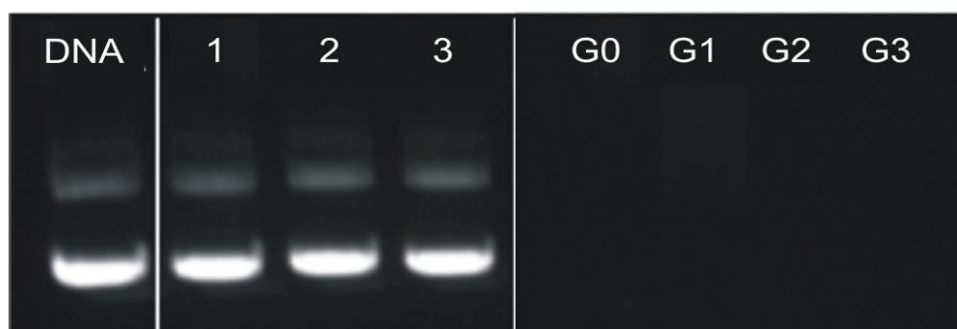


Figure 3.6 Gel electrophoresis experiment [161]

Further investigations on the physico-chemical properties of the obtained polyplexes, their toxicity as well as transfection capacity into the human cells were performed in group of our cooperation partner, Prof. David Oupický and reported in ref. [161]. Briefly, it was found a strong correlation between the number of positive charges per molecule of viologen derivatives, molecular weight, shape or peripheral capping groups on the transfection capabilities. They pointed out that the polyplexes of luciferase plasmid DNA with viologens capped by thymine groups were more stable and exhibited better physico-chemical properties (i.e. hydrodynamic size and ζ -potential) than other analogues viologens. This was assigned to the nucleobases terminal groups that can also contribute on the binding of viologen-thymine derivatives to the plasmid DNA by base pairing interactions.

3.4 Hydrogen-bonded self-assemblies of viologen-thymine derivatives with ssPNA

In this study the oligonucleotide template dA_{40} was replaced by an analogue single stranded PNA 10-mer in order to avoid the electrostatic interaction between the polycationic viologen-thymine derivatives and negatively charged oligonucleotides and to make use exclusively of hydrogen bonding interactions between complementary thymine and adenine nucleobases. Peptide nucleic acids (PNA) are synthetic analogues

of DNA, which mimics very well the structure and properties of DNA [163]. The main structural difference lies in the neutral peptidic backbone of the PNA in contrast with the negatively charged desoxyribose-phosphate backbone of DNA (Figure 3.7).

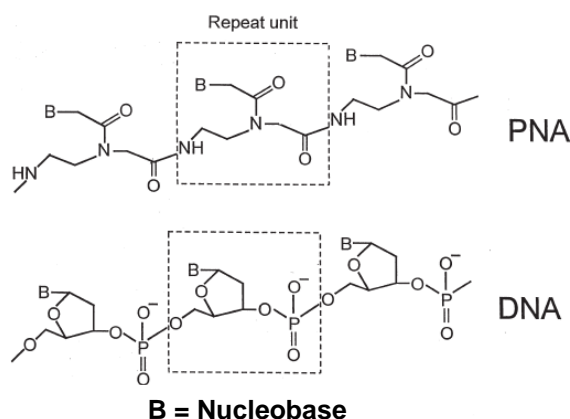


Figure 3.7 The structure of ssPNA compared with ssDNA [164]

The interaction of adenylic PNA oligomer 10-mer (PNA-A₁₀) with four viologen-thymine derivatives, respectively spheroidal viologen-based dendrimers with thymine terminal groups (**G0-3/Cl**), was studied in aqueous solution. The mixtures were prepared by mixing stock aqueous solution of the respective viologen-thymine compound with adenylic PNA 10-mer (PNA-A₁₀) in equimolar ratio T/A at 21°C. The final concentration was adjusted to [T]=[A]=20 μM. The mixtures were characterized by temperature-absorbance dependence experiments (T_m).

The T_m experiments of the corresponding mixtures showed the same sigmoidal hyperchromic effect at 260 nm over the temperature, typically for the cooperative T=A hydrogen bonds breaking in the double helix DNA (Figure 3.8). This result suggests that the interaction mode of the compounds **G0-3/Cl** with the PNA-A₁₀ oligomer takes place by hydrogen bonding between complementary thymine/adenine nucleobases. Unlike the case of interaction with oligonucleotides, no precipitation was observed, indicating that the interaction mode was exclusively by hydrogen bonding.

Extension of the study to PNA of longer chain size, which may enhance the stability of the resulted supramolecular self-assemblies [7], failed due to the low solubility in aqueous solution of the more hydrophobic neutral PNA oligomers compared with the negatively charged ssDNA analogues.

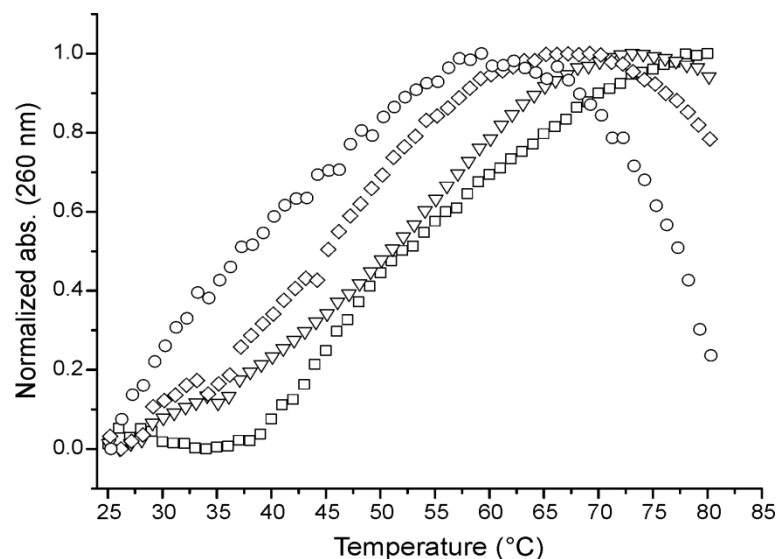


Figure 3.8 Denaturation experiments of aqueous solution mixtures: **G0/Cl⁻** vs PNA-A₁₀ (□), **G1/Cl⁻** vs PNA-A₁₀ (▽), **G2/Cl⁻** vs PNA-A₁₀ (◇), **G3/Cl⁻** vs PNA-A₁₀ (○).

It is important to notice that during the denaturation experiments (T_m), the absorbance at 260 nm decreased irreversibly at elevated temperatures due to a thermal-induced charge-transfer (CT) interaction between viologen as donor and thymine unit as acceptor as confirmed by UV-Vis spectroscopy. In order to demonstrate the thermal-induced CT interaction, the individually aqueous solutions of viologen-nucleobase

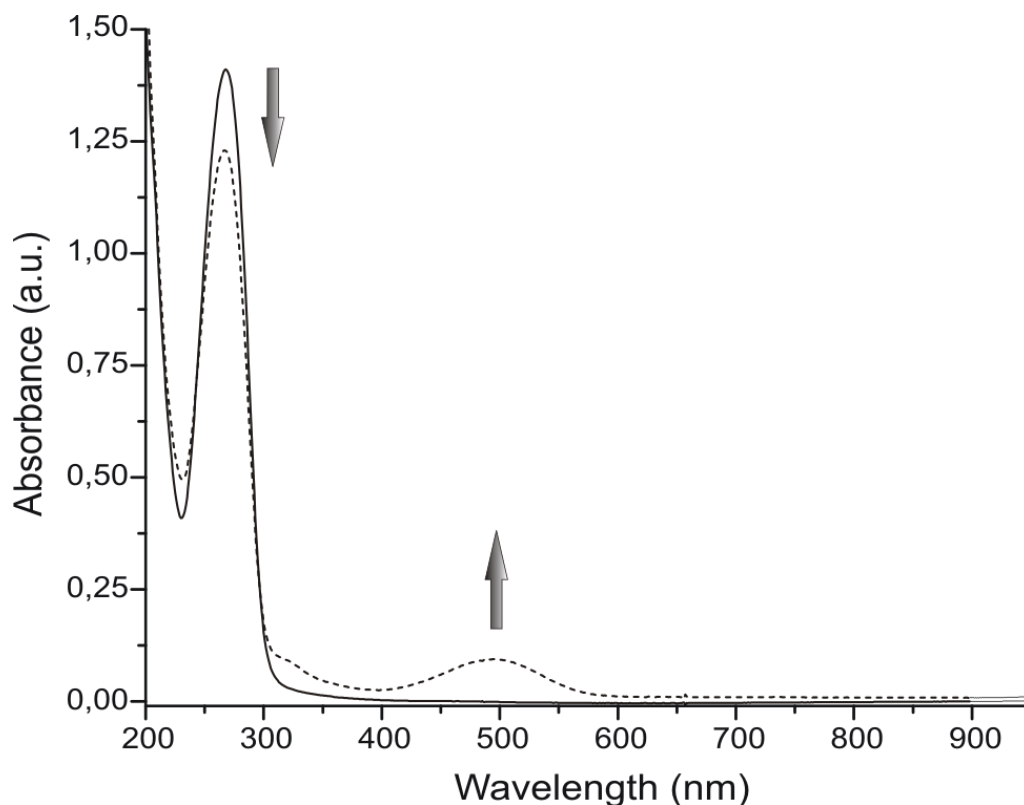


Figure 3.9 UV-Vis spectra of compound **G0/Cl⁻** (0.1 mM) in water: before (continuous line) and after thermal treatment (dashed line)

derivatives **G0-3/Cl⁻** were exposed at 90°C for 12 hours and then characterized by means of UV-Vis spectroscopy. The change in color of the corresponding solution from initially colorless, to pink color after thermal treatment, corresponds in the UV-Vis spectra with evolution of a new broad band in the visible range ($\lambda_{\text{max}} = 500 \text{ nm}$), concomitantly with decreasing of the UV absorption at 260 nm (Figure 3.9). The absorption band in visible range is characterized by a broad shape and low extinction coefficient which is typical for CT bands of 4,4'-bipyridinium dication [141]. The pink color persisted in time after cooling down to ambient temperature (21°C) indicating an irreversible charge transfer interaction.

Conclusions:

In the current study it was investigated the interaction of viologen-thymine derivatives with adenylic oligonucleotides or analogue synthetic ssPNA. The viologen-thymine derivatives **1/Cl⁻** and **G0/Cl⁻**, with relatively low number of positive charges per molecule, have been interacting by thymine-adenine hydrogen bonding with complementary dA₄₀ oligonucleotide leading to the formation of supramolecular aggregates in aqueous solution. The self-assembly aggregation of viologen-nucleobase derivatives in the presence of ssDNA was demonstrated by optical methods. A hypothetical model of the self-assembled aggregates is proposed. In this model the oligonucleotide is expected to act as a template molecule which directs the formation of supramolecular structures with fibrillar conformation. However, the proposed model needs further to be confirmed experimentally by crystallographic analysis or electron microscopic methods. The H-bonded self-assembly approach is promising for tuning optical and optoelectronic properties of the resulted materials due to incorporation of a redox active functionality (i.e. viologen) into a highly-ordered supramolecular matrix.

On the other hand, viologen-thymine derivatives were found to interact electrostatically leading to the partial or total precipitation of the oligonucleotides, strongly depending on the oligonucleotide length and the number of positive charges per viologen-nucleobase derivative.

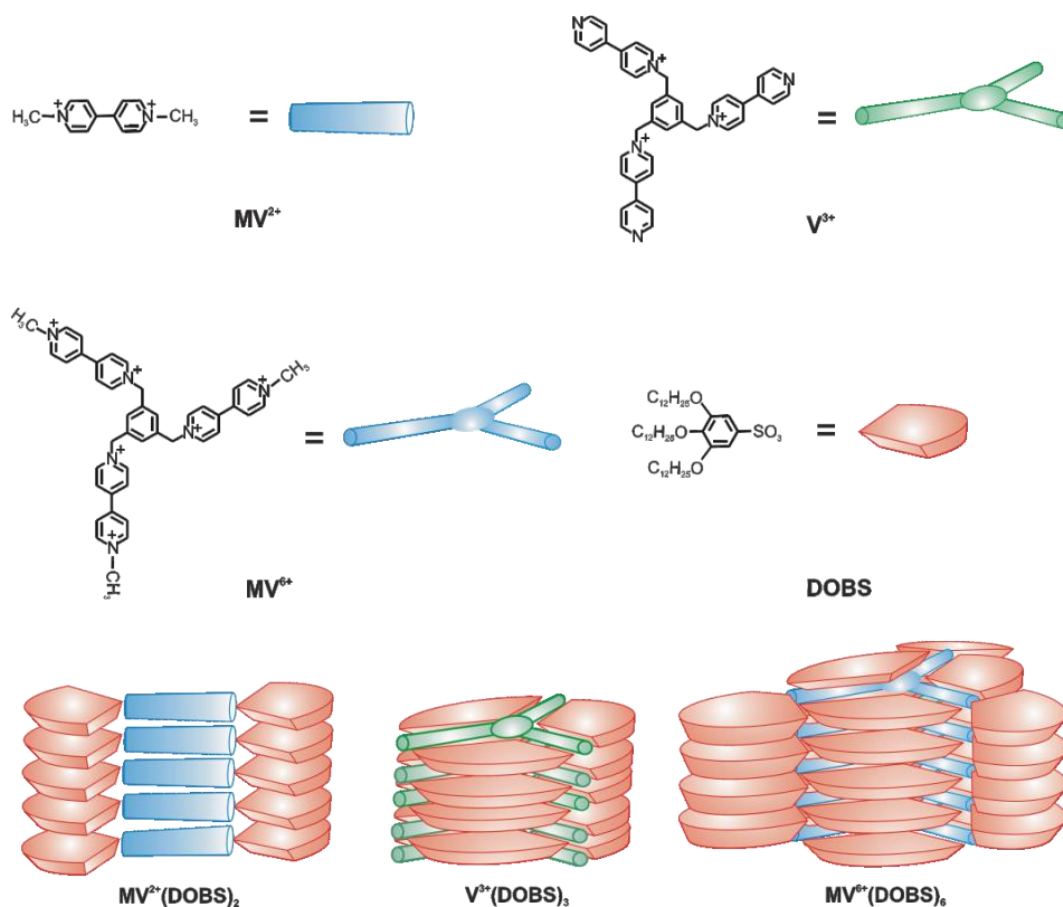
When neutral analogue adenylic ssPNA 10-mer was used as a template to direct the self-assembly process of polycationic viologen-thymine derivatives **G0-3/Cl⁻**, the interaction mode was exclusively by hydrogen bonding leading to the formation of self-assembled aggregates as demonstrated by the T_m experiments.

In an additional study the capacity of polycationic viologen-nucleobase derivatives to condense luciferase plasmid DNA has been investigated. A strong correlation has been found between the number of positive charges per molecule of viologen-thymine derivatives and the capacity to form polyplexes with optimal physicochemical properties that can be used *in vitro* for the DNA transfection. The combined effects of the polycationic scaffold with the thymine group functionality increase the biological significance of the viologen-nucleobase derivatives as potentially gene-delivery vectors in gene therapy.

CHAPTER 4

Mesogenic Viologen-Nucleobase Derivatives with Self-Association Behavior in Low Polar Solvents

Bis-quaternized 4,4'-bipyridinium derivatives (“viologens”) are well known building blocks of special importance, because they allow the generation of functional materials with optoelectronic properties such as electrochromism [111, 112], photochromism [84, 165], thermochromism [166], electron transfer [167, 168] and charge transfer abilities [141, 169]. The viologen-based compounds are an alternative to the classical ionic organic mesogenic cores such as pyridinium or imidazolium salts [70, 76]. They can be used as photochromic and electrochromic additives in a liquid crystalline matrix to construct a “task specific” material. Particularly, the mesogenic ionic complexes of polycationic viologens derivatives (MV^{2+} , V^{3+} and V^{6+}) with anionic cunitic ligands

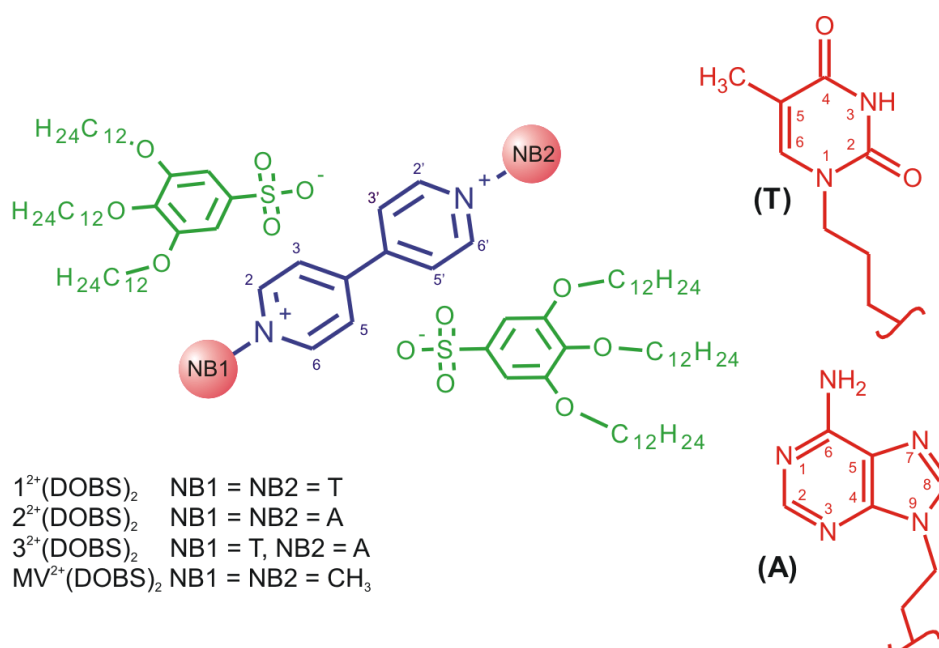


Scheme 4.1 Molecular structures of the viologen units with two (MV^{2+}), three (V^{3+}) and six (MV^{6+}) positive charges, as well as the anionic cunitic ligand ($DOBS^-$) and schematic sketch of the proposed molecular arrangement in the columnar mesophases of the viologen : sulfonate complexes

such as 3,4,5-tris(dodecyloxy)benzene sulfonate (**DOBS**⁻) were prepared in our group by phase transfer catalysis (Scheme 4.1, realized by Dr. Simona Asaftei and published in ref. [22]). The respective new materials exhibited LC properties in a low and broad temperature range (30 - 270°C), ionic conductivity, thermo- or electrochromism.

In this context, the current study represents an extension of above mentioned work and aimed to incorporate 4,4'-bipyridinium derivatives capped by nucleobases (i.e. purine or pyrimidine) into an ionic liquid crystalline matrix. This approach is a promising pathway for tuning the material properties since the nucleobase units, with hydrogen bonding abilities, may influence the overall supramolecular arrangement of the new nanostructured materials.

In the following paragraphs the synthesis and the properties of a new class of redox-active ionic complexes, consisting in ion-pairing of dicationic derivatives (**1-3**)²⁺ with amphiphilic anion 3,4,5-tris(dodecyloxy)benzene sulfonate (**DOBS**⁻) will be discussed (Scheme 4.2).



Scheme 4.2 Ionic complexes of dicationic viologens with amphiphilic anion 3,4,5-tris(dodecyloxy)-benzene sulfonate

The self-association behavior by hydrogen bonding in low-polar media and the influence of solvent nature, temperature or concentration were systematically investigated. The new ionic complexes were further electrochemically characterized in solution and the effect of self-association on the redox properties was addressed. Thermal behavior and electrochromic properties in the bulk state were finally

investigated. A direct comparison with the analogues 1,1'-dimethyl-4,4-bipyridinium, $MV^{2+}(\text{DOBS})_2$ was performed at any point of discussion to reveal the influence of nucleobase capping groups on the physico-chemical properties. This compound was chosen for comparison because is capped by two methyl groups at nitrogen atoms instead nucleobase terminal groups, permitting to discriminate the effect induced by nucleobases.

4.1 Synthesis

Ionic complexes $1^{2+}(\text{DOBS})_2$, $2^{2+}(\text{DOBS})_2$ and $3^{2+}(\text{DOBS})_2$ were prepared in a phase transfer reaction of cationic viologen derivatives **1/I**, **2/I** and **3/I** respectively, with caesium 3,4,5-tris(dodecyloxy)benzene sulfonate (CsDOBS). Derivatives **1-3/I** were synthesized as presented in Chapter 2 to purity higher than 98%. CsDOBS was prepared by Dr. Enfeng Song following a procedure reported in literature [170].

An aqueous solution (0.01 M) of either **1/I** (47 ml), **2/I** (36 ml) or **3/I** (34 ml) respectively, was vigorously mixed with an equal volume of chloroform solution (0.01 M) of hydrophobic CsDOBS [170] for 12 hours at 21°C. During the reaction, the color of the organic phase changed from colorless to yellow, typical for the transfer of viologen units from the aqueous to the chloroform phase. The equal volumes and same concentration of reagents in aqueous and chloroform solution respectively, ensures that the quantity of viologen in the aqueous solution is two-fold higher than the theoretical quantity required for complete ionic exchange of caesium. The ionic complex formed between the viologen dication and 3,4,5-tris(dodecyloxy)benzene sulfonate anion was isolated from the organic phase in excellent yield (>93%) and characterized by means of

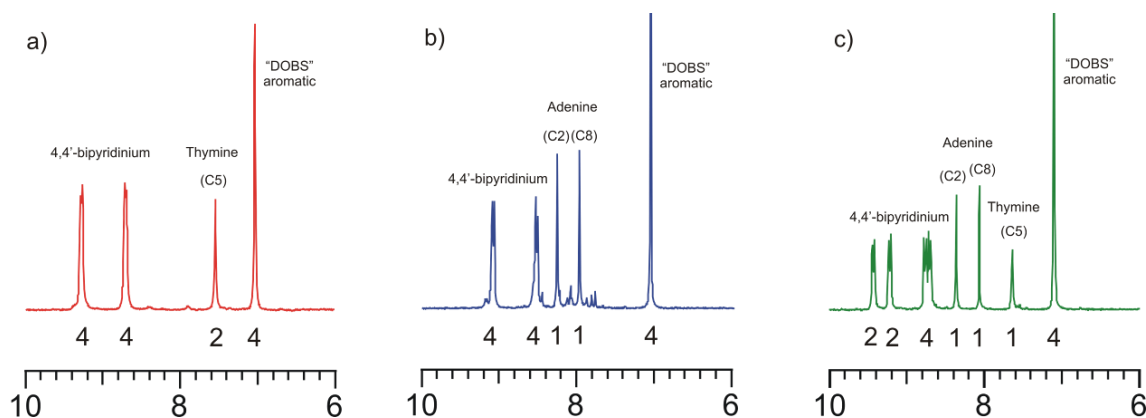


Figure 4.1 ^1H -NMR spectra in the aromatic region of the ionic complexes $1^{2+}(\text{DOBS})_2$ (a), $2^{2+}(\text{DOBS})_2$ (b) and $3^{2+}(\text{DOBS})_2$ (c) in $\text{THF-d}_8/\text{D}_2\text{O}$ (4:1 vol)

$^1\text{H-NMR}$, $^{13}\text{C-NMR}$ and IR spectroscopy and their purity exceeded 98% accordingly with elemental analysis results (cf. Chapter 6 for detailed spectroscopic data and elemental analysis). **Viologen** $^{2+}$ /**DOBS** $^-$ ratio was deduced from the corresponding integral peaks of the ionic components in the $^1\text{H-NMR}$ spectra and was found to be 1:2 (Figure 4.1).

The molar ratio combination (1:2) in the corresponding ionic complexes demonstrates that: (1) the interaction between **Viologen** $^{2+}$ and **DOBS** $^-$ respectively, is electrostatic in nature and, (2) the phase transfer reaction occurred until the caesium was completely replaced by the dicationic viologen from chloroform solution.

4.2 Hydrogen bonded self-association in low-polar solvents

Ionic complexes of viologens capped by nucleobases with amphiphilic anion **DOBS** $^-$ are expected to self-associate in solvents with low polarity (where they are preferentially soluble) due to the ability of nucleobase moieties to undergo in-plane hydrogen bonding. The self-association of ionic complexes $\mathbf{1}^{2+}(\mathbf{DOBS})_2$, $\mathbf{2}^{2+}(\mathbf{DOBS})_2$ and $\mathbf{3}^{2+}(\mathbf{DOBS})_2$ was investigated in solution by $^1\text{H-NMR}$ spectroscopy (i.e. one-dimensional $^1\text{H-NMR}$ and DOSY) and a comparison with the analogues derivative $\mathbf{MV}^{2+}(\mathbf{DOBS})_2$ was performed.

In a first experiment, ionic complexes $\mathbf{1}^{2+}(\mathbf{DOBS})_2$, $\mathbf{2}^{2+}(\mathbf{DOBS})_2$, $\mathbf{3}^{2+}(\mathbf{DOBS})_2$ and $\mathbf{MV}^{2+}(\mathbf{DOBS})_2$ respectively, were analysed in deuterated chloroform solution (50 mM) by means of one-dimensional $^1\text{H-NMR}$ at constant temperature (30°C). The $^1\text{H-NMR}$ spectra in chloroform of the individually ionic complexes is represented in Figure 4.2.

Except from the compound $\mathbf{MV}^{2+}(\mathbf{DOBS})_2$, all the other ionic complexes showed a line broadening of the spectra which increase in the order $\mathbf{1}^{2+}(\mathbf{DOBS})_2 < \mathbf{3}^{2+}(\mathbf{DOBS})_2 < \mathbf{2}^{2+}(\mathbf{DOBS})_2$. The observed line broadening effect arises from the self-association of the molecules into higher molecular weight aggregates [171]. These results suggest that the self-association driving force of viologen-nucleobase derivatives in solvents with low polarity is induced by the nucleobases with hydrogen bonding abilities. Previous research showed that thymine (T) and adenine (A) nucleobases can undergo a multitude of hydrogen bonding motifs in low-polar solvents. These motifs include self-associated cyclic dimers T-T, A-A, trimer A-A-A ($k_{\text{ass}} < 4 \text{ M}^{-1}$) or complementary T-A base-pairing with higher association constant ($k_{\text{ass}} > 100 \text{ M}^{-1}$) [31, 172-175].

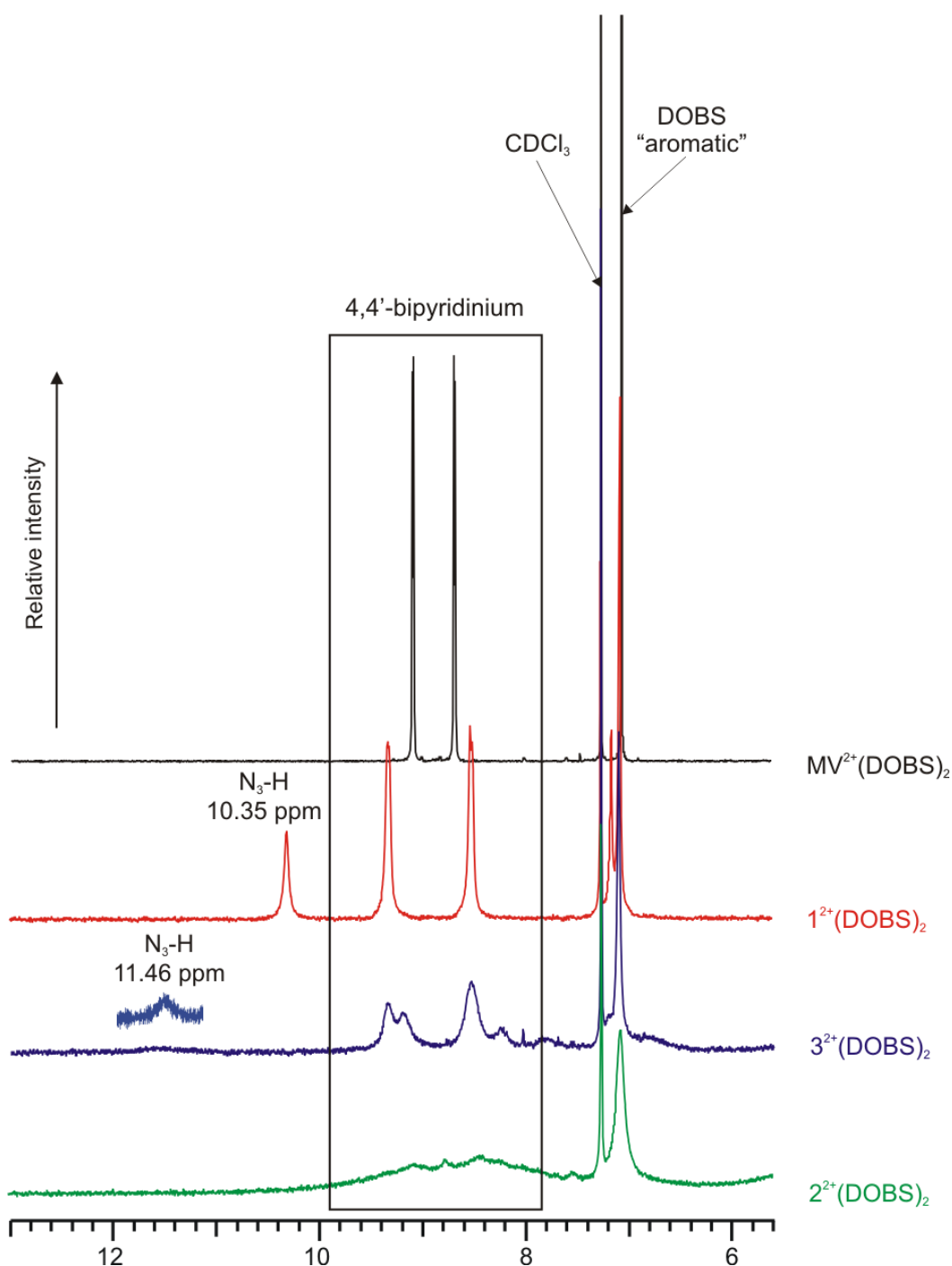


Figure 4.2 ¹H-NMR spectra in the aromatic region of the ionic complexes (50 mM) in CDCl₃ at 30°C

The magnitude of signal attenuation seen in ¹H-NMR spectra can be interpreted as a qualitative appreciation of the self-association degree in solution. Comparing the relative signal broadening of the viologen-nucleobase ionic complexes (Figure 4.2) it can be observed that the compound with the highest degree of self-association is **2²⁺(DOBS)₂**, containing two adenine units, while the ionic complex with the lowest degree of self-association is **1²⁺(DOBS)₂**, containing two thymine units. The ionic complex **3²⁺(DOBS)₂**, containing an adenine and a thymine group, has an intermediary

self-association degree. Remarkably, the ionic complexes, capped by adenine units, exhibited the highest degree of self-association. This is explained by the nature of purinic adenine moiety which contains more hydrogen bonding sites over the thymine, which may enhance the supramolecular self-assembly process of the corresponding viologen-nucleobase molecules [173].

It is noteworthy to say that the thymine *imino* proton ($N_3\text{-H}$, 11.46 ppm) in the compound $3^{2+}(\text{DOBS})_2$ appeared broadened and downfield shifted compared to *imino* proton ($N_3\text{-H}$, 10.35 ppm) in the compound $1^{2+}(\text{DOBS})_2$ (Figure 4.2). This observation suggests that the thymine unit in the compound $3^{2+}(\text{DOBS})_2$ is associated by hydrogen bonding to a higher extent, very probably, with the complementary adenine. To check if the hydrogen bonding of thymine in compound $3^{2+}(\text{DOBS})_2$ occurs intra or intermolecular, the signal of *imino* proton ($N_3\text{-H}$) was monitored over the concentration at constant temperature (30°C). It has been found that the position of *imino* proton was not affected by variation of concentration supporting an intramolecular association of thymine with adenine unit (Figure 4.3). The ethylene and propylene spacers in the compound $3^{2+}(\text{DOBS})_2$ confer enough flexibility to the nucleobases to fold and undergo the proper conformation for intramolecular hydrogen bonding.

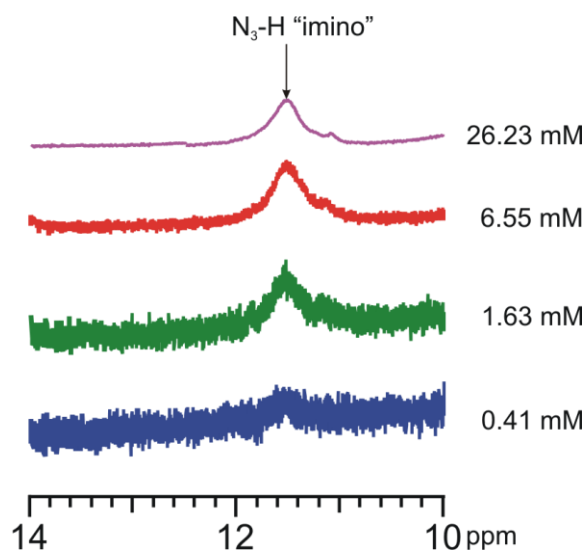


Figure 4.3 ^1H -NMR signal of $N_3\text{-H}$ imino proton for derivative $3^{2+}(\text{DOBS})_2$ in CDCl_3 of different concentrations at 30°C

In a further series of ^1H -NMR experiments it was investigated the self-association behavior of ionic complexes in three different solvents: chloroform, tetrahydrofuran and a mixture of THF:water (4:1 volume ratio).

The results are presented in Figure 4.4. The highest degree of self-association was observed in chloroform in which the peak signals of respective ionic complexes appeared significantly diminished and broadened compared with the other two solvent systems. In THF, a solvent with higher polarity than chloroform, the ionic complexes exhibited a lower broadening of the peaks suggesting lower degree of self-association. When the solvent used was a mixture of THF:water (cf Figure 4.4, black spectra), practically no self-association took place since no line broadening was observed. The self-association of viologen-nucleobase derivatives was inhibited in THF:water, obviously due to the competitive hydrogen bonding with water molecules [176-178]. It can be concluded that the self-assembly process of ionic complexes was strongly influenced by the solvent nature and its ability to compete to hydrogen bonding.

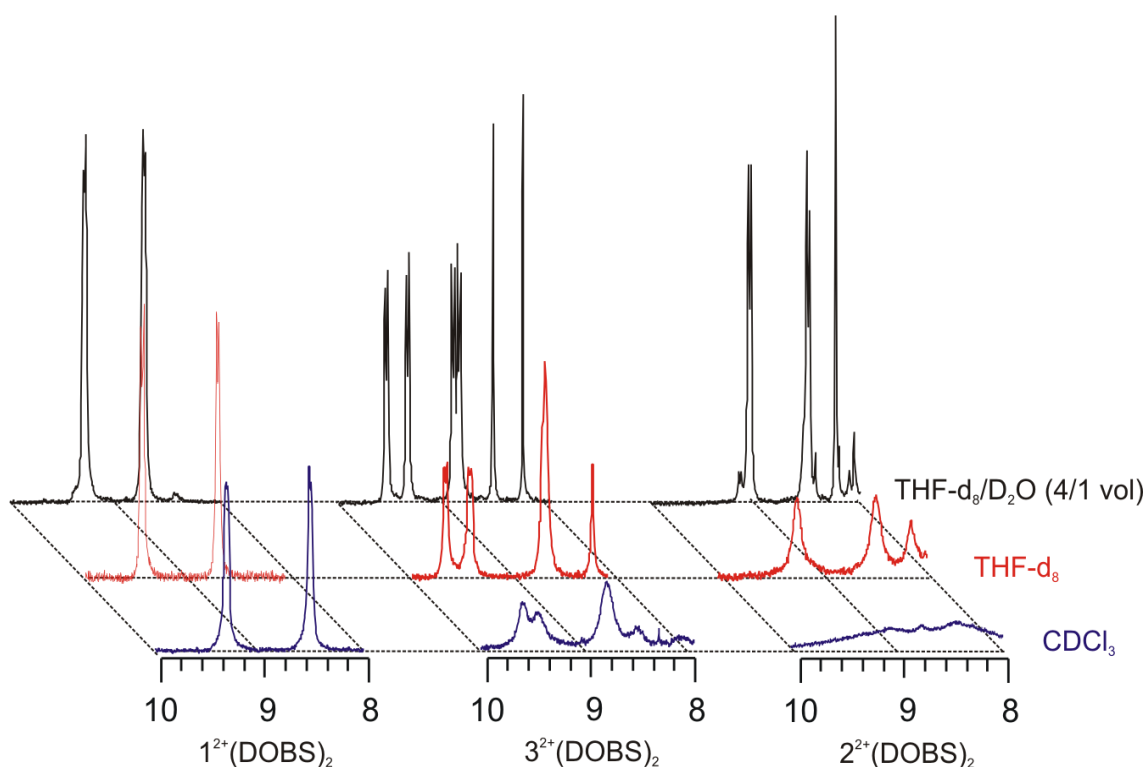


Figure 4.4 $^1\text{H-NMR}$ spectra in the aromatic region of the ionic complexes in different solvent environment at 30°C

The self-association by hydrogen-bonding of ionic complexes was also studied by diffusion-ordered spectroscopy (DOSY). An overlap of the three individual DOSY spectra of ionic complexes $1^{2+}(\text{DOBS})_2$, $2^{2+}(\text{DOBS})_2$ and $3^{2+}(\text{DOBS})_2$ in CDCl_3 at 30°C are presented in Figure 4.5. The diffusion coefficients of the ionic complexes increases in the order $1^{2+}(\text{DOBS})_2 < 3^{2+}(\text{DOBS})_2 < 2^{2+}(\text{DOBS})_2$. The difference in the diffusion coefficients observed in the case of ionic complexes is explained by the

different self-association degree. This trend is in fully agreement with the assumption derived from previously presented one-dimensional $^1\text{H-NMR}$ experiments.

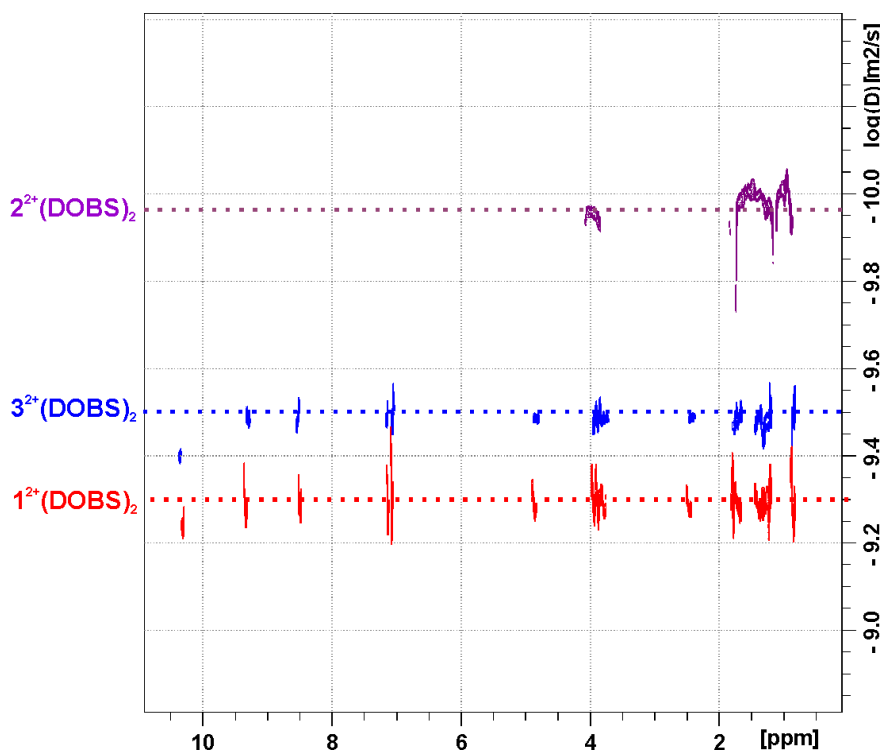


Figure 4.5 Overlapped DOSY spectra of ionic complexes (50 mM) in CDCl_3 at 30°C

The self-association by hydrogen bonding of ionic complexes is an equilibrium process in which the molar ratio of associated and non-associated molecular species depends obviously on the thermodynamic parameters (temperature, concentration) and association constant (K_{ass}). In respect with this, a last series of DOSY experiments were performed with the aimed to investigate the influence of thermodynamic parameters, i.e. temperature and concentration, on the self-association behavior of viologen-nucleobase derivatives. The experiments consisted in monitoring of diffusion coefficients of individually ionic complexes in solution, while the temperature and concentration has been systematically varied.

Figure 4.6 shows the measured diffusion coefficient of compound $2^{2+}(\text{DOBS})_2$ as a function of temperature (a) and concentration (b). From these results it can be concluded that 1) by temperature increase, the self-association degree decreases as a consequence of thermal induced hydrogen bond breaking, and 2) by concentration increase the self-association degree of the molecular species increases.

Combined experiments (DOSY and one-dimensional $^1\text{H-NMR}$) proved that self-association of viologen-nucleobase derivatives is a process strongly influenced by the

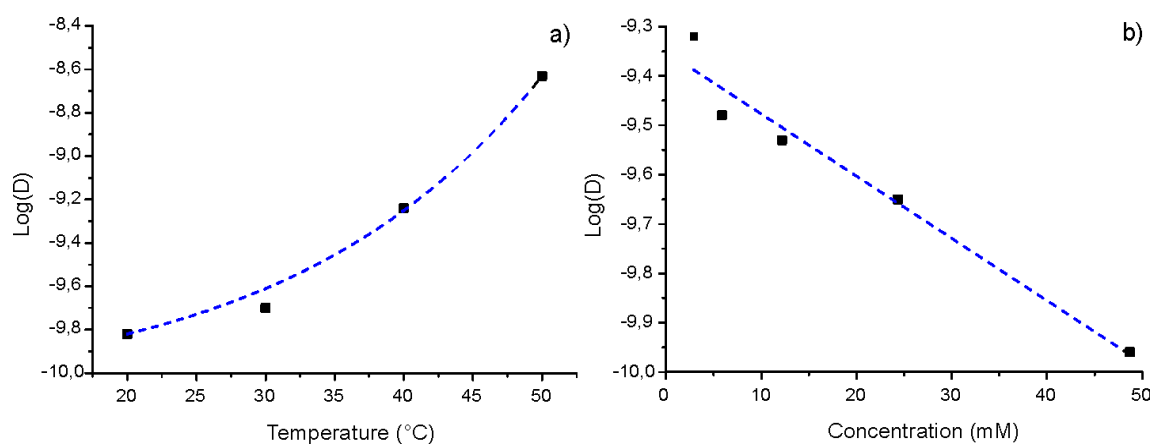


Figure 4.6 Plot of diffusion coefficient (logD) as a function of (a) temperature and (b) concentration determined from DOSY experiments for $2^{2+}(\text{DOBS})_2$ in THF- d_8

nucleobase nature (thymine or adenine), solvent type as well as by the thermodynamic parameters, such as temperature and concentration. The key role of nucleobases in the self-association behavior of viologen-nucleobase ionic complexes was highlighted by direct comparison with the analogue derivative $\text{MV}^{2+}(\text{DOBS})_2$ which did not self-associate in the same environmental conditions.

4.3 Electrochemical properties in low-polar solvents

Electrochemical characterization in solution was performed to study the influence of self-association of ionic complexes on the redox properties of 4,4'-bipyridinium unit. The compounds $1^{2+}(\text{DOBS})_2$, $2^{2+}(\text{DOBS})_2$, $3^{2+}(\text{DOBS})_2$ and analogue derivative $\text{MV}^{2+}(\text{DOBS})_2$ respectively, were investigated by means of cyclic voltammetry at the surface of a glassy carbon electrode at 21°C versus Ag/AgCl (3M KCl) as reference electrode. The analyte concentration was 1mmol/L dissolved in THF containing lithium bis(trifluoromethane)sulfonimide (0.1 mol/L) as supporting electrolyte.

The cyclic voltammograms in Figure 4.7 represent the typical reversible reduction process of the 4,4'-bipyridinium unit from dicationic state (V^{2+}) to radical cation ($\text{V}^{•+}$) and further to the neutral species (V^0). The ratio of the cathodic and anodic current peaks (I_{pc}/I_{pa}) has been determined after baseline correction of the corresponding cyclic voltammograms and satisfies the condition for reversibility ($I_{pc}/I_{pa}=1$) for all four studied compounds. The separation peak potential ($\Delta E=E_{pa}-E_{pc}$) for both reduction steps overcomes the value required for one electron transfer process (<59 mV). This effect is

attributed to the iR drop² rather than to the reversibility of electrochemical process. The iR drop is expected in a solvent with low dielectric permittivity such THF [179].

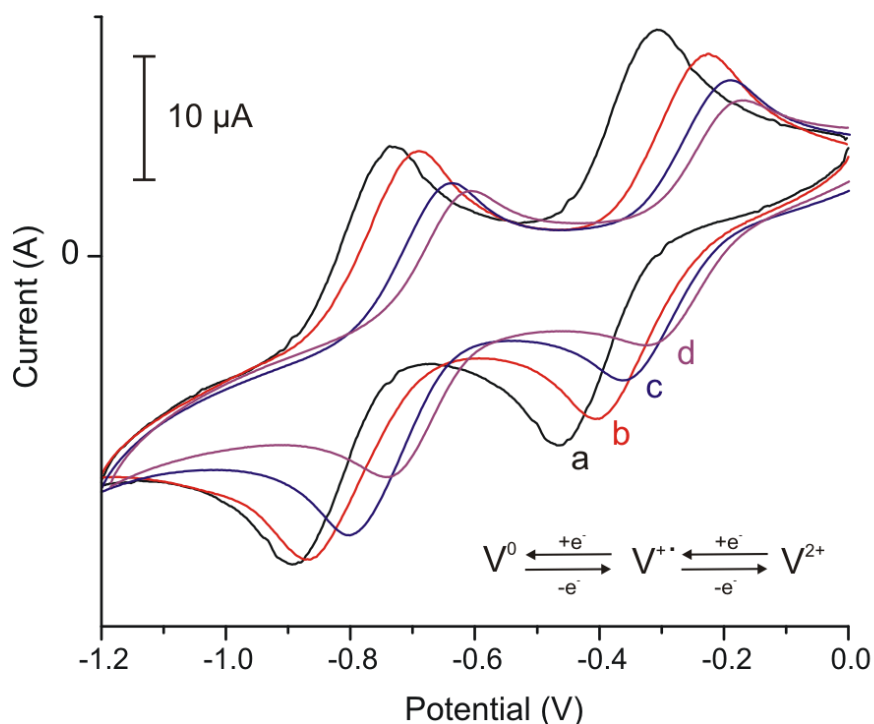


Figure 4.7 Cyclic voltammograms of (0.1 mmol/l) ionic complexes $MV^{2+}(\text{DOBS})_2$ (a), $1^{2+}(\text{DOBS})_2$ (b), $3^{2+}(\text{DOBS})_2$ (c) and $2^{2+}(\text{DOBS})_2$ (d) at $0.6 \text{ V} \cdot \text{s}^{-1}$ scan rate in LiTFSI/THF (0.1 mol/l)

The electrochemical parameters derived from CV measurements are depicted in Table 4.1. The viologen-nucleobase derivatives were reduced at much positive potential then the analogues derivatives $MV^{2+}(\text{DOBS})_2$. On the other hand, the values of formal potentials E^{01} and E^{02} respectively, of viologen-nucleobase ionic complexes follow the same trend as presented in the Chapter 2 for the analogue derivatives $1\text{-}3/\text{PF}_6^-$, measured in DMF/ NaClO_4 electrolyte: the ionic complex $1^{2+}(\text{DOBS})_2$, with two thymine units, was reduced at much negative potential then the ionic complex $2^{2+}(\text{DOBS})_2$, with two adenine units.

The diffusion coefficients of electroactive dicationic species were calculated using the slope of linear regression of the 1st cathodic pick current versus the square root of the scan rate and the Randles–Sevcik equation as presented in Chapter 2, Section 2.2.2. The diffusion coefficient calculated from cyclic voltammetry data (D_{CV}) of the

² iR or *ohmic drop* represents the potential drop between the reference and working electrode caused by the electrolyte conductivity.

corresponding ionic complexes, increase in the order $2^{2+}(\text{DOBS})_2 < 3^{2+}(\text{DOBS})_2 < 1^{2+}(\text{DOBS})_2 < \text{MV}^{2+}(\text{DOBS})_2$ and follow the same trend as the diffusion coefficient values determined from above mentioned DOSY experiments (D_{DOSY}) (cf Table 4.1). However, the diffusion coefficient values obtained from electrochemical data differs from those obtained from DOSY spectroscopy since the experimental condition differs significantly (i.e. concentration, temperature and solvent media) and they are expected to influence the self-association process.

Table 4.1 Electrochemical parameters for the compounds $1^{2+}(\text{DOBS})_2$, $2^{2+}(\text{DOBS})_2$, $3^{2+}(\text{DOBS})_2$ and $\text{MV}^{2+}(\text{DOBS})_2$ from cyclic voltammetry^[a]

Compound	D_{CV} ; D_{DOSY}	ν	E_{pc1} ^[b]	E_{pa1}	E_1° ^[c]	ΔE_1 ^[d]	E_{pc2}	E_{pa2}	E_2°	ΔE_2
$\text{MV}^{2+}(\text{DOBS})_2$	$3.1 \cdot 10^{-6}$;	0.1	-439	-349	-394	90	-850	-759	-805	91
	-	0.3	-447	-320	-384	127	-867	-740	-804	127
		0.6	-454	-310	-382	144	-886	-742	-814	144
		1	-474	-298	-386	176	-896	-737	-817	159
$1^{2+}(\text{DOBS})_2$	$2.1 \cdot 10^{-6}$;	0.1	-374	-244	-309	130	-815	-718	-763	90
	$3.5 \cdot 10^{-6}$	0.3	-383	-239	-311	144	-845	-708	-767	97
		0.6	-396	-227	-312	169	-864	-701	-777	137
		1	-405	-212	-309	193	-881	-684	-783	163
$2^{2+}(\text{DOBS})_2$	$0.6 \cdot 10^{-6}$;	0.1	-342	-198	-248	100	-713	-628	-671	85
	$1.1 \cdot 10^{-6}$	0.3	-298	-181	-243	124	-730	-618	-674	112
		0.6	-305	-169	-248	158	-747	-606	-677	141
		1	-327	-152	-244	183	-762	-598	-680	164
$3^{2+}(\text{DOBS})_2$	$1.3 \cdot 10^{-6}$;	0.1	-332	-225	-279	107	-757	-672	-715	85
	$2.3 \cdot 10^{-6}$	0.3	-347	-200	-274	147	-789	-654	-722	135
		0.6	-352	-195	-274	157	-796	-647	-722	149
		1	-364	-186	-275	178	-820	-642	-731	178

^[a]All potential parameters are expressed in mV versus Ag/AgCl, the diffusion coefficients (D) in $\text{cm}^2 \cdot \text{s}^{-1}$ and the scan rate (ν) in $\text{V} \cdot \text{s}^{-1}$; ^[b] E_{pc1} , E_{pa1} , E_{pc2} and E_{pa2} represent the corresponding half-wave potentials; ^[c] E_1° and E_2° represent the calculated formal potentials; ^[d] ΔE_1 and ΔE_2 represent the separation potentials.

A plot of current peak I_{pc1} against the square root of the scan rate is shown in Figure 4.8. The linear trend of the plot indicates a diffusion-controlled redox process in the range from 0.05 to 1 $\text{V} \cdot \text{s}^{-1}$. In other words, the limiting step that dictates the rate of electron transfer in solution is the diffusion process of the electroactive dicationic viologen species towards the cathode. Since the viologen-nucleobase derivatives were self-

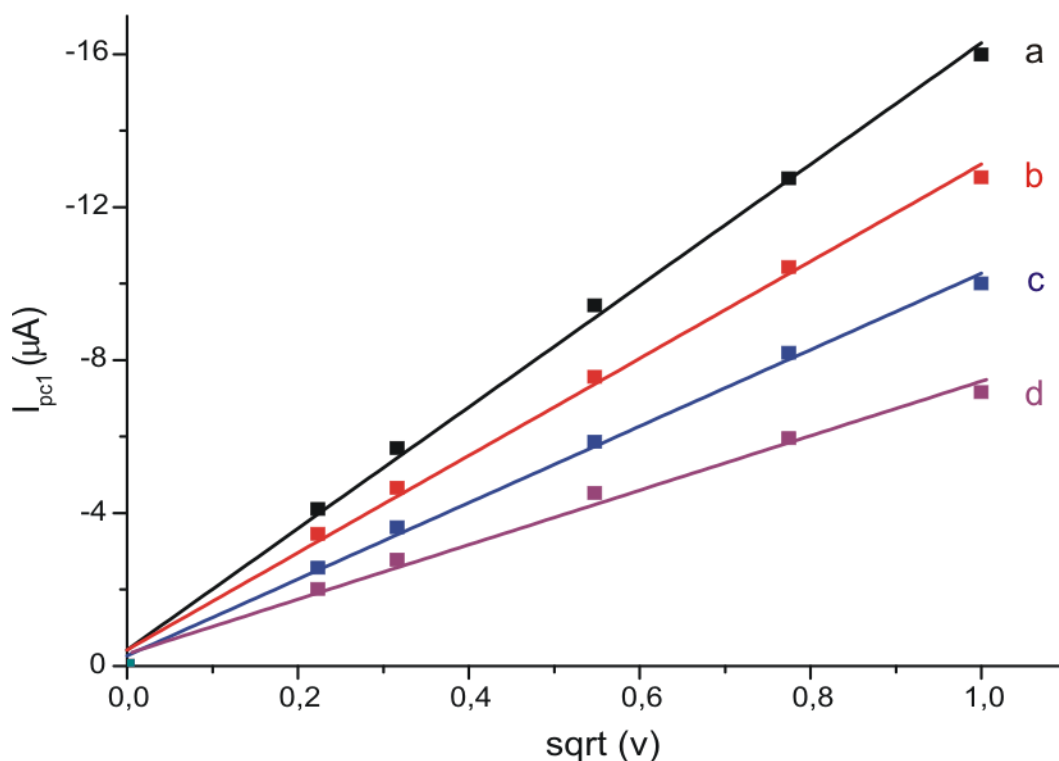


Figure 4.8 Plot of the peak current (I_{pc1}) versus the square root of the scan rate (v), $MV^{2+}(\text{DOBS})_2$ (a), $1^{2+}(\text{DOBS})_2$ (b), $3^{2+}(\text{DOBS})_2$ (c) and $2^{2+}(\text{DOBS})_2$ (d)

associated by hydrogen bonding in THF, as discussed above, the rate of electron transfer was diminished by the slow diffusion of the redox active species, which is reflected in the small value of the slope of linear regression.

To summarize, the electrochemical reduction of viologen-nucleobase ionic complexes $1^{2+}(\text{DOBS})_2$, $2^{2+}(\text{DOBS})_2$ and $3^{2+}(\text{DOBS})_2$ is a one electron two-step reversible process like in the case of analogues derivatives **1-3**/ PF_6^- (cf. Chapter 2). In a media with low polarity (i.e. THF), the rate of electron transfer from cathode to viologen moiety was significantly affected by the slow diffusion in the solution of the self-associated viologen-nucleobase species.

4.4 Thermotropic characterization

Thermal properties of ionic complexes $1^{2+}(\text{DOBS})_2$, $2^{2+}(\text{DOBS})_2$ $3^{2+}(\text{DOBS})_2$ and were investigated by a combination of differential scanning calorimetry (DSC) and thermo-optical polarizing microscopy (TOPM). The DSC program consists in two consecutive heating-cooling cycles recorded with a temperature rate of $10^\circ\text{C}/\text{min}$. The measurements were performed in the temperature range from -60 to 110°C to avoid thermal decomposition. The transition temperature from crystalline to mesophase state

was obtained from the second heating segment. The isotropization transition was determined by direct observation with polarized light microscope. Thermal induced decomposition with loss of mass was checked by thermogravimetric analysis (TGA). To understand the influence of nucleobases capping groups on the thermal properties of viologen-nucleobase derivatives, a comparison with the previously reported analogue $MV^{2+}(\text{DOBS})_2$ [22] was performed.

Figure 4.9 illustrates the corresponding 2nd heating-cooling cycles of ionic complexes. The endothermic peak at 8.2°C for $1^{2+}(\text{DOBS})_2$, -17.7°C for $2^{2+}(\text{DOBS})_2$ and -24°C for $3^{2+}(\text{DOBS})_2$ respectively, corresponds to the melting transition from crystalline to mesophase state as revealed by TOPM (see below). It is noteworthy to say that transition from crystal to LC state of all viologen-nucleobase complexes occurred at considerably low temperature comparing with $MV^{2+}(\text{DOBS})_2$ ($T_m=60^\circ\text{C}$). This is obviously attributed to the presence of thymine and adenine in the chemical structure of the mesogenic unit which influence the supramolecular arrangement, i.e. destabilize the crystalline state.

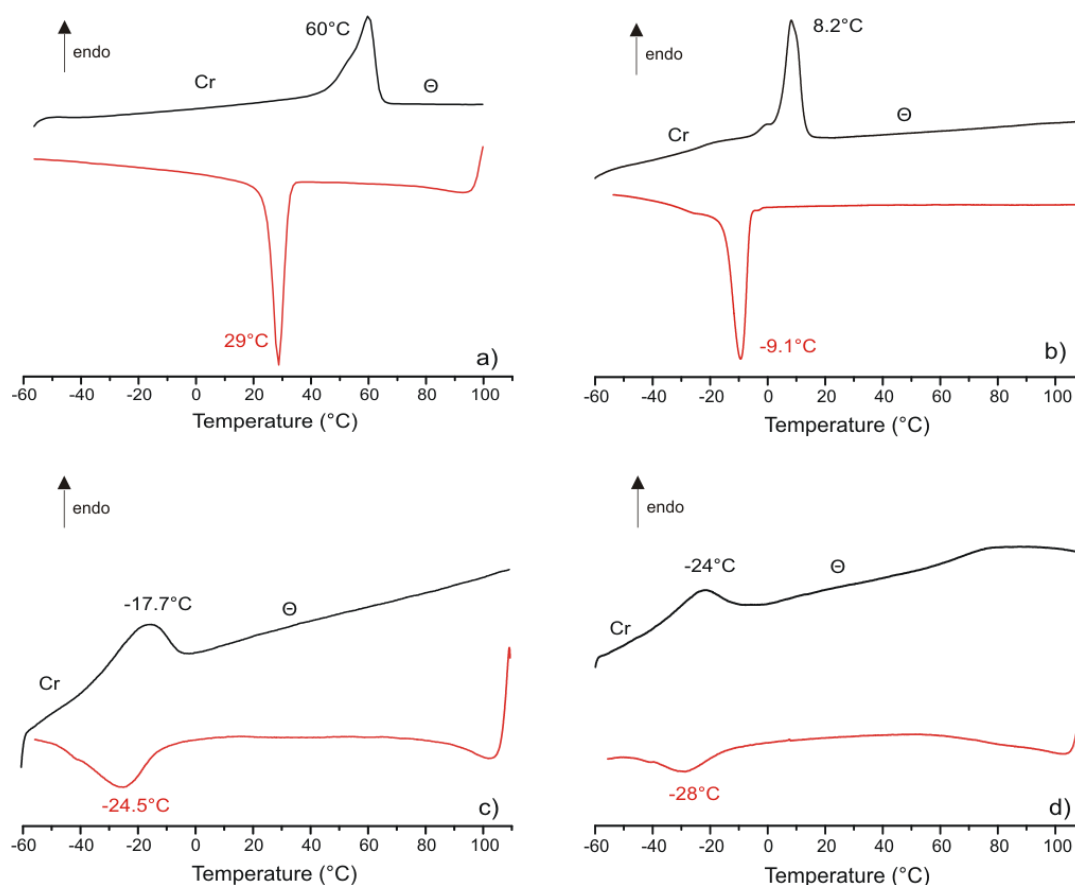


Figure 4.9 DSC 2nd heating-cooling cycle of ionic complexes $MV^{2+}(\text{DOBS})_2$ (a), $1^{2+}(\text{DOBS})_2$ (b), $2^{2+}(\text{DOBS})_2$ (c), and $3^{2+}(\text{DOBS})_2$ (d); Cr = crystalline state, θ = mesophase state. $dT/dt = 10 \text{ K/min}$

The liquid crystalline state of viologen-nucleobase ionic complexes was confirmed by thermo-optical polarized microscopy. Figure 4.10 shows the optical micrographs of derivatives $1^{2+}(\text{DOBS})_2$, $2^{2+}(\text{DOBS})_2$ and $3^{2+}(\text{DOBS})_2$ respectively, at 110°C . The colored domains seen between the cross polarizers above mentioned melting transition seen in DSC indicates that all three viologen-nucleobase derivatives exhibited optical anisotropy. Shearing experiments, performed by mutual sliding of the microscope slides proved the liquid nature of the observed material, hence the compounds are in a mesomorphic state. The undisturbed texture of the mesophase, as obtained by cooling from the isotropic state, has been obtained only from the compound $1^{2+}(\text{DOBS})_2$ which is the only viologen-nucleobase ionic complex stable up to its isotropization temperature. The mesophase texture is different than the one of the compound $\text{MV}^{2+}(\text{DOBS})_2$ revealing the influence of thymine capping units on supramolecular arrangement. Remarkably, the isotropization of $1^{2+}(\text{DOBS})_2$ (192°C) occurred at a considerably lower temperature than for $\text{MV}^{2+}(\text{DOBS})_2$ ($T_{\text{iso}}=270^\circ\text{C}$). The fan-like texture of $1^{2+}(\text{DOBS})_2$ suggests a columnar type mesophase which is an expectable supramolecular arrangement for a discotic mesogen such as 3,4,5-

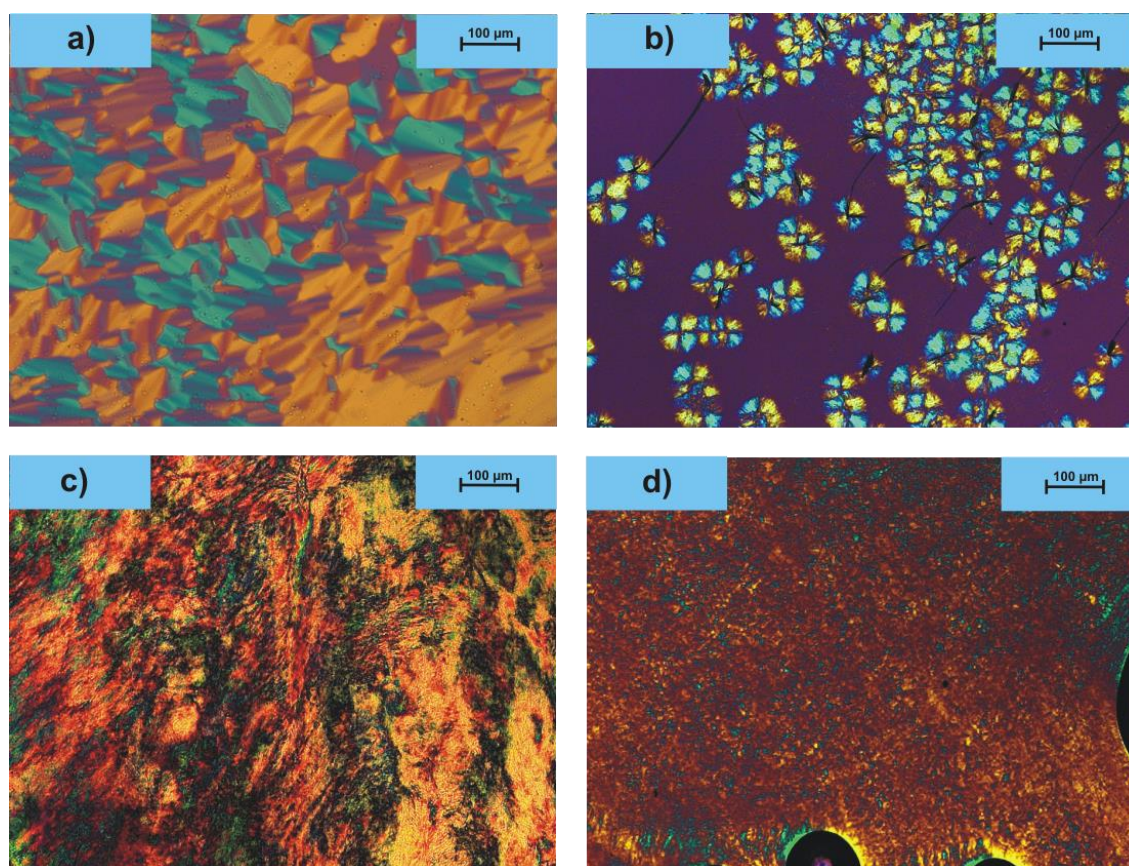


Figure 4.10 The optical micrographs at 110°C between cross polarizers $\text{MV}^{2+}(\text{DOBS})_2$ (a), $1^{2+}(\text{DOBS})_2$ (b), $2^{2+}(\text{DOBS})_2$ (c), and $3^{2+}(\text{DOBS})_2$ (d)

tris(dodecyloxy)benzene sulfonate anion [170]. However, the exact mesophase type of compound $1^{2+}(\text{DOBS})_2$ needs further elucidation by XRD analysis.

The compounds containing adenine, i.e. $2^{2+}(\text{DOBS})_2$ and $3^{2+}(\text{DOBS})_2$, were not thermally stable up to the isotropization point. They changed irreversibly the color into dark brown at elevated temperatures ($>160^\circ\text{C}$) concomitantly with the loss of optical anisotropy. For this reason, it was impossible to obtain an undisturbed texture with characteristic features of the mesophase for these two compounds by cooling from the isotropic state.

Thermogravimetric analysis (Figure 4.11) performed under a helium atmosphere over the temperature range from 30 to 400°C showed the viologen-nucleobase ionic complexes to decompose with loosing of mass at 296°C for compound $1^{2+}(\text{DOBS})_2$, 306°C for compound $2^{2+}(\text{DOBS})_2$ and 300°C for compound $3^{2+}(\text{DOBS})_2$. The viologen-nucleobase ionic complexes were thermally unstable above these temperatures. This is attributed to the chemical instability of 4,4'-bipyridinium in the isotropic state. Notably, the thermal decomposition of analogues derivative $\text{MV}^{2+}(\text{DOBS})_2$ occurred at a temperature value close to those of viologen-nucleobase derivatives (307°C) suggesting that the nucleobases capping groups have a little influence on the thermal decomposition with loosing of mass.

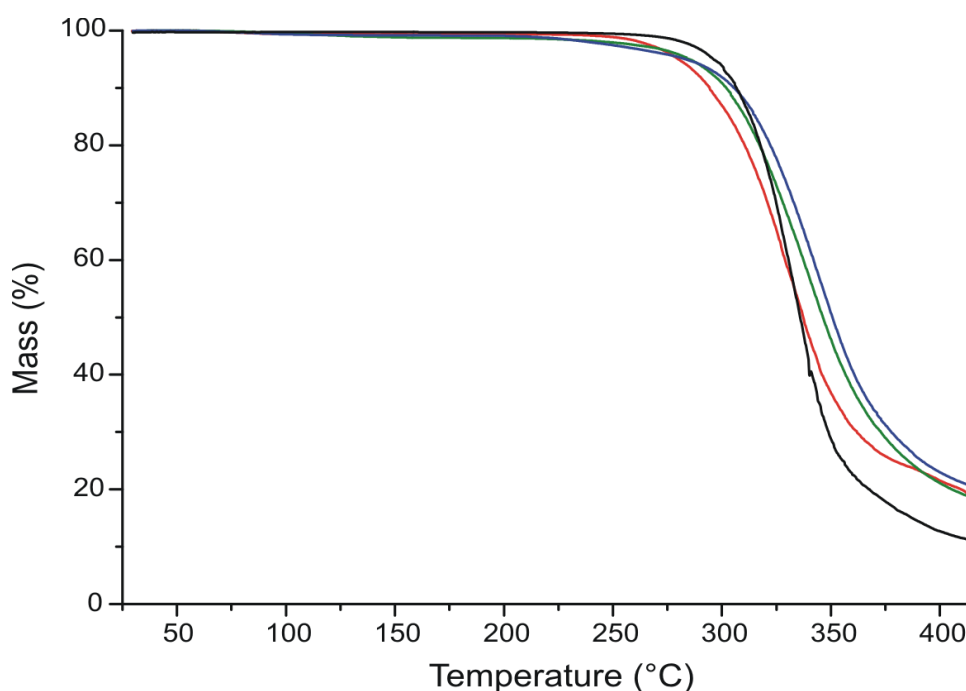


Figure 4.11 TGA analysis of derivatives $1^{2+}(\text{DOBS})_2$ (red line), $2^{2+}(\text{DOBS})_2$ (blue line), $3^{2+}(\text{DOBS})_2$ (green line) and $\text{MV}^{2+}(\text{DOBS})_2$ (black line) in helium atmosphere; $dT/dt=10\text{ K/min}$

The phase transition schemes of derivatives $1^{2+}(\text{DOBS})_2$, $2^{2+}(\text{DOBS})_2$, $3^{2+}(\text{DOBS})_2$ and $\text{MV}^{2+}(\text{DOBS})_2$ respectively, are summarized in Table 4.2.

Table 4.2 Phase transition temperatures and corresponding enthalpies of ionic complexes (DSC onset values, $dT/dt = 10 \text{ }^\circ\text{C}/\text{min}$)

Compound	Phase transition scheme ^[a]
$1^{2+}(\text{DOBS})_2$	Cr, $8.2 \text{ }^\circ\text{C}$ (35) Φ , $192 \text{ }^\circ\text{C}$ I ^[b]
$2^{2+}(\text{DOBS})_2$	Cr, $-17.7 \text{ }^\circ\text{C}$ (22.5) Φ ^[c]
$3^{2+}(\text{DOBS})_2$	Cr, $-24 \text{ }^\circ\text{C}$ (27.5) Φ ^[c]
$\text{MV}^{2+}(\text{DOBS})_2$	Cr, $53 \text{ }^\circ\text{C}$ (52.8), Φ $270 \text{ }^\circ\text{C}$ I ^[b]

^[a] Transition temperatures ($^\circ\text{C}$) and enthalpies (kJ/mol, in parentheses) determined by DSC during the 2nd heating run; ^[b] Isotropization temperatures determined by thermo-optical analysis; ^[c] Thermal unstable up to 160°C ; Cr = solid crystal, Φ = mesophase, I = isotropic phase

4.5 Ionic conductivity and cyclic voltammetry in LC state

Ionic conductivity measurements of ionic complexes $1^{2+}(\text{DOBS})_2$, $2^{2+}(\text{DOBS})_2$ and $3^{2+}(\text{DOBS})_2$, were performed in a two-electrode electrochemical cell “sandwich” setup, consisting of two conductive indium tin oxide (ITO) glass plates connected to an electrical potential source. The sample was confined in the form of a thin film of approx. $50 \text{ }\mu\text{m}$ thickness by compression between the two electrodes.

A constant potential (-2V) was applied between the conductive ITO plates in the temperature range from 30 to $90 \text{ }^\circ\text{C}$. The flowing current observed in the external circuit was monitored over the time. By knowing the temperature ramp of $4 \text{ K}/\text{min}$, the chronoamperometric curves were converted to current/temperature plots (Figure 4.12). The ionic complexes were in LC state in the chosen measurement temperature range. No columbic current was observed during the measurements. Figure 4.12 illustrates two temperature regimes where the conductive properties are distinctive:

- 1) Low temperature regime (below 330 K) in which no current was observed passing between the electrodes. The ionic liquid crystals were highly viscous in this temperature range and they behaved more as insulator materials;
- 2) High temperature regime (above 330 K) in which the ionic complexes become less viscous and an exponential conductive current was observe regime, since the conductive current was increasing with the temperature.

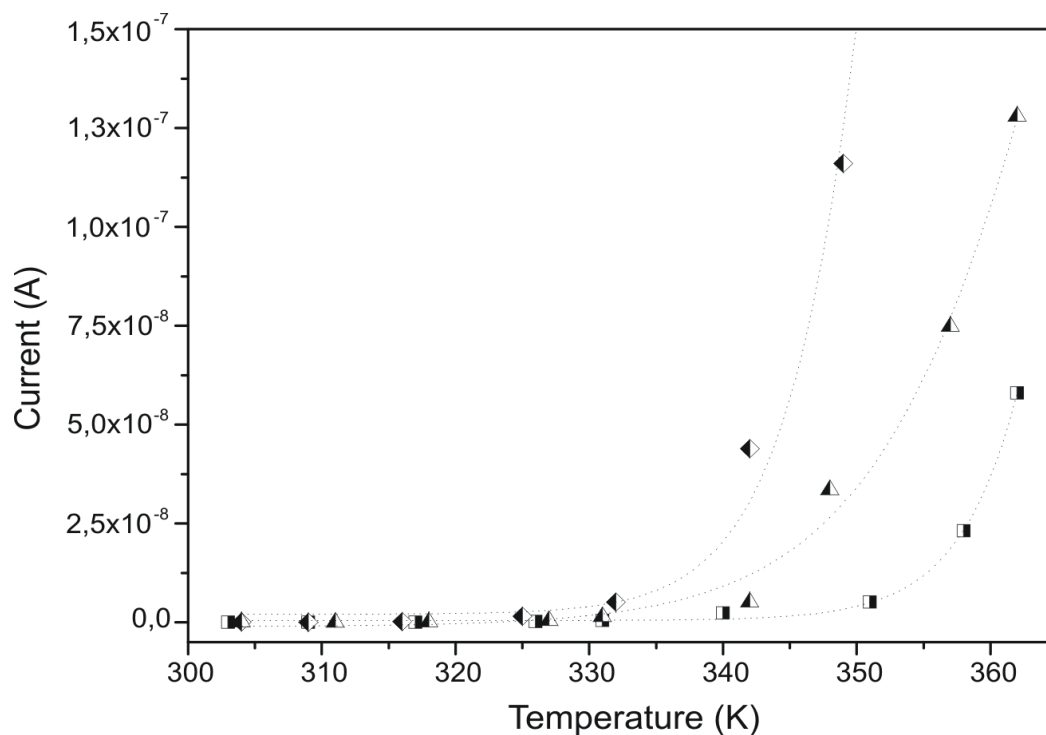


Figure 4.12 Plot of current versus temperature at constant voltage (-2V) for ionic complexes $1^{2+}(\text{DOBS})_2$ (■), $2^{2+}(\text{DOBS})_2$ (◆) and $3^{2+}(\text{DOBS})_2$ (▲)

Figure 4.13 presents the Arrhenius plot of conductivity in the high temperature regime (above 330K) for the ionic complexes $1^{2+}(\text{DOBS})_2$, $2^{2+}(\text{DOBS})_2$ and $3^{2+}(\text{DOBS})_2$ respectively. The activation energy (E_a) was calculated with the formula 4.2 [180]:

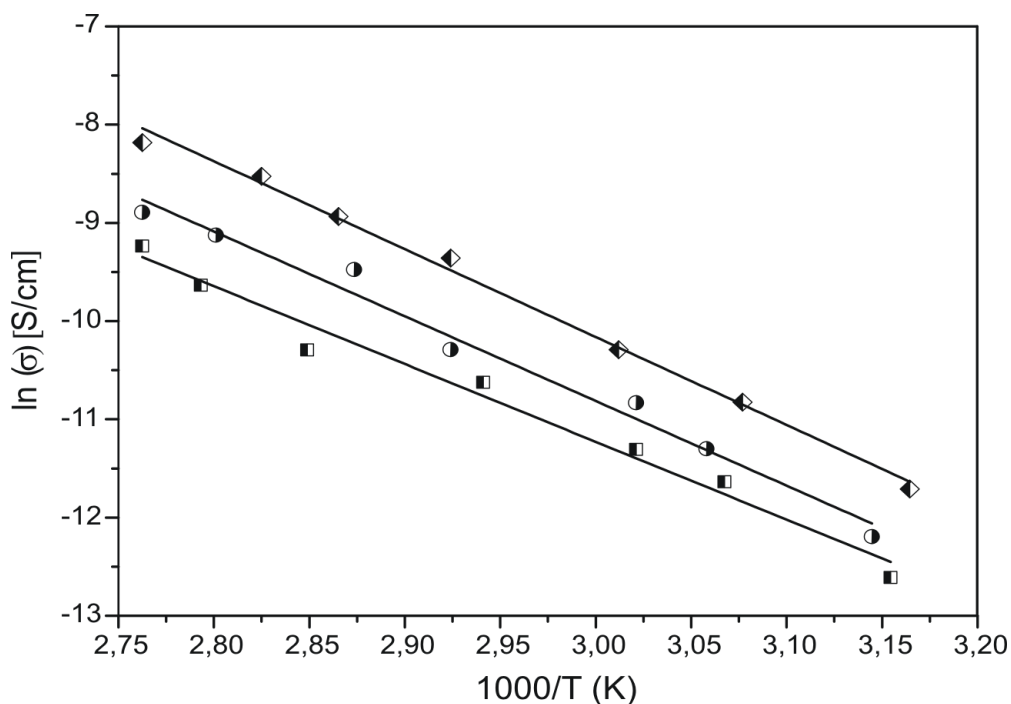


Figure 4.13 Arrhenius plots of ionic conductivity versus reciprocal temperature for ionic complexes $1^{2+}(\text{DOBS})_2$ (■), $2^{2+}(\text{DOBS})_2$ (◆) and $3^{2+}(\text{DOBS})_2$ (▲) at constant voltage (-2V)

$$E_a = - (m \cdot R) \quad (4.2)$$

where m is the slope of Arrhenius plot ($1000 \cdot K$) and R is the gas constant ($8.314 \text{ J} \cdot \text{K}^{-1} \cdot \text{mol}^{-1}$).

The values of activation energy are 65.85 kJ/mol for $1^{2+}(\text{DOBS})_2$, 71.67 kJ/mol for $2^{2+}(\text{DOBS})_2$ and 74.41 kJ/mol for $3^{2+}(\text{DOBS})_2$.

Cyclic voltammetry in the solid state was performed in the same electrochemical setup as for previous ionic conductivity measurements, with a scan rate of $0.01 \text{ V} \cdot \text{s}^{-1}$ at a temperature at which the ionic complexes were in LC state with low viscosity (90°C).

Figure 4.14 shows the corresponding cyclic voltammograms of the compounds

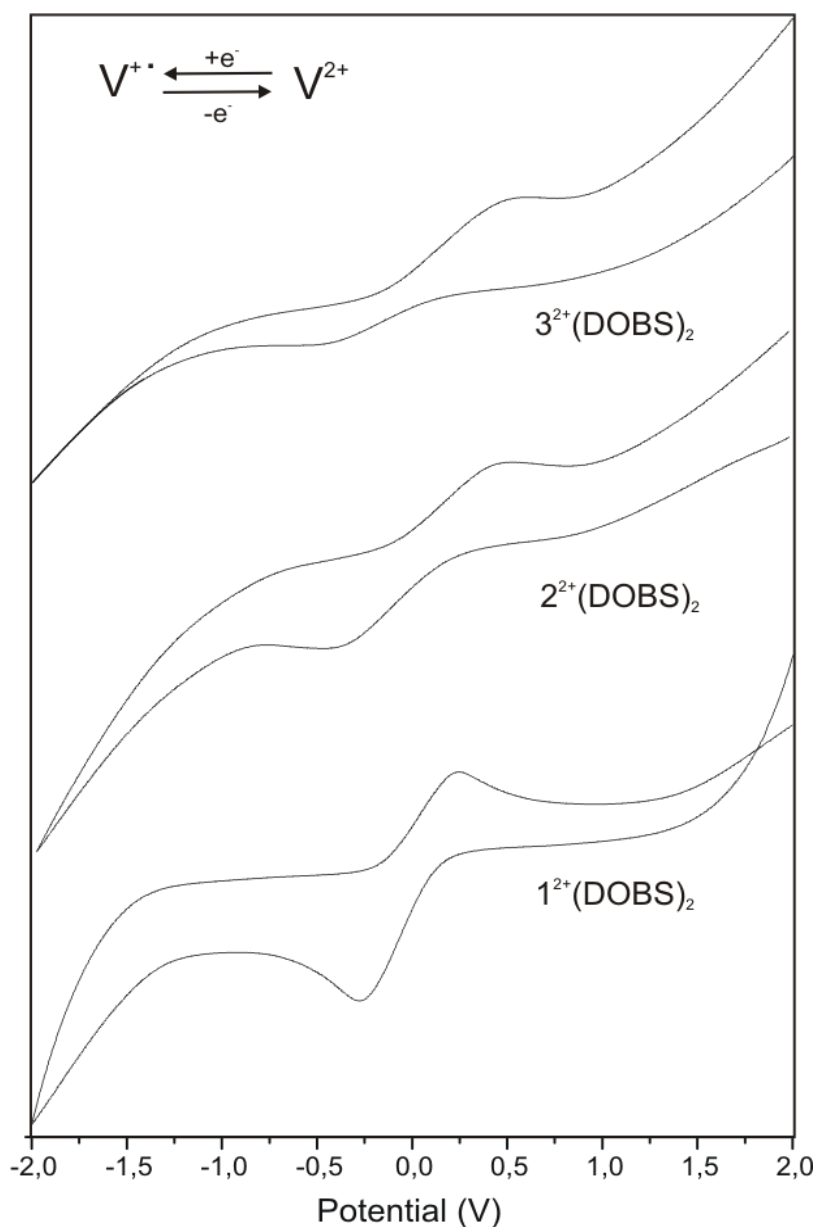


Figure 4.14 Cyclic voltammograms in molten state of the ionic complexes $1^{2+}(\text{DOBS})_2$, $2^{2+}(\text{DOBS})_2$ and $3^{2+}(\text{DOBS})_2$ at 90°C . Scan rate $0.01 \text{ V} \cdot \text{s}^{-1}$

$1^{2+}(\text{DOBS})_2$, $2^{2+}(\text{DOBS})_2$ and $3^{2+}(\text{DOBS})_2$ in molten state. The reversible coulombic current seen in all three cyclic voltammograms represents the reduction of the 4,4'-bipyridinium-nucleobase dicationic species (V^{2+}) to the corresponding radical cationic state (V^+). The hysteresis observed in the CV's of ionic complexes is most probably the result of convective movements which occurred at the surface of the working electrode. Cyclic voltammetry experiments of ionic complexes demonstrated that the mobility of ionic species (i.e. ionic conductivity) has a significant value at elevated temperature, fact that facilitated the electron transfer from the electrode to the redox active viologen species.

4.6 Thermal-induced electrochromism in LC state

A change of the optical properties of the bulk material has been observed when compact films of the compounds $1^{2+}(\text{DOBS})_2$, $2^{2+}(\text{DOBS})_2$ and $3^{2+}(\text{DOBS})_2$ respectively, were heated between two glass plates without any applied voltage. The thin films changed their color instantly (small ΔT) from pale-yellow to blue-green above 110°C (Figure 4.15).

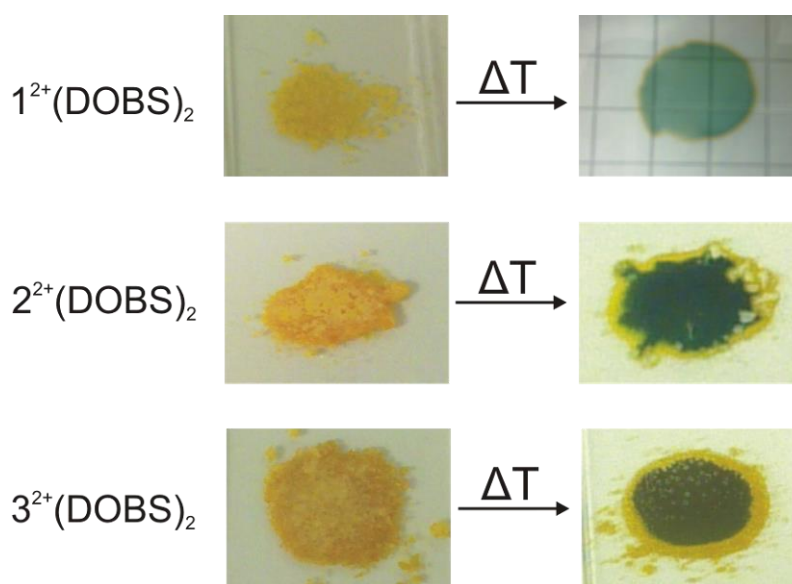


Figure 4.15 Thin-film of ionic complexes $1^{2+}(\text{DOBS})_2$, $2^{2+}(\text{DOBS})_2$ and $3^{2+}(\text{DOBS})_2$ respectively, compressed between two glass slides, before and after thermal treatment

A similar behavior was previously reported for the analogue derivative $MV^{2+}(\text{DOBS})_2$ [22]. The coloration of the bulk material was assigned to the reduction of viologen moiety from the dicationic state (V^{2+}) to the blue colored radical cationic species (V^+). It is noteworthy to say that the color change did not occur at the outer rim of the thin

films where the contact with the air is imminent and the formed radical species are spontaneously oxidized back in the presence of the atmospheric oxygen.

Figure 4.16 illustrates the Vis spectra of the thin films of respective compounds $1^{2+}(\text{DOBS})_2$, $2^{2+}(\text{DOBS})_2$ and $3^{2+}(\text{DOBS})_2$, after exposure at 110°C between two glass plates without any applied voltage. The typical absorption band with a maximum wavelength at 600 nm demonstrates the formation of monomeric radical cationic species ($V^{\bullet+}$). The reversible oxidation of the film (color change from blue-green to yellow) occurred when the film was cooled down at room temperature (approx. 21°C) and stand for more than 12 hours.

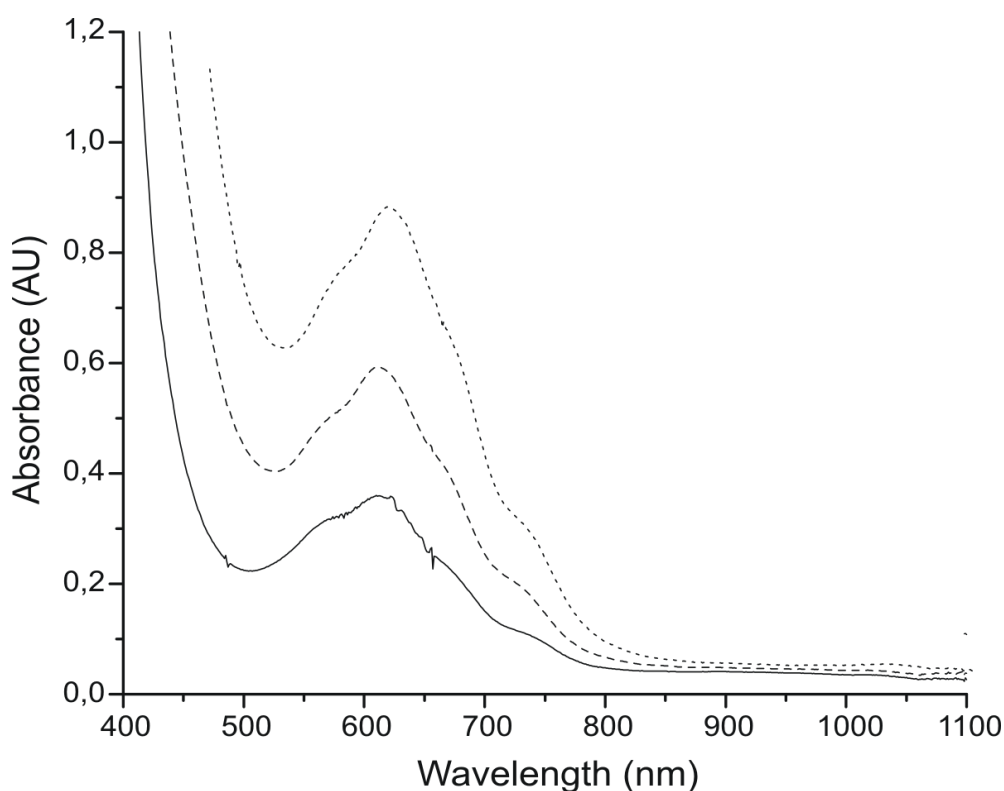


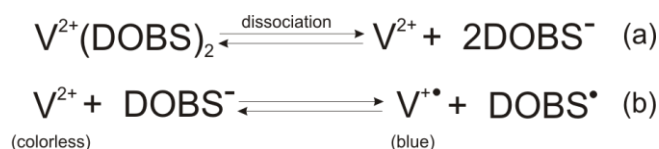
Figure 4.16 VIS spectra of thin-film of viologen-nucleobase ionic complexes $1^{2+}(\text{DOBS})_2$ (continuous line), $2^{2+}(\text{DOBS})_2$ (dotted line) and $3^{2+}(\text{DOBS})_2$ (dashed line) after exposure to 110°C

As previously mentioned, at elevated temperatures (above 60°C) the liquid crystalline compounds $1^{2+}(\text{DOBS})_2$, $2^{2+}(\text{DOBS})_2$ and $3^{2+}(\text{DOBS})_2$ started to behave as 2^{nd} order conductors as a result of increase in ionic mobility. Under this conditions the electron transfer from the anion 3,4,5-tris(dodecyloxy)benzene sulfonate, which act as an electron donor source, to the viologen moiety (electron acceptor) was facilitated. Extensive work of Haramoto [83] and Nanasawa [84] also demonstrated that the long alkylbenzene sulfonate counter anion may act as electron source for the photoreduction of N,N' -diphenylbipyridinium derivatives in LC state. On the other side, Kato et al.

[181, 182] came to the conclusion that the mobility of the ionic species plays a crucial role in the redox activity of the liquid crystal materials combining ionic and electronic functions. More recently, Beneduci et al. (2014) [183] emphasized on the importance of ionic conductivity on the electrochromic properties in the bulk state of the π -conjugated thienoviologens liquid crystals, compounds with similar redox activity such the one reported on this thesis.

Remarkably, the electrochromic reaction of derivatives $1^{2+}(\text{DOBS})_2$, $2^{2+}(\text{DOBS})_2$ and $3^{2+}(\text{DOBS})_2$ did not required any external applied potential like the nanostructured redox liquid crystals reported by Kato or Beneduci [181-183].

In conclusion, the reduction of viologen units occurred spontaneously at a temperature at which the material existed in LC state with sufficiently low viscosity to allow the charge transport in the bulk liquid crystal. A possible mechanism of electron transfer is illustrated in Scheme 4.3.



Scheme 4.3 Thermal-induced electrochromism in viologen-nucleobase derivatives

Summary:

A new class of redox active ionic liquid crystals (ILC's) based on ion pairing of dicationic viologen-nucleobase derivatives $1/\Gamma$ - $3/\Gamma$ with amphiphilic anion 3,4,5-tris(dodecyloxy)benzene sulfonate (DOBS^-) were synthesized and characterized with respect to structure, self-assembly, and electrochemical properties. The viologen-nucleobase derivatives $1^{2+}(\text{DOBS})_2$, $2^{2+}(\text{DOBS})_2$ and $3^{2+}(\text{DOBS})_2$, self-associate in low-polar solvents by hydrogen bonding between nucleobases. $^1\text{H-NMR}$ and DOSY experiments demonstrated the degree of self-association to strongly depend on the nature of the capping groups (i.e. thymine or adenine), solvent polarity, temperature and concentration. The rate of electron transfer during electrochemical reduction of viologen-nucleobase derivatives in THF was significantly diminished as a consequence of self-association by hydrogen bonding. The viologen-nucleobase derivatives $1^{2+}(\text{DOBS})_2$, $2^{2+}(\text{DOBS})_2$ and $3^{2+}(\text{DOBS})_2$ exhibited liquid crystalline properties. The transition from solid crystalline to liquid crystal state occurred at lower temperature compared to the analogue derivative $\text{MV}^{2+}(\text{DOBS})_2$. The compound $1^{2+}(\text{DOBS})_2$,

containing exclusively thymine units, exhibited a stable mesophase until isotropization while the compounds $2^{2+}(\text{DOBS})_2$ and $3^{2+}(\text{DOBS})_2$, containing adenine, were unstable prior transition into the isotropic state. The fan-shaped texture of the mesophase of compound $1^{2+}(\text{DOBS})_2$ suggests a columnar type mesophase. The ionic complexes behaved as 2nd order conductors in the mesophase, at a temperature at which viscosity increased significantly. Ionic mobility facilitated the electron transfer from the anion DOBS^- to the viologen unit, that was readily transformed in the radical cationic state under anaerobic conditions.

This new class of thermotropic viologen-nucleobase derivatives, combining hydrogen-bonding and redox functionalities has a great potential to be used for the construction of optoelectronic devices.

CHAPTER 5**Hydrogen Bonded Layer-by-Layer Deposition of Viologen-Nucleobase Derivatives on Mesoporous TiO₂ Film for Optoelectronic Devices**

This work aims to develop a facile method to assemble viologen-nucleobase derivatives on TiO₂ substrates using the layer-by-layer technique and exploiting the adenine-thymine molecular recognition as driving force.

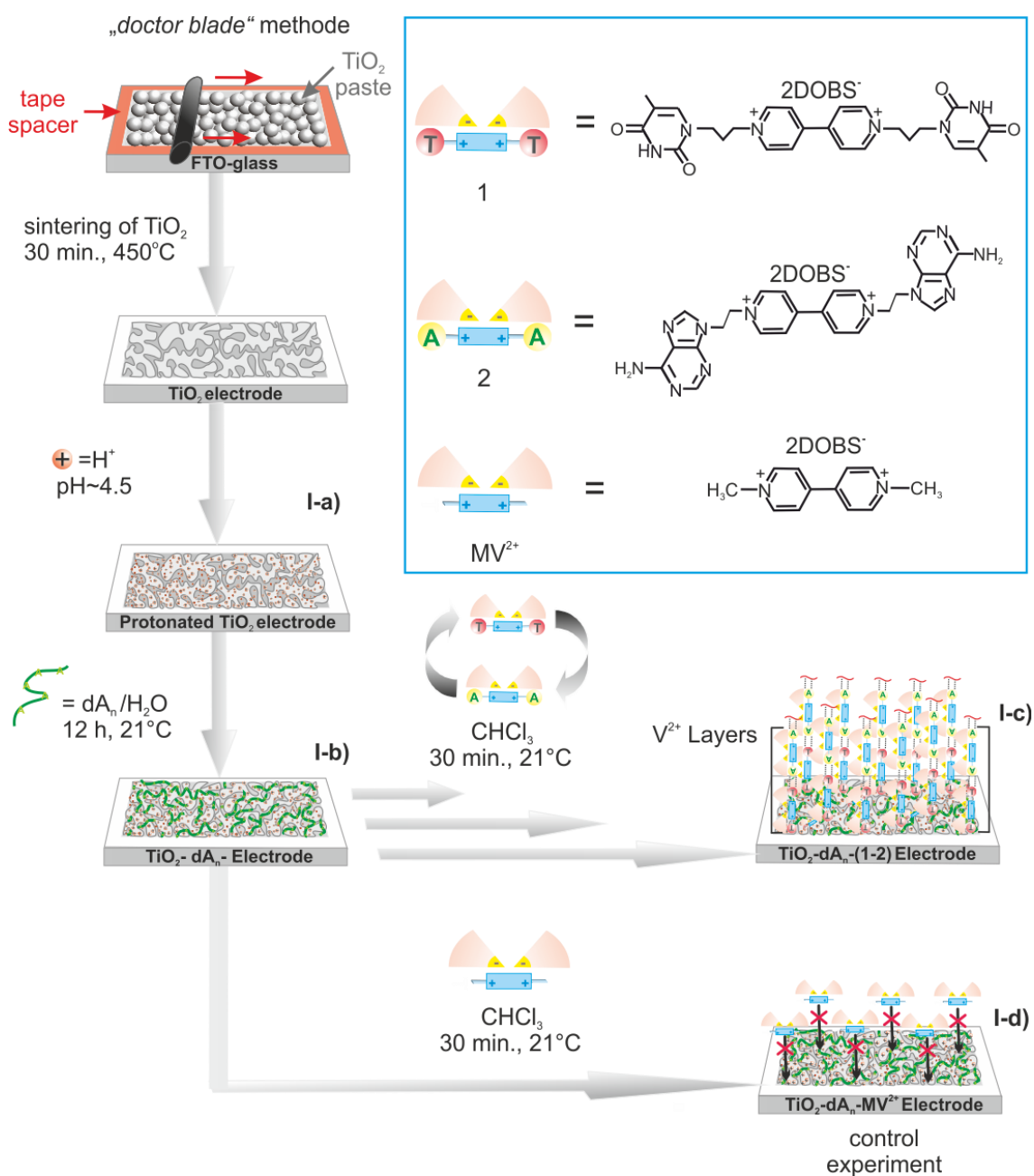
The general concept implies deposition of complementary amphiphilic viologen-nucleobase derivatives **1**²⁺(DOBS)₂ and **2**²⁺(DOBS)₂ on the surface of mesoporous TiO₂ films pre-modified with a layer of an adenylic ssDNA (dA_n) or a phosphonate-viologen-thymine derivative **4/Br**⁻, hereafter referred as “anchoring layer”. The compound **4/Br**⁻ has been specially designed to replace the anchoring function of ssDNA on TiO₂ surface and its synthesis will be discussed.

In a first step, the surface modification is achieved by immersing the mesoporous nanocrystalline TiO₂ film, fabricated by *doctor blade* method, into an aqueous solution of adenylic ssDNA (Scheme 5.1) or into an aqueous solution of phosphonate-viologen-thymine derivative **4/Br**⁻ (Scheme 5.2). The process consisted in coordination of a bifunctional –PO₃H₂ anchoring group onto the inner walls of the mesoporous TiO₂ film as a self-assembled monolayer (SAM). In a second step, the obtained nucleobase-confined surface is exposed to a solution of the complementary viologen-adenine or viologen-thymine derivative, hence further molecules become linked together by hydrogen bonding in low-polar solvent which favors the hydrogen bonding formation.

The strategic route involving ssDNA as anchoring layer is representatively illustrated in Scheme 5.1. In a first set of experiments, the self-assembly process of short single stranded DNA (dA_n) with variable length (dA₁, dA₅, dA₈ and dA₈₀) on the surface of TiO₂ mesoporous film has been systematically investigated (Scheme 5.1, I-a and I-b). The influence of ssDNA length on the stability and respectively surface coverage of self-assembled ssDNA monolayer has been addressed.

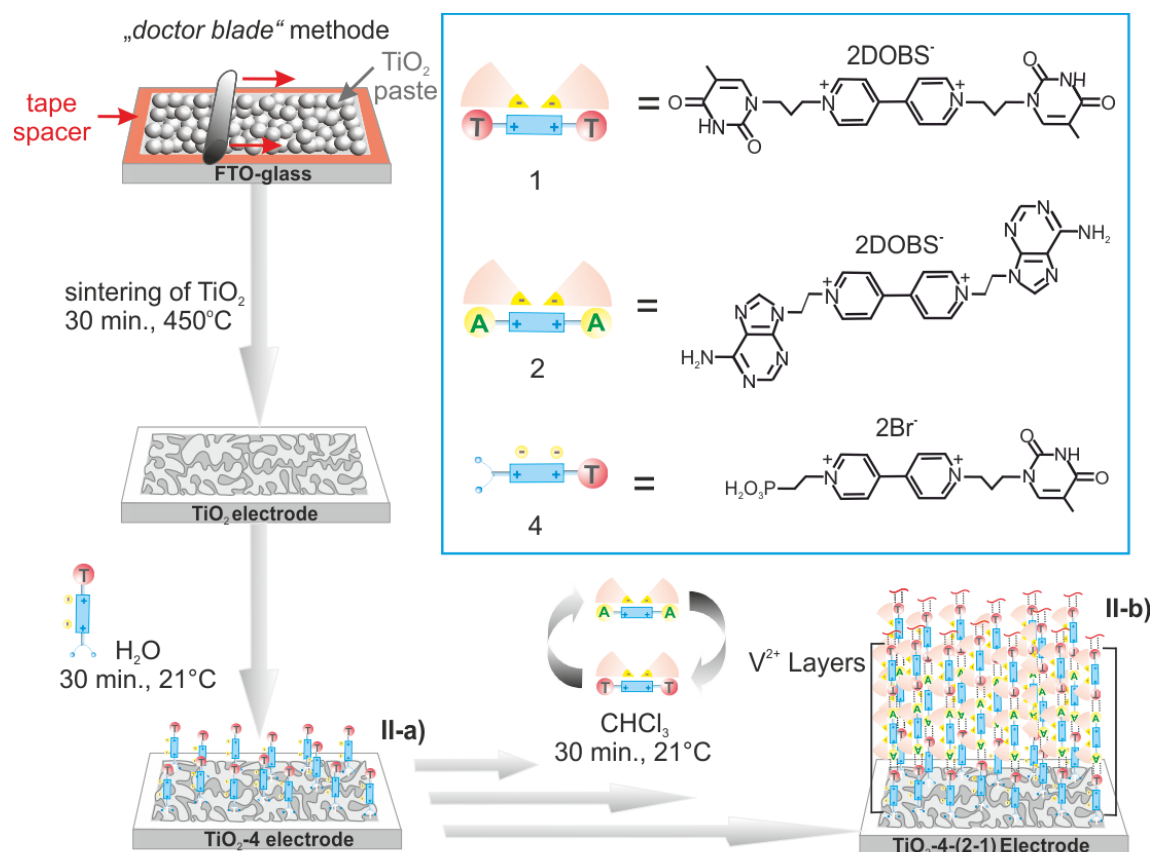
In a second set of experiments, the complementary viologen-nucleobase derivatives $1^{2+}(\text{DOBS})_2$ and $2^{2+}(\text{DOBS})_2$ were adsorbed in repetitive alternating steps on the surface of pre-modified TiO_2 film with oligonucleotide dA_8 (Scheme 5.1, I-c).

The ability of viologen-nucleobase derivatives to bind specifically to the surface ssDNA-modified film was proved in a control experiment where the dA_8 -modified TiO_2 electrode was immersed in a solution of analogue viologen derivative $\text{MV}^{2+}(\text{DOBS})_2$ in the same experimental condition (Scheme 5.1 route I-d).



Scheme 5.1 Hydrogen bonded layer-by-layer deposition of viologen-nucleobase derivatives on mesoporous TiO_2 film. Route Ia-c using dA_n ($n=1, 5, 8, 80$) as anchoring layer. DOBS^- denotes 3,4,5-tris(dodecyloxy)benzene sulfonate anion

The route of modification involving an anchoring layer made from compound **4/Br⁻** is representatively illustrated in Scheme 5.2. The TiO₂ electrode is first functionalized with phosphonate-viologen derivative **4/Br⁻** (Scheme 5.2, II-a) and subsequently modified by LbL technique with complementary viologen-nucleobase derivatives in alternating layers (Scheme 5.2 II-b).



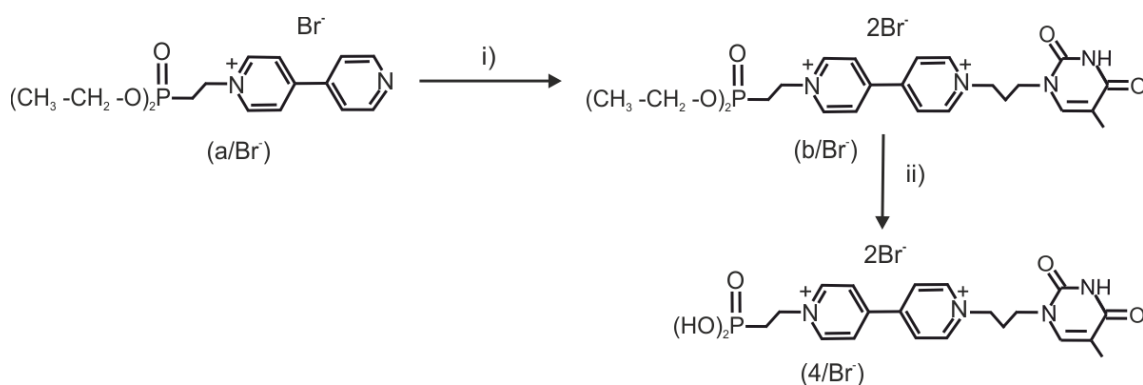
Scheme 5.2 Hydrogen bonded layer-by-layer deposition of viologen-nucleobase derivatives on mesoporous TiO₂ film. Route IIa-b using phosphonate viologen derivative **4/Br⁻** as anchoring layer. DOBS⁻ denotes 3,4,5-tris(dodecyloxy)benzene sulfonate anion

5.1 Synthesis of a phosphonate-viologen derivative **4/Br⁻**

A new asymmetric phosphonate-viologen capped by thymine (compound 1-[3-(5-methyl-2,4-dioxo-3,4-dihydropyrimidin-1(2H)-yl)propyl]-1'-(2-phosphonate)-4,4'-bipyridinium dibromide (**4/Br⁻**)) was synthesized. The molecular design of compound **4/Br⁻** consists of a viologen core capped at one side by a phosphonate group and at the other side by a thymine unit (Scheme 5.3). The advantage of the compound (**4/Br⁻**) over using ssDNA as anchoring layer is that it can bind more tightly to TiO₂ substrate, and can enhance the density of the thymine units at the surface of TiO₂. In consequence, an

increase of the surface concentration of the complementary viologen-nucleobase species that can be adsorbed in the further alternating layers is expected.

Compound **4/Br⁻** was synthesized in two reaction steps (Scheme 5.3). The synthesis started from the precursor derivative 1-[2-(diethoxyphosphoryl)ethyl]-4-(pyridin-4-yl)pyridinium monobromide (**a/Br⁻**) prepared as reported in literature [184] by S. Asaftei (see Chapter 6 for purity and spectroscopic details). In a first step, the compound **a/Br⁻** was alkylated at the nitrogen atom of 4,4'-bipyridine unit by nucleophilic substitution reaction with an excess of 1-(3-bromopropyl)thymine at 80°C for 12 hours. The resulting asymmetrical substituted 4,4'-bipyridinium derivative 1-[3-(5-methyl-2,4-dioxo-3,4-dihydropyrimidin-1(2H)-yl)propyl]-1'-(2-phosphonoethyl)-4,4'-bipyridinium dibromide (**b/Br⁻**) was subsequently hydrolysed in the presence of HBr solution (1M) at 130°C for 72 hours to afford the analogue derivative (**4/Br⁻**) in 87% yield after purification.



Scheme 5.3 Synthesis route of viologen-nucleobase derivative **4/Br⁻**: step i) 1-(3-bromopropyl)thymine, MeCN, 12 h, 80°C, 62%; step ii) 1M HBr, 72 h, 130°C, 87%

The molar integrity of the new synthesized derivatives **b/Br⁻** and **4/Br⁻** respectively was checked by ¹H-NMR spectroscopy (cf. Figure 5.1).

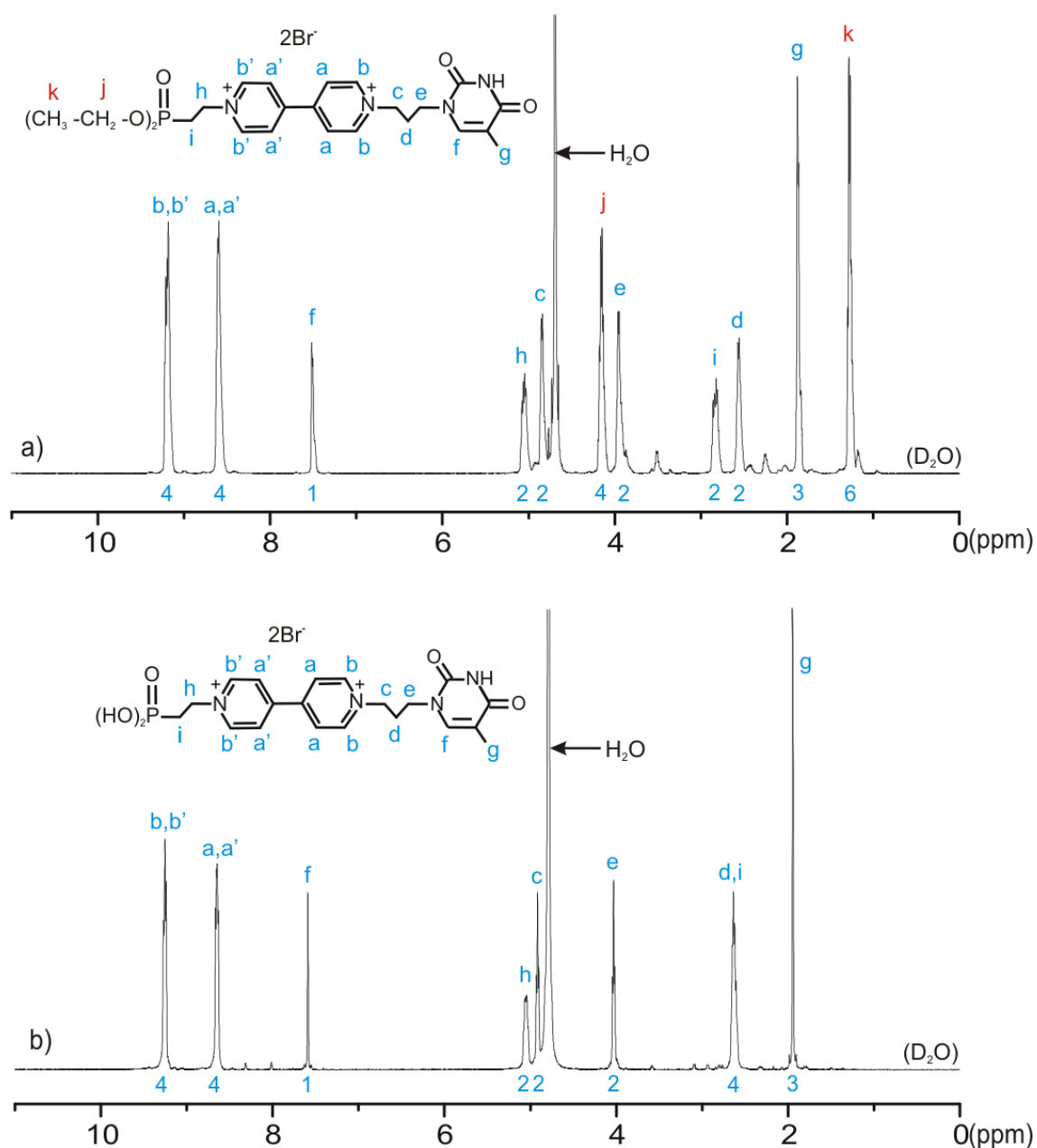


Figure 5.1 $^1\text{H-NMR}$ spectra of b/Br^- (a) and $4/\text{Br}^-$ (b)

5.2 ssDNA-modified TiO_2 film

5.2.1 Preparation and electrochemical characterization

Mesoporous TiO_2 films with a geometrical area (A) in the range $0.43\text{--}0.68\text{ cm}^2$ and $5\text{ }\mu\text{m}$ thickness, coated by the *doctor blade* method on FTO^3 conductive glass, were modified with a series of five adenylic single stranded DNA (dA_n) of different degree of

³ Fluorine doped tin oxide

polymerization n : dA_1 , dA_5 , dA_8 and dA_{80} respectively. The modification was achieved by dip-coating of TiO_2 electrodes in HCl-aqueous solutions of dA_n (pH = 4.5, conc.⁴ = 650 μ M) for 12 hours at 21°C. Successful deposition of ssDNA monolayer on the surface of the TiO_2 electrodes was verified by cyclic voltammetry using the ion-channel sensing principle [185, 186] of the redox anion marker $[Fe(CN)_6]^{4-}$ in aq. KCl (0.1M) electrolyte.

Figure 5.2 illustrates the quasi-reversible one-electron oxidation process of $[Fe(CN)_6]^{4-}$ to $[Fe(CN)_6]^{3-}$ at the surface of unmodified and ssDNA-modified TiO_2 electrodes respectively. The faradaic current resulting from the oxidation of $[Fe(CN)_6]^{4-}$ anions appeared diminished in the case of TiO_2 electrodes modified with dA_n compared to the unmodified TiO_2 electrode (Figure 5.2). The diminishing of the current response was the result of electrostatic repulsion between the marker anions and negatively charged ssDNA layer adsorbed on TiO_2 surface [187]. The adsorption of ssDNA on mineral surfaces and particularly surface oxides such as TiO_2 was discussed previously in literature [188-191]. Those authors claimed that at low pH, nucleic acid bounding occurs predominantly electrostatic between the negatively charged phosphate backbone and the positive sites ($\equiv TiOH_2^+$ or $\equiv Ti^+$) existing at the surface of TiO_2 . In the case of dA_1 -modified TiO_2 electrode a quasi-reversible oxidation process was observed in which the separation peak ($\Delta E=169$ mV) was higher than in the case of the

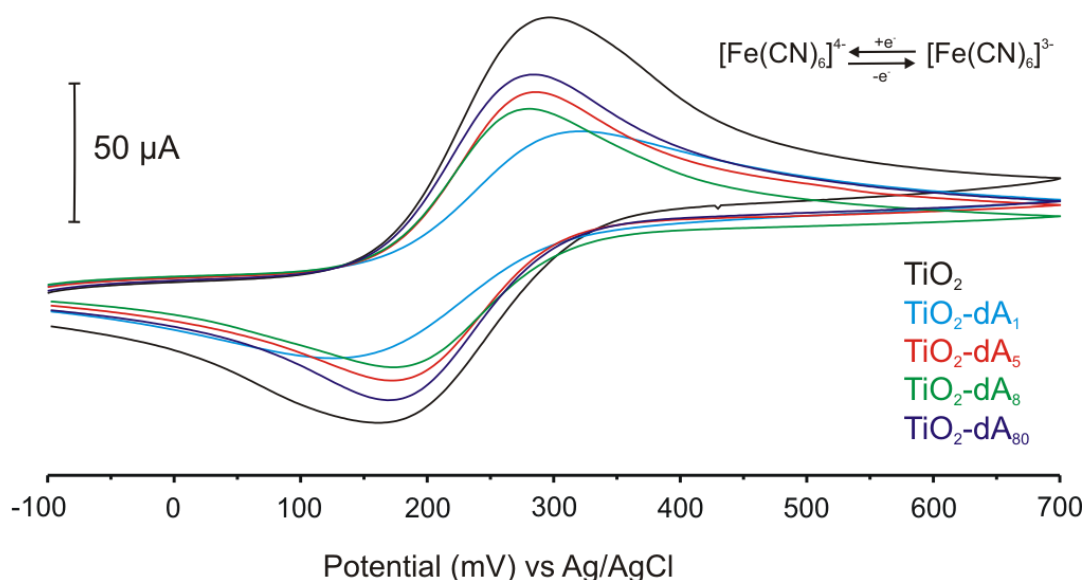


Figure 5.2 CV's of the redox couple $[Fe(CN)_6]^{4-/3-}$ at the surface of TiO_2 electrodes in KCl 0.1 M (scan rate 0.01 $V \cdot s^{-1}$)

⁴ Concentration expressed in monomeric adenylic units

oligonucleotides-modified TiO₂ films (ΔE in the range 97-105 mV). The electrochemical parameters derived from the corresponding cyclic voltammograms are summarized in Table 5.1.

Table 5.1 Electrochemical parameters derived from the CV's of the redox couple [Fe(CN)₆]^{4-/3-} at the surface of TiO₂-dA_n electrodes ^[a]

Electrode name	Geometrical area ^[b]	E _{pa} ^[c]	E _{pc}	E ^o ^[c]	ΔE ^[d]
TiO ₂	0.56	293	176	235	117
TiO ₂ -dA ₁	0.63	313	144	229	169
TiO ₂ -dA ₅	0.60	283	181	232	102
TiO ₂ -dA ₈	0.45	278	181	230	97
TiO ₂ -dA ₈₀	0.56	281	176	229	105

^[a]All potential parameters are expressed in mV versus Ag/AgCl; ^[b]Geometrical area of the TiO₂ electrode (A) expressed in cm² ^[c]E_{pa} and E_{pc} represent the corresponding half-wave potentials; ^[c]E^o represents the formal potential calculated as $E^o = (E_{pa} + E_{pc})/2$; ^[d] ΔE represents the separation potential calculated as $\Delta E = E_{pa} - E_{pc}$.

The analysis of surface concentration of oxidized [Fe(CN)₆]⁴⁺ species (Γ_{Fe}) provides qualitative information regarding the electrostatically immobilized ssDNA layer. This is because the adsorbed ssDNA species on the TiO₂ film reduces the surface available for heterogeneous electron transfer between the TiO₂ electrode and [Fe(CN)₆]⁴⁺ species. In consequence, it is expected that the increase of surface coverage of ssDNA species (Γ_{ssDNA}) at the surface of TiO₂ will cause a decrease of Γ_{Fe} .

Γ_{Fe} has been calculated using the equation 5.1 [192]:

$$\Gamma_{Fe} = Q / n \cdot 96486 \cdot A \text{ [nmol/cm}^2\text{]} \quad (5.1)$$

where Q denotes the electric charge necessary for oxidation of the [Fe(CN)₆]⁴⁺ species determined by the integration of the oxidation peak in the corresponding cyclic voltammogram [C·10⁻⁵], n is the number of the electron transferred (n=1), 96486 is the Faraday constant and A is the geometrical area of the TiO₂ electrode [cm²] (cf. Table 5.1).

Figure 5.3 shows the calculated values of Γ_{Fe} as a function of length of nucleic acid immobilized on TiO_2 surface. It can be seen in the corresponding plot an increase of Γ_{Fe} with the ssDNA length up to 8 monomeric units where above this value tends to remain constant. This observation suggests that the surface coverage of ssDNA immobilized species on mesoporous TiO_2 (Γ_{ssDNA}) decreases with the dA_n size.

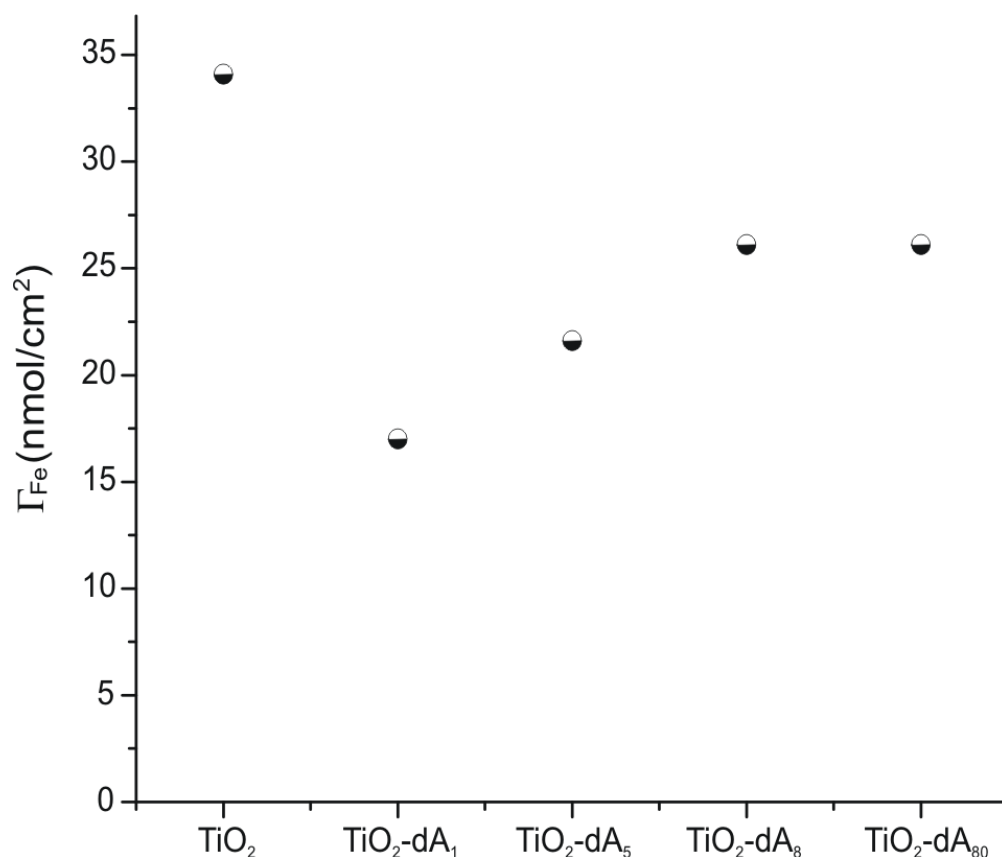


Figure 5.3 Surface coverage of $[\text{Fe}(\text{CN})_6]^{4+}$ species (Γ_{Fe}) at the surface of $\text{TiO}_2\text{-dA}_n$ electrode

5.2.2 Evaluation of ssDNA surface coverage (Γ_{ssDNA})

To confirm the hypothesis of Γ_{ssDNA} dependency with the ssDNA length, as suggested by the previously mentioned CV experiments with redox ion marker, the Γ_{ssDNA} was directly determined.

The experiments consisted in desorption of ssDNA monolayer in NaOH (0.1M aqueous solution) at 90°C for 20 minutes and quantifying the amount of desorbed ssDNA by UV-Vis spectroscopy (cf. experimental part in Chapter 6). The Γ_{ssDNA} was calculated by the formula:

$$\Gamma_{\text{ssDNA}} = \mu / A \quad (5.2)$$

where, μ is the amount of desorbed dA_n (nmol) determined experimentally and A is the geometrical area of the TiO_2 electrode (cm^2).

The desorption conditions (i.e. alkaline media and elevated temperature) were adopted from the reference [189] and are necessary conditions for complete desorption of ssDNA from the TiO_2 surface as that authors claimed. Table 5.2 shows the calculated values of Γ_{ssDNA} .

Table 5.2 Surface concentration (Γ_{ssDNA}) of adsorbed dA_n species on mesoporous TiO_2 film

ssDNA	dA_1	dA_5	dA_8	dA_{80}
Γ_{ssDNA} (nmol/cm ²)	39.60	3.07	1.18	0.10

The results in Table 5.2 point out a decrease of Γ_{ssDNA} with growing length of the applied ssDNA chain. Typically, charged polymers adsorb stronger and faster as their size and number of charges increase. Since the opposite is valid in this case, the explanation lies in the mesoporous structure of TiO_2 film. The mesoporous TiO_2 films, prepared similarly as reported here, have inner pores with diameters ranging between 10 and 15 nm and pore channels with even less space availability [124, 125]. The estimated contour lengths of the oligonucleotides dA_5 , dA_8 , and dA_{80} are 1.65 nm, 2.64 nm and 26.4 nm, respectively. With the increase of ssDNA length, the molecule size becomes comparable with that of the pores diameter even if the real conformation of ssDNA should be a random coil state. In consequence, the surface available for adsorption of long size ssDNA is limited by the hindered diffusion of the species into the inner pores of the film. The decrease of Γ_{ssDNA} as a function of ssDNA size suggests that the small ssDNA molecules (smaller than 8 monomeric units) diffused easier in the channel pores of the mesoporous TiO_2 film ensuring a higher surface coverage of the ssDNA adsorbed species, while long length oligonucleotides are adsorbed just at the outer surface of the film.

5.2.3 Stability of ssDNA monolayer

The stability of adsorbed ssDNA monolayer was tested by desorption experiments in pure water. Water has been chosen as solvent for accelerating ageing tests since it is one of the frequently used media in electrochemical, bio-sensing devices. Desorption of the

DNA monolayer was performed at 21°C for specific periods of time (cf. Chapter 6). The amount of desorbed ssDNA was monitored by UV-Vis spectroscopy.

The amount of desorbed dA_n (related to geometrical area of the TiO_2 electrode) is plotted over the time in the Figure 5.4.

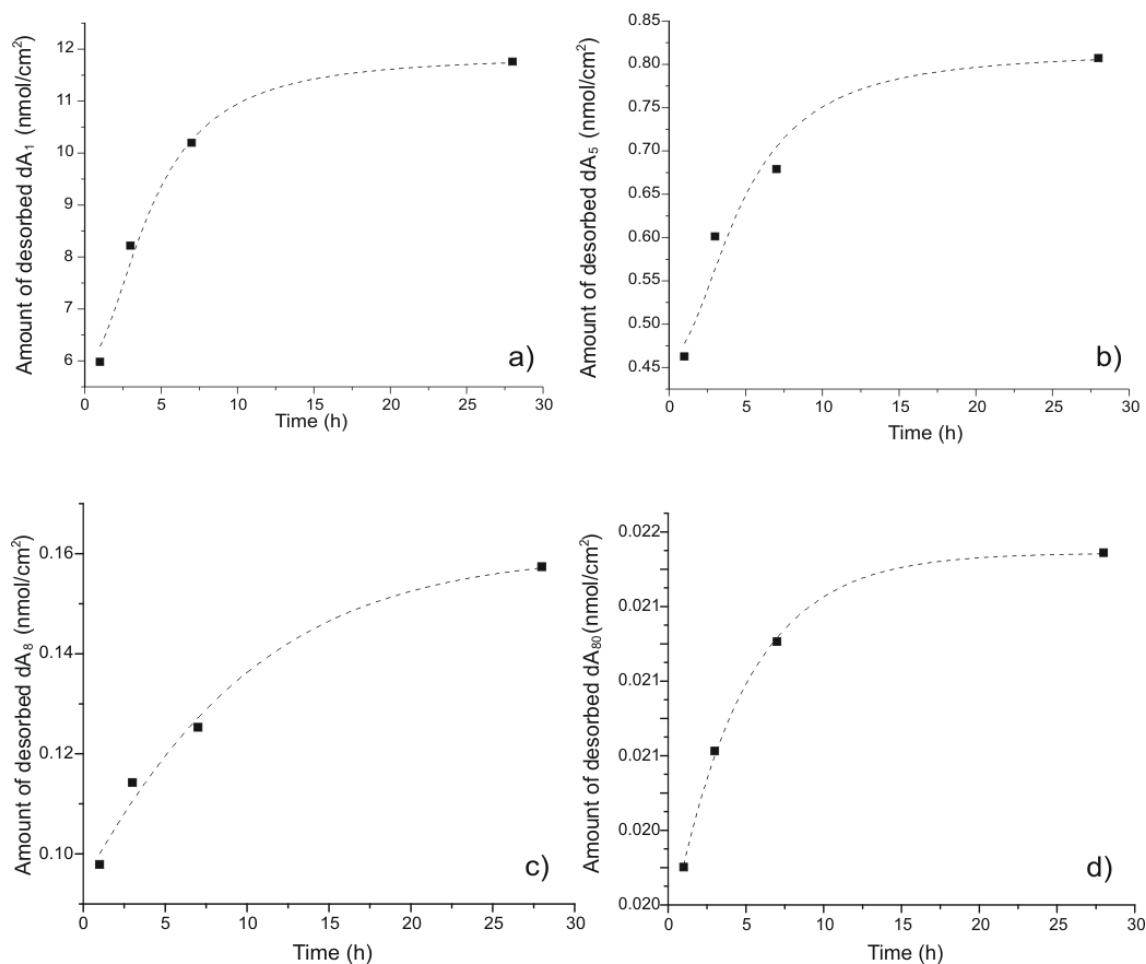


Figure 5.4 Desorbed amount of dA_1 (a), dA_5 (b), dA_8 (c) and dA_{80} (d) respectively, in H_2O at 21°C as a function of time

The results shows that, independently of the ssDNA size, desorption occurred faster in the first five hours and then desorption rich a plateau over the time. The percentage fraction of desorbed ssDNA species was calculated as a ratio between the total amount of ssDNA desorbed from the surface of mesoporous TiO_2 film (determined in the previously discussed experiments from Section 5.2.2) and amount of ssDNA desorbed after 28 hours in pure water.

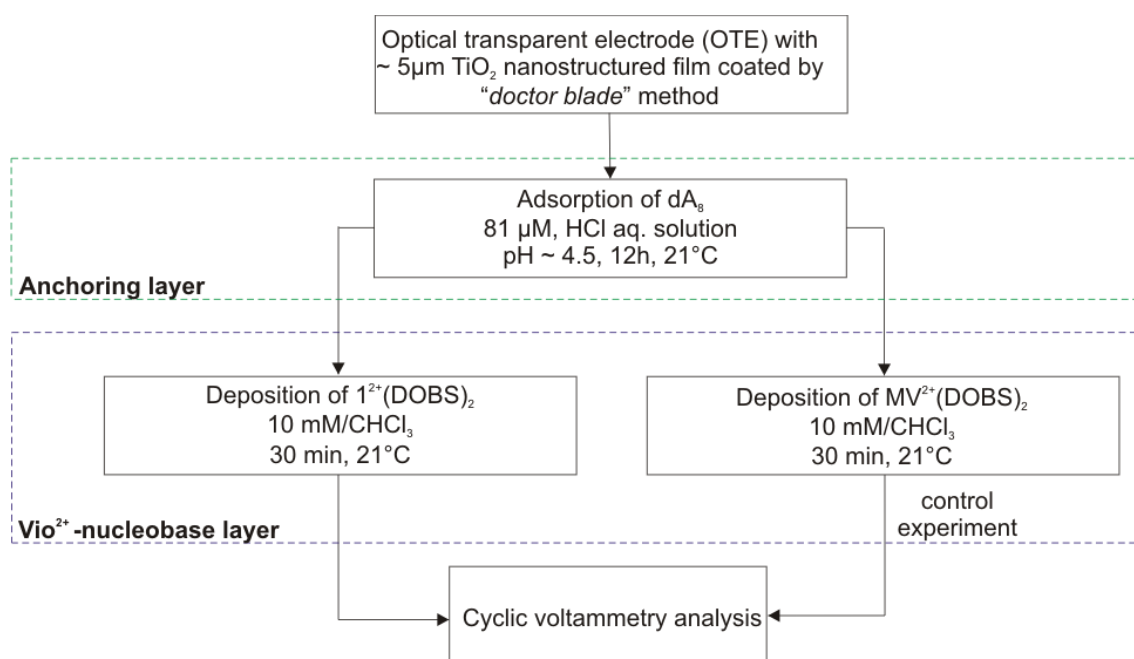
It has been found that after 28 hours of exposure in water of the ssDNA-modified electrodes, 30% of dA_1 , 26% of dA_5 , 14% of dA_8 and 20% of dA_{80} , respectively have been desorbed. These results showed that the ssDNA layer has a relative good stability

in a solvent like water, an issue which is very important for construction of bio-sensing devices. This is in agreement with the study of Suzuki et al. [189] which concluded that the ssDNA are strongly bonded to the TiO₂ surface and complete desorption in water cannot be achieved in mild conditions.

Briefly, the ssDNA was successfully immobilized by dip-coating on the mesoporous TiO₂ film, by electrostatic interaction between negatively charged phosphate backbone of ssDNA and the positive sites existing at the TiO₂ surface. The surface concentration of adsorbed ssDNA species depends on the ssDNA length, presumably due to the spatially hindered access of the high lengths oligonucleotides into the inner pores of the mesoporous TiO₂ film. Aging experiments in pure water showed that ssDNA monolayer has a relatively good stability in time since not more than 30% of the adsorbed species can be removed from the TiO₂ surface, even after 28 hours of desorption. The ssDNA-modified TiO₂ film was used in further experiments as solid support for modification of TiO₂ electrodes with viologen-nucleobase derivatives.

5.3 Deposition of a viologen-thymine derivative by hydrogen bonding on ssDNA-modified TiO₂ surface – proof of the concept

In these experiments the adsorption of a viologen-thymine derivative at the surface of an adenylic ssDNA-modified TiO₂ film via thymine-adenine specific hydrogen bonding



Scheme 5.4 Hydrogen bonded deposition of a viologen-nucleobase derivative on ssDNA-modified TiO₂

interaction will be demonstrated. The experimental methodology is summarized in Scheme 5.4.

The mesoporous TiO₂ film was firstly modified with the oligonucleotide dA₈, which plays the role of anchoring layer, according with the methodology presented in the Section 5.2.1. In the second step, the dA₈-modified TiO₂ electrode was immersed in a 10 mM chloroform solution of viologen-thymine derivative **1**²⁺(**DOBS**)₂. The ionic complex **1**²⁺(**DOBS**)₂ containing hydrophobic anion 3,4,5-tris(dodecyloxy)benzene sulfonate (**DOBS**⁻) as counter anion was chosen in this study because it is soluble in a low-polar solvent such as chloroform, a media which facilitate hydrogen bonding.

To demonstrate the specific thymine-adenine hydrogen bonding of compound **1**²⁺(**DOBS**)₂ with the dA₈-modified TiO₂ surface, a control experiment was performed in which the dA₈-modified TiO₂ film was exposed to a chloroform solution of the analogue 1,1'-dimethyl-4,4'-bipyridinium derivative, **MV**²⁺(**DOBS**)₂, using the same condition of temperature, time and concentration.

The dA₈ anchoring layer formation was proved electrochemically with the redox marker ion [Fe(CN)₆]⁴⁻ as previously discussed in Section 5.2.1 (Figure 5.5a). The viologen layer deposition was checked by monitoring directly the first one-electron reduction step of the immobilized viologen species (Figure 5.5b). The dA₈-modified TiO₂ electrode immersed in the solution of **1**²⁺(**DOBS**)₂ showed a redox process in the negative potential range at about -550 mV versus Ag/AgCl (Figure 5.5b, green line). This reversible electrochemical process was attributed to the first one-electron reduction step of physically adsorbed dicationic species **1**²⁺(**DOBS**)₂ on the surface of the mesoporous film ($\Gamma_{\text{vio}} = 1.93 \text{ nmol/cm}^2$). In contrast, the dA₈-modified TiO₂ electrode exposed to a chloroform solution of compound **MV**²⁺(**DOBS**)₂ did not show any reduction process in the same potential domain (Figure 5.5b, black line). The control experiment confirmed that the interaction mode of the viologen-thymine derivative **1**²⁺(**DOBS**)₂ with the dA₈-modified TiO₂ surface was possible by hydrogen bonding between complementary thymine and surface-confined adenine, while the compound **MV**²⁺(**DOBS**)₂, without capping thymine units, was not able to bind to the surface. This principle of hydrogen bonded deposition of viologen-nucleobase derivatives on the TiO₂ modified surface with ssDNA is an easy and promising method for the construction of electrochemical biosensors or electrochromic devices.

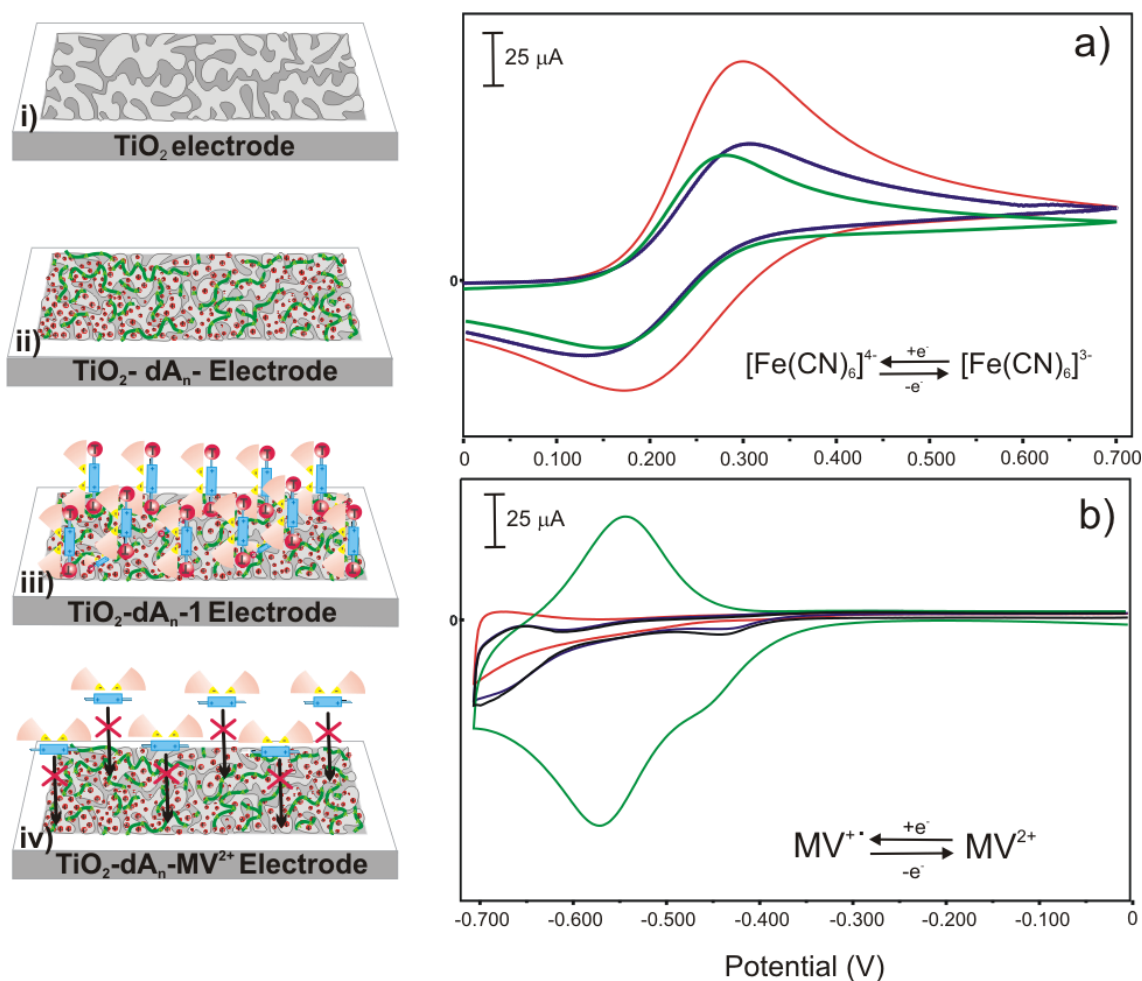


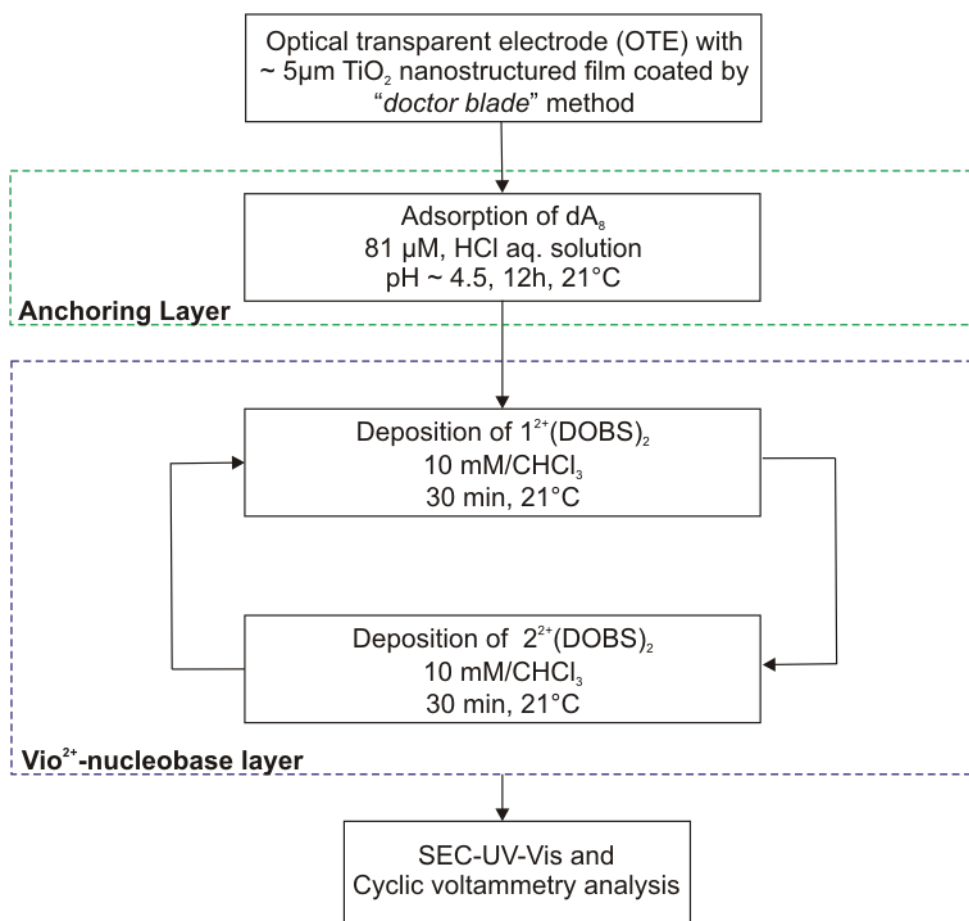
Figure 5.5 Cyclic voltammograms of modified TiO_2 electrodes: (i) --- TiO_2 ; (ii) --- $\text{TiO}_2\text{-dA}_8$; (iii) --- $\text{TiO}_2\text{-dA}_8\text{-1}^{2+}(\text{DOBS})_2$; (iv) --- $\text{TiO}_2\text{-dA}_8\text{-MV}^{2+}(\text{DOBS})_2$. Electrodes were measured in 0.01 M $\text{K}_4[\text{Fe}(\text{CN})_6]$ using $\text{KCl}/\text{H}_2\text{O}$ (0.1M) as supporting electrolyte, Ag/AgCl as reference electrode and Pt as counter electrode at $0.02 \text{ V}\cdot\text{s}^{-1}$ scan rate

5.4 LbL deposition of viologen-nucleobase derivatives on TiO_2 electrode modified with ssDNA as anchoring layer

The hydrogen bonded layer-by-layer deposition technique [100] was employed in the further experiments to enhance the fixation and the surface concentration of redox viologen units on the TiO_2 electrode surface.

The LbL fabrication methodology of TiO_2 electrodes is presented in Scheme 5.5. First, the TiO_2 electrodes were modified with dA_8 oligonucleotide as anchoring layer as presented in Section 5.2.1. Second, the dA_8 -modified TiO_2 films were treated in alternating steps, with 10 mM chloroform solution of complementary viologen-nucleobase derivatives, either $1^{2+}(\text{DOBS})_2$ or $2^{2+}(\text{DOBS})_2$ respectively. An alternating

layer denotes hereafter one single layer of viologen derivative $1^{2+}(\text{DOBS})_2$ or $2^{2+}(\text{DOBS})_2$ deposited after one single adsorption step. The growing of the effective surface concentration of the adsorbed viologen species (Γ_{Viologen}) with the number of deposition steps was verified electrochemically by means of CV and spectroelectrochemically using SEC-UV-Vis.



Scheme 5.5 Hydrogen bonded layer-by-layer deposition of viologen-nucleobase derivatives on dA_8 -modified mesoporous TiO_2 film

The cyclic voltammograms in the Figure 5.6a represent the first one-electron reduction step of deposited viologen layers at the surface of TiO_2 electrodes after one, two and six alternating steps respectively. Notably, the formal potential E^0 was shifted into the positive domain with the increase of the adsorption steps. The electrical charge (Q_{red}) resulted from the reduction process of adsorbed viologen species also increased with the number of alternating adsorption steps. In the CV curves, the electrical charge (Q_{red}) represents the area under the reduction current peak and is proportional with the number of reduced species. The increasing of Q_{red} demonstrates the growing of the viologen layer at the surface of dA_8 -modified TiO_2 electrode.

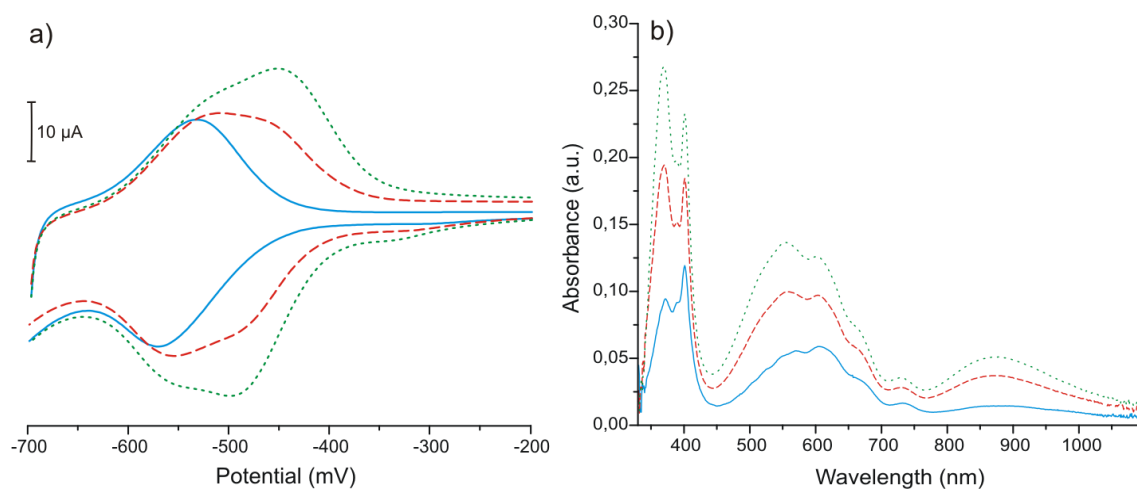


Figure 5.6 2nd scan CV's (a) and Vis spectra at -0.7 V (b) of dA₈-TiO₂ electrodes modified with 1⁺(DOBS)₂ and 2⁺(DOBS)₂ in alternating layers after one (continues line), two (dashed line) and six (dotted line) successive deposition steps; electrolyte KCl (0.1 M) versus Ag/AgCl, scan rate 0.01 V·s⁻¹

Figure 5.6b shows the corresponding Vis spectra recorded at -0.7 V of the dA₈-TiO₂ films modified with alternating viologen layers after one, two and six alternating steps respectively. The growing of the viologen layer with the number of alternating adsorption steps is also suggested by the increase of the absorbance of radical cation species (V^{•+}).

The surface concentration of the adsorbed viologen species in radical cationic state (Γ_{Viologen}) was evaluated from both, electrochemical and spectroelectrochemical data and the values are in good agreement (Table 5.3). Notably, Γ_{Viologen} was not increasing linearly with the number of deposition steps and after more than three steps the slope of the surface coverage decreased with the growing step number. This observation can be explained by two hypotheses: a) the growing of the viologen-nucleobase layer was limited by the sterically hindered diffusion into the inner pores or/and by the space filling between them; b) a fraction of viologen-nucleobase species are bonded with both nucleobases to electrode surface which reduced stepwise the bounding sites for the next deposition steps.

The formation of dimers (V^{•+})₂ from the viologen radical cationic species generated electrochemically at the surface of mesoporous TiO₂ film was observed in the corresponding Vis spectra (see broad adsorption band at 900 nm in Figure 5.6b). This phenomenon is facilitated by the interface of the surface with the aqueous electrolyte (KCl, 0.1M) used in this study. The dimer fraction (%dimer) was determined from spectroscopic data, using the algorithm of calculation from the literature [193]. Briefly,

the surface concentration of the monomer (Γ_M) and of the dimer (Γ_D) was calculated using the following system of equations and molar extinction coefficients of $V^{+\bullet}$ species in monomeric and dimeric form as reported by Komers [194]:

$$A_{600\text{nm}} = \varepsilon_{M, 600\text{nm}} \cdot \Gamma_M + \varepsilon_{D, 600\text{nm}} \cdot \Gamma_D \quad (5.3)$$

$$A_{520\text{nm}} = \varepsilon_{M, 520\text{nm}} \cdot \Gamma_M + \varepsilon_{D, 520\text{nm}} \cdot \Gamma_D \quad (5.4)$$

$$\% \text{dimer} = 2\Gamma_D / (\Gamma_M + 2\Gamma_D) \cdot 100 \quad (5.5)$$

where $A_{600\text{nm}}$ and $A_{520\text{nm}}$ represents the absorbance at $\lambda=600$ and 520 nm respectively. As it was expected, the molar fraction of dimers (%dimer) increased proportionally with the surface concentration of adsorbed viologen species [195] (cf. Table 5.3).

Table 5.3 Electrochemical parameters and surface coverage of viologen species at the surface of d- A_8 modified TiO_2 electrode^[a]

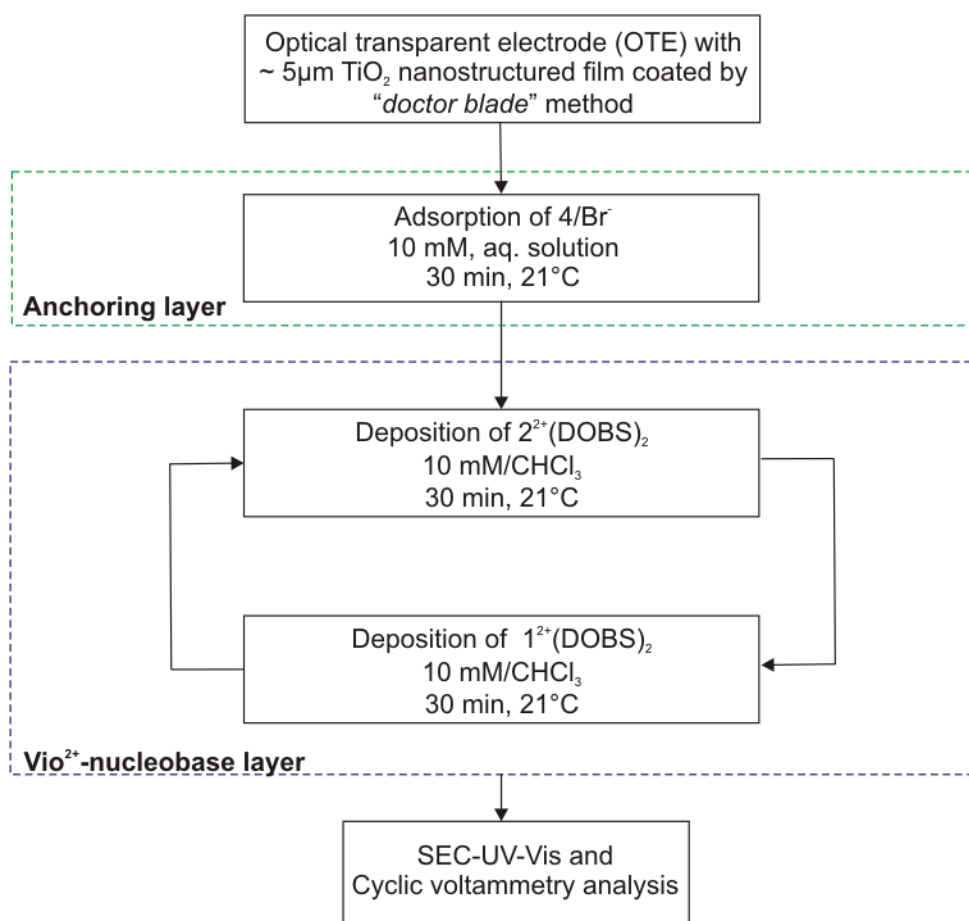
Number of adsorbed steps	$E_{\text{pa}}^{[b]}$ (mV)	E_{pc} (mV)	$E^{0[c]}$ (mV)	$\Delta E^{[d]}$ (mV)	$\Gamma_{\text{CV}}^{[e]}$ (nmol/cm ²)	$\Gamma_{\text{UV-Vis}}^{[f]}$ (nmol/cm ²)	Dimer fraction (%mol)
1	-532	-564	-548	68	1.93	2.61	38
2	-510	-547	-529	37	4.07	4.16	53
6	-457	-496	-477	42	5.82	5.63	58

^[a]All potential parameters are expressed in mV versus. Ag/AgCl ; ^[b] E_{pa} and E_{pc} represent the corresponding half-wave potentials; ^[c] E^0 represents the formal potential calculated as $E^0 = (E_{\text{pa}} + E_{\text{pc}})/2$; ^[d] ΔE represents the separation potential calculated as $\Delta E = E_{\text{pc}} - E_{\text{pa}}$; ^[e] Γ_{CV} represents the surface coverage of viologen species determined from cyclic voltammetry; ^[f] $\Gamma_{\text{UV-Vis}}$ represents the surface coverage of viologen species determined from Vis spectra

In conclusion, the complementary viologen-nucleobase ionic complexes $1^{2+}(\text{DOBS})_2$ and $2^{2+}(\text{DOBS})_2$ were successfully immobilized on the surface of d A_8 -modified TiO_2 film in the form of alternating layers by specific hydrogen bonding interaction of thymine and adenine nucleobase. By using the LbL deposition method, an enhancement of the surface concentration and a better fixation of the redox active species were achieved.

5.5 LbL deposition of viologen-nucleobase derivatives on TiO₂ surface modified with derivative **4/Br⁻** as anchoring layer

The methodology of LbL modification of TiO₂ electrode with viologen-nucleobase derivatives, by using the compound (**4/Br⁻**) as anchoring layer is presented in Scheme 5.6.



Scheme 5.6 Hydrogen bonded layer-by-layer deposition of viologen-nucleobase derivatives on mesoporous TiO₂ film modified with derivative **4/Br⁻** as anchoring layer

The mesoporous TiO₂ film, coated on conductive FTO glass, was first modified with compound **4/Br⁻** by adsorption for 30 minutes in 10 mM aqueous solution of **4/Br⁻** at 21°C. Subsequently, the viologen layer was grown by alternating dip-coating of **4/Br⁻**-modified TiO₂ electrodes from 10 mM chloroform solution of compounds **2²⁺(DOBS)₂** and **1²⁺(DOBS)₂** respectively. The modified TiO₂ films were characterized electrochemically and spectroelectrochemically as described in Section 5.4.

Figure 5.7 shows the corresponding cyclic voltammograms (5.7a) and Vis spectra (5.7b) of the TiO₂ modified films with viologen-nucleobase derivatives in the reduced state

after 1st, 2nd and 6th successive adsorption step. It is noteworthy to say that in the current study first viologen layer is considered already the redox active anchoring layer **4/Br⁻**.

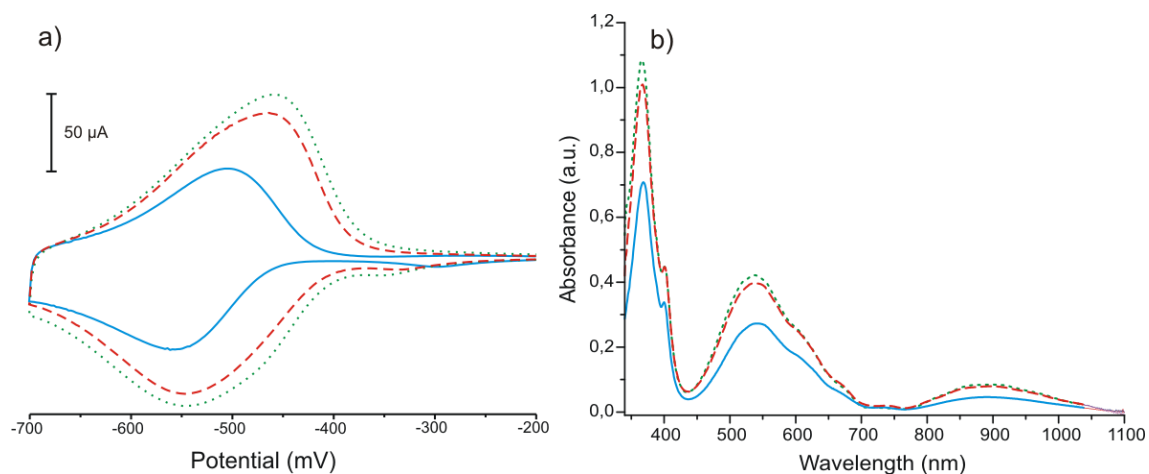


Figure 5.7 CV's (a) and Vis spectra at -0.7 V (b) of **4/Br⁻**-TiO₂ electrodes modified with **2²⁺(DOBS)₂** and **1²⁺(DOBS)₂** in alternating layers after one (continues line), two (dashed line) and six (dotted line) successive deposition steps; electrolyte KCl (0.1 M) versus Ag/AgCl, scan rate 0.01 V·s⁻¹

The number of surface-immobilized viologen species increased with the number of alternating deposition steps similar as in the previous experiments where the viologen-nucleobase derivatives were deposited on the surface of dA₈-modified TiO₂ film. Notably, when compound **4/Br⁻** was used as anchoring layer instead of dA₈ oligonucleotide, a five times higher surface concentration of deposited viologen species was achieved. However, the surface coverage of viologen species remained constant after more than six alternating LbL deposition steps, in the same manner as previously experiment of adsorption of viologen-nucleobase derivatives at the surface of dA₈-modified TiO₂ film. The electrochemical parameters, surface coverage of viologen immobilized species and the corresponding molar fraction of dimer are summarized in Table 5.4.

Table 5.4 Electrochemical parameters and surface coverage of viologen species at the surface of TiO₂ electrode^[a]

Number of adsorbed steps	E _{pa} ^[b] (mV)	E _{pc} (mV)	E ⁰ [c] (mV)	ΔE ^[d] (mV)	Γ _{CV} ^[e] (nmol/cm ²)	Γ _{UV-Vis} ^[f] (nmol/cm ²)	Dimer fraction (%mol)
1	-505	-552	-529	47	10.3	11.3	86
2	-464	-540	-502	76	20.7	20.0	86
6	-449	-537	-493	88	27.6	25.6	88

^[a]All potential parameters are expressed in mV versus Ag/AgCl; ^[b]E_{pa} and E_{pc} represent the corresponding half-wave potentials; ^[c]E⁰ represents the formal potential calculated as E⁰=(E_{pa}+E_{pc})/2; ^[d]ΔE represents the separation potential calculated as ΔE=E_{pc}-E_{pa}; ^[e]Γ_{CV} represents the surface coverage of viologen species determined from cyclic voltammetry; ^[f]Γ_{UV-Vis} represents the surface coverage of viologen species determined from Vis spectra

5.6 Fabrication of an electrochromic device

An electrochromic device (ECD) was fabricated, containing the mesoporous TiO₂ film as the electrochromic component, modified with viologen-nucleobase derivatives accordingly to the methodology and experimental conditions presented in the Section 5.5: the TiO₂ film was first modified with anchoring layer (4/Br⁻) and subsequently, with five alternating layers of complementary derivatives 2²⁺(DOBS)₂ and 1²⁺(DOBS)₂, using LbL technique and adenine-thymine hydrogen bonding interaction.

A schematic representation of the ECD is depicted in Figure 5.8. The device was composed of the following elements: 1) working electrode: mesoporous TiO₂ film (5 μm thickness) modified by LbL technique with viologen-nucleobase derivatives as previously described coated on FTO conductive glass; 2) counter electrode: FTO conductive glass and c) electrolyte solution: lithium bis(trifluoromethane)sulfonimide in MeCN (0.1 M) sandwiched between the CE and WE electrodes and sealed by a rubber frame. The assembled device was connected to a source of potential in three electrode system electrochemical cell, where the pseudo-reference electrode was a silver wire inserted into the electrolyte solution.

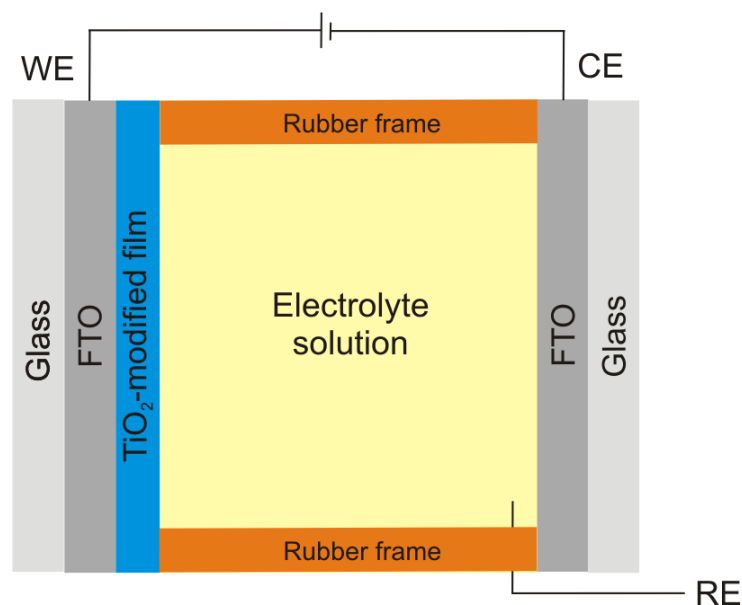


Figure 5.8 Schematic illustration of the side-view of the ECD. Working electrode (WE); Counter electrode (CE); Reference electrode (RE)

Figure 5.9 shows the top-view of the device with a white sheet of paper as contrast background. At 0 V potential the electrochromic display device was transparent as can be observed in the Figure 5.7a. When the potential was switched to -0.7 V, the display

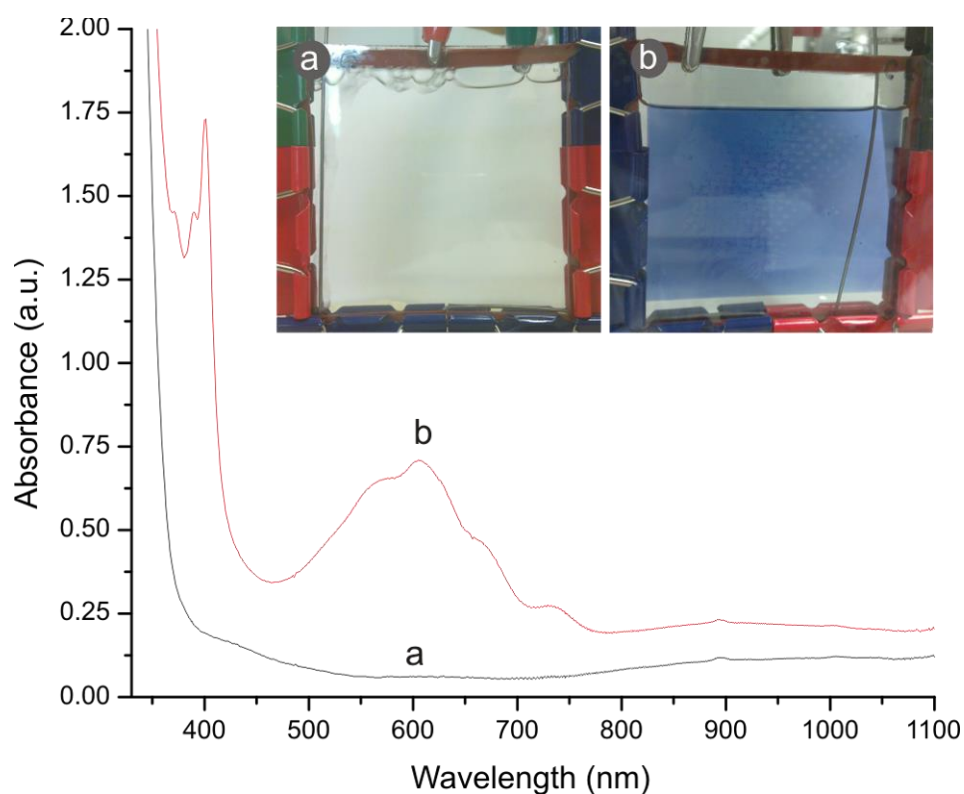


Figure 5.9 Clamp-closed cell 7 x 7 cm in three electrode system, 0.1 M LiTFSI/MeCN electrolyte, Ag wire as pseudo-reference electrode, FTO-glass as counter electrode a) 0 V and b) -0.7 V

changed instantly (within approx. 1 second) its color to blue as a result of the electrochemical reduction of the immobilized viologen species (Figure 5.8b). The decolorization of the electrochromic display was observed when the potential was switched back to 0 V. From the Vis spectra, an effective surface coverage of the electrochromic species of $\Gamma=30 \text{ nmol/cm}^2$ was deduced.

Summary:

The surfaces of nanostructured TiO_2 films coated on the surface of an optical transparent electrode (OTE) have been modified with viologen-nucleobase derivatives by using a layer-by-layer deposition technique. The layers are stabilized by a specific interaction of thymine-adenine base pairs. The TiO_2 was first modified with a monolayer of a single stranded ssDNA, as an anchoring layer. The surface concentration of ssDNA immobilized species (Γ_{ssDNA}) was found to strongly depend on the length of the corresponding ssDNA molecules. The desorption experiments showed that ssDNA monolayer desorbed partially (<30%) in pure water after 28 hours but independently of the ssDNA length. Further has been demonstrated that complementary derivatives $\mathbf{1}^{2+}(\text{DOBS})_2$ can adsorb on the surface of ssDNA-modified TiO_2 due to thymine-adenine hydrogen bonding interaction. A control experiment with analogue derivative $\text{MV}^{2+}(\text{DOBS})_2$, demonstrated that the ssDNA-modified mesoporous TiO_2 film can recognize only complementary viologen-nucleobase species due to the specific hydrogen bonding interaction between complementary nucleobases (T-A). The surface concentration of immobilized viologen species has been enhanced by alternating layer-by-layer deposition steps of complementary derivatives $\mathbf{1}^{2+}(\text{DOBS})_2$ and $\mathbf{2}^{2+}(\text{DOBS})_2$. Moreover, when the asymmetric 4,4'-bipyridinium derivative ($\mathbf{4/Br}^+$), capped by a phosphonate group at one side and a thymine moiety at the other side was used as anchoring layer instead of ssDNA, a considerably increase of immobilized viologen species at the surface of TiO_2 film by a factor of five was observed. The capability of the viologen-nucleobase species to recognize the complementary ssDNA-modified TiO_2 surface is a promising principle for the development of new electrochemical biosensor devices for single stranded DNA. Furthermore, the hydrogen-bonded layer-by-layer deposition of the viologen-nucleobase derivatives can be used as a versatile method to construct electrochromic devices with amplified electrochromic response due to the increase of surface concentration and better fixation of immobilized viologen species.

CHAPTER 6

Experimental part

6.1 Materials

6.1.1 Commercial available chemicals

a) Reagents and solvents used for synthesis

Reagents: potassium carbonate (K_2CO_3), (>99%, Sigma-Aldrich), 4,4'-bipyridine (98%, Aldrich), adenine (>99%, Fluka), thymine (>99%, Sigma-Aldrich), 1,2-dibromoethane (99%, Aldrich), 1,3-dibromopropane (Merck), hexamethyldisilazane (>98%, Merck), trimethylchlorosilane (>99%, Merck), magnesium sulphate (Mg_2SO_4) (anhydrous, >99.5%, Alfa Aesar), ammonium hexafluorophosphate (NH_4PF_6) (99.5%, Alfa Aesar) tetrabutylammonium iodide (98%, Sigma-Aldrich) and tetrabutylammonium chloride (>98%, Fluka) were used as received.

Solvents: acetonitrile (Sigma-Aldrich), dimethylformamide (water content < 150 ppm, VWR), nitrobenzene (99%, Aldrich), diethyl ether (99.5%, Sigma-Aldrich), dichloromethane (99%, Sigma-Aldrich), acetone (99%, Sigma-Aldrich), chloroform (>99%, Sigma-Aldrich) and benzene (>99%, Merck). All purchased solvents were used without further purification. Technical ethanol was distilled prior to be used.

b) Chemicals used for electrochemical, spectroelectrochemical and optical characterization

Solvents: DMF (>99.5%, TCI) and THF (99.9%, Sigma-Aldrich) were used as received.

Supporting electrolytes: sodium perchlorate ($NaClO_4$) (>98%, Sigma-Aldrich), Lithium bis(trifluoromethane)sulfonimide (LiTFSI, 99.9% Sigma-Aldrich) were used as received.

c) Chemicals used for reduction of viologen-nucleobase derivatives $1/Br^-$ - $3/Br^-$

Sodium dithionite ($Na_2S_2O_4$) (86%, Riedel-de Haen), tris(hydroxymethyl)-aminomethane (99.9%, Aldrich), sulfuric acid (H_2SO_4) (95-97%, Sigma Aldrich) were used as received.

d) ssDNA and analogues ssPNA oligomers

Adenylic oligonucleotides (dA_n) were purchased from Eurogentec S.A. and the analogue peptide nucleic acid 10-mer (PNA- A_{10}) from Panagene GmbH without any special chemical modification. All probes were received in lyophilized form and stored at -20°C prior dissolution in corresponding volume of distilled water or phosphate buffer (pH=7, AppliChem).

e) Chemicals and materials used for construction and testing of electrochemical device

TEC glass (from LOF) (coated with fluorine doped tin oxide (FTO), 2.2 mm, 15 Ω/cm^2); titanium dioxide colloidal paste (particle size 14.5- 21.6 nm, surface area 103 $\text{m}^2 \text{g}^{-1}$, NTERA, Dublin, Ireland); potassium chloride; potassium ferrocyanide $\text{K}_4[\text{Fe}(\text{CN})_6]$ (Merck); adenosine 5'-monophosphoric acid (dA_1 , water <5% wt.); oligonucleotides (dA_5 , dA_8 , dA_{80}) were purchased in lyophilized form from Eurogentec S.A. without any special chemical modification.

f) Miscellaneous materials

Conductive glass slides coated with ITO (In-doped SnO_2 , 20 Ω/cm^2) were purchased from BTE (Elsoff, Germany); microscope glass slides (0.8-1 mm thickness, Menzel GmbH).

6.1.2 Synthetized chemicals**a) Viologen-based dendrimers capped by thymine terminal groups G0-G3/Cl⁻**

Dendrimers **G0-G3/Cl⁻** used in interaction with oligonucleotides or analogue PNA oligomer (cf. Chapter 3) were synthetized by Ms. Ana-Maria Lepadatu accordingly with a previously published procedure [3, 4]. Their molecular integrity was checked by means of $^1\text{H-NMR}$ spectroscopy (Figure 6.1). Purity estimated from the corresponding $^1\text{H-NMR}$ spectra was higher than 95%.

G0/Cl⁻ (C₆₃H₆₆Cl₆N₁₂O₆, MW=1299.99)

¹H-NMR (250 MHz, D₂O): δ= 9.25 (d, J=5.44 Hz, 12H), 8.65 (d, J=5.02 Hz, 12H), 7.90 (s, 3H), 7.58 (s, 3H), 6.11 (s, 6H), 4.91 (t, J=6.91 Hz, 6H), 4.02 (t, J=6.44 Hz, 6H), 2.63 (quin, J=6.67 Hz, 6H), 1.93 ppm (s, 9H).

G1/Cl⁻ (C₁₇₄H₁₇₄Cl₁₈N₃₀O₁₂, MW=3515.60)

¹H-NMR (250 MHz, D₂O): δ= 9.25 (dd, J=3.45, 6.59 Hz, 36H), 8.66 (dd, J = 4.71, 7.85 Hz, 36H), 7.91 (s, 6H), 7.87 (s, 6H), 7.56 (s, 6H), 6.10 (s, 24H), 4.91 (t, J=7.06 Hz, 12H), 4.01 (t, J=6.75 Hz, 12H), 2.62 (quin, J=6.67 Hz, 12H), 1.92 ppm (s, 18H).

G2/Cl⁻ (C₃₉₆H₃₉₀Cl₄₂N₆₆O₂₄, MW=7946.79)

¹H-NMR (250 MHz, D₂O): δ= 9.16-9.44 (m, 84H), 8.52-8.80 (m, 84H), 7.91 (s, 15H), 7.87 (s, 15H), 7.57 (s, 12H), 6.11 (s, 60H), 4.91 (t, J=7.20 Hz, 24H), 4.02 (t, J=5.81 Hz, 24H), 2.63 (quin, J=6.99 Hz, 24H), 1.93 ppm (s, 36H).

G3/Cl⁻ (C₈₄₀H₈₂₂Cl₉₀N₁₃₈O₄₈, MW=16809.18)

¹H-NMR (250 MHz, D₂O): δ= 9.01-9.50 (m, 180H), 8.40-8.82 (m, 180H), 7.91 (s, 33H), 7.86 (s, 33H), 7.56 (s, 24H), 6.10 (s, 132H), 4.91 (t, J=7.50 Hz, 48H), 4.01 (t, J=6.12 Hz, 48H), 2.62 (quin, J=7.20 Hz, 48H), 1.91 ppm (s, 72H).

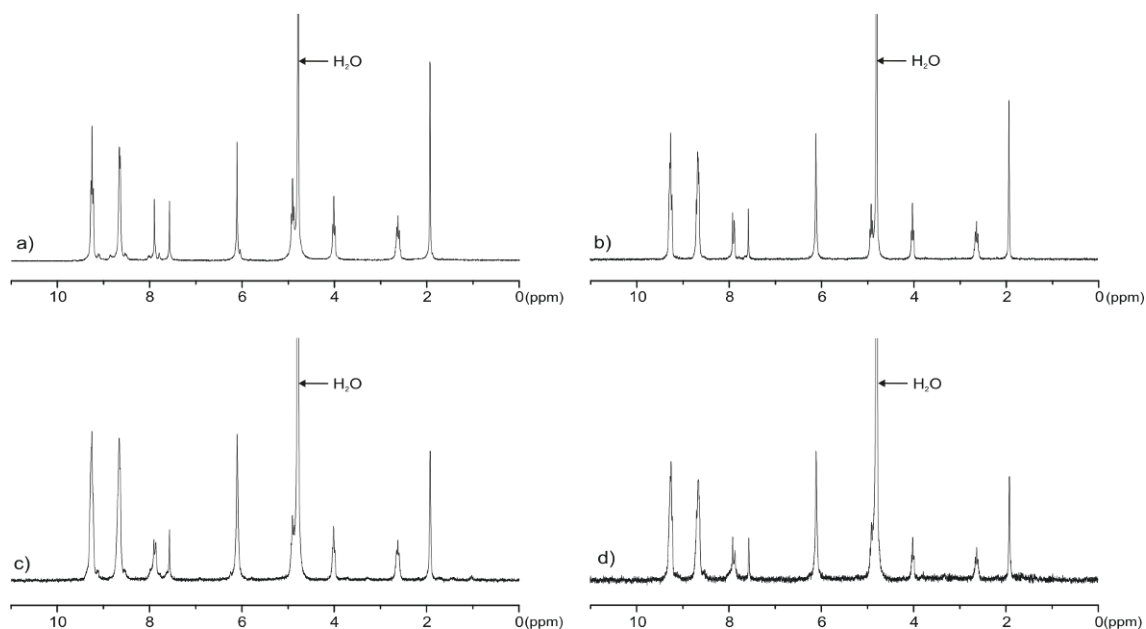


Figure 6.1 ¹H-NMR spectra of viologen-based dendrimers: **G0/Cl⁻** (a), **G1/Cl⁻** (b) **G2/Cl⁻** (c) and **G3/Cl⁻** (d) in D₂O

b) Caesium 3,4,5-tris(dodecyl)benzene sulfonate (CsDOBS)

Caesium 3,4,5-tris(dodecyl)benzene sulfonate used as reagent for the synthesis of ionic liquid crystals discussed in the Chapter 4 was synthesized by Dr. Enfeng Song accordingly with a procedure reported in literature [170] to a purity higher than 98%.

$^1\text{H-NMR}$ (500 MHz, D_2O): $\delta = 7.02$ (s, 2H, aromatic), 3.95-3.91 (m, 6H, OCH_2), 1.71-1.70 (m, 6H, OCH_2CH_2), 1.45-1.41 (m, 6H, $\text{O}(\text{CH}_2)_2\text{CH}_2$), 1.26 (overlapped peaks, 48H, $\text{O}(\text{CH}_2)_3(\text{CH}_2)_8$), 0.88 ppm (t, 9H, CH_3 , $J = 5.0$ Hz).

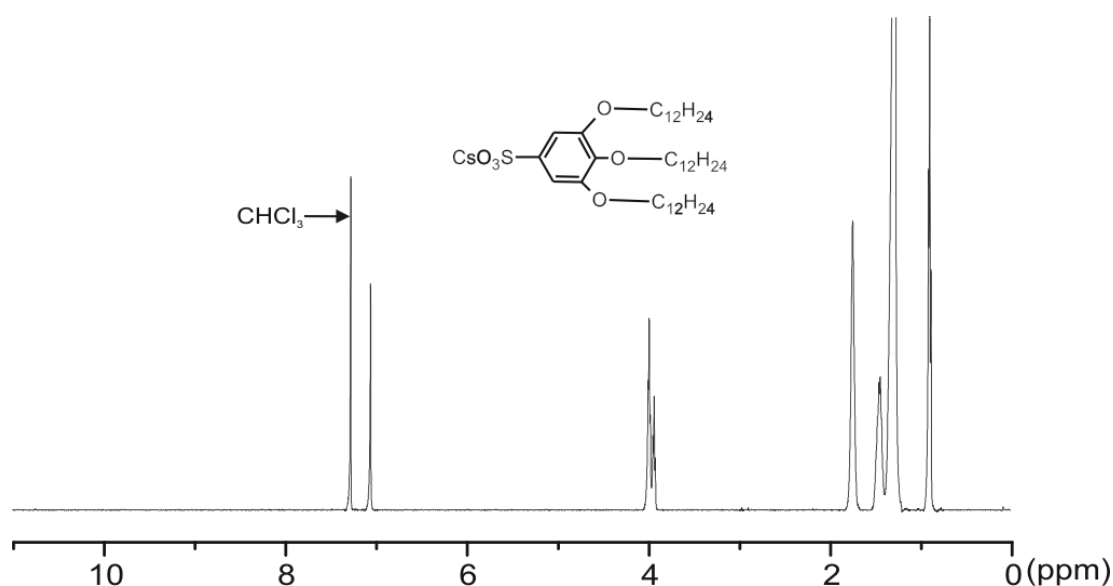


Figure 6.2 $^1\text{H-NMR}$ spectra of CsDOBS in CDCl_3

c) 1-[2-(Diethoxyphosphoryl)ethyl]-4-pyridin-4-ylpyridinium monobromide ($\mathbf{a/Br}^-$)

Derivative 1-[2-(Diethoxyphosphoryl)ethyl]-4-pyridin-4-ylpyridinium monobromide ($\mathbf{a/Br}^-$) used as precursor in the synthesis of 1-[3-(5-methyl-2,4-dioxo-3,4-dihydropyrimidin-1(2H)-yl)propyl]-1'-(2-phosphonate)-4,4'-bipyridinium dibromide ($\mathbf{4/Br}^-$), (cf. Chapter 5) was prepared by Dr. Simona Asaftei following a reported procedure [184] to a purity higher than 95%.

$^1\text{H-NMR}$ (500 MHz, D_2O): $\delta = 9.09$ (d, $J=6.62$ Hz, 2H), 8.85 (d, $J=5.99$ Hz, 2H), 8.53 (d, $J=6.62$ Hz, 2H), 7.99 (d, $J=6.31$ Hz, 2H), 5.03 (m, $J=7.01$ Hz, 2H), 4.17 (m, $J=7.30$ Hz, 4H) 2.85 (m, $J=7.30$ Hz, 2H) 1.29 ppm (t, $J=7.09$ Hz, 6H).

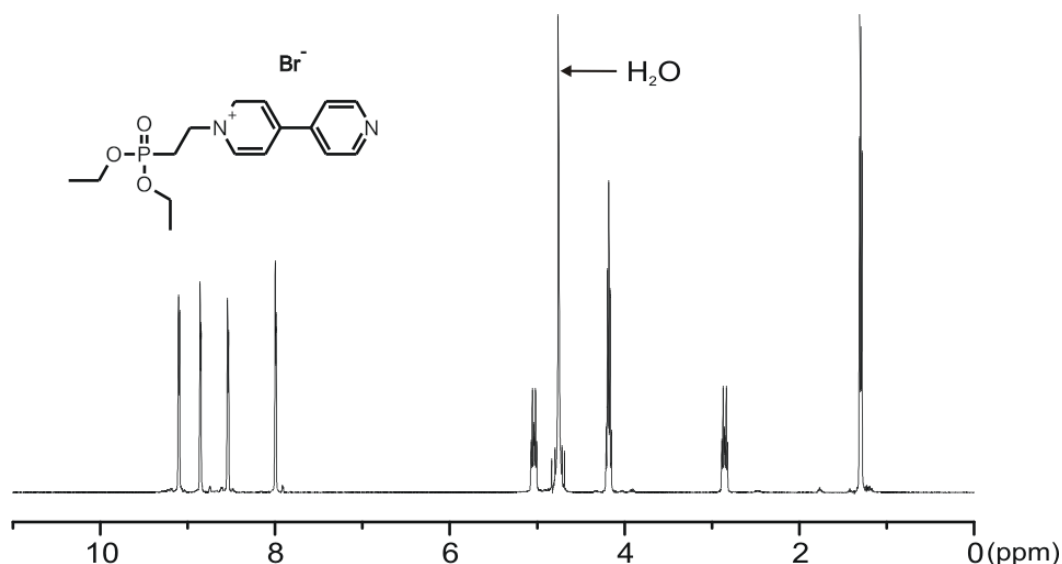
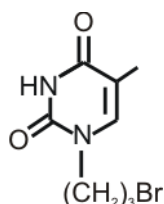


Figure 6.3 $^1\text{H-NMR}$ spectra of precursor 1-[2-(Diethoxyphosphoryl)ethyl]-4-pyridin-4-ylpyridinium monobromide in D_2O

6.2 Synthesis

6.2.1 Synthesis of precursors

6.2.1.1 Synthesis of 1-(3-bromopropyl)-5-methyl-3H-pyrimidine-2,4(1H,3H)-dione [46]



A catalytic amount of trimethylchlorosilane (1.08 ml, 8.54 mmol) was added under nitrogen atmosphere to a suspension of thymine (2.24 g, 17.5 mmol) in hexamethyldisilazane (HMDS; 11.4 ml, 54 mmol) and the mixture was stirred for 21 h under reflux (130°C). Excess HMDS was then removed under reduced pressure to afford crude bis(O-silylated)-thymine. The crude material was taken up in DMF (10 ml), 1,3-dibromopropane (4.6 ml, 45.3 mmol) was added and the mixture was stirred at 80°C for 24 h. Water (150 ml) was then added and after stirring for 10 min, the mixture was filtered. The aqueous filtrate was extracted with diethyl ether (2 x 200 ml) and the combined organic extracts were dried with MgSO_4 (2 g), filtered and evaporated under reduced pressure. Crystallization of the resulted residue from 100 ml ethanol gave white

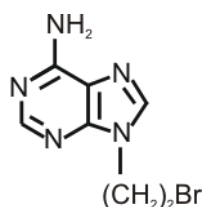
crystals of 1-(3-bromopropyl)-5-methyl-3H-pyrimidine-2,4(1H,3H)-dione (1.5 g, 6.07 mmol, 34.4%). m.p. 140°C.

¹H-NMR (500 MHz, DMSO-*d*₆): δ=11.17 (s, 1H), 7.48 (s, 1H), 3.73 (t, J=7.0 Hz, 2H), 3.51 (t, J=6.5 Hz, 2H), 2.13 (q, J=6.7 Hz, 2H), 1.74 ppm (s, 1H);

¹³C-NMR (125 MHz, DMSO-*d*₆): δ=164.19(s), 151.17(s), 140.38(d), 110.46(s), 47.26(t), 31.29(t), 29.76(t), 12.60 ppm (s);

Elemental analysis calcd (%) for C₈H₁₁BrN₂O₂ (247.09): C 38.89, H 4.49, N 11.34; found: C 39.32, H 4.73, N 11.47.

6.2.1.2 Synthesis of 9-(2-bromoethyl)-9H-purin-6-amine [134]



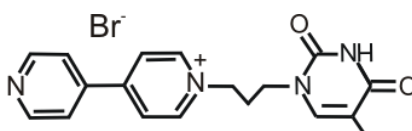
To a solution of adenine (5 g, 37 mmol) dissolved in DMF (200 ml), 1,2-dibromoethane (29.96 g, 159.47 mmol) and K₂CO₃ (11.97 g, 86.58 mmol) were added. The reaction mixture was stirred at room temperature under nitrogen atmosphere. After 48 h the reaction mixture was filtered and the filtrate was evaporated to dryness. The crude material with orange color was washed with water (100 ml) and filtered. The filter cake was dried in vacuum and recrystallized from 100 ml ethanol to obtain 9-(2-bromoethyl)-9H-purin-6-amine (5.49 g, 22.68 mmol, 61%).

¹H-NMR (500 MHz, CD₃CN): δ=8.15 (s, 1H), 8.14 (s, 1H) 7.19 (s, 2H), 5.15 (t, 2H, J=6.2 Hz), 4.93 ppm (t, 2H, J=6.0 Hz);

¹³C-NMR (125 MHz, CD₃CN): δ=155.8 (s), 152.3 (d), 149.4 (s), 140.9 (d), 118.6 (s), 44.6 (t), 31.4 ppm (t);

Elemental analysis calcd (%) for C₇H₈BrN₅ (242): C 34.73, H 3.33, N 28.93; found C 34.99, H 3.40, N 28.87.

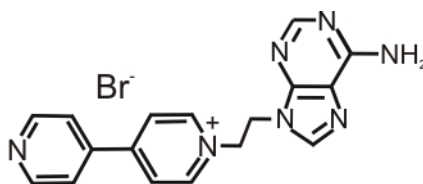
6.2.1.3 Synthesis of 1-[3-(5-methyl-2,4-dioxo-3,4-dihydropyrimidin-1(2H)-yl)propyl]-4-(pyridin-4-yl)pyridinium monobromide (P1/Br⁻)



1-(3-Bromopropyl)-5-methyl-3H-pyrimidine-2,4(1H,3H)-dione (1 g, 4.04 mmol) was dissolved in nitrobenzene (80 ml) and 4,4'-bipyridine (1.29 g, 8.26 mmol) was added. The clear solution was stirred at 110 °C for 48 h. After reaction time, the cold mixture was filtered, and the filtrate was washed consecutively with nitrobenzene (20 ml) and diethyl ether (20 ml). After drying in vacuum (21°C, 12h) a light-yellow solid product (**P1/Br⁻**) was obtained (1.51 g, 3.0 mmol, 68 %).

¹H-NMR (250 MHz, D₂O): δ=9.04 (d, 2H, J=6.3 Hz), 8.82 (d, 2H, J=6.3 Hz), 8.46 (d, 2H, J=6.6 Hz), 7.94 (d, 2H, J=5.3 Hz), 7.50 (s, 1H), 4.81 (t, 2H, J=6.3 Hz), 3.99 (t, 2H, J=6.3 Hz), 2.57 (quin, 2H, J=6 Hz), 1.87 ppm (s, 3H).

6.2.1.4 Synthesis of 1-[2-(6-amino-9H-purin-9-yl)ethyl]-4-(pyridin-4-yl)pyridinium monobromide (**P2/Br⁻**)



9-(2-Bromoethyl)-9H-purin-6-amine (1 g, 4.13 mmol) was dissolved in nitrobenzene (80 ml) and 4,4'-bipyridine (1.29 g, 8.26 mmol) was added. The clear solution was stirred at 110 °C for 48 h. After reaction time the cold mixture was filtered, and the resulted filtrate was washed consecutively with nitrobenzene (20 ml) and diethyl ether (20 ml). After drying in vacuum (21°C, 12h) a yellow solid product (**P2/Br⁻**) was obtained (1.51 g, 3.0 mmol, 92%).

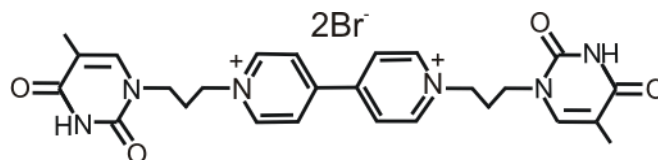
¹H-NMR (500 MHz, D₂O): δ=8.75 (d, 2H, J=6.0 Hz), 8.69 (d, 2H, J=7.0 Hz), 8.26 (d, 2H, J=6.5 Hz), 8.15 (s, 1H), 7.86 (s, 1H), 7.80 (d, 2H, J=6.0 Hz), 5.16 (t, 2H, J=5.2 Hz), 4.93 ppm (t, 2H, J=5.2 Hz);

¹³C-NMR (125 MHz, D₂O): δ=155.68(s), 155.03(s), 152.71(d), 150.15(d), 149.04(s), 145.22(d), 142.16(d), 141.91(s), 126.39(d), 122.43(d), 118.09(s), 60.85(t), 44.07 ppm (t);

Elemental analysis calcd (%) for **P2** as PF₆⁻ salt C₁₇H₁₆F₆N₇P (463.3): C 44.07, H 3.48, N 21.16; found: C 43.94, H 3.37, N 21.27.

6.2.2 Synthesis of viologen-nucleobase derivatives 1/An⁻-3/An⁻

6.2.2.1 Synthesis of 1,1'-Bis[3-(5-methyl-2,4-dioxo-3,4-dihydropyrimidin-1(2H)-yl)propyl]-4-(pyridin-4-yl)-pyridinium dibromide (1/Br⁻)



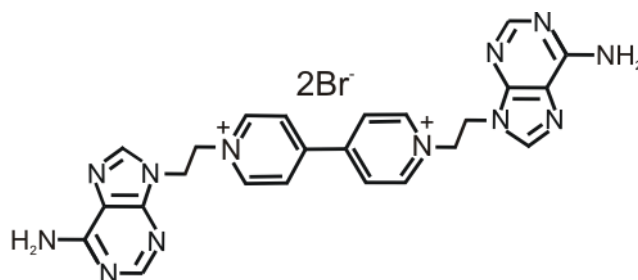
1-(3-Bromopropyl)-5-methyl-3H-pyrimidine-2,4(1H,3H)-dione (1.756 g, 7.1 mmol) and 4,4'-bipyridine (0.24 g, 1.54 mmol) were dissolved in dry DMF (60 mL) and stirred at 80°C for 4 days. The resulted light-yellow precipitate was filtered, washed with DMF (20 ml), diethyl ether (20 ml) and dried in ultra-high vacuum at 45°C to afford product **1/Br⁻** (0.76 g, 1.16 mmol, 76%).

¹H-NMR (500 MHz, D₂O): δ=9.26 (d, J=6.62 Hz, 4H), 8.66 (d, J=6.30 Hz, 4H), 7.60 (s, 2H), 4.93 (t, J=7.25 Hz, 4H), 4.05 (t, J=6.62 Hz, 4H), 2.65 (quin, J=6.70 Hz, 4H), 1.96 ppm (s, 6H);

¹³C-NMR (125 MHz, D₂O): δ=166.87(s), 152.31(s), 150.31(s), 145.76(d), 142.49(d), 127.16(d), 111.47(s), 59.43(t), 45.25(t), 29.53(t), 11.33 ppm (q);

Elemental analysis calcd (%) for **1** as PF₆⁻ salt C₂₆H₃₀F₁₂N₆O₄P₂ (780.48): C 40.0, H: 3.87, N 10.77; found C 39.69, H 3.60, N 10.71.

6.2.2.2 Synthesis of 1,1'-bis[2-(6-amino-9H-purin-9-yl)ethyl]-4-(pyridin-4-yl)pyridinium dibromide (2/Br⁻)



1-[2-(6-Amino-9H-purin-9-yl)ethyl]-4-(pyridin-4-yl)pyridinium monobromide (0.382 g, 0.96 mmol) and 9-(2-bromoethyl)-9H-purin-6-amine (0.6 g, 2.48 mmol) were dissolved in distilled water (30 ml) and stirred at 80°C for 17 days. At the 10th and 14th day after reaction start, a new quantity of 9-(2-bromoethyl)-9H-purin-6-amine was added (0.2 g, respectively 0.12 g). After 17 days, reaction mixture was cooled down to 21°C and

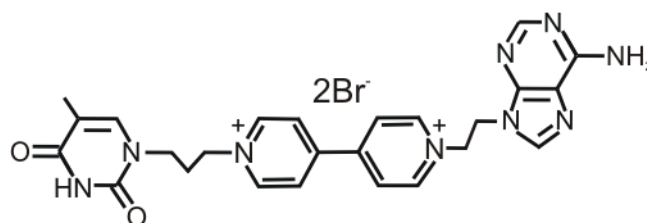
subsequently, acetone (80 ml) was added. The resulted precipitate was separated by filtration, washed with acetone (10 ml) and dried under reduced pressure to afford product **2/Br⁻** (0.523 g, 0.82 mmol, 85%).

¹H-NMR (250 MHz, DMSO-*d*₆): δ=9.19 (d, J=6.91 Hz, 4H), 8.63 (d, J=6.91 Hz, 4H), 8.11 (s, 2H), 7.78 (s, 2H), 7.26 (br. s., 4H), 5.14 (t, J=5.30 Hz, 4H), 4.85 ppm (t, J=4.10 Hz, 4H);

¹³C-NMR (125 MHz, D₂O): δ=155.82(s), 152.75(d), 150.69(s), 149.19(s), 146.21(d), 142.02(d), 127.34(d), 118.19(s), 61.52(t), 44.09 ppm (t);

Elemental analysis calcd (%) for **2** as PF₆⁻ salt C₂₄H₂₄F₁₂N₁₂P₂ + 0.8 H₂O (770.46 + 14.4): C 37.41, H 3.14, N 21.82; found: C 36.73, H 3.29, N 21.41.

6.2.2.3 Synthesis of 1-[2-(6-amino-9H-purin-9-yl)ethyl]-1'-[3-(5-methyl-2,4-dioxo-3,4-dihydropyrimidin-1(2H)-yl)propyl]-4-(pyridin-4-yl)pyridinium dihexafluorophosphate (**3/PF₆⁻**)



1-[2-(6-Amino-9H-purin-9-yl)ethyl]-4-(pyridin-4-yl)pyridinium monohexafluorophosphate (0.45 g, 0.97 mmol) and 1-(3-bromopropyl)-5-methylpyrimidine-2,4(1H,3H)-dione (0.72 g, 2.19 mmol) were dissolved in dry DMF (20 ml) and stirred at 80°C for 70 hours. The resulted precipitate was filtered, washed with DMF (5 ml) and subsequently with acetone (20 ml). After drying in vacuum, the resulted solid was dissolved in water (20 ml) and treated with aqueous solution of NH₄PF₆ (4 ml, 10% wt). The resulted precipitate was separated by filtration, washed with water (5 ml) and dried in vacuum to obtained product **3/PF₆⁻** as a white solid yield 281 mg (0.281 g, 0.44 mmol, 45%).

¹H-NMR (250 MHz, CD₃CN): δ=9.78 (br. s, 1H), 8.94 (d, J=6.91 Hz, 2H), 8.67 (d, J=6.91 Hz, 2H), 8.34 (d, J=6.91 Hz, 2H), 8.23 (d, J=6.59 Hz, 2H), 7.94 (s, 1H), 7.79 (s, 1H), 7.23 (s, 1H), 6.22 (br. s., 2H), 5.07 (t, J=5.70 Hz, 2H), 4.80 (t, J=5.00 Hz, 2H), 4.67 (t, J=7.06 Hz, 2H), 3.79 (t, J=6.12 Hz, 2H), 2.40 (quin, J=1.00 Hz, 2H), 1.85 ppm (s, 3H);

$^{13}\text{C-NMR}$ (125 MHz, CD_3CN): $\delta=165.78(\text{s})$, $157.43(\text{s})$, $154.05(\text{d})$, $152.90(\text{s})$, $151.96(\text{s})$, $151.70(\text{s})$, $151.20(\text{s})$, $147.69(\text{d})$, $147.37(\text{d})$, $142.32(\text{d})$, $142.08(\text{d})$, $128.65(\text{d})$, $128.54(\text{d})$, $120.26(\text{s})$, $111.93(\text{s})$, $63.02(\text{t})$, $60.93(\text{t})$, $45.43(\text{t})$, $45.40(\text{t})$, $31.86(\text{t})$, 12.73 ppm (q);

Elemental analysis calcd (%) for **3** as PF_6^- salt $\text{C}_{25}\text{H}_{27}\text{F}_{12}\text{N}_9\text{O}_2\text{P}_2 + 0.1 \text{H}_2\text{O}$ (775.48 + 1.8): C 38.72, H 3.51, N 16.26; found: C 38.63, H 3.53, N 16.22.

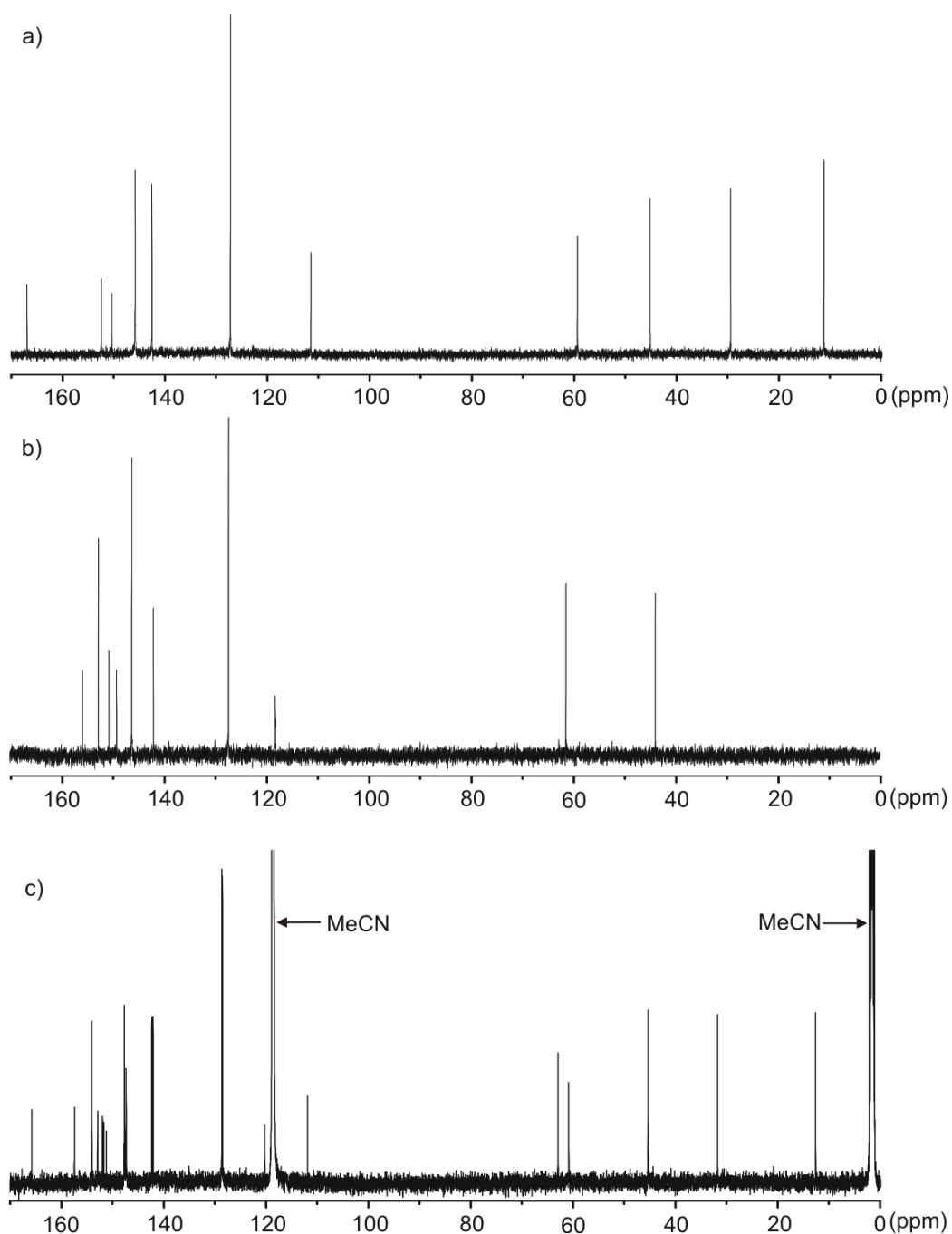


Figure 6.4 $^{13}\text{C-NMR}$ spectra (125.7 MHz) of **1/Br⁻** in D_2O (a), **2/Br⁻** in D_2O (b), **3/PF₆⁻** in acetonitrile- d_3 (c)

6.2.3 Synthesis of ionic complexes $1^{2+}(\text{DOBS})_2$, $2^{2+}(\text{DOBS})_2$ and $3^{2+}(\text{DOBS})_2$

General procedure:

Equal volumes of aqueous solution (0.01 M) of $1/\text{I}$, $2/\text{I}$ or $3/\text{I}$ respectively, and chloroform solution of caesium 3,4,5-tris(dodecyloxy)benzene sulfonate (0.01 M) were vigorously stirred at ambient temperature for 12 hours at 21°C. Further on, the organic phase was separated, washed two times with 20 ml distilled water, dry over MgSO_4 and subsequently evaporated under reduced pressure. The resulted yellow solid was freeze-dried from 40 ml benzene to obtain the ionic complexes $1^{2+}(\text{DOBS})_2$, $2^{2+}(\text{DOBS})_2$ and $3^{2+}(\text{DOBS})_2$ respectively. The amount of corresponding reactants and reaction products are presented in Table 6.1:

Table 6.1 Corresponding amounts of reactants and reaction products

Ionic complex	Viologen-nucleobase deriv. mg (mmol)	CsDOBS mg (mmol)	Product mg (yield%)
$1^{2+}(\text{DOBS})_2$	351 (0.471)	397 (0.471)	432 (96%)
$2^{2+}(\text{DOBS})_2$	252 (0.343)	289 (0.343)	311 (96%)
$3^{2+}(\text{DOBS})_2$	262 (0.354)	298 (0.354)	313 (93%)

1,1'-Bis[3-(5-methyl-2,4-dioxo-3,4-dihydropyrimidin-1(2H)-yl)propyl]-4-(pyridin-4-yl)-pyridinium di-[3,4,5-tris(dodecyl)benzene sulfonate]; $1^{2+}(\text{DOBS})_2$

$^1\text{H-NMR}$ (250 MHz, $\text{THF-}d_8/\text{D}_2\text{O}$, 4/1(vol)): $\delta=9.29$ (d, $J=5.34$ Hz, 4 H), 8.72 (d, $J=5.34$ Hz, 4 H), 7.56 (s, 2 H), 7.05 (s, 4 H), 4.90 (t, $J=6.28$ Hz, 4 H), 3.92 - 4.08 (m, 16 H), 2.54 (quin, $J=7.30$ Hz, 4 H), 1.77 (s, 6 H), 1.41 - 1.57 (m, 12 H), 1.16 - 1.40 (m, 108 H), 0.86 ppm (t, $J=6.30$ Hz, 18 H);

$^{13}\text{C-NMR}$ (62.9 MHz, $\text{THF-}d_8/\text{D}_2\text{O}$, 4/1(vol)): $\delta=165.74$ (s), 153.50(s), 152.93(s), 151.30(s), 147.04(d), 142.52(d), 141.90(s), 140.25(s), 128.51(d), 111.63(s), 105.73(d), 73.71(t), 69.93(t), 60.30(t), 46.02(t), 32.96(t), 31.51(t), 30.41-31.03(t, overlapped peaks), 27.37(t), 23.64(t), 14.56(q), 12.33 ppm (q);

IR (ATR, cm^{-1}): 3056(w), 2921(s), 2852(m), 1681(s), 1585(m), 1463(m), 1421(m), 1380(m), 1313(m), 1180(s), 1108(s), 1041(s), 840(m), 721(w), 651(s);

Elemental analysis calcd (%) for $C_{110}H_{184}N_6O_{16}S_2+2.45 H_2O$ (1910.8+44.1): C 67.95, H 9.41, N 3.92 S 3.34%; found: C 67.58, H 9.74, N 4.3, S 3.28.

1,1'-Bis[2-(6-amino-9H-purin-9-yl)ethyl]-4-(pyridin-4-yl)pyridinium di-[3,4,5-tris(dodecyl)benzene sulfonate]; 2²⁺(DOBS)₂

¹H-NMR (250 MHz, THF-*d*₈/D₂O, 4/1(vol)): δ=9.08 (d, *J*=6.59 Hz, 4 H), 8.52 (d, *J*=6.91 Hz, 4 H), 8.25 (s, 2 H), 7.96 (s, 2 H), 7.05 (s, 4 H), 5.29 (t, *J*=5.34 Hz), 5.01 (t, *J*=5.34 Hz, 4 H), 3.96 (t, *J*=5.97 Hz, 8 H), 3.86 (t, *J*=6.28 Hz, 4 H), 1.40 - 1.56 (m, 12 H), 1.15 - 1.40 (m, 108 H), 0.85 ppm (18 H, t, *J*=6.28 Hz);

¹³C-NMR (62.9 MHz, THF-*d*₈/D₂O, 4/1(vol)): δ=156.96(s), 153.73(d), 153.52(s), 151.70(s), 150.41(s), 147.50(d), 142.79(d), 141.73(s), 140.26(s), 128.55(d), 119.43(s), 105.72(d), 73.70(t), 69.93(t), 62.13(t), 44.92(t), 32.96(t), 31.52(t), 30.86-30.40(t, overlapped peaks), 27.39(t), 23.64(t), 14.58 ppm (q);

IR (ATR, cm⁻¹): 3338 (br), 2921(s), 2852(m), 1685(m), 1639(m), 1585(m), 1463(m), 1421(m), 1382(m), 1311(m), 1228(m), 1176(m), 1108(s), 1043(s), 956(w), 836(w), 719(m), 647(s);

Elemental analysis calcd (%) for $C_{108}H_{178}N_{12}O_{12}S_2+1.85 H_2O$ (1900.8+33.3): C 66.92, H 9.29, N 8.85, S 3.33; found: C 67.07, H 9.47, N 8.69, S 3.32.

1-[2-(6-Amino-9H-purin-9-yl)ethyl]-1'-[3-(5-methyl-2,4-dioxo-3,4-dihydropyrimidin-1(2H)-yl)propyl]-4-(pyridin-4-yl)pyridinium di-[3,4,5-tris(dodecyl)benzene sulfonate]; 3²⁺(DOBS)₂

¹H-NMR (250 MHz, THF-*d*₈/D₂O, 4/1(vol)): δ=9.27 (d, *J*=6.59 Hz, 2 H), 9.07 (d, *J*=6.59 Hz, 2 H), 8.63 (d, *J*=6.59 Hz, 2 H), 8.57 (d, *J*=6.91 Hz, 2 H), 8.25 (s, 1 H), 7.96 (s, 1 H), 7.55 (s, 1 H), 7.04 (s, 4 H), 5.29 (t, *J*=5.34 Hz, 2 H), 5.01 (t, *J*=5.49 Hz, 2 H), 4.88 (t, *J*=7.06 Hz, 2 H), 3.77 - 4.01 (m, 14 H), 2.53 (quin, *J*=7.14 Hz, 2 H), 1.78 (s, 3 H), 1.40 - 1.58 (m, 12 H), 1.12 - 1.40 (m, 108 H), 0.85 ppm (t, *J*=6.28 Hz, 18 H);

¹³C-NMR (62.9 MHz, THF-*d*₈/D₂O, 4/1(vol)): δ=166.02(s), 157.06(s), 153.87(d), 153.51(s), 153.03(s), 152.01(s), 151.05(s), 150.42(s), 147.40(d), 147.11(d), 142.74(d), 142.65(d), 141.76(s), 140.26(s), 128.59(d), 128.45(d), 119.44(s), 111.79(s), 105.72(d),

73.70(t), 69.93(t), 62.07(t), 60.37(t), 46.03(t), 44.91(t), 32.96(t), 31.52(t), 31.05-30.40(t, overlapped peaks), 27.38(t), 23.64(t), 14.57(q), 12.35 ppm (q);

IR (ATR, cm^{-1}): 3446 (br), 3058(w), 2921(s), 2852(m), 1681(m), 1639(m), 1585(m), 1463(m), 1421(m), 1380(m), 1313(m), 1228(m), 1180(m), 1108(s), 1043(s), 960(w), 836(w), 651(s);

Elemental analysis calcd (%) for $\text{C}_{109}\text{H}_{181}\text{N}_9\text{O}_{14}\text{S}_2+1.3 \text{H}_2\text{O}$ (1905.8+23.4): C 67.72, H 9.42, N 6.40, S 3.38; found: C 67.86, H 9.59, N 6.53, S 3.32.

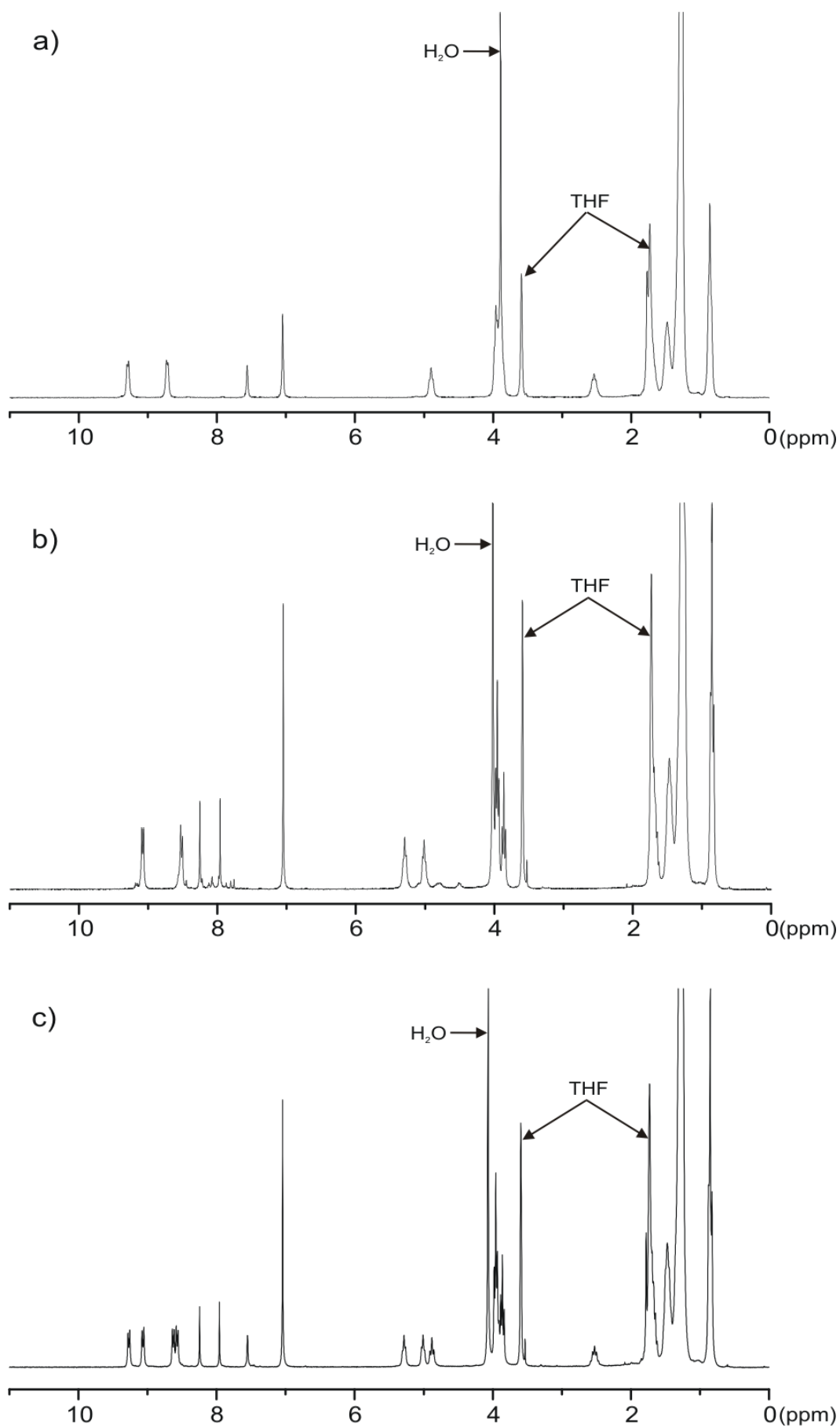


Figure 6.5 $^1\text{H-NMR}$ spectra (250 MHz) of $1^{2+}(\text{DOBS})_2$ (a), $2^{2+}(\text{DOBS})_2$ (b) and $3^{2+}(\text{DOBS})_2$ (c) in $\text{THF-}d_8/\text{D}_2\text{O}$, 4/1(vol)

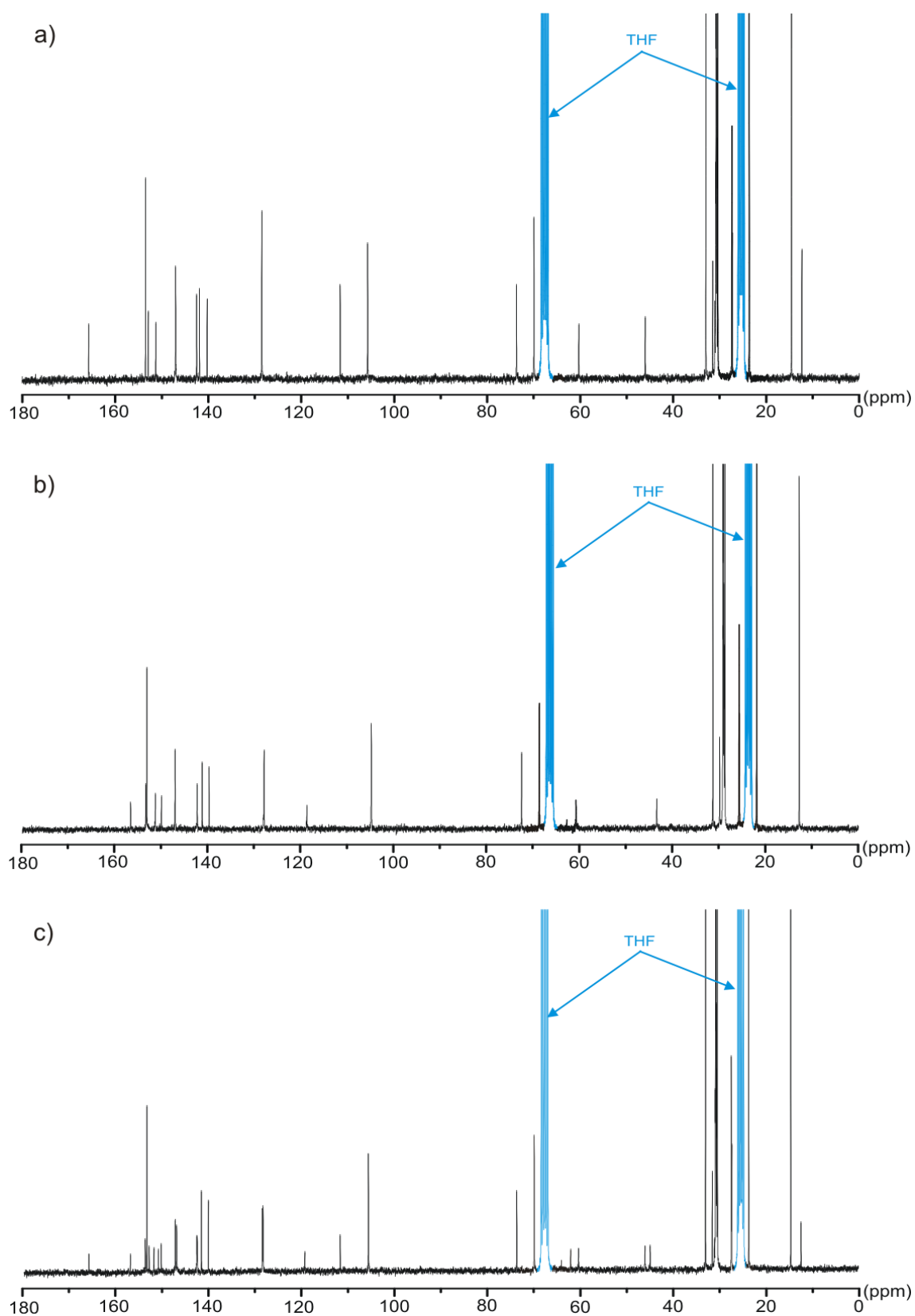


Figure 6.6 ^{13}C -NMR spectra (62.9 MHz) of $1^{2+}(\text{DOBS})_2$ (a), $2^{2+}(\text{DOBS})_2$ (b) and $3^{2+}(\text{DOBS})_2$ (c) in THF- d_8 / D_2O , 4/1(vol)

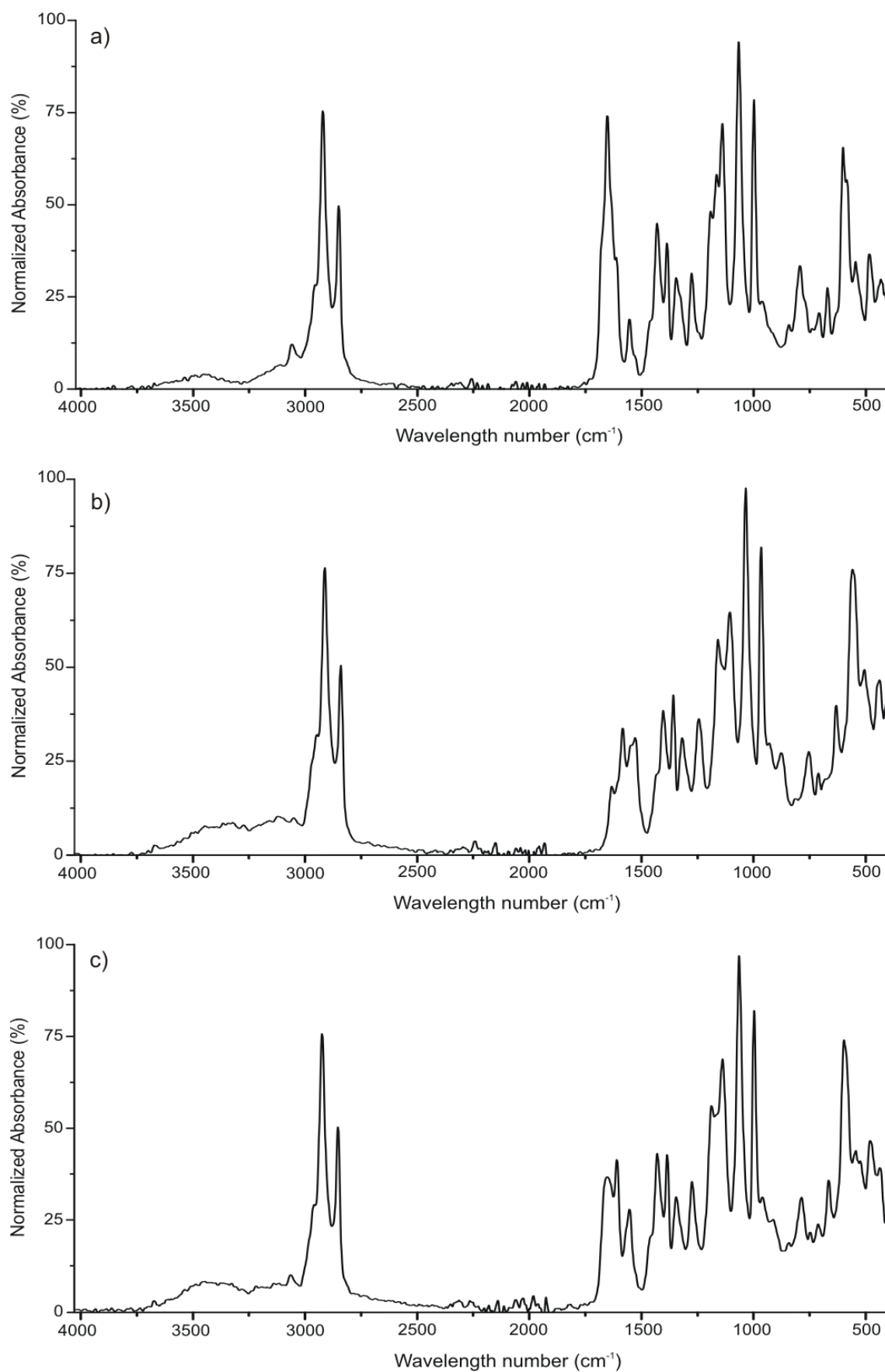
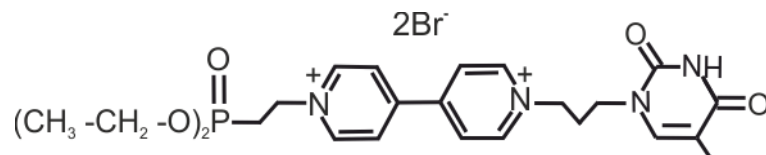


Figure 6.7 IR spectra in absorption mode of $1^{2+}(\text{DOBS})_2$ (a), $2^{2+}(\text{DOBS})_2$ (b) and $3^{2+}(\text{DOBS})_2$ (c) measured in the frequency range 4000-500 cm^{-1} with 30 scans by ATR technique

6.2.4 Synthesis of phosphonate-viologen derivatives

6.2.4.1 Synthesis of 1-[3-(5-methyl-2,4-dioxo-3,4-dihydropyrimidin-1(2H)-yl)propyl]-1'-(2-phosphonoethyl)-4,4'-bipyridinium dibromide (**b/Br⁻**)

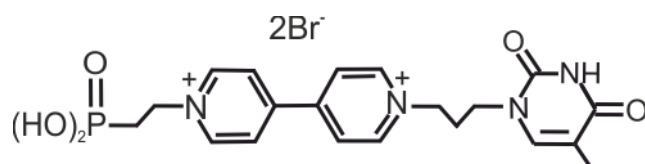


1-[2-(Diethoxyphosphoryl)ethyl]-4-(pyridin-4-yl)pyridinium monobromide (300 mg, 0.75 mmol) and 1-(3-bromopropyl)-5-methyl-pyridine-2,4(1H,3H)dione (548 mg, 2.22 mmol) were dissolved in acetonitrile (10 ml) and heated under stirring for 12 hours at 80°C. The resulted precipitate was filtered, washed with acetonitrile (10 ml), Et₂O (10 ml) and dried in vacuum for 12 hours to afford the pure compound (**b/Br⁻**) (300 mg, 0.46 mmol, 62%).

¹H-NMR (500 MHz, D₂O): δ=9.34 (dd, J=6.60 Hz, 2H), δ=9.31 (dd, J=6.60 Hz, 2H) 8.73 (dd, J=6.46 Hz, 4H), 7.63 (s, 1H), 5.05 (quin, J=5.70 Hz, 2H), 4.92 (t, J=7.25 Hz, 2H), 4.03 (t, J=6.31 Hz, 2H), 2.62 (tt, J=6.90 Hz, 4H), 1.95 ppm (s, 3H).

¹³C-NMR (125 MHz, DMSO-d₆): δ=164.19(s), 151.17(s), 140.38(d), 110.46(s), 47.26(t), 31.29(t), 29.76(t), 12.60 ppm (s).

6.2.4.2 Synthesis of 1-[3-(5-methyl-2,4-dioxo-3,4-dihydropyrimidin-1(2H)-yl)propyl]-1'-(2-phosphonate)-4,4'-bipyridinium dibromide (**4/Br⁻**)



Precursor derivative 1-[3-(5-methyl-2,4-dioxo-3,4-dihydropyrimidin-1(2H)-yl)propyl]-1'-(2-phosphonoethyl)-4,4'-bipyridinium dibromide (**b/Br⁻**) (200 mg, 0.31 mmol) was heated together with 20 ml of HBr (1M, 72 h, 130°C) under reflux. The cold mother liquor was evaporated. The resulted solid was isolated and dried for 24 hours in vacuum (160 mg, 0.27 mmol, 87%).

¹H-NMR (500 MHz, D₂O): δ=9.25 (dd, J=6.60 Hz, 4H), 8.65 (dd, J=6.46 Hz, 4H), 7.59 (s, 1H), 5.05 (quin, J=5.70 Hz, 2H), 4.92 (t, J=7.25 Hz, 2H), 4.03 (t, J=6.31 Hz, 2H), 2.62 (tt, J=6.90 Hz, 4H), 1.95 ppm (s, 3H).

6.3 Methods

6.3.1 General techniques of characterization

6.3.1.1 ^1H - and ^{13}C -NMR spectroscopy

^1H - and ^{13}C -NMR spectra were recorded on Bruker AMX-500 spectrometer; ^1H : 500.13 MHz or 250 MHz, ^{13}C : 125.7 MHz or 62.9 MHz; chemical shifts δ are given in ppm relative to the solvent signal peaks as internal standard.

6.3.1.2 Elemental analysis (EA)

Elemental analyses were made on a VarioMICRO cube device.

6.3.1.3 Infrared Spectroscopy (IR)

IR analysis was performed on a Bruker FT-IR Spectrophotometer Vertex 70 using ATR technique.

6.3.1.4 Cyclic voltammetry (CV)

Cyclic voltammetry experiments were performed under argon in a three electrode electrochemical cell with the potentiostat PGSTAT 302N from AUTOLAB controlled by a PC running under GPES from Windows, version 4.9 (ECO Chemie B.V.). A glassy carbon electrode (GCE) from Metrohm (Germany) with an electrochemical active surface area of $A=0.031\text{ cm}^2$ was used as working electrode. The surface of the working electrode was polished before the measurement with Al_2O_3 . The reference electrode was Ag/AgCl (3M, KCl in water) and the counter electrode a Pt wire.

6.3.1.5 Spectroelectrochemistry (SEC-UV-Vis)

The cell used for SEC-UV-Vis measurements of compounds **1-3**/ PF_6^- in solution was a H-Type spectroelectrochemical bulk electrolysis cell [196]. The reference electrode was Ag/AgCl immersed in an electrolyte vessel filled with LiCl (2M in ethanol), separated from the cell by a glass frit and the counter electrode was a Pt-foil. The working electrode was 0,039 g of graphitized carbon felt GFA-5 of approximately 0.021 m^2 BET area from SGL carbon with an unknown electrochemically active area. Absorbance changes were measured in conjunction with an Agilent 8453 Diode Array Spectrophotometer. The path length of the quartz cuvette was 0.2 cm and the blank sample was a solution of pure electrolyte solution.

6.3.1.6 Denaturation experiments (T_m)

T_m experiments of the mixtures of viologen-thymine derivatives **1**/Cl⁻, respectively dendrimers **G0-3**/Cl⁻ with oligonucleotides (dA_n) and analogue peptide nucleic acid (A₁₀-PNA) in phosphate buffer solution (pH=7) were performed with a Cary 100 UV-Vis Spectrophotometer. The measurement consisted in monitoring the absorbance at a fixed wavelength (260 nm) while the sample was heated from 20 to 80°C with 1°C/min ramp temperature after 5 minutes of equilibration time.

6.3.1.7 Circular dichroism spectroscopy (CD)

Circular dichroism (CD) spectra were recorded using a J-600 Spectropolarimeter (Jasco, Japan) in a quartz cuvette with 1 cm pathlength at 21°C.

6.3.1.8 Diffusion-ordered spectroscopy (DOSY)

DOSY experiments were measured on a Bruker AMX-500 spectrometer using Bruker pulse program ledbgp2s. Diffusion time (D20) was 60 ms, the length of the diffusion gradient variable between 600 – 2500 μs (P30) and the gradient recovery delays 200 μs (D16) in deuterated chloroform or tetrahydrofuran. Temperature-dependence DOSY measurements were applied to a sample of respective ionic complex (50 mM) in the temperature range from 20 to 50°C. Concentration-dependence DOSY experiments were performed at 30°C on samples of different concentration ranging from 3 mM to 50 mM of ionic. Deuterated solvent used for temperature and concentration-dependence experiments was THF-d₈.

6.3.1.9 Differential scanning calorimetry (DSC)

DSC measurements were performed on samples of about 4-12 mg. Phase transitions were measured on a Netzsch DSC 204 'Phoenix' differential scanning calorimeter. The heating and cooling rates were 10°C/min. Indium, tin and cyclohexane were used as calibration standards.

6.3.1.10 Thermo-optical polarizing microscopy (TOPM)

A Zeiss AXIOPLAN 2 polarizing microscope, equipped with a Mettler FP 80 hot stage was used. Pictures were taken using a digital Zeiss AxioCam MRC4 camera with a resolution of 4 megapixels in combination with Zeiss AxioVision software.

6.3.1.11 Ionic conductivity and electrochemical characterization of ILC's

5-7 mg solid material $1^{2+}(\text{DOBS})_2$, $2^{2+}(\text{DOBS})_2$ and $3^{2+}(\text{DOBS})_2$ respectively, was placed between two ITO conductive glass slides, heated at 51°C and compressed to obtain a uniform film with a rectangular surface area of 0.25 cm^2 and approx. $50\text{ }\mu\text{m}$ thickness. The conductivity experiments were performed in two-electrode system setup by applying a potential of -2V between the two ITO electrodes. The flow current in the external electrical circuit was monitored upon the time while the temperature was ramped with $4^\circ\text{C}/\text{min}$ in the range from 30 to 90°C . The cyclic voltammetry measurements were performed in the same two-electrode electrochemical setup with $0.01\text{ V}\cdot\text{s}^{-1}$ scan rate at 110°C .

6.3.1.12 UV-Vis characterization of ILC's in bulk state

3-5 mg of the compound $1^{2+}(\text{DOBS})_2$, $2^{2+}(\text{DOBS})_2$ and $3^{2+}(\text{DOBS})_2$ respectively, was placed between two microscope glass slides ($0.8\text{-}1\text{ mm}$ thickness, Menzel GmbH) and exposed to the temperature of 110°C on a pre-heated plate for a period of 3-5 seconds. The resulted compressed film between the glass slides was analysed with a Spectrophotometer Agilent 8453 Diode-Array. Two overlapped microscope slides were used as blank reference.

6.3.1.13 Electrochemical and spectroelectrochemical characterization of modified TiO_2 film

The ssDNA-modified TiO_2 electrodes were characterized by cyclic voltammetry in 0.1 M KCl electrolyte solution containing 1 mM $\text{K}_4[\text{Fe}(\text{CN})_6]$ in a three electrode system using Ag/AgCl (KCl, 3M) as reference electrode and a Pt wire as counter electrode. The CV's were performed at 23°C with $10\text{ mV}\cdot\text{s}^{-1}$ after purging the electrolyte solution with argon for at least 30 minutes.

The electrochemical characterization of deposited viologen-nucleobase layer was performed in KCl/ H_2O electrolyte (0.1M) in the absence of $\text{K}_4[\text{Fe}(\text{CN})_6]$ ion marker. Vis spectra of the modified TiO_2 film were record in the same electrochemical setup as previously mentioned for cyclic voltammetry experiments at -0.7 V potential after 5 seconds equilibration time, in conjunction with an Agilent 8453 Spectrophotometer. The blank was an unmodified mesoporous TiO_2 electrode.

6.3.2 Preparative procedures

6.3.2.1 Chemical reduction of compounds **1/Br⁻**, **2/Br⁻** or **3/Br⁻** with Na₂S₂O₄

2 ml solution of compound **1/Br⁻**, **2/Br⁻** or **3/Br⁻** (0.5 mM), in Tris-H₂SO₄ buffer (pH=8.5) was purged with nitrogen for at least 10 minutes and then 0.05 ml of freshly prepared solution of Na₂S₂O₄ (10 mM) in Tris-H₂SO₄ buffer (pH=8.5) were added under nitrogen atmosphere. The evolution of the reduction reaction of the compounds **1/Br⁻**, **2/Br⁻** and **3/Br⁻** was monitored *in situ* by UV-Vis spectroscopy using an Agilent 8453 Diode Array Spectrophotometer.

The buffer Tris-H₂SO₄ was prepared by dissolving Tris(hydroxymethyl)amino-methane salt (1,21 g) in 70 ml water and the pH was corrected to 8.5 with 2.4 ml solution H₂SO₄ (1 mol·l⁻¹). The solution volume was adjusted to 100 ml with distilled water.

6.3.2.2 Mixture preparation of 4,4'-bipyridinium-thymine derivatives with oligonucleotides or analogue peptide nucleic acids

Corresponding volumes of aqueous stock solutions of oligonucleotide (dA_n) or peptide nucleic acid PNA-A₁₀ and respectively viologen-nucleobase derivatives (**1/Cl⁻**, **G0-3/Cl⁻**) were mixed in a phosphate buffer (pH = 7) to afford an equimolar ratio of thymine/adenine ([T] = [A] = 20 μM). The solution mixtures were then stored at 4°C prior optical characterization.

6.3.2.3 Preparation of mesoporous TiO₂ film [197]

Conductive TEC-glass substrate was cleaned according with procedure reported in the reference [198]. Titanium dioxide colloidal paste was applied to the cleaned substrate by *doctor blade* method masked with a Tesa[®] scotch tape and air dried for 15 min. After removing the mask, the coated film was heated in an oven from 25°C to 450 °C and thermostated for 30 min (temperature was increased with a rate of 5°C/min). The sintered mesoporous TiO₂ film has a thickness of about 4-5 μm with an average pore diameter of 10-15 nm as previously reported [125].

6.3.2.4 Modification of mesoporous TiO₂ film with ssDNA

Mesoporous TiO₂ electrodes were immersed in HCl-acidified aqueous solution (pH=4.5) of respective 5'-adenylic nucleic acids (dA₁, dA₅, dA₈ or dA₈₀). The concentration of the ssDNA (expressed in monomeric adenylic units) was 650 μM.

After exposure for 12 hours at 21°C, the electrodes were rinsed with distilled water and dried in air atmosphere.

6.3.2.5 Modification of mesoporous TiO₂ film with derivative (4/Br⁻)

Mesoporous TiO₂ electrodes were exposed to a solution (10 mM) of derivative 4/Br⁻ in water at 21°C for 30 minutes. Subsequently, the electrodes were rinsed with pure solvent and dried in air atmosphere.

6.3.2.6 LbL deposition of viologen-nucleobase derivatives on modified mesoporous TiO₂ film

Modified TiO₂ electrodes with ssDNA or phosphonate-viologen-thymine derivative 4/Br⁻, were exposed in alternating steps to a chloroform solution (10 mM) of complementary viologen nucleobase derivatives 1²⁺(DOBS)₂ and 2²⁺(DOBS)₂ respectively, at 60°C for 5 minutes and subsequently cooled down to room temperature (21°C) over 30 minutes. The modified electrodes were further washed with pure solvent and dry in air atmosphere.

6.3.2.7 Desorption experiments in alkali media for determination of total surface coverage of ssDNA species

The modified TiO₂ electrodes with a layer of dA_n (n = 1, 5, 8, 80), were immersed in NaOH solution (0.1 M, 1ml) and heated to 90°C for 20 minutes. The alkali aqueous solutions were further monitored by UV-Vis spectroscopy in a quartz cuvette (1 cm pathlength). The amount of desorbed ssDNA was calculated with the Lambert Beer law using the corresponding extinction coefficients listed in the Table 6.2.

Table 6.2 Extinction coefficients of nucleic acids at 260 nm wavelength

ssDNA	dA ₁	dA ₅	dA ₈	dA ₈₀
$\epsilon_{260\text{nm}}$ (L * mol ⁻¹ * cm ⁻¹)	15400	63400	99400	963400

6.3.2.8 Desorption experiments in accelerated aging conditions

The modified TiO₂ electrodes with a layer of dA₁, dA₅, dA₈ or dA₈₀ respectively, were immersed in distilled water (1 ml) for 1, 3, 7 and respectively 28 hours at 23°C. The solutions were investigated by UV-Vis spectroscopy in a quartz cuvette (1cm pathlength) and the amount of the desorbed dA_n was calculated using the Lambert-Beer law and extinction coefficients presented in Table 6.2.

6.4 Numerical experimental data

Table 6.3 Reaction kinetic for **P1/Br⁻** and **P2/Br⁻** in nitrobenzene at 110°C (Figure 2.2)

Time (h)	Conversion of 1-(3-bromopropyl)thymine (wt%)	Conversion of 9-(2-bromoethyl)adenine (wt%)
0	0	0
2	4.3	20
4	8.3	35.35
6	12.4	45.35
9	17.7	55.15
12	22.5	63.65
27	38.1	76.95
51	52.8	82.85
75	59.8	82.85
99	64.4	82.85
171	71.1	82.85
243	73.1	82.85

Table 6.4 Concentration dependency of molar extinction coefficient (ϵ) at 404 nm of compound **1/PF₆⁻**: a) in the absence or b) in the presence of 0.1 mol/l TBAPF₆ (Figure 2.6)

In the presence of TBAPF ₆		In the absence of TBAPF ₆	
Log(conc.) (mol/l)	ϵ ($10^3 \cdot \text{l} \cdot \text{mol}^{-1} \cdot \text{cm}^{-1}$)	Log(conc.) (mol/l)	ϵ ($10^3 \cdot \text{l} \cdot \text{mol}^{-1} \cdot \text{cm}^{-1}$)
-4.22185	1.09717	-3.30103	0.52461
-4.52288	1.29033	-4	1.14751
-4.82391	1.13733	-5	2.5669
-5.12494	1.06667	-5.60206	5.9288

Table 6.5 Plot of normalized absorbance at 600 nm for compounds **1-3/PF₆⁻** versus potential (Figure 2.8b)

Potential (mV)	1/PF ₆ ⁻		2/PF ₆ ⁻		3/PF ₆ ⁻	
	Abs. (a.u.)	Normalized abs.	Abs. (a.u.)	Normalized abs.	Abs. (a.u.)	Normalized abs.
0	-0.00703	0.0012	0.00861	9.44341E-5	-0.0039	0.00258
-50	-0.00737	0	0.00859	0	-0.0043	8.58972E-4
-100	-0.00735	7.08341E-5	0.00859	3.02189E-5	-0.0045	0
-150	-0.00732	1.77085E-4	0.0098	0.00459	-0.0041	0.0018
-200	-0.00608	0.00457	0.01741	0.03334	-8.6E-4	0.01449
-250	-0.00339	0.0141	0.05475	0.17438	0.01883	0.09136
-300	0.05235	0.21151	0.147	0.52284	0.08229	0.33914
-350	0.1482	0.55098	0.2142	0.77668	0.17016	0.68222
-400	0.22244	0.81392	0.246	0.8968	0.21499	0.85725
-450	0.25488	0.92881	0.25831	0.9433	0.23353	0.92964
-500	0.26564	0.96692	0.26201	0.95728	0.24064	0.9574
-550	0.27037	0.98367	0.26618	0.97303	0.24456	0.97271

Table 6.6 Plot of peak current (I_{pc1}) versus the square root of the scan rate (v) for the compounds **1/PF₆⁻** - **3/PF₆⁻** (Figure 2.9b)

Sqrt(v)	I_{pc} (μ A)		
	1/PF ₆ ⁻	2/PF ₆ ⁻	3/PF ₆ ⁻
0.3162	-1.988	-1.921	-2.051
0.5477	-3.625	-3.552	-3.656
0.7745	-5.502	-5.557	-5.517
1	-7.178	-7.011	-7.311

Table 6.7 Amount of precipitated dA₄₀ as a function of number of positive charges per molecule of viologen-thymine derivative (Figure 3.4a)

Number of positive charges/molecule	Precipitated amount of dA ₄₀ (%)
2	24
6	71
18	98
42	97
90	98

Table 6.8 Amount of precipitated dA_n as a function of oligonucleotide length in the presence of G0/CI (Figure 3.4b)

Number of monomeric units in dA _n	Precipitated amount of dA _n (%)
20	23.5
40	60
80	79.5
140	99.9

Table 6.9 Plot of diffusion coefficient (logD) as a function of temperature determined from DOSY experiments for 2²⁺(DOBS)₂ in THF-d₈ (Figure 4.6a)

Temperature (°C)	Log(D)
20	-9.82
30	-9.7
40	-9.24
50	-8.63

Table 6.10 Plot of diffusion coefficient (logD) as a function of concentration determined from DOSY experiments for $2^{2+}(\text{DOBS})_2$ in THF- d_8 (Figure 4.6b)

Concentration (mM)	Log(D)
48.71	-9.96
24.36	-9.65
12.18	-9.53
5.87	-9.48

Table 6.11 Plot of the peak current (I_{pc1}) versus the square root of the scan rate (ν) for the compounds $MV^{2+}(\text{DOBS})_2$, $1^{2+}(\text{DOBS})_2$, $2^{2+}(\text{DOBS})_2$ and $3^{2+}(\text{DOBS})_2$ (Figure 4.8)

Sqrt(ν)	I_{pc1} (μA)			
	$1^{2+}(\text{DOBS})_2$	$2^{2+}(\text{DOBS})_2$	$3^{2+}(\text{DOBS})_2$	$MV^{2+}(\text{DOBS})_2$
0.2236	-3.46	-2.01	-2.57	-4.1
0.31622	-4.66	-2.78	-3.63	-6.69
0.5477	-7.56	-4.52	-5.86	-9.43
0.7745	-10.43	-5.96	-8.19	-12.75
1	-12.78	-7.16	-10	-15.99

Table 6.12 Plot of current versus temperature at constant voltage (-2V) for ionic complexes $1^{2+}(\text{DOBS})_2$, $2^{2+}(\text{DOBS})_2$ and $3^{2+}(\text{DOBS})_2$ (Figure 4.12)

$1^{2+}(\text{DOBS})_2$		$2^{2+}(\text{DOBS})_2$		$3^{2+}(\text{DOBS})_2$	
Temp. (K)	Current (A)	Temp. (K)	Current (A)	Temp. (K)	Current (A)
303	5.49E-11	304	7.93E-11	304	7.32E-11
309	4.88E-11	309	2.44E-11	311	5.70E-11
317	2.44E-11	316	1.95E-10	318	6.40E-11
326	2.31E-10	325	1.50E-09	327	5.00E-10
331	4.91E-10	332	5.11E-09	331	1.47E-09
340	2.37E-09	342	4.39E-08	342	5.11E-09
351	5.08E-09	349	1.16E-07	348	3.35E-08
358	2.31E-08	354	2.99E-07	357	7.48E-08
362	5.80E-08	362	6.55E-07	362	1.28E-07
371	1.50E-07				
378	4.80E-07				

Table 6.13 Arrhenius plots of ionic conductivity versus reciprocal temperature for ionic complexes $1^{2+}(\text{DOBS})_2$, $2^{2+}(\text{DOBS})_2$, and $3^{2+}(\text{DOBS})_2$ at constant voltage (-2V) (Figure 4.13)

$1^{2+}(\text{DOBS})_2$		$2^{2+}(\text{DOBS})_2$		$3^{2+}(\text{DOBS})_2$	
1000/T (K)	ln(σ) (S/cm)	1000/T (K)	ln(σ) (S/cm)	1000/T (K)	ln(σ) (S/cm)
3.30033	-12.2604	3.289474	-12.1007	3.289474	-12.1355
3.236246	-12.3116	3.236246	-12.6126	3.215434	-12.2441
3.154574	-12.6126	3.164557	-11.71	3.144654	-12.1938
3.067485	-11.6364	3.076923	-10.8239	3.058104	-11.301
3.021148	-11.3089	3.012048	-10.2916	3.021148	-10.8327
2.941176	-10.6253	2.923977	-9.35754	2.923977	-10.2916
2.849003	-10.2941	2.86533	-8.93554	2.873563	-9.47496
2.793296	-9.63639	2.824859	-8.52433	2.80112	-9.1261
2.762431	-9.23657	2.762431	-8.18376	2.762431	-8.89279
2.695418	-8.82391				
2.645503	-8.31876				

Table 6.14 Surface coverage of $[\text{Fe}(\text{CN})_6]^{4-}$ species (Γ_{Fe}) at the surface of $\text{TiO}_2\text{-dA}_n$ electrode (Figure 5.3)

Electrode name	Γ_{Fe} (nmol/cm ²)
TiO2	34.1
TiO2-dA ₁	17
TiO2-dA ₅	21.6
TiO2-dA ₈	26.1
TiO2-dA ₈₀	26.1

Table 6.15 Desorption kinetic of dA_1 , dA_5 , dA_8 and dA_{80} monolayer respectively, in H_2O at $21^\circ C$ (Figure 5.4)

Time (h)	Amount of desorbed dA_n (nmol/cm ²)			
	dA_1	dA_5	dA_8	dA_{80}
1	5.98295	0.46268	0.09788	0.0204
3	8.21536	0.60132	0.11427	0.02102
7	10.19577	0.67912	0.12531	0.02161
28	11.75686	0.80716	0.15736	0.02209

Summary and outlook

The main subject of this thesis is the synthesis and investigation of the properties and potential applications of a new class of hybrid compounds consisting of a rigid, electroactive 4,4'-bipyridinium core capped by nucleobase terminal groups with hydrogen bonding abilities.

Within this work the following objectives were accomplished:

(i) A new series of small molecules consisting in a redox active 4,4'-bipyridinium unit carrying thymine or/and adenine as capping groups was synthesized. The synthesis strategy implied the regioselective alkylation of thymine and adenine bases respectively, followed by coupling of the alkylated precursors to 4,4'-bipyridine unit via Menshutkin reaction. Electrochemical, spectroelectrochemical and optical investigations revealed an intramolecular charge transfer (CT) relationship between nucleobases as donors and 4,4'-bipyridinium unit as acceptor which is accompanied by a change in color and a shift of the reduction potentials (approx. 60 mV).

(ii) The viologen-nucleobase derivatives, particularly viologens capped by thymine, were used as building blocks to create self-assembled functional nanostructures in the presence of complementary templates such as oligonucleotides or ssPNA analogues via thymine-adenine interactions. The viologen-thymine derivatives were found to partially precipitate oligonucleotides or plasmid DNA by mean of coulombic interactions and form stable polyplexes that could be used as potential gene delivery vectors. It was found that the number of positive charges, as well as the number of thymine units per viologen-thymine derivative determines whether the interaction with DNA is dominated by electrostatic or by hydrogen bonding interactions.

(iii) New electroactive ionic liquid crystals were prepared by ion pairing of viologen-nucleobase dicationic species with amphiphilic 3,4,5-tris(dodecyloxy)benzene sulfonate anion. The nucleobases with ability to self-associate by hydrogen bonding were found to influence not just the thermotropic behavior, by decreasing transition temperature from crystalline to mesophase state, but also the supramolecular arrangement in solution.

(iv) A versatile approach to functionalize mesoporous TiO₂ film with viologen-nucleobase derivatives was developed consisting of hydrogen bonding layer-by-layer

deposition of viologen-nucleobase derivatives on TiO_2 surface using the thymine-adenine molecular recognition as driving force for immobilization. This method is promising and represents an easy way to construct optoelectronic device components as was demonstrated with the construction of a switchable electrochromic device.

Outlook:

There are still aspects that remain open to explore regarding the dual functional derivatives. For example, new molecules based on combination of 4,4'-bipyridinium redox core with the other nucleobases (guanine, cytosine) will lead to an enhancement of self-assembly process. This is because the association constant of guanine with cytosine it is higher than that of adenine with thymine, obviously due to the ability of the former couple to make three hydrogen bonds instead two hydrogen bonds [199]. However the low solubility in organic solvents combined with low regioselectivity of guanine and cytosine makes difficult up to date the alkylation of this nucleobases. If this issue will be achieved in practice by the organic chemists, new functional molecules such the one in Figure 7.1 can be designed.

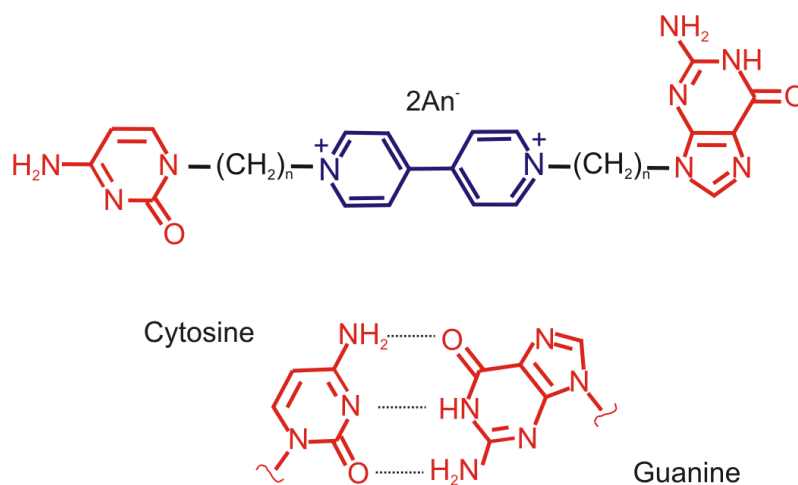


Figure 7.1 Viologen derivatives capped by guanine and cytosine bases and the Watson - Crick Model of the G-C base pair

The high ability of such compounds to self-assembly in solution or in the solid state will possibly lead to new intriguing functional materials like redox active gels [200] that are responsive to external stimuli such as temperature, pH or concentration.

Zusammenfassung und Ausblick

Das Hauptthema dieser Arbeit ist die Synthese und die Untersuchung der Eigenschaften, so wie der potentiellen Anwendungen einer neuen Klasse von Hybridmaterialien bestehend aus einem starren, elektroaktiven 4,4'-Bipyridinium-Kern flankiert von zwei Nucleobasen-Endgruppen, welche die Fähigkeit zur Ausbildung von Wasserstoffbrückenbindungen besitzen.

In dieser Arbeit wurden folgende Ziele erreicht:

(i) Eine neue Serie kleiner Moleküle bestehend aus einer redoxaktiven 4,4'-Bipyridinium-Einheit, die Thymin- und/oder Adenin-Endgruppen trägt, wurde synthetisiert. Die Synthese beinhaltete die regioselektive Alkylierung von Thymin- und Adenin-Basen gefolgt von der Kupplung der alkylierten Vorstufe an die 4,4'-Bipyridinium-Einheit mittels Menschutkin-Reaktion. Elektrochemische, spektroelektrochemische und optische Untersuchungen offenbarten einen intramolekularen Ladungstransfer zwischen der Nucleobase als Donor und der 4,4'-Bipyridinium-Einheit als Akzeptor, der von einer Farbveränderung und einer Verschiebung der Reduktionspotentiale (ca. 60 mV) begleitet wird.

(ii) Die Viologen-Nucleobasen-Derivate, insbesondere Viologene mit Thymin-Endgruppen, wurden als Bausteine benutzt, um in Gegenwart von kovalenten Ketten mit angebondenen komplementären Nucleobasen wie Oligonucleotiden oder ssPNS-Analoga, selbstorganisierende, funktionelle Nanostrukturen mittels Thymin-Adenin-Wechselwirkungen herzustellen. Die Viologen-Thymin-Derivate waren zum Teil in der Lage, Oligonucleotide oder Plasmid-DNS mittels Coulomb-Wechselwirkung auszufällen, aber auch in Lösung stabile Polypexe zu bilden, die potentiell als Vektoren für Gentransport benutzt werden könnten. Es wurde herausgefunden, dass die Anzahl der positiven Ladungen, sowie die Anzahl der Thymin-Einheiten pro Viologen-Thymin-Derivat bestimmen, ob die Wechselwirkung mit der DNS durch elektrostatische Wechselwirkung oder durch Wasserstoffbrückenbindungen dominiert wird.

(iii) Neue elektroaktive ionische Flüssigkristalle wurden durch Salzbildung von Viologen-Nucleobasen-Dikationen mit amphiphilen 3,4,5-Tris-(dodecyloxy-)benzolsulfonatanionen hergestellt. Mit ihrer Fähigkeit zur Selbstorganisation mittels

Wasserstoffbrückenbindungen beeinflussen nicht nur das thermotrope Verhalten, sondern auch die supramolekulare Anordnung in Lösung.

(iv) Ein vielseitiger Ansatz zur Funktionalisierung mesoporöser TiO_2 -Filme mit Viologen-Nukleobasen-Derivaten wurde entwickelt, bestehend aus Wasserstoffbrückenbindungs-unterstützte schichtweiser Abscheidung („Layer-by-Layer deposition“) von Viologen-Nukleobasen-Derivaten auf TiO_2 -Oberflächen, wobei die molekulare Erkennung der Thymin-Adenin-Paare als treibende Kraft für die Immobilisierung. Diese Methode ist vielversprechend und stellt einen einfachen Weg dar um optoelektronische Bauelemente zu konstruieren, wie mit der Herstellung eines schaltbaren, elektrochromen Displays gezeigt wurde.

Ausblick:

Es gibt weitere Aspekte, bezüglich der doppelfunktionellen Derivate die zu weiteren Untersuchungen herausfordern. So würden zum Beispiel neue Moleküle durch Kombination des 4,4'-Bipyridinium-Redoxkerns mit den Nukleobasen Guanin und Cytosin zur Verstärkung des Selbstorganisationsprozesses führen können weil die Assoziationskonstante von Guanin mit Cytosin höher ist als diejenige von Adenin mit Thymin. Dies erscheint offensichtlich, da das genannte Paare drei anstelle von zwei Wasserstoffbrückenbindungen auszubilden vermag [199]. Allerdings macht die geringe Löslichkeit in organischen Lösungsmitteln in zusammen mit der geringen Regioselektivität von Guanin und Cytosin die Alkylierung der Nukleobasen schwierig. Wenn diese Problematik in der Praxis durch organische Chemikers gelöst wird, können neue Materialien, wie die in Abbildung 7.1 gezeigt, hergestellt werden.

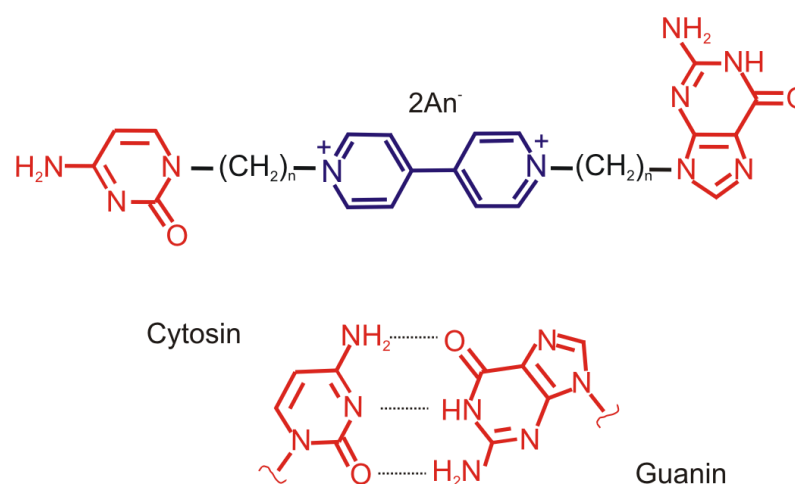


Figure 7.1 Viologenderivate flankierend substituiert mit Guanin- und Cytosinbasen-Endgruppen, sowie dem Watson-Crick-Model des G-C-Basenpaares

Die starke Fähigkeit dieser Verbindungen zur Selbstorganisation in Lösung oder im festen Zustand wird möglicherweise zu neuen, faszinierenden, funktionellen Materialien führen. Beispiele wären redoxaktive Gele [200], die reaktionsfähig gegenüber äußeren Stimuli wie Temperatur, pH oder Konzentration sind.

Abbreviations

^{13}C -NMR	carbon nuclear magnetic resonance
^1H -NMR	proton nuclear magnetic resonance
a. u.	adimensional unit
CD	circular dichroism spectroscopy
CT	charge transfer
CV	cyclic voltammetry
dA _n	adenylic oligonucleotide of degree of polymerization n
DMF	dimethylformamide
DNA	desoxyribonucleic acid
DOBS	3,4,5-tris(dodecyloxy)benzene sulfonate
dsDNA	double stranded DNA
EBr	ethidium bromide
ET	electron transfer
FTO	fluorine doped tin oxide
HBr	hydrobromic acid
HMDS	hexamethyldisilazane
ILC	ionic liquid crystal
I _{pa}	anodic peak current
I _{pc}	cathodic peak current
ITO	indium tin oxide
LbL	layer-by-layer assembly
LC	liquid crystal
LiTFSI	lithium bis(trifluoromethane)sulfonimide
MW	molecular weight

NaClO ₄	sodium perchlorate
OTE	optical transparent electrode
PF ₆ ⁻	hexafluorophosphate anion
PNA	peptide nucleic acid
ppm	parts per million
RNA	ribonucleic acid
SAM	self-assembled monolayer
SEC-UV-Vis	spectroelectrochemical UV-Vis
ssDNA	single stranded DNA
ssPNA	single stranded PNA
TiO ₂	titanium dioxide
T _m	DNA “melting temperature” as obtained from denaturation experiment
UV-Vis	ultraviolet-visible spectral range
ε	molar extinction coefficient
λ	wavelength
λ _{max}	wavelength of maximum absorption

References

1. M. White, C., M. Fernandez Gonzalez, D. A. Bardwell, L. H. Rees, J. C. Jeffery, M. D. Ward, N. Armaroli, G. Calogero, and F. Barigelletti, *Derivatives of luminescent metal-polypyridyl complexes with pendant adenine or thymine groups: building blocks for supramolecular assemblies based on hydrogen bonding*. Journal of the Chemical Society, Dalton Transactions, 1997(5): p. 727-736.
2. Maiya, B.G. and M. Sirish, *A Porphyrin-Anthracene Supramolecular System Assembled via Complementary Nucleic Acid Base Pairing*. Journal of Porphyrins and Phthalocyanines, 1998. **02**(04): p. 327-335.
3. Asaftei, S., A.M. Lepadatu, and M. Ciobanu, *Novel Compounds with a Viologen Skeleton and N-Heterocycles on the Peripheries: Electrochemical and Spectroscopic Properties*. Helvetica Chimica Acta, 2011. **94**(6): p. 1091-1101.
4. Asaftei, S., D. Huskens, and D. Schols, *HIV-1 X4 Activities of Polycationic "Viologen" Based Dendrimers by Interaction with the Chemokine Receptor CXCR4: Study of Structure-Activity Relationship*. Journal of Medicinal Chemistry, 2012. **55**(23): p. 10405-10413.
5. Yang, W., P.F. Xia, and M.S. Wong, *Highly Ordered Assembly of π -Stacked Distyrylbenzenes by Oligoadenines*. Organic Letters, 2010. **12**(18): p. 4018-4021.
6. Janssen, P.G.A., N.J.M. Brankaert, X. Vila, and A.P.H.J. Schenning, *ssDNA templated assembly of oligonucleotides and bivalent naphthalene guests*. Soft Matter, 2010. **6**(7): p. 1494-1502.
7. Janssen, P.G.A., S. Jabbari-Farouji, M. Surin, X. Vila, J.C. Gielen, T.F.A. de Greef, M.R.J. Vos, P.H.H. Bomans, N.A.J.M. Sommerdijk, P.C.M. Christianen, P. Leclère, R. Lazzaroni, P. van der Schoot, E.W. Meijer, and A.P.H.J. Schenning, *Insights into Templated Supramolecular Polymerization: Binding of Naphthalene Derivatives to ssDNA Templates of Different Lengths*. Journal of the American Chemical Society, 2008. **131**(3): p. 1222-1231.
8. Janssen, P.G.A., J. Vandenbergh, J.L.J. van Dongen, E.W. Meijer, and A.P.H.J. Schenning, *ssDNA Templated Self-Assembly of Chromophores*. Journal of the American Chemical Society, 2007. **129**(19): p. 6078-6079.
9. Iwaura, R., F.J.M. Hoeben, M. Masuda, A.P.H.J. Schenning, E.W. Meijer, and T. Shimizu, *Molecular-Level Helical Stack of a Nucleotide-Appended Oligo(*p*-phenylenevinylene) Directed by Supramolecular Self-Assembly with a Complementary Oligonucleotide as a Template*. Journal of the American Chemical Society, 2006. **128**(40): p. 13298-13304.
10. Lo, P.K. and H.F. Sleiman, *Synthesis and Molecular Recognition of Conjugated Polymer with DNA-Mimetic Properties*. Macromolecules, 2008. **41**(15): p. 5590-5603.

11. Monk, P.M.S., *The Viologens* 1998, Chichester: John Wiley & Sons Ltd.
12. Anderson, T., *Ueber die Producte der trocknen Destillation thierischer Materien*. Justus Liebigs Annalen der Chemie, 1855. **94**(3): p. 358-365.
13. Menshutkin, N., *Beiträgen zur Kenntnis der Affinitätskoeffizienten der Alkylhaloide und der organischen Amine*. Z. Physik. Chem., 1890. **5**: p. 589.
14. Bird, C.L. and A.T. Kuhn, *Electrochemistry of the viologens*. Chemical Society Reviews, 1981. **10**(1): p. 49-82.
15. Möller, M., S. Asaftei, D. Corr, M. Ryan, and L. Walder, *Switchable Electrochromic Images Based on a Combined Top-Down Bottom-Up Approach*. Advanced Materials, 2004. **16**(17): p. 1558-1562.
16. Kim, H.J., J.K. Seo, Y.J. Kim, H.K. Jeong, G.I. Lim, Y.S. Choi, and W.I. Lee, *Formation of ultrafast-switching viologen-anchored TiO₂ electrochromic device by introducing Sb-doped SnO₂ nanoparticles*. Solar Energy Materials and Solar Cells, 2009. **93**(12): p. 2108-2112.
17. Santa-Nokki, H., J. Kallioinen, and J. Korppi-Tommola, *A dye-sensitized solar cell driven electrochromic device*. Photochemical & Photobiological Sciences, 2007. **6**(1): p. 63-66.
18. Kim, Y., G.G. Malliaras, C.K. Ober, and E. Kim, *An Electrochemical Glucose Sensor from an Organically Modified Nanocomposite of Viologen and TiO₂*. Journal of Nanoscience and Nanotechnology, 2010. **10**(10): p. 6869-6873.
19. Sharrett, Z., S. Gamsey, L. Hirayama, B. Viložny, J.T. Suri, R.A. Wessling, and B. Singaram, *Exploring the use of APTS as a fluorescent reporter dye for continuous glucose sensing*. Organic & Biomolecular Chemistry, 2009. **7**(7): p. 1461-1470.
20. Bhowmik, P., H. Han, I. Nedeltchev, and J. Cebe, *Room-Temperature Thermotropic Ionic Liquid Crystals: Viologen Bis(Triflimide) Salts*. Molecular Crystals and Liquid Crystals, 2004. **419**(1): p. 27-46.
21. Tanabe, K., T. Yasuda, M. Yoshio, and T. Kato, *Viologen-Based Redox-Active Ionic Liquid Crystals Forming Columnar Phases*. Organic Letters, 2007. **9**(21): p. 4271-4274.
22. Asaftei, S., M. Ciobanu, A.M. Lepadatu, E. Song, and U. Beginn, *Thermotropic ionic liquid crystals by molecular assembly and ion pairing of 4,4'-bipyridinium derivatives and tris(dodecyloxy)benzene sulfonates in a non-polar solvent*. Journal of Materials Chemistry, 2012. **22**(29): p. 14426-14437.
23. Nantalaksakul, A., D.R. Reddy, C. Bardeen, and S. Thayumanavan, *Light Harvesting Dendrimers*. Photosynthesis Research, 2006. **87**(1): p. 133-150.
24. Ageishi, K., T. Endo, and M. Okawara, *Reduction of aldehydes and ketones by sodium dithionite using viologens as electron transfer catalyst*. Journal of Polymer Science: Polymer Chemistry Edition, 1983. **21**(1): p. 175-181.

25. Mayhew, S.G., *The Redox Potential of Dithionite and SO₂ from Equilibrium Reactions with Flavodoxins, Methyl Viologen and Hydrogen plus Hydrogenase*. European Journal of Biochemistry, 1978. **85**(2): p. 535-547.
26. De Vries, J.G. and R.M. Kellogg, *Reduction of aldehydes and ketones by sodium dithionite*. The Journal of Organic Chemistry, 1980. **45**(21): p. 4126-4129.
27. Corbin, J.L. and G.D. Watt, *A chemical preparation of pure reduced viologens for use as biomolecular reducing reagents*. Analytical Biochemistry, 1990. **186**(1): p. 86-89.
28. Rusling, J.F. and S.L. Suib, *Characterizing Materials with Cyclic Voltammetry*. Advanced Materials, 1994. **6**(12): p. 922-930.
29. Kissinger, P.T. and W.R. Heineman, *Cyclic voltammetry*. Journal of Chemical Education, 1983. **60**(9): p. 702.
30. Scholz, F., *Electroanalytical Methodes: Guide to Experiments and Applications* 2010, Berlin Heidelberg: Springer-Verlag.
31. Sivakova, S. and S.J. Rowan, *Nucleobases as supramolecular motifs*. Chemical Society Reviews, 2005. **34**(1): p. 9-21.
32. Rebek, J., B. Askew, P. Ballester, C. Buhr, S. Jones, D. Nemeth, and K. Williams, *Molecular recognition: hydrogen bonding and stacking interactions stabilize a model for nucleic acid structure*. Journal of the American Chemical Society, 1987. **109**(16): p. 5033-5035.
33. Askew, B., P. Ballester, C. Buhr, K.S. Jeong, S. Jones, K. Parris, K. Williams, and J. Rebek, *Molecular recognition with convergent functional groups. VI. Synthetic and structural studies with a model receptor for nucleic acid components*. Journal of the American Chemical Society, 1989. **111**(3): p. 1082-1090.
34. Zimmerman, S.C., W. Wu, and Z. Zeng, *Complexation of nucleotide bases by molecular tweezers with active site carboxylic acids: effects of microenvironment*. Journal of the American Chemical Society, 1991. **113**(1): p. 196-201.
35. Rieth, L.R., R.F. Eaton, and G.W. Coates, *Polymerization of Ureidopyrimidinone-Functionalized Olefins by Using Late-Transition Metal Ziegler-Natta Catalysts: Synthesis of Thermoplastic Elastomeric Polyolefins*. Angewandte Chemie International Edition, 2001. **40**(11): p. 2153-2156.
36. Thibault, R.J., P.J. Hotchkiss, M. Gray, and V.M. Rotello, *Thermally Reversible Formation of Microspheres through Non-Covalent Polymer Cross-Linking*. Journal of the American Chemical Society, 2003. **125**(37): p. 11249-11252.
37. Lin, D.C., B. Yurke, and N.A. Langrana, *Mechanical properties of a reversible, DNA-crosslinked polyacrylamide hydrogel*. Journal of Biomechanical Engineering, 2004. **126**(1): p. 104-110.
38. Brunsveld, L., B.J.B. Folmer, E.W. Meijer, and R.P. Sijbesma, *Supramolecular Polymers*. Chemical Reviews, 2001. **101**(12): p. 4071-4098.

39. Araki, K. and I. Yoshikawa, *Nucleobase-Containing Gelators*, in *Low Molecular Mass Gelator* 2005, Springer Berlin Heidelberg. p. 133-165.
40. Ulbricht, T.L.V., *Purines, Pyrimidines and Nucleotides: Ant the Chemistry of Nucleic Acids* 1964, London: Pergamon Press Ltd.
41. Dezor-Mazur, M., H. Koraniak, J.J. Langer, and K. Golankiewicz, *Intramolecular cyclization of 1-(3-bromopropyl)uracils*. *Journal of the Chemical Society, Perkin Transactions 2*, 1989(9): p. 1209-1212.
42. Nawrot, B., O. Michalak, S. Olejniczak, M.W. Wieczorek, T. Lis, and W.J. Stec, *Alkylolation of thymine with 1,2-dibromoethane*. *Tetrahedron*, 2001. **57**(18): p. 3979-3985.
43. Itahara, T., *NMR study of stacking interactions between adenine and xanthine rings*. *Journal of the Chemical Society, Perkin Transactions 2*, 1998(6): p. 1455-1462.
44. Nowick, J.S., J.S. Chen, and G. Noronha, *Molecular recognition in micelles: the roles of hydrogen bonding and hydrophobicity in adenine-thymine base-pairing in SDS micelles*. *Journal of the American Chemical Society*, 1993. **115**(17): p. 7636-7644.
45. Iwamura, H., N.J. Leonard, and J. Eisinger, *Synthetic Spectroscopic Models Related to Coenzymes and Base Pairs, VII. Stacking Interactions in tRNA; the „Bend” at Dimethylguanosine*. *Proc Natl Acad Sci U S A*, 1970. **65**(4): p. 1025-1032.
46. Baret, N., J.-P. Dulcere, J. Rodriguez, J.-M. Pons, and R. Faure, *The Cohalogenation of 1-N-Vinylpyrimidinediones: A New Approach to Nucleoside Analogs*. *European Journal of Organic Chemistry*, 2000. **2000**(8): p. 1507-1516.
47. Lehn, J.-M., *Perspectives in Supramolecular Chemistry—From Molecular Recognition towards Molecular Information Processing and Self-Organization*. *Angewandte Chemie International Edition in English*, 1990. **29**(11): p. 1304-1319.
48. Lehn, J.-M., *Supramolecular Chemistry - Concepts and Perspectives* 1995, Weinheim: Wiley-VCH.
49. Deng, W., H. Yamaguchi, Y. Takashima, and A. Harada, *A Chemical-Responsive Supramolecular Hydrogel from Modified Cyclodextrins*. *Angewandte Chemie*, 2007. **119**(27): p. 5236-5239.
50. Suzuki, M., M. Yumoto, M. Kimura, H. Shirai, and K. Hanabusa, *A Family of Low-Molecular-Weight Hydrogelators Based on L-Lysine Derivatives with a Positively Charged Terminal Group*. *Chemistry – A European Journal*, 2003. **9**(1): p. 348-354.
51. Ajayaghosh, A. and V.K. Praveen, *π -Organogels of Self-Assembled p-Phenylenevinylenes: Soft Materials with Distinct Size, Shape, and Functions*. *Accounts of Chemical Research*, 2007. **40**(8): p. 644-656.

-
52. Ryu, J.-H., H.-J. Kim, Z. Huang, E. Lee, and M. Lee, *Self-Assembling Molecular Dumbbells: From Nanohelices to Nanocapsules Triggered by Guest Intercalation*. *Angewandte Chemie*, 2006. **118**(32): p. 5430-5433.
 53. Yoshikawa, I., J. Sawayama, and K. Araki, *Highly Stable Giant Supramolecular Vesicles Composed of 2D Hydrogen-Bonded Sheet Structures of Guanosine Derivatives*. *Angewandte Chemie*, 2008. **120**(6): p. 1054-1057.
 54. Aprahamian, I., T. Yasuda, T. Ikeda, S. Saha, W.R. Dichtel, K. Isoda, T. Kato, and J.F. Stoddart, *A Liquid-Crystalline Bistable [2]Rotaxane*. *Angewandte Chemie*, 2007. **119**(25): p. 4759-4763.
 55. Sivakova, S., J. Wu, C.J. Campo, P.T. Mather, and S.J. Rowan, *Liquid-Crystalline Supramolecular Polymers Formed through Complementary Nucleobase-Pair Interactions*. *Chemistry – A European Journal*, 2006. **12**(2): p. 446-456.
 56. Berl, V., M. Schmutz, M.J. Krische, R.G. Khoury, and J.-M. Lehn, *Supramolecular Polymers Generated from Heterocomplementary Monomers Linked through Multiple Hydrogen-Bonding Arrays—Formation, Characterization, and Properties*. *Chemistry – A European Journal*, 2002. **8**(5): p. 1227-1244.
 57. Iwaura, R., K. Yoshida, M. Masuda, M. Ohnishi-Kameyama, M. Yoshida, and T. Shimizu, *Oligonucleotide-Templated Self-Assembly of Nucleotide Bolaamphiphiles: DNA-Like Nanofibers Edged by a Double-Helical Arrangement of A–T Base Pairs*. *Angewandte Chemie International Edition*, 2003. **42**(9): p. 1009-1012.
 58. Iwaura, R., M. Ohnishi-Kameyama, and T. Iizawa, *Construction of Helical J-Aggregates Self-Assembled from a Thymidylic Acid Appended Anthracene Dye and DNA as a Template*. *Chemistry – A European Journal*, 2009. **15**(15): p. 3729-3735.
 59. Ruiz-Carretero, A., P.G.A. Janssen, A. Kaeser, and A.P.H.J. Schenning, *DNA-templated assembly of dyes and extended [small pi]-conjugated systems*. *Chemical Communications*, 2011. **47**(15): p. 4340-4347.
 60. Stevens, A.L., P.G.A. Janssen, A. Ruiz-Carretero, M. Surin, A.P.H.J. Schenning, and L.M. Herz, *Energy Transfer in Single-Stranded DNA-Templated Stacks of Naphthalene Chromophores*. *The Journal of Physical Chemistry C*, 2011. **115**(21): p. 10550-10560.
 61. Janssen, P.G.A., N. Meeuwenoord, G. van der Marel, S. Jabbari-Farouji, P. van der Schoot, M. Surin, Z. Tomovic, E.W. Meijer, and A.P.H.J. Schenning, *ssPNA templated assembly of oligo(p-phenylenevinylene)s*. *Chemical Communications*, 2010. **46**(1): p. 109-111.
 62. Lo, P.K. and H.F. Sleiman, *Nucleobase-Templated Polymerization: Copying the Chain Length and Polydispersity of Living Polymers into Conjugated Polymers*. *Journal of the American Chemical Society*, 2009. **131**(12): p. 4182-4183.

63. Liu, Y., Z. Wang, and X. Zhang, *Characterization of supramolecular polymers*. Chemical Society Reviews, 2012. **41**(18): p. 5922-5932.
64. Johnson Jr, C.S., *Diffusion ordered nuclear magnetic resonance spectroscopy: principles and applications*. Progress in Nuclear Magnetic Resonance Spectroscopy, 1999. **34**(3-4): p. 203-256.
65. Sackmann, H., *Franklin D. Saeva. Liquid Crystals - the Fourth State of Matter*. Marcel Dekker, Inc., New York and Basel; 1979 491 Seiten. Preis SFr. 106. Kristall und Technik, 1981. **16**(4): p. 527-527.
66. Karim, M.A., *Electro-optical displays*1992: CRC Press.
67. Hussain, A., A.S. Pina, and A.C.A. Roque, *Bio-recognition and detection using liquid crystals*. Biosensors and Bioelectronics, 2009. **25**(1): p. 1-8.
68. Ohm, C., M. Brehmer, and R. Zentel, *Liquid Crystalline Elastomers as Actuators and Sensors*. Advanced Materials, 2010. **22**(31): p. 3366-3387.
69. Tocnaye, J.L.D.B.D.L., *Engineering liquid crystals for optimal uses in optical communication systems*. Liquid Crystals, 2004. **31**(2): p. 241-269.
70. Axenov, K.V. and S. Laschat, *Thermotropic Ionic Liquid Crystals*. Materials, 2011. **4**(1): p. 206-259.
71. Beginn, U., *Thermotropic columnar mesophases from N-H...O, and N...H-O hydrogen bond supramolecular mesogenes*. Progress in Polymer Science, 2003. **28**(7): p. 1049-1105.
72. Höhne, G.W.H., W.F. Hemminger, and H.J. Flammersheim, *Diferential Scanning Calorimetry - Second Edition*2003: Springer-Verlag Berlin Heidelberg.
73. Collings, P.J. and M. Hird, *Introduction to Liquid Crystals - Chemsitry and Physics*2009: Taylor & Francis Ltd.
74. Carlton, R., *Thermal Microscopy*, in *Pharmaceutical Microscopy*2011, Springer New York. p. 65-84.
75. Dierking, I., *Textures of Liquid Crystals*2003, Weinheim: Wiley-VCH Verlag.
76. Binnemans, K., *Ionic Liquid Crystals*. Chemical Reviews, 2005. **105**(11): p. 4148-4204.
77. Kato, T. and K. Tanabe, *Electro- and Photoactive Molecular Assemblies of Liquid Crystals and Physical Gels*. Chemistry Letters, 2009. **38**(7): p. 634-639.
78. Tabushi, I., K. Yamamura, and K. Kominami, *Electric stimulus-response behavior of liquid-crystalline viologen*. Journal of the American Chemical Society, 1986. **108**(20): p. 6409-6410.

79. Causin, V. and G. Saielli, *Effect of asymmetric substitution on the mesomorphic behaviour of low-melting viologen salts of bis(trifluoromethanesulfonyl)amide*. *Journal of Materials Chemistry*, 2009. **19**(48): p. 9153-9162.
80. Bonchio, M., M. Carraro, G. Casella, V. Causin, F. Rastrelli, and G. Saielli, *Thermal behaviour and electrochemical properties of bis(trifluoromethanesulfonyl)amide and dodecatungstosilicate viologen dimers*. *Physical Chemistry Chemical Physics*, 2012. **14**(8): p. 2710-2717.
81. Casella, G., V. Causin, F. Rastrelli, and G. Saielli, *Viologen-based ionic liquid crystals: induction of a smectic A phase by dimerisation*. *Physical Chemistry Chemical Physics*, 2014. **16**(11): p. 5048-5051.
82. Kamogawa, H. and T. Ono, *Redox photochromism in films of viologens and related compounds bearing long-chain alkyl groups*. *Chemistry of Materials*, 1991. **3**(6): p. 1020-1023.
83. Haramoto, Y., M. Yin, Y. Matukawa, S. Ujiie, and M. Nanasawa, *A new ionic liquid crystal compound with viologen group in the principal structure*. *Liquid Crystals*, 1995. **19**(3): p. 319-320.
84. Nanasawa, M., Y. Matsukawa, J. Jing Ji, and Y. Haramoto, *Redox photochromism of viologen in organized solid state*. *Journal of Photochemistry and Photobiology A: Chemistry*, 1997. **109**(1): p. 35-38.
85. Decher, G. and J.-D. Hong, *Buildup of ultrathin multilayer films by a self-assembly process, I consecutive adsorption of anionic and cationic bipolar amphiphiles on charged surfaces*. *Makromolekulare Chemie. Macromolecular Symposia*, 1991. **46**(1): p. 321-327.
86. Quinn, J.F., A.P.R. Johnston, G.K. Such, A.N. Zelikin, and F. Caruso, *Next generation, sequentially assembled ultrathin films: beyond electrostatics*. *Chemical Society Reviews*, 2007. **36**(5): p. 707-718.
87. Manna, U., S. Bharani, and S. Patil, *Layer-by-Layer Self-Assembly of Modified Hyaluronic Acid/Chitosan Based on Hydrogen Bonding*. *Biomacromolecules*, 2009. **10**(9): p. 2632-2639.
88. Wang, L., Z. Wang, X. Zhang, J. Shen, L. Chi, and H. Fuchs, *A new approach for the fabrication of an alternating multilayer film of poly(4-vinylpyridine) and poly(acrylic acid) based on hydrogen bonding*. *Macromolecular Rapid Communications*, 1997. **18**(6): p. 509-514.
89. Stockton, W.B. and M.F. Rubner, *Molecular-Level Processing of Conjugated Polymers. 4. Layer-by-Layer Manipulation of Polyaniline via Hydrogen-Bonding Interactions*. *Macromolecules*, 1997. **30**(9): p. 2717-2725.
90. Kharlampieva, E., V. Kozlovskaya, and S.A. Sukhishvili, *Layer-by-Layer Hydrogen-Bonded Polymer Films: From Fundamentals to Applications*. *Advanced Materials*, 2009. **21**(30): p. 3053-3065.

91. Guan, Y., Y. Zhang, T. Zhou, and S. Zhou, *Stability of hydrogen-bonded hydroxypropylcellulose/poly(acrylic acid) microcapsules in aqueous solutions*. *Soft Matter*, 2009. **5**(4): p. 842-849.
92. Hou, S., J. Wang, and C.R. Martin, *Template-Synthesized DNA Nanotubes*. *Journal of the American Chemical Society*, 2005. **127**(24): p. 8586-8587.
93. Johnston, A.P.R., H. Mitomo, E.S. Read, and F. Caruso, *Compositional and Structural Engineering of DNA Multilayer Films*. *Langmuir*, 2006. **22**(7): p. 3251-3258.
94. Kotov, N.A., *Layer-by-layer self-assembly: The contribution of hydrophobic interactions*. *Nanostructured Materials*, 1999. **12**(5-8): p. 789-796.
95. Zhao, W., J.-J. Xu, and H.-Y. Chen, *Electrochemical Biosensors Based on Layer-by-Layer Assemblies*. *Electroanalysis*, 2006. **18**(18): p. 1737-1748.
96. Jana, S., S. Pande, A.K. Sinha, S. Sarkar, M. Pradhan, M. Basu, Y. Negishi, A. Pal, and T. Pal, *Layer-by-Layer Deposition of Silver/Gold Nanoparticles for Catalytic Reduction of Nitroaromatics*. *Journal of Nanoscience and Nanotechnology*, 2010. **10**(2): p. 847-859.
97. Majumdar, H.S., A. Bandyopadhyay, and A.J. Pal, *Data-storage devices based on layer-by-layer self-assembled films of a phthalocyanine derivative*. *Organic Electronics*, 2003. **4**(1): p. 39-44.
98. Petty, M.C., *Molecular Electronics: From Principles to Practice* 2007, Chichester: John Wiley & Sons Ltd. .
99. Soh, S., X. Chen, S.J. Vella, W. Choi, J. Gong, and G.M. Whitesides, *Layer-by-layer films for tunable and rewritable control of contact electrification*. *Soft Matter*, 2013. **9**(43): p. 10233-10238.
100. Iost, R.M. and F.N. Crespilho, *Layer-by-layer self-assembly and electrochemistry: Applications in biosensing and bioelectronics*. *Biosensors and Bioelectronics*, 2012. **31**(1): p. 1-10.
101. Decher, G., *Fuzzy Nanoassemblies: Toward Layered Polymeric Multicomposites*. *Science*, 1997. **277**(5330): p. 1232-1237.
102. Wang, L., S. Cui, Z. Wang, X. Zhang, M. Jiang, L. Chi, and H. Fuchs, *Multilayer Assemblies of Copolymer PSOH and PVP on the Basis of Hydrogen Bonding*. *Langmuir*, 2000. **16**(26): p. 10490-10494.
103. Fu, Y., H. Chen, D. Qiu, Z. Wang, and X. Zhang, *Multilayer Assemblies of Poly(4-vinylpyridine) and Poly(acrylic acid) Bearing Photoisomeric Spironaphthoxazine via Hydrogen Bonding*. *Langmuir*, 2002. **18**(12): p. 4989-4995.
104. Zhang, H., Y. Fu, D. Wang, L. Wang, Z. Wang, and X. Zhang, *Hydrogen-Bonding-Directed Layer-by-Layer Assembly of Dendrimer and Poly(4-*

- vinylpyridine) and Micropore Formation by Post-Base Treatment*. Langmuir, 2003. **19**(20): p. 8497-8502.
105. Zhang, H., Z. Wang, Y. Zhang, and X. Zhang, *Hydrogen-Bonding-Directed Layer-by-Layer Assembly of Poly(4-vinylpyridine) and Poly(4-vinylphenol): Effect of Solvent Composition on Multilayer Buildup*. Langmuir, 2004. **20**(21): p. 9366-9370.
106. Zhang, X., H. Chen, and H. Zhang, *Layer-by-layer assembly: from conventional to unconventional methods*. Chemical Communications, 2007(14): p. 1395-1405.
107. Kharlampieva, E. and S.A. Sukhishvili, *Hydrogen-Bonded Layer-by-Layer Polymer Films*. Journal of Macromolecular Science, Part C, 2006. **46**(4): p. 377-395.
108. Park, J.S., G.S. Lee, Y.-J. Lee, Y.S. Park, and K.B. Yoon, *Organization of Microcrystals on Glass by Adenine–Thymine Hydrogen Bonding*. Journal of the American Chemical Society, 2002. **124**(45): p. 13366-13367.
109. Cosnier, S., C. Gondran, A. Senillou, M. Grätzel, and N. Vlachopoulos, *Mesoporous TiO₂ films: New catalytic electrode fabricating amperometric biosensors based on oxidases*. Electroanalysis, 1997. **9**(18): p. 1387-1392.
110. Renault, C., V. Balland, E. Martinez-Ferrero, L. Nicole, C. Sanchez, and B. Limoges, *Highly ordered transparent mesoporous TiO₂ thin films: an attractive matrix for efficient immobilization and spectroelectrochemical characterization of cytochrome c*. Chemical Communications, 2009(48): p. 7494-7496.
111. Choi, S.Y., M. Mamak, N. Coombs, N. Chopra, and G.A. Ozin, *Electrochromic Performance of Viologen-Modified Periodic Mesoporous Nanocrystalline Anatase Electrodes*. Nano Letters, 2004. **4**(7): p. 1231-1235.
112. Campus, F., P. Bonhôte, M. Grätzel, S. Heinen, and L. Walder, *Electrochromic devices based on surface-modified nanocrystalline TiO₂ thin-film electrodes*. Solar Energy Materials and Solar Cells, 1999. **56**(3–4): p. 281-297.
113. Cinnsealach, R., G. Boschloo, S. Nagaraja Rao, and D. Fitzmaurice, *Coloured electrochromic windows based on nanostructured TiO₂ films modified by adsorbed redox chromophores*. Solar Energy Materials and Solar Cells, 1999. **57**(2): p. 107-125.
114. Cummins, D., G. Boschloo, M. Ryan, D. Corr, S.N. Rao, and D. Fitzmaurice, *Ultrafast Electrochromic Windows Based on Redox-Chromophore Modified Nanostructured Semiconducting and Conducting Films*. The Journal of Physical Chemistry B, 2000. **104**(48): p. 11449-11459.
115. Jheong, H., Y. Kim, J. Pan, T.-Y. Won, and W. Lee, *Electrochromic property of the viologen-anchored mesoporous TiO₂ films*. Journal of Electroceramics, 2006. **17**(2-4): p. 929-932.

116. Bach, U., D. Lupo, P. Comte, J.E. Moser, F. Weissortel, J. Salbeck, H. Spreitzer, and M. Grätzel, *Solid-state dye-sensitized mesoporous TiO₂ solar cells with high photon-to-electron conversion efficiencies*. *Nature*, 1998. **395**(6702): p. 583-585.
117. Zúkalová, M., A. Zúkal, L. Kavan, M.K. Nazeeruddin, P. Liska, and M. Grätzel, *Organized Mesoporous TiO₂ Films Exhibiting Greatly Enhanced Performance in Dye-Sensitized Solar Cells*. *Nano Letters*, 2005. **5**(9): p. 1789-1792.
118. Kim, E.-Y., D.S. Kim, and B.-T. Ahn, *Synthesis of Mesoporous TiO₂ and Its Application to Photocatalytic Activation of Methylene Blue and E. coli*. *Bulletin of Korean Chemistry Society*, 2009. **30**(1): p. 193-196.
119. Fan, S., C. Li, G. Yang, and L. Zhang, *Influence of TiCl₄ treatment on performance of dye-sensitized solar cell assembled with nano-TiO₂ coating deposited by vacuum cold spraying*. *Rare Metals*, 2006. **25**(6, Supplement 1): p. 163-168.
120. Fan, S.-Q., C.-J. Li, G.-J. Yang, L.-Z. Zhang, J.-C. Gao, and Y.-X. Xi, *Fabrication of Nano-TiO₂ Coating for Dye-Sensitized Solar Cell by Vacuum Cold Spraying at Room Temperature*. *Journal of Thermal Spray Technology*, 2007. **16**(5-6): p. 893-897.
121. Ma, T., T. Kida, M. Akiyama, K. Inoue, S. Tsunematsu, K. Yao, H. Noma, and E. Abe, *Preparation and properties of nanostructured TiO₂ electrode by a polymer organic-medium screen-printing technique*. *Electrochemistry Communications*, 2003. **5**(4): p. 369-372.
122. Ramasamy, E., W.J. Lee, D.Y. Lee, and J.S. Song, *Portable, parallel grid dye-sensitized solar cell module prepared by screen printing*. *Journal of Power Sources*, 2007. **165**(1): p. 446-449.
123. Masuda, Y., T. Sugiyama, W.S. Seo, and K. Koumoto, *Deposition Mechanism of Anatase TiO₂ on Self-Assembled Monolayers from an Aqueous Solution*. *Chemistry of Materials*, 2003. **15**(12): p. 2469-2476.
124. Kavan, L., J. Rathouský, M. Grätzel, V. Shklover, and A. Zúkal, *Mesoporous thin film TiO₂ electrodes*. *Microporous and Mesoporous Materials*, 2001. **44-45**(0): p. 653-659.
125. Grätzel, M., *Perspectives for dye-sensitized nanocrystalline solar cells*. *Progress in Photovoltaics: Research and Applications*, 2000. **8**(1): p. 171-185.
126. Monk, P.M.S., R.J. Mortimer, and D.R. Rosseinsky, *Electrochromism and Electrochromic Devices* 2007, New York: Cambridge University Press.
127. Diebold, U., *The surface science of titanium dioxide*. *Surface Science Reports*, 2003. **48**(5-8): p. 53-229.
128. Thomas, A.G. and K.L. Syres, *Adsorption of organic molecules on rutile TiO₂ and anatase TiO₂ single crystal surfaces*. *Chemical Society Reviews*, 2012. **41**(11): p. 4207-4217.

129. Vlachopoulos, N., J. Nissfolk, M. Möller, A. Briançon, D. Corr, C. Grave, N. Leyland, R. Mesmer, F. Pichot, M. Ryan, G. Boschloo, and A. Hagfeldt, *Electrochemical aspects of display technology based on nanostructured titanium dioxide with attached viologen chromophores*. *Electrochimica Acta*, 2008. **53**(11): p. 4065-4071.
130. Granqvist, C.-G., *Electrochromic materials: Out of a niche*. *Nat Mater*, 2006. **5**(2): p. 89-90.
131. Sheina, G.G., E.D. Radchenko, S.A. Egupov, Y.P. Blagoy, and V.M. Orlov, *Charge transfer interactions between nucleic acid bases and strong acceptors*. *International Journal of Quantum Chemistry*, 1979. **16**(2): p. 387-394.
132. Schall, O.F. and G.W. Gokel, *Molecular Boxes Derived from Crown Ethers and Nucleotide Bases: Probes for Hoogsteen vs Watson-Crick H-Bonding and Other Base-Base Interactions in Self-Assembly Processes*. *Journal of the American Chemical Society*, 1994. **116**(14): p. 6089-6100.
133. Vorbrüggen, H. and B. Bennua, *Nucleoside syntheses, XXVI) A new simplified nucleoside synthesis*. *Chemische Berichte*, 1981. **114**(4): p. 1279-1286.
134. Fkyerat, A., M. Demeunynck, J.F. Constant, P. Michon, and J. Lhomme, *A new class of artificial nucleases that recognize and cleave apurinic sites in DNA with great selectivity and efficiency*. *Journal of the American Chemical Society*, 1993. **115**(22): p. 9952-9959.
135. Barral, K., S. Priet, J. Sire, J. Neyts, J. Balzarini, B. Canard, and K. Alvarez, *Synthesis, in Vitro Antiviral Evaluation, and Stability Studies of Novel α -Borano-Nucleotide Analogues of 9-[2-(Phosphonomethoxy)ethyl]adenine and (R)-9-[2-(Phosphonomethoxy)propyl]adenine*. *Journal of Medicinal Chemistry*, 2006. **49**(26): p. 7799-7806.
136. *Nucleic Acids from A to Z*, ed. S. Müller 2008, Weinheim: Wiley-VCH Verlag GmbH & Co.
137. Gasa, T.B., J.M. Spruell, W.R. Dichtel, T.J. Sørensen, D. Philp, J.F. Stoddart, and P. Kuzmič, *Complexation between Methyl Viologen (Paraquat) Bis(Hexafluorophosphate) and Dibenzo[24]Crown-8 Revisited*. *Chemistry – A European Journal*, 2009. **15**(1): p. 106-116.
138. Biasutti, M.A., S.G. Bertolotti, and C.M. Previtali, *Charge Transfer Complexes Between Indole Derivatives and Methyl Viologen in Normal and Reverse Micellar Systems*. *Journal of the Brazilian Chemical Society*, 1998. **9**: p. 63-68.
139. Park, J.W., B.A. Lee, and S.Y. Lee, *Linkage Length Dependence of Intramolecular Photoinduced Electron Transfer Reactions in Aromatic Donor–Viologen Acceptor Molecules Linked by Polymethylene Bridges*. *The Journal of Physical Chemistry B*, 1998. **102**(42): p. 8209-8215.
140. Park, J.W., H.J. Song, Y.J. Cho, and K.K. Park, *Thermodynamics and Kinetics of Formation of Orientationally Isomeric [2]Pseudorotaxanes between α -Cyclodextrin and Aliphatic Chain-Linked Aromatic Donor-Viologen Acceptor*

- Compounds*. The Journal of Physical Chemistry C, 2007. **111**(50): p. 18605-18614.
141. Monk, P.M.S., N.M. Hodgkinson, and R.D. Partridge, *The colours of charge-transfer complexes of methyl viologen: effects of donor, ionic strength and solvent*. Dyes and Pigments, 1999. **43**(3): p. 241-251.
142. Zhang, Q., T. Wu, X. Bu, T. Tran, and P. Feng, *Ion Pair Charge-Transfer Salts Based on Metal Chalcogenide Clusters and Methyl Viologen Cations*. Chemistry of Materials, 2008. **20**(13): p. 4170-4172.
143. Kunkely, H. and A. Vogler, *Optical charge transfer in the ion pairs methyl viologen²⁺ guanosine-5'-monophosphate²⁻ and adenosine-5'-triphosphate²⁻*. Chemical Physics Letters, 2001. **345**(3-4): p. 309-311.
144. Moriwaki, H., *Complexes of Paraquat with Guanine Bases Detected by Electrospray Ionization-Mass Spectrometry*. Journal of the Mass Spectrometry Society of Japan, 2002. **50**(1): p. 18-20.
145. Jalilov, A.S., S. Patwardhan, A. Singh, T. Simeon, A.A. Sarjeant, G.C. Schatz, and F.D. Lewis, *Structure and electronic spectra of purine-methyl viologen charge transfer complexes*. The Journal of Physical Chemistry B, 2014. **118**(1): p. 125-133.
146. Hünig, S. and W. Schenk, *Über zweistufige Redoxsysteme, XXVI. Einfluß von N-Substituenten in 4,4'-Bipyridylen auf das Redoxverhalten, die Radikalstabilität und die Elektronenspektren*. Liebigs Annalen der Chemie, 1979. **1979**(10): p. 1523-1533.
147. Lever, A.B.P., B.S. Ramaswamy, and S. Licocchia, *Sensitized photoreduction of methyl viologen by metalloporphyrins*. Journal of Photochemistry, 1982. **19**(2): p. 173-182.
148. Ford, W.E. and G. Tollin, *Direct Observation of Electron Transfer Across a Lipid Bilayer: Pulsed Laser Photolysis of an Asymmetric Vesicle System Containing Chlorophyll, Methyl Viologen and EDTA*. Photochemistry and Photobiology, 1982. **35**(6): p. 809-819.
149. Kalyanasundaram, K., J. Kiwi, and M. Grätzel, *Hydrogen Evolution from Water by Visible Light, a Homogeneous Three Component Test System for Redox Catalysis*. Helvetica Chimica Acta, 1978. **61**(7): p. 2720-2730.
150. McKenna, C.E., W.G. Gutheil, and W. Song, *A method for preparing analytically pure sodium dithionite. Dithionite quality and observed nitrogenase-specific activities*. Biochimica et Biophysica Acta (BBA) - General Subjects, 1991. **1075**(1): p. 109-117.
151. Park, K.K., C.H. Oh, and W.K. Joung, *Sodium dithionite reduction of nitroarenes using viologen as an electron phase-transfer catalyst*. Tetrahedron Letters, 1993. **34**(46): p. 7445-7446.

-
152. Lin, Y. and C. Mao, *Bio-inspired supramolecular self-assembly towards soft nanomaterials*. *Frontiers of Materials Science*, 2011. **5**(3): p. 247-265.
 153. Sugimoto, T., T. Suzuki, S. Shinkai, and K. Sada, *A Double-Stranded Helix by Complexation of Two Polymer Chains with a Helical Supramolecular Assembly*. *Journal of the American Chemical Society*, 2006. **129**(2): p. 270-271.
 154. Grimsdale, A.C. and K. Müllen, *The Chemistry of Organic Nanomaterials*. *Angewandte Chemie International Edition*, 2005. **44**(35): p. 5592-5629.
 155. Hoeben, F.J.M., P. Jonkheijm, E.W. Meijer, and A.P.H.J. Schenning, *About Supramolecular Assemblies of π -Conjugated Systems*. *Chemical Reviews*, 2005. **105**(4): p. 1491-1546.
 156. Bloomfield, V.A., *DNA condensation by multivalent cations*. *Biopolymers*, 1997. **44**(3): p. 269-282.
 157. Froehlich, E., J.S. Mandeville, C.M. Weinert, L. Kreplak, and H.A. Tajmir-Riahi, *Bundling and Aggregation of DNA by Cationic Dendrimers*. *Biomacromolecules*, 2010. **12**(2): p. 511-517.
 158. Raspaud, E., M. Olvera de la Cruz, J.L. Sikorav, and F. Livolant, *Precipitation of DNA by Polyamines: A Polyelectrolyte Behavior*. *Biophysical Journal*, 1998. **74**(1): p. 381-393.
 159. He, S., P.G. Arscott, and V.A. Bloomfield, *Condensation of DNA by multivalent cations: Experimental studies of condensation kinetics*. *Biopolymers*, 2000. **53**(4): p. 329-341.
 160. Zimmer, C., E. Birch-Hirschfeld, and R. Weiss, *CD studies on the conformation of some deoxyoligonucleotides containing adenine and thymine residues*. *Nucleic Acids Research*, 1974. **1**(8): p. 1017-1030.
 161. Li, J., A.-M. Lepadatu, Y. Zhu, M. Ciobanu, Y. Wang, S.C. Asaftei, and D. Oupický, *Examination of Structure–Activity Relationship of Viologen-Based Dendrimers as CXCR4 Antagonists and Gene Carriers*. *Bioconjugate Chemistry*, 2014. **25**(5): p. 907-917.
 162. Bongard, D., *Synthese und Charakterisierung von alkylverbrückten Viologendendrimern für die Transfektion in eukaryotische Zellen*, 2008, University of Osnabrück.
 163. Hyrup, B. and P.E. Nielsen, *Peptide Nucleic Acids (PNA): Synthesis, properties and potential applications*. *Bioorganic & Medicinal Chemistry*, 1996. **4**(1): p. 5-23.
 164. Wang, J., *DNA biosensors based on Peptide Nucleic Acid (PNA) recognition layers. A review*. *Biosensors and Bioelectronics*, 1998. **13**(7–8): p. 757-762.
 165. Sun, J.-K., P. Wang, Q.-X. Yao, Y.-J. Chen, Z.-H. Li, Y.-F. Zhang, L.-M. Wu, and J. Zhang, *Solvent- and anion-controlled photochromism of viologen-based*

- metal-organic hybrid materials*. Journal of Materials Chemistry, 2012. **22**(24): p. 12212-12219.
166. Kinuta, T., T. Sato, N. Tajima, R. Kuroda, Y. Matsubara, and Y. Imai, *Solid-state thermochromism observed in charge-transfer complex composed of binaphthol and viologen*. Journal of Molecular Structure, 2010. **982**(1–3): p. 45-49.
167. Hoogvliet, J.C., L.C. Lievense, C. van Dijk, and C. Veeger, *Electron transfer between the hydrogenase from *Desulfovibrio vulgaris* (Hildenborough) and viologens*. European Journal of Biochemistry, 1988. **174**(2): p. 281-285.
168. Krishnamurthy, S., I.V. Lightcap, and P.V. Kamat, *Electron transfer between methyl viologen radicals and graphene oxide: Reduction, electron storage and discharge*. Journal of Photochemistry and Photobiology A: Chemistry, 2011. **221**(2–3): p. 214-219.
169. Moore, J.S. and S.I. Stupp, *Charge-transfer and thermochromic phenomena in solid polyelectrolytes*. Macromolecules, 1986. **19**(7): p. 1815-1824.
170. Beginn, U., L. Yan, S.N. Chvalun, M.A. Shcherbina, A. Bakirov, and M. Möller, *Thermotropic columnar mesophases of wedge-shaped benzenesulfonic acid mesogens*. Liquid Crystals, 2008. **35**(9): p. 1073-1093.
171. Escuder, B., M. Llusar, and J.F. Miravet, *Insight on the NMR Study of Supramolecular Gels and Its Application to Monitor Molecular Recognition on Self-Assembled Fibers*. The Journal of Organic Chemistry, 2006. **71**(20): p. 7747-7752.
172. Bazzi, H.S. and H.F. Sleiman, *Adenine-Containing Block Copolymers via Ring-Opening Metathesis Polymerization: Synthesis and Self-Assembly into Rod Morphologies*. Macromolecules, 2002. **35**(26): p. 9617-9620.
173. Biemann, L., T. Haber, D. Maydt, K. Schaper, and K. Kleinermanns, *Structural assignment of adenine aggregates in CDCl₃*. J Chem Phys, 2008. **128**(19): p. 195103.
174. Wilson, A.J., *Non-covalent polymer assembly using arrays of hydrogen-bonds*. Soft Matter, 2007. **3**(4): p. 409-425.
175. Kyogoku, Y., R.C. Lord, and A. Rich, *The effect of substituents on the hydrogen bonding of adenine and uracil derivatives*. Proc Natl Acad Sci U S A, 1967. **57**(2): p. 250-257.
176. Spencer, J.N., C.L. Campanella, E.M. Harris, and W.S. Wolbach, *Solvent effects on hydrogen-bond formation*. The Journal of Physical Chemistry, 1985. **89**(10): p. 1888-1891.
177. Cook, J.L., C.A. Hunter, C.M.R. Low, A. Perez-Velasco, and J.G. Vinter, *Solvent Effects on Hydrogen Bonding*. Angewandte Chemie International Edition, 2007. **46**(20): p. 3706-3709.

-
178. Ouhib, F., M. Raynal, B. Jouvelet, B. Isare, and L. Bouteiller, *Hydrogen bonded supramolecular polymers in moderately polar solvents*. Chemical Communications, 2011. **47**(38): p. 10683-10685.
179. Funston, A., J.P. Kirby, J.R. Miller, L. Pospíšil, J. Fiedler, M. Hromadová, M. Gál, J. Pecka, M. Valášek, Z. Zawada, P. Rempala, and J. Michl, *One-Electron Reduction of an "Extended Viologen" p-Phenylene-bis-4,4'-(1-aryl-2,6-diphenylpyridinium) Dication*. The Journal of Physical Chemistry A, 2005. **109**(48): p. 10862-10869.
180. Bockris, J.O.M. and R.K.N. Amulya, *Modern Electrochemistry*. 2nd Edition ed. Vol. 1. 1998: Kluwer Academic Publishers.
181. Yazaki, S., M. Funahashi, and T. Kato, *An Electrochromic Nanostructured Liquid Crystal Consisting of π -Conjugated and Ionic Moieties*. Journal of the American Chemical Society, 2008. **130**(40): p. 13206-13207.
182. Yazaki, S., M. Funahashi, J. Kagimoto, H. Ohno, and T. Kato, *Nanostructured Liquid Crystals Combining Ionic and Electronic Functions*. Journal of the American Chemical Society, 2010. **132**(22): p. 7702-7708.
183. Beneduci, A., S. Cospito, M. La Deda, L. Veltri, and G. Chidichimo, *Electrofluorochromism in pi-conjugated ionic liquid crystals*. Nature Communication, 2014. **5**: p. 3105.
184. Heinen, S., *Elektroaktive Dendrimere mit Viologengerüst*, 1999, Universität Osnabrück, Institut für Chemie: Osnabrück.
185. Umezawa, Y. and H. Aoki, *Peer Reviewed: Ion Channel Sensors Based on Artificial Receptors*. Analytical Chemistry, 2004. **76**(17): p. 320 A-326 A.
186. Schön, P., T.H. Degefa, S. Asaftei, W. Meyer, and L. Walder, *Charge Propagation in "Ion Channel Sensors" Based on Protein-Modified Electrodes and Redox Marker Ions*. Journal of the American Chemical Society, 2005. **127**(32): p. 11486-11496.
187. Aoki, H., P. Bühlmann, and Y. Umezawa, *Electrochemical Detection of a One-Base Mismatch in an Oligonucleotide Using Ion-Channel Sensors with Self-Assembled PNA Monolayers*. Electroanalysis, 2000. **12**(16): p. 1272-1276.
188. Cleaves, H.J., C.M. Jonsson, C.L. Jonsson, D.A. Sverjensky, and R.M. Hazen., *Adsorption of Nucleic Acid Components on Rutile (TiO₂) Surfaces*. Astrobiology, 2010. **10**(3): p. 311-323.
189. Suzuki, H., T. Amano, T. Toyooka, and Y. Ibuki, *Preparation of DNA-Adsorbed TiO₂ Particles with High Performance for Purification of Chemical Pollutants*. Environmental Science & Technology, 2008. **42**(21): p. 8076-8082.
190. Zhang, X., F. Wang, B. Liu, E.Y. Kelly, M.R. Servos, and J. Liu, *Adsorption of DNA Oligonucleotides by Titanium Dioxide Nanoparticles*. Langmuir, 2014. **30**(3): p. 839-845.

-
191. James Cleaves Ii, H., E. Crapster-Pregont, C.M. Jonsson, C.L. Jonsson, D.A. Sverjensky, and R.A. Hazen, *The adsorption of short single-stranded DNA oligomers to mineral surfaces*. Chemosphere, 2011. **83**(11): p. 1560-1567.
 192. Asaftei, S. and L. Walder, *Modification of Mesoporous TiO₂ Electrodes with Cross-Linkable B12 Derivatives*. Langmuir, 2006. **22**(13): p. 5544-5547.
 193. Baker, W.S., B.I. Lemon, and R.M. Crooks, *Electrochemical and Spectroscopic Characterization of Viologen-Functionalized Poly(Amidoamine) Dendrimers†*. The Journal of Physical Chemistry B, 2001. **105**(37): p. 8885-8894.
 194. Komers, K., *Methylviologen Cation Radical and its Dimer in Buffered Aqueous Solutions: Visible Spectroscopy and Polarography* Journal of Chemical Research (M), 1994(8): p. 1649 - 1662.
 195. Felderhoff, M., S. Heinen, N. Molisho, S. Webersinn, and L. Walder, *Molecular Suppression of the Pimerization of Viologens (=4,4'-Bipyridinium Derivatives) Attached to Nanocrystalline Titanium Dioxide Thin-Film Electrodes*. Helvetica Chimica Acta, 2000. **83**(1): p. 181-192.
 196. Steiger, B. and L. Walder, *A Reduction Catalyst Powered by Its Own 10-Electron Battery: Synthesis and properties of a pentaviologen-linked corrinatocobalt complex*. Helvetica Chimica Acta, 1992. **75**(1): p. 90-108.
 197. Taffa, D.H., *Post Grafting of Mesoporous TiO₂ Electrodes: Host Guest Interactions and Pore Size Tuning*, in *Institute of Chemistry2010*, University of Osnabrück: Osnabrück.
 198. Hillebrandt, H., G. Wiegand, M. Tanaka, and E. Sackmann, *High Electric Resistance Polymer/Lipid Composite Films on Indium–Tin–Oxide Electrodes*. Langmuir, 1999. **15**(24): p. 8451-8459.
 199. Tanaka, H., D. Shiomi, T. Ise, K. Sato, and T. Takui, *Cytosine-guanine base pairing in a hydrogen-bonded complex of stable open-shell molecules with S = 1 spins*. CrystEngComm, 2007. **9**(9): p. 767-771.
 200. Sui, X., X. Feng, M.A. Hempenius, and G.J. Vancso, *Redox active gels: synthesis, structures and applications*. Journal of Materials Chemistry B, 2013. **1**(12): p. 1658-1672.

Curriculum Vitae

PERSONAL INFORMATION

Name: MARIUS CIOBANU

Address: Mecklenburger Str. 4, 49088 Osnabrück (Germany)

Tel.: +49 175 777 82 43

E-mail: maciobanu@uos.de

Date of birth: 23/03/1985

RESEARCH EXPERIENCE

01/2010 - 03/2014 **Research Assistant**

Department of Organic Materials Chemistry, Institute of Chemistry of New Materials, University of Osnabrück, research group OMC I

06/2013 - 03/2014 **Assistant Editor in Chemistry**

De Gruyter Open
voluntary, part-time; Responsibilities: building databases

02/2009 - 09/2009 **Graduate Assistant**

Department of Organic Materials Chemistry, Institute of Chemistry of New Materials, University of Osnabrück, research group OMC I

EDUCATION

04/2010 – 04/2015 **PhD Studies in Chemistry**

Institute of Chemistry of New Materials, University of Osnabrück, research group OMC I, Prof. U. Beginn / Prof. S. Asaftei

10/2004 - 07/2009 **Chemical Engineering Studies**

Food production technology, Faculty of Engineering, University of Bacau (Romania)

02/2009 - 09/2009 **Research internship**

Institute of Chemistry of New Materials, University of Osnabrück, research group OMC I, Prof. S. Asaftei
Topic: *Electrochemical studies of heterogeneous interactions between the surface effectors and biomolecules*

04/2007 - 08/2007 **Semester Abroad in Erasmus Program** at Institute of Chemistry of New Materials, University of Osnabrück (Germany)

10/2000 - 08/2004 **High School**
National College "Vasile Alecsandri", Bacau (Romania)

PUBLICATIONS AND PARTICIPATION TO CONFERENCES

Publications (2015), M. Ciobanu, S. Asaftei, *Nucleobase Appended Viologens: Building Blocks for New Optoelectronic Materials*, *Optical Materials*, 42, p. 262-269.

(2015), M. Ciobanu, A. Lepadatu, S. Asaftei, *Chemical and Electrochemical Studies of Carbon Black Surface by Treatment with Ozone and Nitrogen Oxide*, *Materials Today: Proceedings*, (manuscript submitted).

(2014), J. Li, A. Lepadatu, Y. Zhu, M. Ciobanu, Y. Wang, S. Asaftei, D. Oupicky, *Examination of Structure-Activity Relationship of Viologen-Based Dendrimers as CXCR4 Antagonists and Gene Carriers*, *Bioconjugate Chemistry*, 25(5), p. 907-917.

(2012), S. Asaftei, M. Ciobanu, A. M. Lepadatu, E. Song, U. Beginn, *Thermotropic ionic liquid crystals by molecular assembly and ion pairing of 4,4'-bipyridinium derivatives and tris(dodecyloxy)benzene sulfonates in a non-polar solvent*, *Journal of Materials Chemistry*, 22, p. 14426-14437.

(2011), S. Asaftei, A. M. Lepadatu, M. Ciobanu, *Novel Compounds with a Viologen Skeleton and N-Heterocycles on the Peripheries: Electrochemical and Spectroscopic Properties*, *Helvetica Chimica Acta*, 94, p. 1091–1101.

Conferences (Oral Presentation), *Hydrogen-Bonded Layer-by-Layer Modification of Mesoporous TiO₂ Films for Electrochemical Devices*, 3rd International Conference on Competitive Materials and Technology Processes, 6th – 10th October 2014, Miskolc-Lillafüred, Hungary.

(Poster), M. Ciobanu, A.-M. Lepadatu, S. Asaftei, *Chemical and Electrochemical Studies of Carbon Black Surface by Treatment with Ozone and Nitrogen Oxide*, The International Conference on Diamond and Carbon Materials, 8th – 11th September 2014, Madrid, Spain.

(Poster), Marius Ciobanu, Simona Asaftei, *Thermal-induced Electrochromism in Viologen-Nucleobase Derivatives with Ionic Liquid Crystalline Properties* – 7th International Symposium on Flexible Organic Electronics 2014, 9th -12th July 2014, Thessaloniki, Greece.

(Poster), Marius Ciobanu, Simona Asaftei, *Electrochemical and Spectroscopic Study of Supramolecular Aggregation of a New Class of Viologen-Nucleobase Derivatives in Low-Polar Solvents* at Scientific Forum Chemistry 2013, German Chemical Society (GDCh), 1st – 4th September 2013, Darmstadt, Germany.

(Poster), Marius Ciobanu, Simona Asaftei, *Self-assembled Supramolecular Structures by Hydrogen Bonding of 4,4'-bipyridinium-thymine Derivatives and Oligoadenines as Template* at the Lecture conference ORCHEM 2012, German Chemical Society (GDCh), 24th – 26th September 2012, Weimar, Germany.

(Poster), Simona Asaftei, Marius Ciobanu, Ana-Maria Lepadatu, Uwe Beginn, Enfeng Song, *New Supramolecular Aggregates of Viologen Derivatives with Liquid Crystalline or Molecular Recognition Properties* at Scientific Forum Chemistry 2011, German Chemical Society (GDCh), 4th – 7th September 2011, Bremen, Germany.

(Poster) Simona Asaftei, Ana-Maria Lepadatu, Marius Ciobanu, Dominique Schols, *Electrochemical and Chemical Properties of Novel Compounds with Viologen Skeleton and N-Heterocycles in the Periphery as Possible Antiviral Agents* at Scientific Forum Chemistry 2011, German Chemical Society (GDCh), 4th – 7th September 2011, Bremen, Germany.

(Oral presentation), *Molecular-Assemble of a Derivative of 4,4'-bipyridinium Salt and Tris(dodecyloxy)benzene Sulfonate by Ion-Pairing in Nonpolar Solvent* -International Conference of Applied Sciences. Chemistry and Chemical Engineering, University of Bacau, 28th – 30th April 2011, Bacau, Romania.

Erklärung über die Eigenständigkeit der erbrachten wissenschaftlichen Leistung

Ich erkläre hiermit, dass ich die vorliegende Arbeit ohne unzulässige Hilfe Dritter und ohne Benutzung anderer als der angegebenen Hilfsmittel angefertigt habe. Die aus anderen Quellen direkt oder indirekt übernommenen Daten und Konzepte sind unter Angabe der Quelle gekennzeichnet. Niemand hat von mir unmittelbar oder mittelbar geldwerte Leistungen für Arbeiten erhalten, die im Zusammenhang mit dem Inhalt der vorgelegten Dissertation stehen.

Die Arbeit wurde bisher weder im In- noch im Ausland in gleicher oder ähnlicher Form einer anderen Prüfungsbehörde vorgelegt.

Osnabrück, 12. März 2015

Marius Ciobanu